TeV gamma-ray emission from accreting binary pulsars

Vincent Mannings

TeV Gamma-Ray Emission From Accreting Binary Pulsars

By

Vincent Mannings

1990

A thesis submitted to the University of Durham in accordance with the regulations for admittance to the degree of Doctor of Philosophy

Department of Physics

University of Durham

TeV Gamma-Ray Emission From Accreting Binary Pulsars

Vincent Mannings

Department of Physics

University of Durham

Ph.D. 1990

ABSTRACT

The high-mass X-ray binary SMC X-1 has been observed during the interval 1986-1989 at a threshold γ-ray energy of 0.4 TeV using the University of Durham Mark III air Cerenkov telescope at Narrabri. The Cerenkov arrival time series recorded during these observations have been tested for periodicity at the contemporary pulse period of the SMC X-1 X-ray pulsar. This period analysis was performed using a new technique - introduced in the present work - which is designed for TeV γ-ray source candidates in binary systems and which simultaneously seeks evidence for pulsed TeV γ-ray emission and information on the location of the emission site within the binary.

Results are also presented from the period analysis of data accumulated at Narrabri during observations of the low-mass X-ray binaries X0021.8-7221 (in the globular cluster 47 Tucanae) and GX 1+4.

X-ray binaries as a class of TeV γ-ray source are considered and their properties compared. Previous models which invoke the interaction of beams of high-energy particles with material within the environment of a binary system are discussed. One of these models is adapted in the present work in order to propose a simple explanation of the narrow TeV γ-ray orbital light curve observed for the high-mass binary Centaurus X-3. The new model accounts for the γ-ray emission from Cen X-3 in terms of the collisions of ultrarelativistic protons with an accretion wake trailing the X-ray pulsar. This model, which incorporates the steering of charged particles in the magnetosphere of the massive primary star, is also applied to the Vela X-1 binary in order to investigate claims that TeV γ-ray outbursts observed during X-ray eclipse arise at particle collisions with the limb of the supergiant companion.

TeV γ-Ray Emission From Accreting Binary Pulsars

Table of Contents

PREFACE

The present work is concerned with the analysis and interpretation of data obtained with the University of Durham Mark III telescope at Narrabri, New South Wales, Australia.

The author has participated with the operation and maintenance of the Mark III telescope during a total of five Moon-free periods and has assisted with the collection of data on the principal X-ray binary source candidates studied in this thesis (SMC X-1, X0021.8-7221, and GX 1+4) together with various other objects including Cen X-3, Vela X-1, SS433, LMC X-4, Sco X-1, GX 5-1, SN 1987a in the Large Magellanic Cloud, and the active Galaxy Centaurus A. The author also participated with the construction and testing of a second air Cerenkov telescope (the Mark IV) which has now joined the Mark III at Narrabri.

Along with his colleagues, the author has been involved in all stages of the routine processing of data prior to analysis.

The main contribution of the author has been the development of a new method for the analysis of data on TeV γ-ray pulsar source candidates in X-ray binary systems. He has quantified the potential spatial resolution offered by the necessity to tranform Cerenkov arrival times to the binary system rest frame (in order to compensate for Doppler shifting) and was completely responsible for the application of this new technique to the full SMC X-1 database collected at Narrabri and for the calibration and interpretation of the results. In addition he was responsible for the period analysis of the X0021.8-7221 and GX 1+4 data.

The author has briefly discussed previous models of TeV γ-ray emission in X-ray binary systems and is entirely responsible for adapting one of them - and writing all relevant software - to suggest an explanation of the observed properties of the pulsed γ-ray emission from Cen X-3 and Vela X-1.

None of the material presented in this thesis has been submitted previously for admittance to a degree in this or any other university.

Acknowledgements

My supervisor Ted Turver is thanked for his guidance, ideas and support throughout the course of my studies in Durham.

Alberto Carramiñana, my good friend and colleague, is thanked for his companionship over these last three years and for keeping me sane during the completion of this thesis. I will never forget our long chats about X-ray binaries, pulsars, γ-rays, cosmic rays, and other bits and pieces of the universe, not to mention the numerous cups of coffee which kept us going as we wrote our theses long into the dark evenings. A pleasure to know you, Alberto. And Esperanza too ! I would also like to thank Lowry McComb for the many useful discussions we've had (and his patience !), and for his pleasant company at Narrabri. My good friends Pete Edwards and Jo Lee are thanked for their friendship and for putting up with my company during the last couple of weeks of this thesis ! My warmest wishes are also offered to Penny Dunbabin, Chris Bowden, and Stella Bradbury. Best of luck to you for the future. Very best wishes are also extended to Nigel, Eric, Cyril, Keith, Paula, Audrey and Jack.

The Science and Engineering Research Council is thanked for my Research Studentship. Many thanks to Professor Arnold Wolfendale and to Professor Alan Martin for the provision of the facilities of the Department of Physics, University of Durham, and to the University of Sydney for the lease of the Narrabri site.

Chapter 1

Introduction

1.1 The Present Work

The ground-based detection of optical Cerenkov radiation from photon-induced cascades in the Earth's atmosphere is the most cost-effective method currently available for the monitoring of celestial source candidates for emission in the energy range ~ 10^{11} to 10^{14} eV. In 1986 September the Durham University TeV γ-Ray Astronomy Group commissioned the Mark III air Cerenkov telescope at a site in New South Wales, Australia. This instrument had, by 1990 September, observed a total of 32 γ-ray source candidates to yield 2660 hours of data. The potential γ-ray sources selected for observation have included 16 X-ray binary systems, 13 radio pulsars, the Galactic centre, the supernova SN1987a in the Large Magellanic Cloud, and the nearby active galaxy Centaurus A.

Successful detections of high-energy γ-ray emission with the Mark III telescope have so far been confined to the X-ray binary source class, namely the high-mass binaries Vela X-1 and Centaurus X-3, and the low-mass binary Scorpius X-1. The wind-driven supergiant X-ray binary Vela X-1 was observed during 1986-1988. See Carraminana *et al.* (1989a). Evidence has been found for persistent γ-ray pulsations at the X-ray period of

approximately five minutes. The time-averaged luminosity at energies > 0.3 TeV is estimated to be ~ 4 x 10^{34} ergs s^{-1}. These results confirm the first observations of Vela X-1 at TeV γ-ray energies by North *et al.* (1987). Centaurus X-3 was discovered to be a source of high-energy γ-ray emission by the Durham Group and has been observed since 1987 (Brazier *et al.* (1990a). This binary comprises a 4.8-second X-ray pulsar in a 2-day orbit about an OB companion star. Pulsed γ-ray emission is detected only when the neutron star is within the vicinity of the ascending node of the orbit, or X-ray phase 0.75. The peak luminosity is ~ 4 x 10^{36} ergs s^{-1} (E > 0.25 TeV). The low-mass X-ray binary Scorpius X-1 has been observed since 1988. Evidence is found (Brazier *et al.* 1990b) for persistent unpulsed γ-ray emission at a luminosity ~ 2 x 10^{34} ergs s^{-1} (E > 0.3 TeV).

These detections can be placed in context by inspecting the catalogue of known TeV γ-ray sources in Table 1.1. The list is short and totals just 21 sources spread across five classes of object: X-ray binaries, cataclysmic variables, radio pulsars, supernova remnants, and galaxies. Of these 21 sources, only 9 - all within the Galaxy - have been confirmed by subsequent observations. It can be seen that the addition of Vela X-1, Centaurus X-3 and Scorpius X-1 to this list following the observations with the Mark III telescope has brought the number of confirmed X-ray binary TeV γ-ray sources up to 6, or $^{2}/_{3}$ of the total number of confirmed sources. The X-ray binaries are therefore the dominant class of known sources of high-energy γ-ray radiation at this time.

TABLE 1.1

SOURCE	REFERENCE	CONFIRMED
X-RAY BINARIES		
Cygnus X-3	Brazier *et al.* (1990c)	√
Hercules X-1	Brazier *et al.* (1990d)	√
4U0115+63	Brazier *et al.* (1990d)	√
Vela X-1	Carraminana *et al.* (1989a)	√
Centaurus X-3	Brazier *et al.* (1990a)	√
Scorpius X-1	Brazier *et al.* (1990b)	√
X0021.8-7221	de Jager *et al.* (1990)	X
1E2259+586	Brazier *et al.* (1990d)	X
LMC X-4	Brazier *et al.* (1990e)	X
CATACLYSMIC VARIABLES		
AE Aquarii	Brink *et al.* (1990)	X
RADIO PULSARS		
Crab	Dowthwaite *et al.* (1984a)	√
Vela	Bhat *et al.* (1987)	√
PSR1855+09	Brazier *et al.* (1990h)	X
PSR1937+21	Chadwick *et al.* (1987)	X
PSR1953+29	Chadwick *et al.* (1985a)	X
PSR1509-58	Nel *et al.* (1990)	X
PSR1957+20	de Jager *et al.* (1989a)	X
SUPERNOVA REMNANTS		
Crab Nebula	Weekes *et al.* (1989)	√
GALAXIES		
Galactic Plane	Dowthwaite *et al.* (1985)	X
Centaurus A	Grindlay *et al.* (1975)	X
M31 (Andromeda)	Dowthwaite *et al.* (1984b)	X

TeV γ-Ray Source Catalogue

The emission of pulsed TeV γ-rays from the X-ray binary systems is explored in this thesis. The experimental and analytical methods are described briefly first. Chapter 2 is concerned with the air Cerenkov technique. The design of the Mark III facility at Narrabri is described in Chapter 3, together with the procedures adopted for the pre-analysis processing of the data. The methods employed for the period analysis of Cerenkov arrival time series are outlined and compared in Chapter 4.

New results will be presented from the analysis and interpretation of the databases accumulated during observations of three X-ray pulsars: SMC X-1, X0021.8-7221, and GX 1+4. The astrophysical background to these analyses is developed in Chapters 5 and 6. Chapter 5 deals with the classification and general properties of X-ray binary systems and provides a brief account of the energetics of mass transfer. The results of the previous detections of TeV γ-rays from examples in this source class are quickly reviewed in Chapter 6.

The high-mass binary system SMC X-1 consists of a 0.71-s X-ray pulsar in a 3.9-day orbit about a supergiant companion star. A uniform secular X-ray pulse period derivative $\sim -10^{-11}$ s s^{-1} has been measured during nearly twenty years of X-ray observations. This steady spin-up has a timescale $(P/\dot{P}) \sim 2 \times 10^3$ yr. Roche lobe overflow drives the X-ray source, which radiates typically at the Eddington limit $\sim 10^{38}$ ergs s^{-1}. It is the most powerful X-ray source in the Small Magellanic Cloud and is one of the most

luminous X-ray binaries known.

The Durham Group have performed the first TeV γ-ray observations of SMC X-1. These data are employed in the present work in order to introduce a new approach to the period analysis of Cerenkov arrival time series recorded during observations of TeV γ-ray source candidates in X-ray binary systems. Details of the Narrabri database are given in Chapter 7, following a discussion of the results of the X-ray and optical measurements. The SMC X-1 database has been tested for pulse periodicity at the contemporary X-ray pulse period. In order to accomplish this, the arrival times of the Cerenkov events registered at the telescope must first be transformed to the rest frame of the binary in order to remove the effect of the Doppler shifting in the value of the putative γ-ray pulse period due to the orbital motion of the pulsar. It will be seen that the particular values of the SMC X-1 pulse period and the orbital elements require a comparatively accurate knowledge of the relative orientation of the pulsar and the companion star at any given time if pulse phase coherence is to be maintained. However, since the SMC X-1 orbital parameters are well known from the measurements at X-ray energies, these special demands on the period analysis of the Narrabri database can, in principle, be utilised to investigate the location of a γ-ray emission site in the SMC X-1 binary. The potential spatial resolution is such that a distinction could be made between a γ-ray source positioned at the neutron star and one that is located towards the outer edge of the accretion disk. This possibility

is investigated in Chapters 8 and 9, where the results of the analyses are presented. Although periodic components pulsed at a period consistent with the X-ray pulse period are identified, the low strengths of these components, coupled with the necessary number of analysis trials, means that the confidence level is low and, formally the results must be said to be consistent with a chance origin. However, there is qualitative evidence which suggests that pulsed γ-rays may have been recorded and that the origin of this emission may be within the vicinity of the SMC X-1 X-ray pulsar.

X0021.8-7221 is a low-mass binary in the core of the nearby globular cluster 47 Tucanae. Transient two-minute X-ray pulsations have been reported by Auriere, Koch-Miramond and Ortolani (1989) following the analysis of data which was obtained by the *Einstein* observatory during 1979. The X-ray luminosity is typically ~ 10^{34} ergs s^{-1}. Evidence for TeV γ-rays from 47 Tucanae which were pulsed at the X-ray pulse period has been claimed by de Jager *et al.* (1990) using the data from a series of observations performed during 1989. The time-averaged luminosity is ~ 10^{35} ergs s^{-1} ($E > 2.8$ TeV). The Durham Group have monitored 47 Tucanae from Narrabri during five observing sequences in the interval 1988 July to 1990 September. Period analysis of the Narrabri database is presented in Chapter 10. These data provide no evidence for pulse periodicity. A 3σ upper limit of 7×10^{34} ergs s^{-1} ($E > 0.4$ TeV) is placed on the time-averaged luminosity of emission from 47 Tucanae pulsed at the X-

ray period of X0021.8-7221.

The unusual low-mass binary GX 1+4 is located near to the Galactic centre and consists of a two-minute X-ray pulsar in orbit about a red giant star. Optical spectrophotometry reveals that the binary is embedded within a cocoon of gas of radius ~ 2 x 10^3 lt-sec. The X-ray intensity is highly variable and was observed close to the Eddington limit during the 1970s. Since then the X-ray power has fallen off to < 10^{36} ergs s^{-1}. Episodes of rapid spin-up and spin-down have been witnessed at X-ray energies; the spin-up timescale is ~ 40 years, which is one of the shortest of all known X-ray pulsars. A tentative identification of GX 1+4 with the Galactic centre 511-keV electron-positron annihilation line source has been made by McClintock and Leventhal (1989). The Durham Group monitored GX 1+4 during a short sequence of observations in 1988. The results of the analysis of the data taken during these observations are given in Chapter 10, where a 3σ upper limit on the luminosity of L ~ 4 x 10^{34} ergs s^{-1} (E > 0.25 TeV) is placed for pulsed γ-ray emission from GX 1+4 at the contemporary X-ray pulse period.

The observed characteristics of TeV γ-ray emission from the X-ray binaries are considered in Chapter 11. Constraints on models of γ-ray emission imposed by the results of the measurements are discussed. Approximately one third of the X-ray binaries detected at TeV energies to date show some indication that ultrarelativistic particles may be transported far from the neutron star and deposited in material at several possible

locations: these include the outer edge of a neutron star accretion disk, the accretion wake trailing behind a neutron star, and perhaps even the limb of a companion star. A simple model is proposed in Chapter 11 in order to account for the observed TeV γ-ray orbital light curve of Centaurus X-3. This postulates the acceleration of protons to ultrahigh energies in the immediate vicinity of the neutron star and their injection into the environment of the accretion disk. Their trajectories are then computed in the magnetosphere of the companion star to test the feasibility of the idea that the detected γ-rays are the products of neutral pion decay following high-energy nucleon collisions within the Centaurus X-3 accretion wake. Proton trajectories are also computed for the parameters of the Vela X-1 binary in order to examine the suggestion by North *et al.* (1987) and Raubenheimer *et al.* (1989) that short-term bursts of TeV γ-ray emission may be produced by particle interactions with the limb of the supergiant primary star.

The remainder of the present chapter is divided into two sections. Section 1.2 is a brief account of the different methods which are currently employed to detect γ-rays at energies below $E \sim 10^{10}$ eV and above $E \sim 10^{14}$ eV. This serves to provide a frame of reference for the air Cerenkov technique described in the following chapter. Section 1.3 concentrates on the mechanisms for the production and loss of γ-rays in astronomical environments.

1.2 Techniques in Gamma-Ray Astronomy

1.2.1 Introduction

The γ-ray portion of the electromagnetic spectrum can be subdivided into three broad energy bands, each corresponding to the techniques by which γ-rays from astronomical sources are detected. These regions are shown in Figure 1.1. Gaps exist at the lower and upper bounds on the air Cerenkov band. Around photon energies ~ 10 to ~ 100 GeV the typical source fluxes have fallen off to such low levels that they are beneath the limiting sensitivities of the spacecraft experiments conducted so far; at the same time the Cerenkov components in the cascades generated in the atmosphere by such photons are well below the detection thresholds of contemporary ground-based instruments. Similarly, photons at energies between ~ 5 to ~ 50 TeV typically are too few in number for the air Cerenkov observatories, and too low in energy to generate sufficient particle fluxes for the ground-based air shower arrays.

1.2.2 Gamma-Rays in the Energy Range 0.1 MeV to 30 GeV

Detailed accounts of the instrumentation used in contemporary γ-ray astronomy are provided by Hillier (1984), Ramana Murthy and Wolfendale (1986), Weekes (1988), and Hartman (1989).

The Compton scattering of electrons is the dominant process of interaction with matter for γ-rays of energy between ~ 0.1 MeV

Figure 1.1

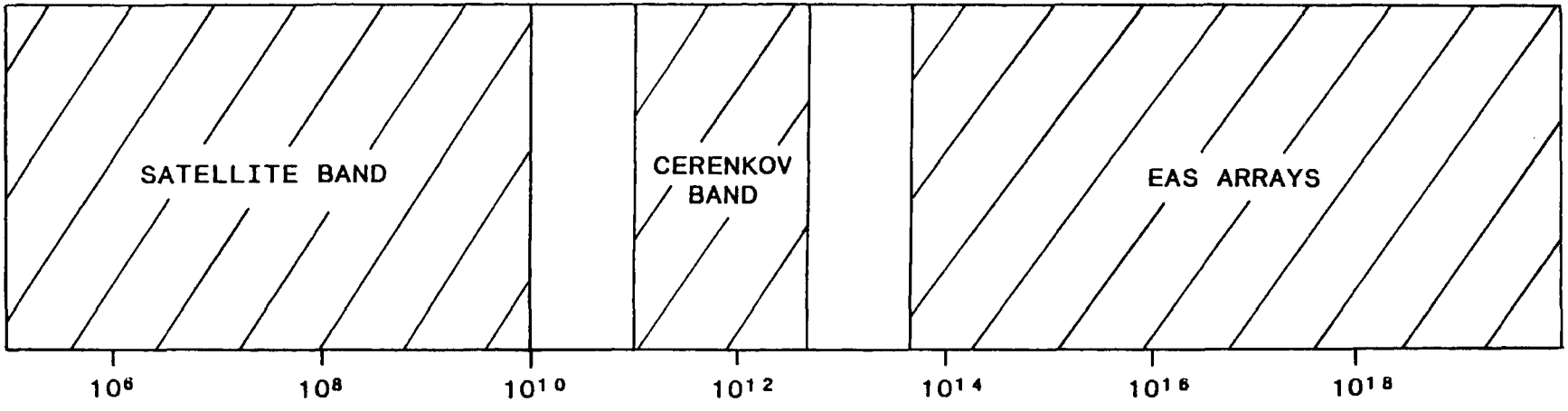

The γ-Ray Region of the Electromagnetic Spectrum

Cross-hatched energy ranges indicate bands covered by contemporary experimental techniques

and ~ 3 MeV. A γ-ray loses just a small fraction of its energy in a single Compton scattering so that detectors which make use of this process need to be massive if the photon is to undergo many scatterings and the total energy is to be absorbed. For this reason, scintillation counters are often used. Scintillators convert into optical fluorescent light a fraction of the energy of a scattered electron lost to ionisation. These are coupled to a photosensor (often a photomultiplier tube) which then converts the light into an electric signal which can be amplified and processed.

At the lower end of this energy band the direction of motion of the scattered electron is only weakly correlated with the direction of the γ-ray. Moreover, since the low energy electron suffers multiple scatterings in the detector, information on its initial direction of motion is soon lost. Collimators placed in front of the scintillation detector must instead be used to infer the direction of motion of the incident γ-ray photon. The OSSE instrument (*Oriented Scintillation Spectrometer Experiment*) aboard the Gamma-Ray Observatory (GRO) is sensitive to the energy range 0.1 to 10 MeV and comprises four large collimated NaI scintillators with a field of view of 5°x11° FWHM.

So-called 'Compton telescopes' are constructed for the detection of primary photon energies ~ 3 MeV. At these energies the scattering angle of an electron is sufficiently small that its direction of motion essentially defines that of the incident γ-ray. Both the secondary electron and the secondary photon

can be used in Compton telescopes. The GRO COMPTEL instrument has an energy range 1-30 MeV and an angular resolution ~ 1°. The detectors are a liquid scintillator and a NaI crystal scintillator.

Electron-positron pair production becomes the most probable interaction process with matter for γ-rays at energies above a few MeV. Much directional information can now be obtained, for the direction of motion of the secondary particles is very closely aligned with the direction of the primary photon. The secondary electrons also have much greater energies than those involved in the lower energy Compton scattering process and can therefore penetrate larger thicknesses of material. This permits the use of spark chambers to observe the tracks of the secondary particles. These consist of a stack of parallel metal plates in a gas-filled chamber (usually a mixture of neon and argon). Alternate plates are at earth potential. Triggering detectors aligned with the stack respond to a secondary charged particle by applying a large voltage pulse to the interleaving plates. A spark is then observed between each pair of plates as a result of breakdown through the trail of ion pairs in the gas along the track of the particle. The GRO EGRET instrument (*Energetic Gamma-Ray Experiment Telescope*) is sensitive to the energy range ~ 20 MeV to ~30 GeV. The detector system includes a multilevel thin plate spark chamber which is similar to those which were carried by the SAS-2 AND COS-B satellite experiments of the 1970s. However the angular resolution is better. For point sources of

moderate flux, the position determination is expected to be accurate to ~ 10 minutes of arc. Spatial variations in the energy spectrum of diffuse sources should be measurable on a scale ~ few degrees. The Soviet-French GAMMA-I experiment was launched in 1990 July. It uses a spark chamber assembly and is designed principally for the energy range 50 to 500 MeV. At these energies the GAMMA-I angular resolution is marginally better than that of EGRET. The greater collecting area of the latter instrument however means that it may be sensitive up to energies ~ 30 GeV, at which the directional information provided by the secondary particles is much greater.

A fourth instrument will be carried by GRO, in addition to the OSSE, COMPTEL and EGRET experiments: the wide-field BATSE instrument (*Burst and Transient Source Experiment*) will be sensitive to the energy range 50-600 keV and will monitor γ-ray burst events to a time resolution ~ 100 microsecond with an angular resolution ~ 1°. Orginally due for launch in 1988, the Gamma-Ray Observatory is currently scheduled for a Space Shuttle flight in the spring of 1991.

1.2.3 Gamma-Rays Above ~ 50 TeV

A brief outline of the techniques used in PeV and EeV γ-ray astronomy is given here, together with details of some of the exciting recent reports of ultrahigh energy emission from X-ray binary sources.

γ-rays with energy in excess of E ~ 50 TeV arriving at the Earth's atmosphere generate cascade showers which produce a detectable particle flux consisting mainly of electrons, positrons and muons over an area ~ 100 m radius at ground level. Horizontal arrays of particle detectors - usually fast scintillators coupled to photomultiplier tubes - are employed to sample the particle density and the time of arrival across the shower front. Each detector has a solid angle acceptance $\approx 2\pi$ steradians so that no information on arrival direction can be obtained from a single component of the array. Instead, the arrival times recorded at several detectors must be used to reconstruct the direction of the primary γ-ray: for two timing detectors separated by a distance d which record events separated in time by an amount Δt, the projected zenith angle in a vertical plane containing the detectors is just $\theta = \sin^{-1}(c\Delta t/d)$. A third detector must be used to fix the direction in two dimensions. In practice the arrival times from many detectors are used and a least squares fit is made to the shower front. The current generation of PeV γ-ray experiments typically have detectors with ~ 1 ns time resolution, collection areas ~ 1 m^2, and separations ~ 10 m. Arrival directions can be measured to an accuracy ~ 1°.

By far the majority of the particles detected by the PeV exeperiments originate in the extensive air showers (EAS) generated by primary cosmic rays. Besides electrons, positrons and muons (~ 5 % electron component), the EAS include pions, nucleons, and other hadrons, totalling ~ 20 % of the muon

component. The γ-ray showers must be identified in the presence of this large, isotropic background by searching for significant fluctuations in the angular and temporal distributions of the showers registered by an array. Samorski and Stamm (1983a,b) operated the Kiel array during 1976-1979 and found a 4.4 σ excess of air showers in the direction of Cygnus X-3 which was modulated with the X-ray cycle of 4.8 hours. This excess was only recognised when an 'age cut' was applied to the data in order to improve the signal-to-noise ratio. The energy of a γ-ray electromagnetic cascade is dispersed much faster in the atmosphere than that of a nuclear-electromagnetic shower in which a significant fraction of the energy is carried to greater depths by the relatively stable hadrons. In consequence, the ground-level lateral distribution of electrons and positrons is much flatter for γ-ray showers than for the cosmic ray EAS. The data may therefore be sorted according to this distribution in order to enrich the fractional γ-ray content.

Lloyd-Evans *et al.* (1983a,b) confirmed the identification of Cygnus X-3 as a source of PeV emission using air shower data obtained with the Haverah Park array (UK) during 1979-1982.

A second method which has been proposed to improve the signal-to-noise ratio is to inspect the muon content of showers. Charged pions are produced in both γ-ray showers and EAS, which subsequently decay to positive and negative muons in a rest frame time $\sim 10^{-8}$ s. (Other pion decay products are photons, electrons, positrons, neutrinos and antineutrinos). However, the

ratio of the cross-sections for pion production in the two types of showers is small,

$$\sigma(\gamma + N \longrightarrow \pi\pm + \ldots) \; / \; \sigma(p + N \longrightarrow \pi\pm + \ldots) \sim 10^{-2}$$

- see e.g. Ramana Murthy and Wolfendale (1986) - so it is expected that few muons would be sampled in a γ-ray shower compared with the number detected in an EAS. The predicted ratio is $\approx$ 1:10. Low muon density could then be used to sort the showers and remove a large fraction of the cosmic ray background. This prediction has been called into question by the observation of a high muon content in showers ascribed to γ-rays from Cygnus X-3. See Samorski and Stamm (1983c) for measurements of muon densities with the Kiel array which indicate an eight-fold increase over the expected muon component; Marshak *et al.* (1985) report evidence for high muon content using the Soudan-1 underground detector, and Battistoni *et al.* (1985) claim evidence for the detection of an X-ray phase modulated muon flux in the direction of Cygnus X-3 using the Mt Blanc NUSEX experiment. See also Elbert (1985) for a discussion of these results. Dingus *et al.* (1988, 1989) report evidence for the detection of two short bursts of pulsed PeV emission from the low-mass binary Hercules X-1 during 1986 using the CYGNUS PeV experiment at Los Alamos. Again the muon content of the air showers is claimed to be much higher than that expected for γ-ray cascades, and is observed to be comparable with that expected from hadronic showers.

The South Pole is now the site of a successful PeV γ-ray experiment which is being operated jointly by the University of Leeds and the Bartol Research Institute, Delaware. This site has three attractive features, in addition to providing the opportunity to monitor Southern Hemisphere candidate sources for PeV emission. First, all sources are circumpolar and so may be observed continuously. Second, the South Pole is 2.8 km above mean sea level so that the air showers suffer correspondingly less attenuation before reaching a detector array. Third, the elevation of any given source candidate is constant, which means that the local rate of background cosmic rays is effectively unchanging. The Leeds-Bartol SPASE array (*South Pole Air Shower Experiment*) has provided evidence for a new source of PeV emission. SPASE is located ~ 10^2 m from the South Pole and has been operating since 1987. It is essentially a scaled-down version of the array at Haverah Park and consists of 24 1 m^2 scintillators arranged 30 m apart in a series of interlocking hexagons. An excess of showers at the 5σ level has been found with this instrument using the data collected during a period of four months in the southern winter of 1987. See Hillas (1990). The 3^o x 3^o region of sky in which this excess is observed includes the Be X-ray binary 4U1145-619 and the high-mass X-ray binary 1E1145-614.

The highest energies for which a claim has been made for emission from a point source are in excess of E ~ 5 x 10^{17} eV. Cassiday *et al.* (1989) report evidence for an excess of showers observed with the Fly's Eye facility (Utah) in the direction of

Cygnus X-3. (The claim has also been discussed by Kazanas (1989) within the context of the detections of Cygnus X-3 at PeV and TeV energies). This experiment uses the Earth's atmosphere itself as a scintillator and maps the nitrogen fluorescence stimulated by air showers. It is not known if the primaries are γ-rays; it is possible that they are neutrons which, at these highly relativistic energies, would suffer little attenuation by spontaneous decay over the ~ 11 kpc journey from Cygnus X-3. Evidence for an excess of particle showers in the direction of Cygnus X-3 at $E > 5 \times 10^{17}$ eV has also been claimed recently by Teshima *et al.* (1990) following analysis of data obtained with the Akeno 20 km^2 array in Japan. If the results of these two experiments are confirmed by subsequent observations, then they will have provided the first direct evidence for EeV cosmic ray acceleration within the Galaxy.

1.3 Gamma-Ray Production and Loss Processes

1.3.1 Introduction

Continuum emission and absorption processes will be outlined quickly here. Useful reference sources are Harwit (1973), Tucker (1975), Rybicki and Lightman (1979), Lang (1986), and Katz (1987). γ-ray lines arising from e^-e^+ annihilation, neutron capture reactions, and de-excitation of nuclei are outside the scope of this work; details of γ-ray line astronomy can be found

in Hillier (1984) and Ramana Murthy and Wolfendale (1986).

Continuum radiation mechanisms - thermal, bremsstrahlung, magnetobremsstrahlung, curvature, inverse Compton, and spontaneous neutral pion decay - are illustrated schematically in Figure 1.2. These processes are each described briefly in Section 1.3.2. Losses due to photon-matter and photon-photon interactions are considered in Section 1.3.3. It will be seen that the emission of γ-rays with energies in excess of E ~ 1 TeV in stellar environments is usually considered to require the presence of highly relativistic particles. The mechanisms which have been proposed for particle acceleration to ultrahigh energies are outlined in Section 1.3.4.

1.3.2 Continuum Radiation Processes

i) Thermal Radiation

The photon energy (E_{max}) at the peak of the radiation spectrum of a blackbody at temperature T is determined by differentiating the Planck formula with respect to frequency. This just gives the Wien displacement law,

$$E_{max}\ (\mathrm{MeV}) \approx 5 \times 10^{-10}\ T(\mathrm{K}) \qquad (1)$$

Blackbody temperatures in excess of $T \sim 10^{10}$ K are therefore required in order to obtain appreciable production of γ-rays

Figure 1.2

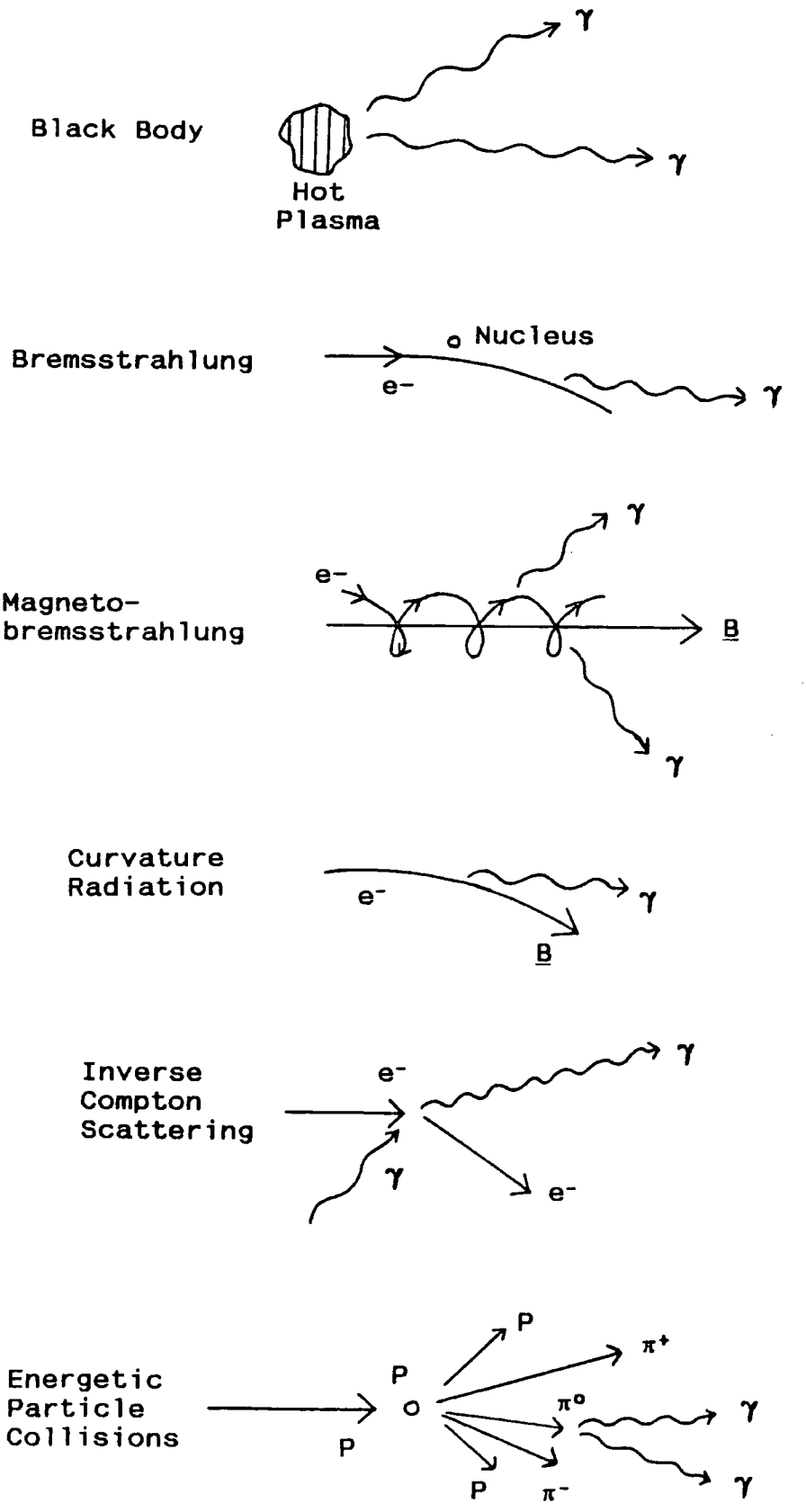

Continuum Radiation Processes

above an energy ~ 1 MeV. Such temperatures are reached only in highly energetic explosive phenomena such as a supernova core bounce; significant blackbody emission at TeV energies needs a value of T ~ 10^{16} K, which is unknown outside the hot Big Bang models of the early universe.

ii) <u>Bremsstrahlung Radiation</u>

The total energy radiated per unit time in all directions by a particle of charge q experiencing an acceleration $\dot{v}$ is given by

$$\frac{dW}{dt} = \frac{2}{3}\frac{q^2}{c^3}\dot{v}^2 \qquad (2)$$

with all quantities in c.g.s units. See Lang (1986). A factor of γ^6 is introduced on the right-hand side of this equation when the velocity is large, where $\gamma = \sqrt{[1-(v/c)^2]}$. Such radiation is called bremsstrahlung when a charge enters the Coulomb field of a second charge, magnetobremsstrahlung when it spirals about a magnetic field line, curvature when the particle is constrained to travel along a magnetic field line which is itself curved, and inverse Compton when it interacts with the electromagnetic field of a photon.

For a non-relativistic electron of instantaneous speed v encountering the Coulomb field of a charge Ze, the total bremsstralung energy radiated in all directions in the frequency

interval ν to ν+dν is given by

$$W(\nu)d\nu \quad \alpha \quad \left[\frac{Z}{\nu b}\right]^2 d\nu \qquad (3)$$

where b is the impact parameter, or the perpendicular distance from the target charge to the original path of the electron. The radiation spectrum of a single electron is flat up to the critical frequency $\nu_c \approx \nu/b$ where it falls off rapidly to zero. For astrophysical applications the spectrum of bremsstrahlung radiation from a thermal plasma is usually required. The energy emitted per unit volume per unit time is

$$j(\nu) \quad \alpha \quad Z^2 N_e N_i (1/T^{1}/_{2}) \exp(-h\nu/kT) \qquad (4)$$

(See Tucker 1975). N_e is the number density of electrons, N_i that of ions of charge Ze, and T is temperature. So, the theremal bremsstrahlung spectrum is also flat at low frequencies, and falls off exponentially at high frequencies. A bremsstrahlung spectrum has been fitted, for example, to optical and X-ray measurements of the low-mass X-ray binary Sco X-1 for $N_e \sim 10^{16}$ cm^{-3} and $T \sim 10^8$ K; X-rays from the Coma Cluster of galaxies have been fitted using $N_e \sim 10^{-3}$ cm^{-3} and $T \sim 10^8$ K (Tucker 1975 and references therein).

iii) Magnetobremsstrahlung Radiation

A non-relativistic charge q moving with velocity $\underline{v}$ in a uniform magnetic field $\underline{B}$ experiences the Lorentz force $\underline{F}$,

$$\underline{F} = \frac{q}{c}(\underline{v} \times \underline{B}) \qquad (5)$$

The charge therefore moves in a helix about the direction of the magnetic field. The acceleration of the charge causes it to radiate; this magnetobremsstrahlung radiation is known as cyclotron radiation when the speed of the charge is non-relativistic and synchrotron radiation in the relativistic case. The cyclotron frequency (ω) is easily determined using equation 5:

$$mr\omega^2 = mv\omega = \frac{q}{c} vB_p$$

$$\omega = \frac{qB_p}{mc} \qquad (6)$$

where m is the charge mass and B_p is the component of the magnetic field perpendicular to the velocity of the charge. Equations 2 and 5 provide the total power radiated by the charge through cyclotron radiation:

$$\frac{dW}{dt} = \frac{2}{3}\frac{q^4 B_p{}^2 v^2}{m^2 c^3} \qquad (7)$$

This emission occurs predominantly at photon frequencies near to the cyclotron frequency, which is directly proportional to the magnetic field strength (equation 6). Note the mass dependence in equation 7: for a given speed, v, cyclotron radiation is far more important for electrons than for protons.

In the rest frame of the observer, electrons at relativistic energies are no longer seen to radiate isotropically; instead, the emission - synchrotron radiation - is tightly beamed along the instantaneous direction of motion of the electron. (The angular width of the beam is $\theta \sim \gamma^{-1}$). The observer therefore witnesses bursts of emission as the electron spirals about the magnetic field line. For photon frequencies in Hz, field strengths (B) in Gauss, and electron energies (E_e) in MeV, the spectrum of the synchrotron radiation peaks at a frequency

$$\nu \sim 10^6 B E_e{}^2 \qquad (8)$$

See Hillier (1984). A 1 MeV synchrotron γ-ray ($\nu \sim 10^{20}$ Hz) therefore requires the product $BE_e{}^2$ to be $\sim 10^{14}$. Thus only very energetic electrons moving in strong magnetic fields will emit synchrotron radiation at γ-ray frequencies. The importance of synchrotron radiation to γ-ray astronomy is that when it is

observed in lower energy regions of the electromagnetic spectrum it indicates the presence of relativistic electrons which may produce γ-rays through other processes such as bremsstrahlung emission or inverse Compton scattering.

iv) Curvature Radiation

Consider high energy electrons emerging from the polar caps of a neutron star: these are constrained to move along the field lines of the exceptionally strong pulsar magnetosphere. Any motion of the electrons transverse to the field lines is very quickly damped by synchrotron radiation. Since the field lines are curved, the particles are accelerated and, from the point of view of the observer's rest frame, emit radiation along their direction of motion. The spectrum of curvature radiation is similar to that of bremsstrahlung and the energies of the radiated photons extend as high as those of the electrons. The characteristic photon energy (E_c) is given by

$$E_c\,(eV) \approx \frac{3hc\gamma^3}{4\pi r_c} = \frac{3 \times 10^{-5}\ \gamma^3}{r_c\,(cm)} \qquad (9)$$

(Ramana Murthy and Wolfendale (1986) and references therein) where r_c is the radius of curvature of the magnetic field line. Substituting $E_e/m_e c^2$ for γ and adopting a typical value of r_c -

10^8 cm ($\approx 10^2$ neutron star radii), equation 9 predicts that an electron with total energy ~ 50 TeV would be required to produce curvature γ-rays at the 250 GeV threshold energy of the Durham University Mark III γ-ray telescope. Usov (1983) predicts the emission of high-energy γ-rays from millisecond radio pulsars via curvature radiation; Cohen and Mustafa (1986) adopt this process to propose an explanation for the observations of TeV and PeV γ-rays from Hercules X-1.

v) <u>Inverse Compton Scattering</u>

In the collision of a fast electron of total energy $E_e = \gamma m_o c^2$ with a low energy photon of energy $E_{ph} = h\nu$, the energy, E_c, of the Compton boosted photon is given by

$$E_c = \frac{4}{3} \gamma^2 E_{ph} \qquad \gamma h\nu << m_o c^2 \qquad (10a)$$

and

$$E_c \sim E_e \qquad \gamma h\nu >> m_o c^2 \qquad (10b)$$

See Rybicki and Lightman (1979) and Lang (1986). This process can be important for γ-ray production; for instance, an optical starlight photon (E_{ph} ~ 2 eV << $m_o c^2$) will be scattered to an energy ~ 40 MeV by a 10^{13} eV electron.

vi) Neutral Pion Decay

Neutral pions can be created in collisions between high-energy nucleons and in the annihilation of nucleons with antinucleons; in the case of a collision between two protons, the simplest interaction which involves pion production is

$$p + p \longrightarrow p + p + \pi^0$$

Other important pion-producing reactions include

$$p + p \longrightarrow p + p + n_1(\pi^+ + \pi^-) + n_2\pi^0$$

$$p + p \longrightarrow p + n + \pi^+ + n_3(\pi^+ + \pi^-) + n_4\pi^0$$

$$p + p \longrightarrow n + n + 2\pi^+ + n_5(\pi^+ + \pi^-) + n_6\pi^0$$

$$p + p \longrightarrow D + \pi^+ + n_7(\pi^+ + \pi^-) + n_8\pi^0$$

where n_1 to n_8 are positive integers.

The neutral pion is an unstable particle and decays after a rest frame mean life $t \sim 10^{-16}$ s (or γt for an observer's frame in which the pion has total energy $\gamma m_0 c^2$), normally into a pair of γ-rays:

$$\pi_0 \longrightarrow h\nu + h\nu$$

Other pion decay modes (with total branching fraction ~ 1 %) are

$$\pi^o \longrightarrow h\nu + e^+ + e^-$$
$$\pi^o \longrightarrow 2e^+ + 2e^-$$
$$\pi^o \longrightarrow h\nu + h\nu + h\nu$$

Thus when the pion decays at rest (with mass m_o) to two photons, the energy of each γ-ray is $0.5m_oc^2$, or approximately 67 MeV. Much higher energy γ-rays are possible when the kinetic energies of the colliding protons greatly exceed the thresold energy required for neutral pion production.

Table 1.2 summarises the conditions required for continuum γ-ray production via the six processes outlined here. Entries are made for the generation of γ-rays at energies of 1 MeV, 1 GeV, and 1 TeV. (Extended from a table published by Ramana Murthy and Wolfendale 1986).

1.3.3 γ-Ray Loss Processes

i) Photon-Matter Interactions

It has already been mentioned that absorption of γ-rays is insignificant above photon energies ~ 1 MeV, after which e^-e^+ pair production in the Coloumb field of a nucleus is the principal process of interaction with matter. At TeV energies

Table 1.2

Mechanism	$E(\gamma)$ = 1 MeV	$E(\gamma)$ = 1 GeV	$E(\gamma)$ = 1 TeV
1) Black Body	T ~ 10^{10} K	T ~ 10^{13} K	T ~ 10^{16} K
2) Bremsstrahlung	$E(e^-) \geq$ 2 MeV	$\geq$ 2 GeV	$\geq$ 2 TeV
3) Synchrotron			
a)	B = 1 G $E(e^-)$ ~ 10^{13} eV	~ 10^{14} eV	~ 10^{16} eV
b)	B = 10^4 G $E(e^-)$ ~ 10^{11} eV	~ 10^{12} eV	~ 10^{14} eV
4) Curvature ($r = 10^8$ cm)	$E(e^-)$ ~ 10^{12} eV	~ 10^{13} eV	~ 10^{14} eV
5) Inverse Compton			
a) Against 2.7 K Cosmic Background (E_{ph} ~ 10^{-3} eV)	$E(e^-)$ ~ 10^{10} eV	~ 10^{12} eV	~ 10^{13} eV
b) Against optical starlight (E_{ph} ~ 1 eV)	$E(e^-)$ ~ 10^8 eV	~ 10^{10} eV	~ 10^{12} eV
c) Against X-rays (E_{ph} ~ 10^4 eV)	$E(e^-)$ ~ 10^6 eV	~ 10^9 eV	~ 10^{12} eV
6) P-P Collisions —> π^o —> 2γ		$E(P) \geq 10^{10}$ eV	$\geq 10^{13}$ eV

Parameters for Continuum γ-Ray Emission
(Listed for three γ-ray energies)

Adapted from Ramana Murthy & Wolfendale (1986)

the radiation length for pair production - defined as the penetration depth in a medium after which the incident γ-ray flux has been depleted by a factor of $^1/_e$ - corresponds to a column density ~ 40 g cm^{-2}; the Earth's atmosphere offers ~ 30 radiation lengths at vertical incidence and is therefore an efficient absorber. The radiation length is often exceeded in the environments of accreting neutron stars in X-ray binary systems, thereby placing constraints on the location of regions of observable TeV γ-ray emission.

ii) <u>Photon-Photon Interactions</u>

A γ-ray of energy E_1 meeting a second photon of energy E_2 will give rise to a particle pair, each of mass m, if the γ-ray energy exceeds a threshold value given by

$$E_1 > E_t = \frac{2m^2c^4}{E_2(1-\cos\theta)} \qquad (11)$$

where θ is the angle formed by the two photon trajectories prior to interaction. (See Ramana Murthy and Wolfendale 1986). If attention is restricted to the formation of e^-e^+ pairs in head-on collisions, then the threshold energy is just $E_t(eV) \approx 0.26 \times 10^{12}/E_2$. Thus for the 2.7 K background ($E_2 \approx 6 \times 10^{-4}$ eV), γ-rays at energies in excess of $E_t \sim 4 \times 10^{14}$ eV can pair produce. For optical starlight the threshold is at a value ~ 10^{11} eV, while for X-rays the γ-rays must exceed $E_t \sim 3 \times 10^8$ eV. Away

from compact luminous sources, photon-photon collisions are infrequent at most γ-ray energies, since the spatial density of target photons in astronomical environments is usually very small. Figure 1.3 shows the mean-free-path for γ-rays, as a function of energy, before being lost to e^-e^+ pair production on the various background radiation fields, which include optical and infrared starlight, the microwave background, and radio waves. Note that the claims for the detection of PeV γ-rays from Cygnus X-3 ($d \sim 11$ kpc $\approx 10^{23}$ cm) noted earlier demand an upward revision of the values of the mean-free-paths plotted in the vicinity of this energy in Figure 1.3. At γ-ray energies $\leq$ 1 TeV, the universe is essentially transparent out to distances comparable with the Hubble radius.

iii) <u>e^-e^+ Pair Production in Strong Magnetic Fields</u>

Electron-positron pair production occurs via the interaction of photons with high <u>B</u>-field energy densities, such as those found in the magnetospheres of pulsars. If B_t is the strength of the field component transverse to the direction of the γ-ray, the photon energy threshold for pair production is given by

$$E_t(\text{eV}) \approx 4 \times 10^{18}/B_t(\text{G}) \qquad (12)$$

See Manchester and Taylor (1977). Field strengths near the surfaces of neutron stars have been measured at values $\sim 10^{12}$ G (Nagase 1989 and references therein), for which γ-rays in excess

Figure 1.3

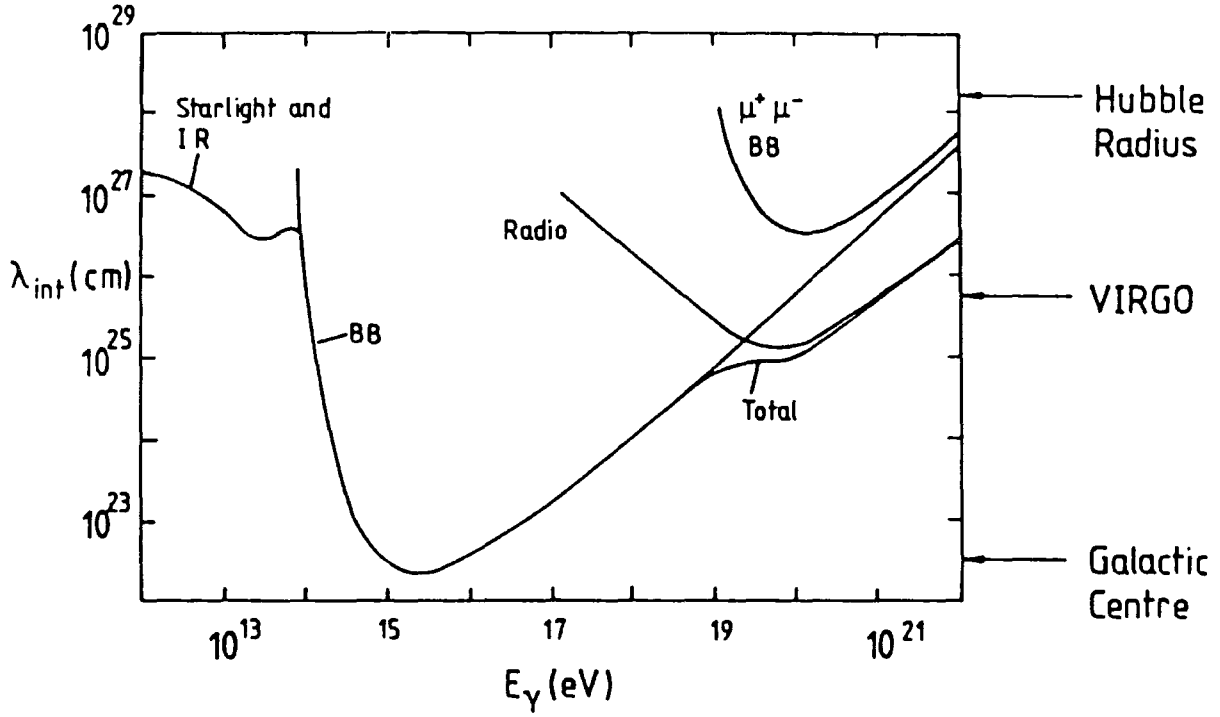

Mean free paths of γ-rays on the various background radiation fields as a function of γ-ray energy.

(From Ramana Murthy & Wolfendale 1986)

Unless otherwise indicated, the attenuation process is e^-,e^+ production.

BB: 2.7 K cosmic background black body radiation (energy density $\approx$ 0.24 eV cm^{-3} $\approx$ 400 photons cm^{-3})

Virgo: galaxy cluster at centre of local super-cluster

of E ~ 4 MeV would be absorbed. Of interest to the present thesis is the distance ($r-r_N$) from the neutron star surface at which the threshold energy rises to 1 TeV: taking the value of the magnetic dipole moment $B(r)r^3$ to be constant and adopting a value for the neutron star radius $r_N = 10^4$ m then, with equation 12 supplying E_t = 1 TeV for $B_t(r) = 10^{12}(r/r_N)^3 = 4 \times 10^6$ G, r has a value $\approx 60r_N$. The TeV γ-rays observed from X-ray binaries containing such highly magnetised neutron stars must therefore be produced at considerable distances from the X-ray emission regions, which are located at the bases of the accretion columns at the magnetic polar caps.

1.3.4 Ultrahigh Energy Particle Acceleration

All current models of the observed TeV and PeV γ-ray emission from astronomical sources invoke the acceleration of particles to ultrarelativistic energies. For the isolated pulsar sources, high-energy photons are then thought to be emitted either by inverse Compton scattering or curvature radiation. See for example Usov (1983), Cheng, Ho and Ruderman (1986a,b) and Cohen and Mustafa (1987). For the X-ray binary systems, it is usually suggested that the particle acceleration is followed by the interaction of the particle beams with material in the environment of the neutron star or at the limb of the companion, followed by the decay of neutral pions to high-energy γ-rays. References to models of this type are given in Chapter 11 of the present work.

Four particle acceleration mechanisms have been studied, all of which use accretion energy or the neutron star rotation energy as the power source. These are the dynamo mechanism, shock acceleration, magnetic reconnection, and plasma turbulence. Each of these acceleration processes will be outlined very briefly here, with particular reference to the accreting binary systems. For further details and references to the literature, recent sources include Katz and Smith (1988), Kazanas (1988), Nagle, Gaisser and Protheroe (1988), Harding (1989, 1990), and Harding and Gaisser (1990).

i) Disk Dynamo Mechanism

In this mechanism, the rotation of a pulsar magnetosphere induces large-scale $\underline{v} \times \underline{B}$ electric fields within a highly conducting, differentially rotating accretion disk; if v(r) is the Keplerian velocity at radial distance r and B(r) is the magnetic field strength then the electric potential over a small distance Δr is just

$$\frac{\Delta V}{\Delta r} \approx \frac{F}{e} = \frac{1}{c} |\underline{v} \times \underline{B}| \qquad (13)$$

so that the particle energy (E) accessible with this mechanism is

$$E \approx \frac{e\Delta r}{c} |\underline{v} \times \underline{B}| \qquad (14)$$

A serious problem with the dynamo model is that, in the presence of a disk plasma which is free to move along the field lines but not across them (since the Larmor radius is very small in the strong pulsar fields) the field lines are equipotentials; the potential drop is developed only normal to the magnetic field and so the particles cannot be accelerated. The potential in equation 13 is fully realizable only in a vacuum; within the disk only a very small fraction can go to acceleration.

ii) Shock Acceleration

Fermi acceleration in shocks has been proposed for the acceleration of charged particles to high energies in, e.g. supernovae, stellar winds from hot stars, pulsar winds in supernova remnants, and pulsar winds in X-ray binaries containing a rapidly spinning, non-accreting neutron star. Shock acceleration in such environments has been reviewed by Quenby (1986). See also Harding (1989, 1990), Harding and Gaisser (1990), and references therein. The idea is that particles can travel back and forth across a shock front by scattering from magnetic irregularities, gaining some energy during each traversal. Kazanas and Ellison (1986) have proposed shock acceleration in the accretion flow in Cygnus X-3. Harding and

Gaisser (1990) have considered a shock front at the interface between a pulsar wind and a companion star wind, where the ram (inertia) pressures of the two winds balance. (Alternatively, in the absence of a companion star wind, the pulsar wind could interact with the atmosphere or the magnetosphere of the companion, where the pulsar wind pressure is then balanced by the gas or magnetic pressures). The acceleration of protons in such shocks could produce observable high-energy γ-rays through interactions with the companion star wind or the atmosphere.

iii) Magnetic Reconnection

Differential Keplerian rotation in an accretion disk, together with uneven accretion rates, can stress the pulsar magnetic field lines threading the disk plasma. Wang (1986) has suggested that sporadic high-energy γ-ray emission in X-ray binaries may occur when this stress is released during episodes of reconnection of the tangled field lines in neutral sheets within the disk, along which high induced electric potential drops may be established. Particles could then be accelerated along these voltage drops.

iv) Plasma Turbulence

Katz and Smith (1988) have employed plasma turbulence to model proton acceleration in accreting binaries. If a magnetic field is present in a turbulent plasma, then the induced electric fields will be randomly oriented. Particles can then be

accelerated or decelerated by these fields but, since a particle will experience a greater number of head-on 'collisions' with voltage drops than it will with receding ones, the net result is that it gains more kinetic energy than it loses.

Table 1.3 is adapted from one published by Harding (1989) and is a summary of the acceleration models mentioned here. Included are the values estimated by Harding for the maximum proton energies (E_p^{max}) available with each of these mechanisms. Note the similarity of the four expressions for E_p^{max}, which is a consequence of the fact that charged particles are most efficiently accelerated by electric fields which, in astrophysical sources, arise readily through induction by moving magnetic fields.

Table 1.3

Acceleration Mechanism	Power Source: Pulsar rotation	Power Source: Mass accretion by transfer from companion star
	L_{max} ~ 10^{43} ergs/s	L_{max} ~ 10^{38} ergs/s
1) Dynamo	$E^{max}_p \approx e \frac{\underline{v} \times \underline{B}}{c} \Delta r$	
	$< 10^{14}$ eV	$< 10^{16}$ eV
2) Shock	$E^{max}_p \approx e \frac{u_1}{c} B r_s$	
	u_1 = fluid speed into shock	
	r_s = shock radius	
	$E^{max}_p < 10^{18}$ eV	$< 10^{16}$ eV
3) Magnetic Reconnection		$E^{max}_p < e \frac{v_f}{c} B \Delta r$
		v_f = maximum rate of $\underline{B}$-field line flow into reconnection region
		$E^{max}_p < 10^{14}$ eV
4) Plasma Turbulence		$E^{max}_p \approx eB\Delta r < 10^{16}$ eV

Maximum Proton Energies Predicted for Acceleration Near Pulsars

(Adapted from Harding 1989)

Chapter 2

The Air Cerenkov Technique for the Detection of TeV γ-Rays

2.1 Introduction

The steepness of the high energy photon spectra typical of point sources means that the fluxes of γ-rays with energies above E ~ 10 GeV arriving at the Earth are very low. The weakness of the fluxes means that observations from satellites are not practicable at this time: the only method currently available for the observation of TeV γ-rays is to sample the optical Cerenkov light which arrives at ground level from photon-induced particle cascades in the Earth's atmosphere. Consider the high-mass X-ray binary SMC X-1 as an example. This binary was monitored with the Durham Group's ground-based air Cerenkov observatory (Australia) for a total $\approx$ 30 hr from 1987 July 21 to 31, during which ~ 3 x 10^4 Cerenkov events were registered. Evidence has been found for a periodic component in the Cerenkov arrival time series with a strength which is $\approx$ 3 % of the cosmic ray background. With an effective collecting area for the telescope ~ 10^4 m^2, this corresponds to an average flux of γ-rays from SMC X-1 ~ 30 m^{-2} yr^{-1} (E > 0.4 TeV). Such a flux of photons is, for example, only ~ 0.25 % of the typical source flux measured at E > 10^2 MeV with the COS-B satellite (Ramana

Murthy and Wolfendale 1986). The direct observation of TeV γ-rays from space-borne platforms would therefore require instruments with prohibitively large collecting areas operated for very long intervals of time.

The ground-based technique does in fact have a number of advantages: the detection medium (the atmosphere) has zero cost, a huge effective collecting area is provided by the size of the Cerenkov light pool at ground level, and the contemporary instrumentation required to detect the Cerenkov light is comparatively simple and has low running costs.

The aim of the present chapter is to make a concise sketch of the air Cerenkov method in order to provide the experimental background to the period analysis of Cerenkov arrival time series considered later. Further details of the method are given by Jelley (1967), Ramana Murthy and Wolfendale (1986), and Weekes (1988).

Air showers generated by γ-rays and cosmic rays are described in Section 2.2 of the present chapter. Section 2.3 provides an account of the geometry and energetics of the Cerenkov emission process. Properties of the Cerenkov light component in air showers are considered in Section 2.4. Section 2.5 is concerned with the basic design requirements of ground-based TeV γ-ray telescopes. The experimental techniques employed for the enhancement of signal-to-noise - geometrical discrimination, Cerenkov imaging and pulse shape discrimination - are considered

in Section 2.6. Section 2.7 provides details of the various TeV γ-ray observatories currently operating worldwide.

2.2 Air Showers

(i) γ-Ray Air Showers

Photons of energy greater than E ~ 1 MeV produce an electron-positron pair upon interacting with the electromagnetic field of an atomic nucleus. At γ-ray energies ~ 1 TeV, a flux of photons is depleted by a factor of $^1/_e$ to pair production upon passing through a medium of column density $\approx$ 38 g cm^{-2} ($\equiv$ one 'radiation length'). The Earth's atmosphere has a column density $\approx$ 1030 g cm^{-2} ($\approx$ 27 radiation lengths) at mean sea level, so that a primary TeV γ-ray is almost immediately absorbed. The creation of a very energetic e^--e^+ pair high in the atmosphere initiates a cascade of bremsstrahlung photon emission and e^--e^+ pair production, which is represented by a flow-chart loop in Figure 2.1; during each circuit of the loop, the number of bremsstrahlung photons and e^--e^+ pairs grows exponentially, and the energy of the primary γ-ray is divided correspondingly. Bremsstrahlung emission of γ-rays is the leading $e^{-/+}$ energy loss process at energies greater than E ~ 80 MeV. Other loss mechanisms include optical Cerenkov emission (when E > 21 MeV in air: see below) and the much weaker fluorescence emission which is produced from the excitation of atmospheric nitrogen and oxygen. Ionization becomes the dominant loss process at particle

Figure 2.1

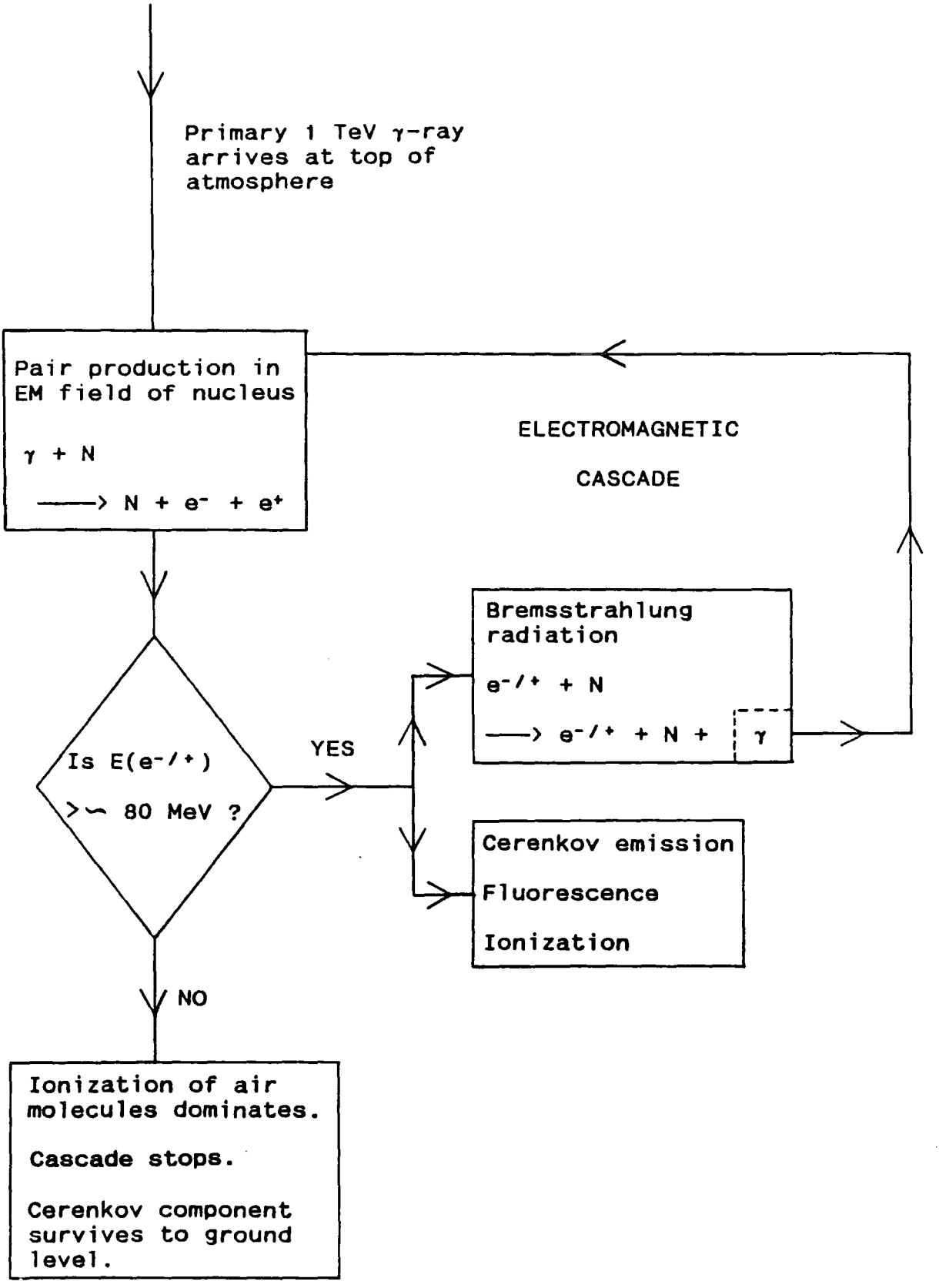

Air Shower Initiated by 1 TeV γ-Ray

energies less than E ~ 80 MeV: by this stage the photon/pair-production loop has therefore reached a maximum, after which the development of the cascade is terminated abruptly.

The altitude at which a shower maximises can be calculated approximately in the following way. Let the energy at which ionization and bremsstrahlung losses become comparable be E_{crit}. The radiation lengths for pair production and bremmsstrahlung emission are approximately equal so that the number of electrons, positrons and bremsstrahlung photons developed after n radiation lengths is just ~ 2^n. If E_o is the energy of the primary γ-ray then the total number of radiation lengths (N) traversed down to the altitude of shower maximium is

$$2^N \approx \frac{E_o}{E_{crit}} \qquad (1)$$

So, with ln 2 ≈ 1,

$$N \approx \ln (E_o/E_{crit}) \qquad (2)$$

By this simple picture, approximately 10^4 particles and bremsstrahlung photons are generated following the arrival of a primary γ-ray of energy 1 TeV. The column density (σ) over a distance Δy in a material of mass density $\rho(y)$ is

$$\sigma = \int_{y}^{y+\Delta y} \rho(y)dy \qquad (3)$$

The density of the atmosphere falls off exponentially with altitude, so that the number of radiation lengths traversed down to shower maximum is

$$N \approx \frac{-1}{L} \int_{oo}^{y_{max}} \rho_o \exp(-y/h_o)\, dy \qquad (4)$$

where L is one radiation length (= 38 g cm^{-2}), y_{max} is the altitude of the shower maximum, ρ_o is the density of air at mean sea level, and h_o is the scale height (≈ 8 km) of the atmosphere. Substituting for N from equation 2 into 4 and performing the integration,

$$y_{max} = -h_o \ln \left[\frac{L \ln(E_o/E_{crit})}{\rho_o h_o} \right] \qquad (5)$$

It can be seen that there is a logarithmic dependence of the value of y_{max} upon the energy of the primary. With $\rho_o h_o \approx 1030$ g cm^{-2} (equation 3) and E_o = 1 TeV, the cascade is found to peak at an altitude $y_{max} \approx 8$ km.

Alhough the electrons and positrons are quickly absorbed in the atmosphere after shower maximum, the Cerenkov component of the shower survives to ground level since the atmosphere is transparent at optical photon energies. This penetrating component is easily detectable with contemporary instrumentation.

(ii) <u>Cosmic Ray Air Showers</u>

If air showers were induced only by high-energy γ-rays then the identification of astronomical sources would be quite straightforward. However, TeV γ-ray astronomy has a very serious noise problem due to the random background of high energy cosmic ray charged particles arriving isotropically at the Earth. Consider first the electron component of the cosmic rays: high energy electrons arrive at the Earth with a flux that is comparable with the typical γ-ray flux from a discrete source. Air showers arising from cosmic ray electrons and γ-rays are indistinguishable, for the loop in Figure 2.1 can be initiated simply by bremsstrahlung emission from a primary electron in the Coulomb field of a nucleus. Worse still, electrons are only a minor component of the cosmic ray population. They are much less massive than protons and so radiate most of their energy in the

weak Galactic magnetic fields. Cosmic ray protons and heavier nuclei arriving at the Earth outnumber the electrons by a factor ~ 100 at E > 1 GeV (e.g. Meyer 1975). The cosmic ray primary energy spectrum is shown in Figure 2.2. The integral spectral index steepens from ≈ -1.6 to ≈ -1.8 at E ~ 10^{15} eV. The origin of this "knee" is unknown: it may indicate different production mechanisms in the two energy regimes, or it may be that cosmic rays at the higher energies can escape more easily from the Galaxy. The spectrum changes again at the highest energies, starting at the "ankle" at E ~ 10^{19} eV. This portion of the spectrum may have an extragalactic origin.

Protons are the major component of cosmic rays at TeV energies and make by far the largest contribution to the background in TeV γ-ray observations. At proton energies ~ 1 TeV the radiation length in matter is ~ 80 g cm^{-2}, or approximately twice that of a γ-ray of equal energy. In the proton air shower cascades, the primary collides with a target nucleus high in the atmosphere, leading to the production of multiple pions (with ~ 50 % of the primary proton energy) and secondary nucleons. The primary proton can survive the first interaction and continue on to further collisions; similarly, the secondary nucleons go on to additional collisions and pion production.

For high energy primaries, the energy which goes to pion production is shared approximately equally by the three charge species (π^-, π^o, π^+). The charged pions may decay (rest frame half-life ~ 10^{-8} s), giving rise to muons, electrons, neutrinos,

Figure 2.2

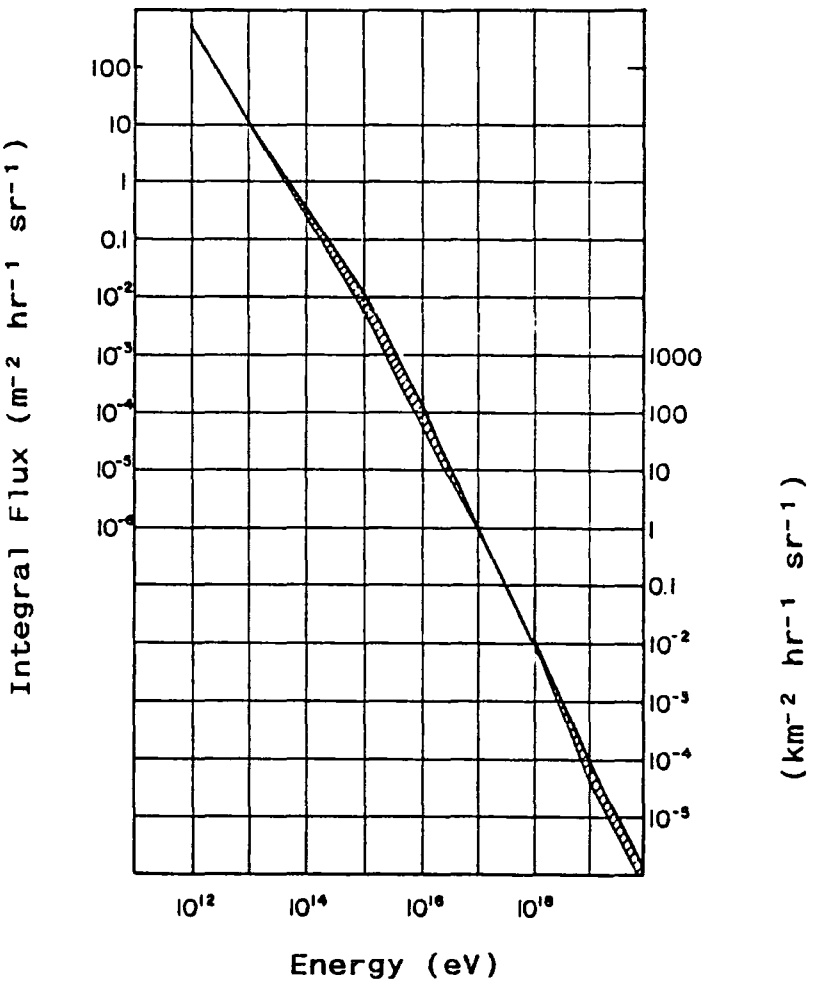

Spectrum of primary cosmic rays at top of atmosphere. The cross-hatching represents experimental uncertainties.

(From Gaisser 1982)

and the corresponding antiparticles. If ( ) denotes the type of neutrino (i.e. muon or electron) then the principal charged pion decays are:

$$\pi^{+/-} \longrightarrow \mu^{+/-} + \nu(\mu)/\bar{\nu}(\mu) \quad (\sim 100\ \%\ \text{of decays})$$

$$\pi^{+/-} \longrightarrow e^{+/-} + \gamma + \nu(e)/\bar{\nu}(e) \quad (\sim 3\ \%)$$

$$\pi^{+/-} \longrightarrow e^{+/-} + \nu(e)/\nu(\bar{e}) \quad (\sim 1\ \%)$$

$$\pi^{+/-} \longrightarrow \mu^{+/-} + \gamma + \nu(\mu)/\bar{\nu}(\mu) \quad (\sim 1\ \%)$$

The muon has a rest mass $\approx$ 200 times that of the electron, so it can travel through the atmosphere without radiating too much energy via bremsstrahlung interactions. The muon is unstable:

$$\mu^{+/-} \longrightarrow e^{+/-} + \nu(e)/\bar{\nu}(e) + \nu(\mu)/\bar{\nu}(\mu) \quad (\sim 100\ \%\ \text{of decays})$$

However, the rest frame half-life is relatively long ($\sim 10^{-6}$ s) so that the energetic muons can survive to ground level. As indicated in Chapter 1, detecting the muons is of great interest to PeV γ-ray astronomers since their presence in a shower may indicate that it was most likely initiated by a hadron.

Significant Cerenkov fluxes follow the almost immediate electromagnetic decay of the neutral pions to two γ-rays (rest frame half-life ~ 10^{-16} s):

$$\pi^{o} \longrightarrow \gamma + \gamma \quad (\sim 100\ \%\ \text{of decays})$$

$$\pi^{o} \longrightarrow \gamma + e^{+} + e^{-} \quad (\sim 1\ \%)$$

$$\pi^{o} \longrightarrow 2e^{+} + 2e^{-} \quad (\sim 1\ \%)$$

$$\pi^{o} \longrightarrow \gamma + \gamma + \gamma \quad (\sim 1\ \%)$$

The π^{o} decay γ-rays then act as catalysts for e^{-}-e^{+} pair production/bremsstrahlung cascade loops, which generate optical Cerenkov radiation. The multiplicity of the π^{o}'s means that the hadron air showers are multi-cored: the Cerenkov photon distributions are therefore considerably more irregular than for the γ-ray showers. Since up to ~ $^{1}/_{3}$ of the primary cosmic ray energy is converted to π^{o}'s, the hadron air showers produce up to $^{1}/_{3}$ as many Cerenkov photons as γ-ray showers of equivalent primary energy. The hadron shower Cerenkov component is therefore readily detectable at ground level: the challenge to TeV γ-ray astronomy is therefore to design telescopes which will maximise the signal-to-noise ratio and permit the identification of sources in the presence of this very strong background. Some recent successes have been achieved in discriminating between the two types of showers and these will be discussed after considering the general properties of Cerenkov radiation.

2.3 Cerenkov Radiation

Cerenkov (1934-1938) performed the first systematic experimental investigation of the optical continuum emission radiated in the direction of motion of fast electrons in transparent liquids and solids. In so doing, he confirmed the quantitative predictions of a classical theoretical treatment developed simultaneously by Vavilov (1934) and Tamm and Frank (1937), with respect to the total electron energy loss, the spectral distribution of the radiation, and the angle of emission. A simple outline of the geometry and the energetics of this phenomenon is presented here and is based on the work of Blackett (1948), Boley (1964) and Jelley (1968). See also Harwit (1973) and Lang (1986).

A charged particle passing swiftly with speed v through a dielectric appears to the atoms along its path as a rapidly time-varying electric field. Each atom responds by polarizing, which results in electromagnetic radiation from the transient induced dipole moment. The radiation from many path elements interferes destructively when $v \leq c_m$, the local speed of light in the dielectric, and is not observable at large distances from the particle track. Coherent emission can arise only when $v > c_m$; the Huygens construction in Figure 2.3 shows the geometry required for constructive interference. Since it is demanded that the particle should travel the distance AC in exactly the time (Δt) taken by radiation emitted at A to reach B then:

Figure 2.3

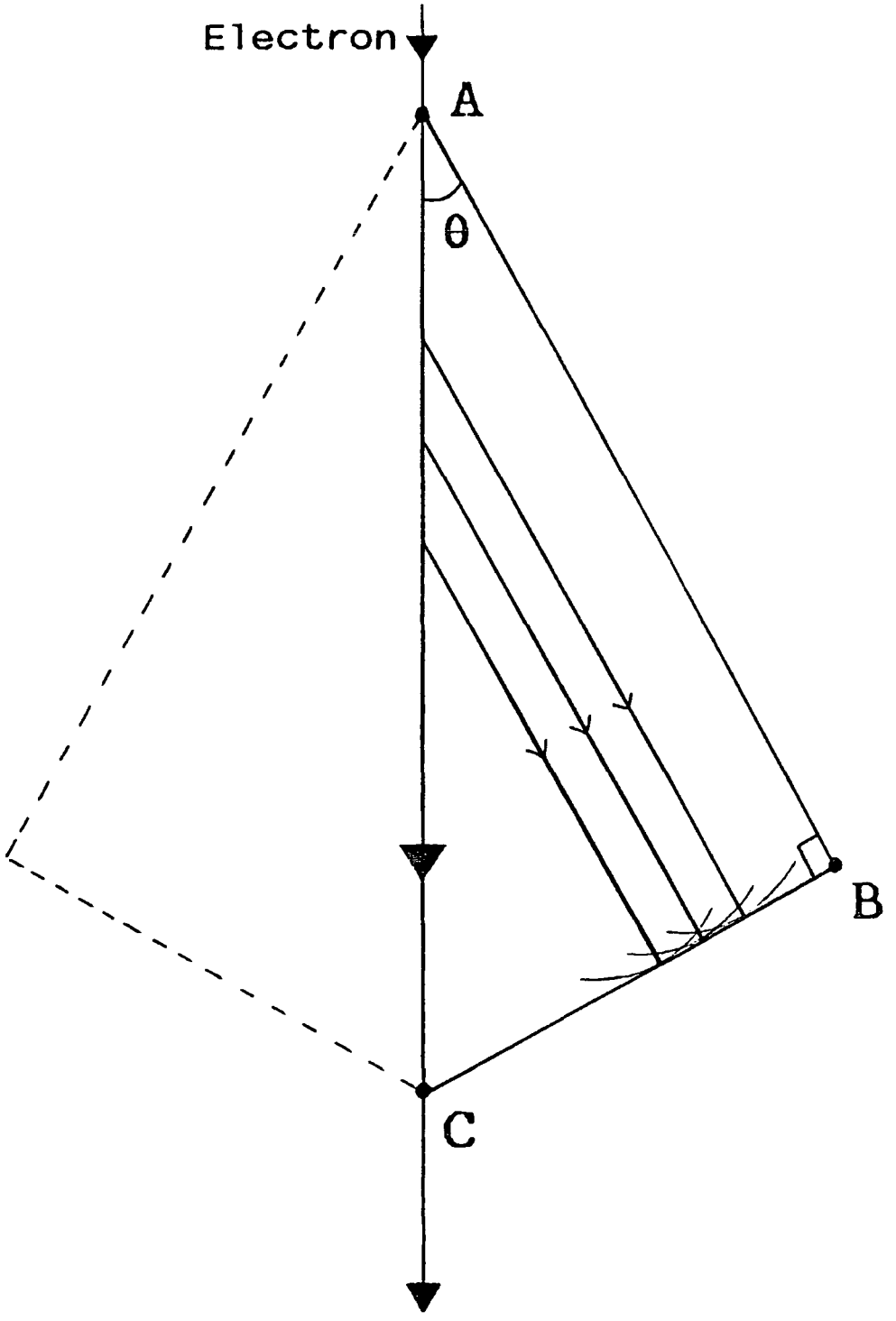

Cerenkov Emission Geometry

$$\Delta t = \frac{AC}{v} = \frac{AB}{c_m} \qquad (6)$$

Only radiation emitted at angle θ to the track of the particle will therefore be coherent:

$$\cos\theta = \frac{AB}{AC} = \frac{c_m}{v} = \frac{c}{nv} \qquad (7)$$

where n is the refractive index and c is the speed of light in vacuo. The emission angle is clearly not defined in the case $v < c_m$. Thus if $\beta \equiv v/c$,

$$\cos\theta = (\beta n)^{-1} \qquad (8)$$

The maximum angle of emission is then $\theta_{max} = \cos^{-1}(1/n)$ which, in the case of air at STP ($n = 1.000293$), gives $\theta_{max} \approx 1.4^{\circ}$. The wavefront has a shape which is approximately conical, since the geometrical requirements for constructive interference possess symmetry about the track of the particle.

The refractive index of any medium is less than unity for photons at X-ray energies and higher. With $\beta < 1$, equation 8 therefore shows that the radiation is limited to the radio,

infrared, optical and UV bands of the spectrum.

Equation 8 also supplies a value for the velocity threshold of the particle. No radiation will be observed when $\beta < 1/n$. The threshold energy of an electron travelling in air is then $E_{min} = m_o c^2 \gamma_{min} = E_o(1 - n^{-2})^{-1/2} \approx 21.1$ MeV. For muons, $E_{min} \approx 4.4$ GeV and for protons $E_{min} \approx 38.7$ GeV.

The rate at which energy (E) is radiated per unit distance along the track of a particle of charge Ze is (Tamm and Frank 1937):

$$\frac{dE}{dl} = \frac{Z^2 e^2}{c^2} \int \left[1 - (\beta n(\omega))^{-2} \right] \omega \, d\omega \qquad (9)$$

where E is in ergs, l is in cm, the charge e is in E.S.U., and ω is the angular frequency of the radiation in Hz. The spectrum of the radiation is therefore continuous. Notice also how this rate of energy loss by the particle is essentially independent of its speed, for $\beta \approx 1$ by the very nature of the Cerenkov effect. The value of the refractive index of air changes by less then 3 % across the visible spectrum from $\lambda \approx 400$ nm to 700 nm (i.e. dispersion is negligible), thus equation 9 gives for an electron travelling in air:

$$\left.\frac{dE}{dl}\right|_{visible} \approx -2 \times 10^{29} \frac{e^2}{c^2}\left[1 - (\beta n)^{-2}\right] \qquad (10)$$

$$\approx -8 \times 10^{-13} \text{ erg cm}^{-1} \quad (\beta \approx 1)$$

This corresponds to approximately 0.2 optical photons cm^{-1} along the track of the electron. By differentiating equation 9 with respect to frequency, the spectral intensity of the Cerenkov emission is seen to be simply proportional to photon frequency for low-dispersion media. The Cerenkov emission spectrum in air peaks at around 350 nm and the radiation is thus predominantly blue. Absorption by atmospheric ozone becomes increasingly important at shorter wavelengths: the linear spectrum breaks down shortly after the peak, and there is an absoprtion cut-off around λ = 280 nm.

2.4 Air Shower Cerenkov Radiation

Blackett (1948) was the first to point out that Cerenkov radiation should be generated by cosmic ray air showers, which were known to include electrons of energies in excess of the 21 MeV threshold. However, he calculated that such radiation should amount to just 0.01 % of the the total night sky optical background. Air shower experiments distinguish the Cerenkov emission from this strong background by using fast electronics to

exploit the very short duration (≈ 5 ns: see below) of a Cerenkov pulse. No other atmospheric or astrophysical processes are known which contribute to the background light on this timescale. Galbraith and Jelley (1953, 1955) were the first to succeed in detecting Cerenkov emission from cosmic ray air showers. They used a simple optical flux collector and a focal plane photomultiplier tube with a rise time matched to the anticipated duration of the pulses. The air Cerenkov technique was first applied - though without success - to the detection of TeV γ-rays by Chudakov *et al.* (1962).

(i) General Properties of a Shower

The refractive index of air decreases with increasing altitude (y) as

$$n(y) = 1 + R_o \exp(-y/h_o) \qquad (11)$$

where h_o is the scale height of the atmosphere, and the constant $R_o = 0.000293$. This equation for n(y) can be substituted directly into the expressions derived earlier for the electron energy threshold for Cerenkov radiation, the photon yield, and the Cerenkov opening angle, so that the variation of these quantities with altitude can be explored. See Figure 2.4. Much of the electromagnetic cascade occurs between altitudes of 16 and

Figure 2.4

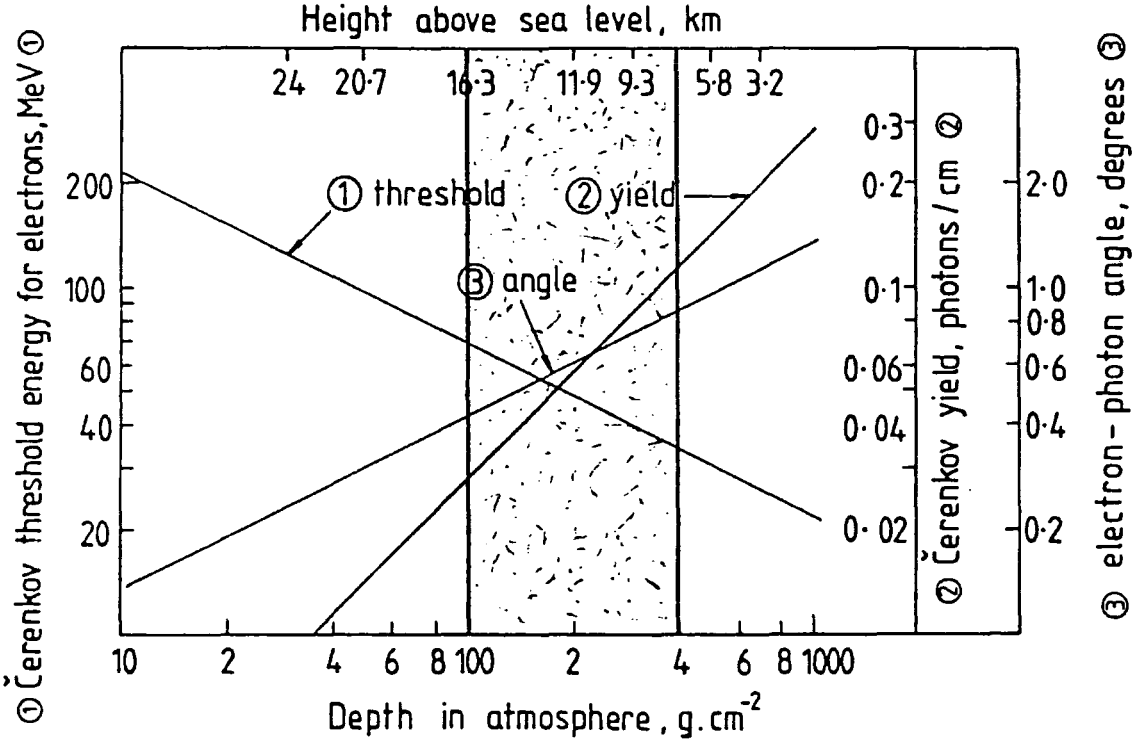

Variation with altitude in the atmosphere of

1) e^- threshold energy for Cerenkov emission

2) Cerenkov photon yield

3) Beaming angle

Dashed region is the most relevant to air showers

(From Ramana Murthy & Wolfendale 1986)

8 km (≡ 100 to 400 g cm^{-2} in the direction of shower development), where E_{th} decreases from ≈ 70 to 35 MeV, the yield increases from ≈ 0.04 to 0.1 photons cm^{-1} and the emission angle rises from ≈ 0°.4 to 0°.9.

(ii) <u>Dispersive Processes</u>

(a) The lateral development of a γ-ray air shower is largely determined by multiple Coulomb scattering of electrons and positrons in the electromagnetic fields of atmospheric nuclei. The root-mean-square scattering angle is inversely proportional to the energy (E) of a charged particle (e.g. Lang 1986). It has a value ≈ 1° at electron energies ~ 1 GeV and increases to ~ 10° at shower maximum.

(b) The deflection of air shower particles by the geomagnetic field may have a significant effect upon the distribution of Cerenkov light. Calculations by Browning and Turver (1977) for 0.1 TeV vertical showers indicate that the expected size of the Cerenkov light pool at ground level is ~10 % greater when the field is taken into account, with a consequent reduction in the average photon density.

(c) The effect of refraction of Cerenkov light in the air can be quantified roughly by letting a ray of light produced high in the atmosphere enter a dense, lower atmosphere characterised by a slab of air with n = 1.000293 throughout. If the actual and

refracted zenith angles* are Z and Z' respectively then, for small angles,

$$R = n - 1 = \frac{\sin Z}{\sin Z'} - 1 \approx \frac{\Delta Z}{Z'} \qquad (12)$$

Thus, $\Delta Z \sim RZ'$, which is $<< \theta$, the half-angle of Cerenkov emission. The difference in the zenith angles remains negligible at all values of Z. Refraction is therefore unimportant.

(iii) <u>Spatial Distribution of Cerenkov Light at Ground Level</u>

A first estimate of the radius of a Cerenkov light pool at ground level can be made using the information displayed in Figure 2.4. The air shower maximum occurs near the base of the cascade ($h \approx 8$ km) where the Cerenkov emission half-angle $\theta \approx 0^{o}.9$. Then, $r_{pool} \approx h\tan\theta \approx 130$ m. The light pool radius was studied by Macrae (1985), who performed air shower simulations for a primary γ-ray energy of 1 TeV in order to obtain predictions of the properties of light pools at the 1.5-km altitude of the former Durham University γ-ray observatory at Dugway, Utah. The pool radius was defined as the distance from the shower core at which the photon density falls to $^{1}/_{e}$ of the

*Zenith angle is the angular separation of the local zenith and the direction of observation.

core value. Pool radii for vertical showers were found to vary from ~ 110 m for cascades maximising early in the atmosphere, to just 45 m for the (late) showers developing deep in the atmosphere. The average distance of the cascade maximum will, for a given primary energy, grow with increasing zenith angle (since the depth of the intervening column of air will increase): this therefore leads to larger light pools at the ground. Macrae finds radii of between 70 and 130 m at Z = 10°, depending on the age of the 1 TeV shower. At larger zenith angles, even late (deep) showers were found to produce pool radii in excess of ~ 115m.

The effective collecting area of a telescope at ground level is defined by the size of the light pool and is therefore ~ 10^4 m, i.e. a γ-ray cascade axis may lie anywhere within ~ 10^2 m of the instrument and yet the Cerenkov light will still be detected.

Expected peak areal photon densities at ground level range from ~ 100 m^{-2} (early developing showers) to ~ 400 m^{-2} (late developing showers) for vertical 1 TeV cascades. The density falls with increasing zenith angle as a consequence of the greater average distance to the cascade maximum, the tilt of the Cerenkov light cone with respect to the ground plane, and the enhanced atmospheric attenuation *en route* to the observer. The average intensity of the Cerenkov light observed at any given zenith angle is expected to increase with the energy of the primary γ-ray since more energy is available for the production of particle pairs above threshold, leading to larger cascades.

Of equal importance, the atmospheric absorption and inverse-square attenuation will decrease as the average altitude of cascade maximum reduces with increasing primary energy.

(iv) Duration of a Cerenkov Pulse

This may be estimated very easily. Since the fundamental requirement for Cerenkov emission is that the electron speed v exceeds c_m, the air shower photons lag behind the electrons. Let all electrons take speed $v \approx c$, the speed of light in vacuo. The photon speed $c_m = c/n = c[1+R(y)]^{-1}$, where y is altitude and the function R is (equation 11) just $R = n(y) - 1 = R_o \exp(-y/h_o)$. With $R_o = 0.000293$ (corresponding to air at S.T.P.) and $h_o \approx 8$ km,

$$\Delta t = \left[\frac{nd}{c}\right]_{photon} - \left[\frac{d}{c}\right]_{electron} \approx 2 \text{ ns} \qquad (13)$$

where the vertical extent of the cascade, $d \approx 8$ km, and a typical altitude of 12 km has been taken in order to compute n. The duration of the pulse is extended to ~ 3 to 5 ns by Coulomb scattering of the shower particles and the consequent range of path lengths to the detector. Note that the disk of Cerenkov light is very thin and has a depth ~ $c\Delta t$ ~ 1 m.

2.5 Basic Design Requirements For TeV γ-Ray Telescopes

Gamma-ray telescopes deployed for the detection of Cerenkov emission from air showers consist essentially of a flux collector, which needs to be a mirror of only moderate optical quality, and one or more focal-plane photosensors (usually photomultiplier tubes). Cerenkov events can be identified in the presence of the night-sky background noise (due to star-light and air glow) by discriminating at a suitable threshold level. The threshold γ-ray energy of the telescope would then be limited by the gain of the phototube used which, in turn, is limited by the maximum permissable noise counting rate. The background can be almost entirely rejected by taking fast coincidence between multiple mirror-phototube combinations. The Durham group has demonstrated (Brazier *et al.* 1989a) that, for a given total mirror area, three-fold coincidence offers the best compromise between the Cerenkov event rate registered and the complexity of the signal-processing hardware required. The ability to identify a weak γ-ray signal is then limited only by fluctuations in the arrival rate of the random cosmic ray background.

The cosmic ray event rate (B) recorded at a telescope is directly proportional to the solid angle (Ω) of sky viewed by the mirror-phototube combination, the area (A) of the mirror, and the observation time (T):

$$B \alpha \Omega A T \qquad (14)$$

The excess count rate due to a γ-ray signal from a point source is

$$S \alpha A T \tag{15}$$

Let φ be the half-angle of the field of view, so that Ω can be replaced by $\pi\varphi^2$. Then, assuming that the arrival rate of the cosmic ray events follows Poissonian statistics, the ratio of the signal rate to the standard deviation of the background rate is

$$\frac{S}{\sqrt{B}} \alpha \sqrt{(AT)}\ \varphi^{-1} \tag{16}$$

which is a direct measure of the statistical significance of a DC source detection. The signal-to-noise ratio is therefore a slowly increasing function of mirror area and collection time.

Enlarging the area of the mirror decreases the Cerenkov light pool photon density threshold and therefore increases the effective collection area for a given primary γ-ray energy. A more important advantage of increasing A is the reduction of the γ-ray energy threshold of the telscope.

The benefits of lengthening the observation time are limited according to the nature of the γ-ray source. For transient sources, the value of T is clearly bounded by the duration of emission. The measurement of DC (unpulsed) sources can be

frustrated by unstable atmospheric conditions during the course of an observation.

The signal-to-noise ratio can also be increased by narrowing the field of view of the telescope but this is limited to the angular width of the Cerenkov light cone, below which the amount of light collected falls, as does the detection efficiency of the telescope. Patterson and Hillas (1989) have simulated air showers in order to quantify the optimum design specifications for a TeV γ-ray telescope. A field of view of $\approx 1.5^{\circ}$ is suggested as being the most favourable. Similar values were determined experimentally by the Durham group using an array of Cerenkov telescopes at Dugway, Utah (Gibson *et al.* 1982).

2.6 Air Shower Discrimination

Given that an air Cerenkov telescope has been designed with the above requirements in mind, the signal-to-noise ratio can be improved further if a significant fraction of the cosmic ray component registered at the telescope can be identified and rejected. Geometrical discrimination, Cerenkov imaging, and pulse shape discrimination are three methods which have been developed in order to try to distinguish between air showers generated by photons and hadrons.

(i) Geometrical Discrimination

The Durham Group operates two independent telescopes at Narrabri, New South Wales. Both instruments comprise three paraxial flux collectors, each with a focal plane set of seven photomultiplier tubes. Each set of phototubes is arranged so that a central tube is directed to a γ-ray source candidate whilst the remaining six tubes form an encircling 'guard ring' which monitors regions of the sky centred at angles of 2° from the direction of the source. The field of view observed by each phototube has a width $\approx 1^{\circ}$. The central tubes of the three flux collectors comprise a single on-axis detector channel. Six off-axis detector channels are formed by the corresponding guard ring phototubes at each of the focal planes. On-source or off-source Cerenkov events are identified by demanding fast three-fold coincidence between the three elements of at least one of the channels. An air shower generated by a γ-ray is expected to be centred approximately upon the source and will therefore usually trigger the on-axis channel only. Cosmic ray air showers however can be centred just beyond the field of view of the on-source channel and yet still contribute enough Cerenkov light to trigger an on-axis response, in addition to being registered by one or more of the off-axis channels. Events recorded simultaneously by the on-axis channel and an off-axis channel may therefore be rejected; this is performed routinely during pre-analysis processing of the data. It is found that approximately 60 % of the Cerenkov events which trigger the on-axis channel can be eliminated in this way with little or no loss of the candidate

γ-ray events. The signal-to-noise ratio is therefore improved by a factor ≈ 2. This rejection technique is referred to as the 'hardware cut' since it relies upon the phototube threshold levels, which are set automatically before the beginning of an observation with the telscope.

A second level of hadron rejection is accomplished by inspecting sub-threshold off-axis phototube responses. (Discrimination levels are defined in the data processing software prior to analysis, hence this second rejection procedure is known as the 'software cut'). This permits a further *a priori* enhancement of the signal-to-noise ratio by up to 10 %. These two selection methods will be considered in more detail in Chapter 3. Examples of the results of both types of selection are shown in Figure 2.5a and are taken from the period analysis of a Cerenkov arrival time series recorded during a four-hour observation of SMC X-1 on 1987 July 23.

(ii) <u>Cerenkov Imaging</u>

Rejection of the cosmic ray background by making a detailed inspection of the angular distribution of Cerenkov light from air showers has been pioneered by the Whipple Collaboration, which operates a single optical reflector (diameter 10 m) located at Mount Hopkins, Arizona. This technique has been described by Kwok (1989), Weekes *et al.* (1989), and Lang *et al.* (1990). A total of 109 phototubes at the focal plane of the telescope are

Figure 2.5a

Durham University Mark III Telescope:

Geometrical Shower Discrimination

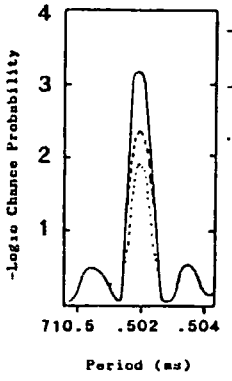

—— Hardware & Software Selection

---- Hardware Selection

····· No Selection

Results of test for uniformity in phase of SMC X-1 time series recorded on 1987 July 23

SMC X-1 23/07/87	Total Events	% Rejected	% Signal Strength	Gamma-Ray Candidates	Chance Prob.
No Selection	9517	-	2.14	204	1.3×10^{-2}
Hardware Selection	8235	34	2.89	180	5.5×10^{-3}
Software Selection	5557	11	3.54	197	9.5×10^{-4}

Figure 2.5b

Whipple Collaboration: Air Shower Discrimination By Cerenkov Imaging

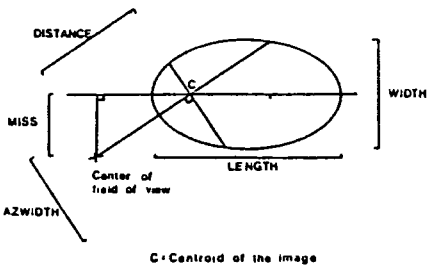

Definition of image parameters

(Adapted from Weekes *et al.* 1989)

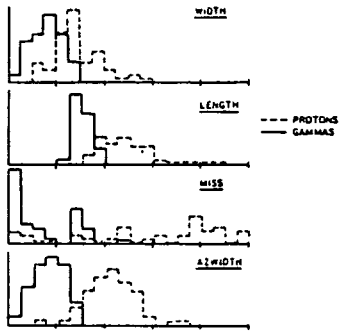

Image parameter distribution predicted by simulations for γ-ray source at zenith and an isotropic cosmic ray background

Horizontal scale: degrees
Vertical: arbitrary linear scale

Figure 2.5c

Riverside & Caltech: Shower Discrimination by Inspection of Temporal Distribution of Pulse

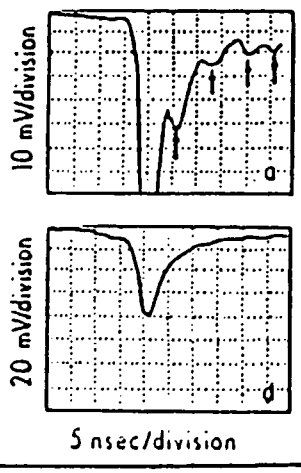

OSCILLOSCOPE TRACES OF CERENKOV PULSES

Hadron Candidate.

Multiple kinks, large tail offset, pulse height > 100 mV

Gamma-Ray Candidate.

No kinks, no tail offset, pulse height = 80 mV.

(Adapted from Tumer *et al.* 1990)

used to record an image of the field of view, which has an angular width of 3°.5. Simulations of the response of this instrument to air showers generated by γ-rays and protons were performed in order to examine the distributions of the angular sizes, shapes, and orientations of shower images. As described in Section 2.2, the proton showers have multi-cored electromagnetic cascades, compared with the single core of a γ-ray air shower: the distribution of Cerenkov photons in the proton showers is therefore expected to be broader and less regular. Figure 2.5b defines the image parameters and shows their expected distributions for the two types of shower. The discrimination criteria established by the simulations were applied by Weekes *et al.* (1989) to data collected during observations of the Crab Nebula. This led to the elimination of more than 98 % of the proton background and has provided the most statistically significant detection of TeV γ-rays to date. It should be noted that the same photon/hadron discrimination criteria fail when applied to data which were accumulated on other γ-ray source candidates using an earlier, simpler, focal-plane detector package.

(iii) Pulse Shape Discrimination

Tumer *et al.* (1990) have examined the temporal distribution of Cerenkov pulses recorded during observations of the Crab Nebula using a pair of 11 m diameter solar collectors at the Sandia

Laboratories, Albuquerque, New Mexico. As with Cerenkov imaging, the technique rests upon the expectation that hadron-induced air showers of a given primary energy have, on average, a more anisotropic distribution of cascade particles than is found in the showers generated by γ-rays of equal energy. The Cerenkov radiation produced by this component of anisotropic secondaries makes a significant contribution to the pulse recorded at the telescope. This light is received at a slightly later time than the light from the main body of the cascade, due to the differences in the path lengths through the atmosphere. Because the secondaries are small in total, their number and distribution will fluctuate widely from shower to shower. It is therefore predicted that pulses from hadronic showers will, when displayed as a function of time, exhibit tails which tend to be more extended and considerably more uneven than the pulses generated by γ-ray air showers. Adopting such features as the criteria for discrimination, Tumer *et al.* (1990) analysed video tape recordings of oscilloscope traces of Cerenkov pulses recorded during drift-scan observations of the Crab Nebula. Two examples of the oscilloscope traces are shown in Figure 2.5c. Approximately 95 % of the cosmic ray background was rejected and, with just 1.5 hr of such data, the technique was sufficient to identify a DC (unpulsed) excess in the on-source drift-scan measurements which is significant at the 4.2 σ level.

2.7 Current TeV γ-Ray Observatories

Air Cerenkov telescopes are in operation at thirteen sites worldwide at the present time (1990 September) and a fourteenth experiment is currently being commissioned in the Republic of Ireland; five of these observatories are located in the Southern Hemisphere. Details of each experiment are listed in Table 2.1, which provides the name of the research group, the location of the telescope site, and the year in which the telescope was commissioned, together with information on the flux collector and the detector package.

2.8 Summary

By good fortune, the Earth's atmosphere is an excellent medium for the detection of TeV γ-rays. Air has a low refractive index and, consequently, produces tight Cerenkov beaming which gives good angular resolution and permits the identification of point sources of high energy γ-ray emission. At the same time, the column density of the atmosphere is sufficient to produce air shower maxima at altitudes which are great enough to provide a very large effective collecting area on the ground: given the typical source distances and luminosities, this large collecting area is vital if the γ-ray flux is to be detectable.

A major drawback of the air Cerenkov technique is the existence of a strong isotropic background due to hadronic air showers. Some recent success has been achieved in isolating the

Research Group	Location	Commission Date	Flux Collector	Detector Package	Comments	Reference
Durham University	Narrabri, NSW, Australia 30° 29' S 149° 39' E 210 m asl	1986	Mk III 3 x 11 m² paraxial dishes. Focal length = 2.5 m.	7 PMTs at each focal plane operated in fast triple coincidence between 3 dishes	On-axis PMT channel with 6-channel anti-coincidence guard ring	Brazier *et al.* (1989a, 1990)
		1988 La Palma 1990 Narrabri	Mk IV 3 x 6 m² paraxial dishes.	" " " "	" " " "	" "
Whipple Collaboration	Mt Hopkins, Arizona 31° 41' N 110° 53' W 2320 m asl	1983	Single ~70 m² dish of 248 0.61 m spherical mirrors.	High resolution camera formed by 109 PMTs in 5 concentric hexagonal rings	Discrimination by Cerenkov imaging	Cawley *et al.* (1990)
Adelaide University	Woomera, S. Australia 31° 06' S 136° 47' E	1989	3 x 10 m² paraxial dishes. Focal length = 2.7 m	PMT triplets run in fast 3-fold coincidence between dishes	Multi-tube camera for imaging is planned	Gregory *et al.* (1990)
Tata Institute	Pachmarhi, India 22° 28' N 78° 26' E (formerly at Ootacamund)	1986	20-element array of parabolic mirrors. 12 x 1.5 m diam. 8 x 0.9 m diam.	Single PMT at focus of each mirror	Array elements grouped in 4 banks. Majority logic (3/4) to trigger on shower	Acharya *et al.* (1990)
Bhabha Atomic Research Centre	Gulmarg 34° N 77° E 2743 m asl	1985	6 x 0.9 m diam. parabolic mirror. Focal length 0.4 m	Single PMT at focus of each mirror	Operated as 2 banks of 3 telescopes	Koul *et al.* (1989)
JANZOS Collaboration	Black Birch, South Island, New Zealand. 1640 m asl	1987	3 x 2m diameter parabolic mirrors	28 PMTs at focus of each mirror	Mirrors at vertices of 80 m equilateral triangle. Drift scan only.	Bond *et al.* (1990)

Table 2.1 Currently Operational TeV γ-Ray Observatories

Research Group	Location	Commission Date	Flux Collector	Detector Package	Comments	Reference
Potchefstroom University	Nooitgedacht, South Africa 26° 54' S 27° 11' E 1438 m asl	1985	Four telescopes with three 1.5 m parabolic mirrors	Single PMT per focus	3 telescopes at vertices of equi-lateral triangle of side 48 m, 1 at centre.	de Jager *et al.* (1986)
Haleakala Collaboration	Mt. Haleakala, Maui, Hawaii. 21° N 156° W 2950 m asl	1985	6 x 1.5m diameter spherical mirrors on single mount	6 PMTs at each focus	3 PMTs of each set of 6 on-source, 3 PMTs off-source. 0.2 TeV threshold.	Resvanis *et al.* (1987)
Riverside & Caltech	Albuquerque, New Mexico. 34° N 107° W	1987	2 x 11m solar collector dishes, 40 m apart	Single PMT at each focus	0.2 TeV threshold. Hadron rejection by pulse shape inspection	Tumer *et al.* (1990)
Wisconsin Collaboration	South Pole	1990	10 x 0.8m diam. mirrors	2 PMTs per focus; 3° apart for on-source, off-source monitoring	Operated in conjunction with SPASE PeV array	Morse (1990)
AsGat Collaboration	Odeillo, French Pyrenees. 42° N 2° E 1700 m asl	1988	7 x 7m diam. parabolic mirrors	7 PMTs per focus. Signals summed at each telescope	0.3 TeV threshold. Telescopes at centre and apices of 60 m side hexagon	Basiuk *et al.* (1990)
Beijing Institute HE Physics	Xing Long, China. 40° 24' N 117° 30' E 940 m asl	1990	3 x 1.5m diam. paraxial parabolic mirrors on single altazimuth mount	Single PMT at each focus	Operational prototype of this instrument exists in Beijing	Jiang *et al.* (1990)
St. Patrick's College, Eire	Experiment under construction	1990 (expected)	Two 1x0.8 m Fresnel lenses on single altazimuth mount. 1.12 m focal length.	Single tube per focus for 2-fold coincidence	Automatic operation of array of such instruments planned, with 2-way communication to remote station.	Cawley *et al.* (1990)

Table 2.1 cont.

γ-ray component by examining the angular and temporal distribution of the Cerenkov light.

A second disadvantage, though one shared by optical astronomers, is that the technique requires clear, Moon-free skies. However, the observing duty cycle for the Durham University observatory at Narrabri is, at $\approx$ 15 %, enough to provide an average ~ 100 hours of clear viewing per dark period.

Chapter 3

University of Durham Mark III γ-Ray Telescope: Data Collection and Data Processing

3.1 Introduction

The Mark III γ-ray telescope was constructed during 1986 September at a site approximately 20 km south of the town of Narrabri, New South Wales, Australia (30° 29' S, 149° 39' E; altitude 210 m a.s.l.). The identification of an air Cerenkov event is made using fast 3-fold coincidence in the responses of one or more of seven channels of photomultiplier tubes which are located at the prime foci of three 11 m^2 flux collectors. The telescope is automatically steered on a central alt-azimuth mount and attains a threshold γ-ray energy of 250 GeV at the zenith.

This chapter is divided into three sections. The principal components of the Mark III telescope are described in Section 3.2. The processing of signals transmitted from the focal plane detectors to the telescope control room is considered in Section 3.3. The chapter concludes with a description of the subsequent processing of the data at the University of Durham, which includes the routine adjustments made to all Cerenkov arrival times and the procedures adopted for the standard selection of data for analysis.

3.2 The Mark III γ-Ray Telescope

3.2.1 Introduction

The key components of the Mark III telescope are described briefly here; these include the flux collectors, the focal plane detectors, the electronic recording channels, the telescope drives and the supporting Local Area Network of microcomputers. Three observing modes employed with the telescope (tracking, source-chopping, drift scanning) are also described. See Brazier *et al.* (1989a) for further details on the design of the telescope.

3.2.2 The Flux Collectors

Three paraxial collectors of area ≈ 11 m^2 were each constructed from a closely-packed array of 0.3 m^2 spherical mirrors arranged as a symmetric distribution of seven hexagons. The configuration of the mirror dishes can be seen in the photograph of the Mark III in Plate 1. The shape of the resultant reflecting surface formed by the individual mirrors is approximately parabolic so that the light collected by all mirrors on a single dish can be brought close to a unique focus.

The telescope has a field of view of 1°.1 FWHM which is defined by a photomultiplier tube of 46mm sensitive diameter and an individual mirror focal length of 2.45m; tests performed earlier

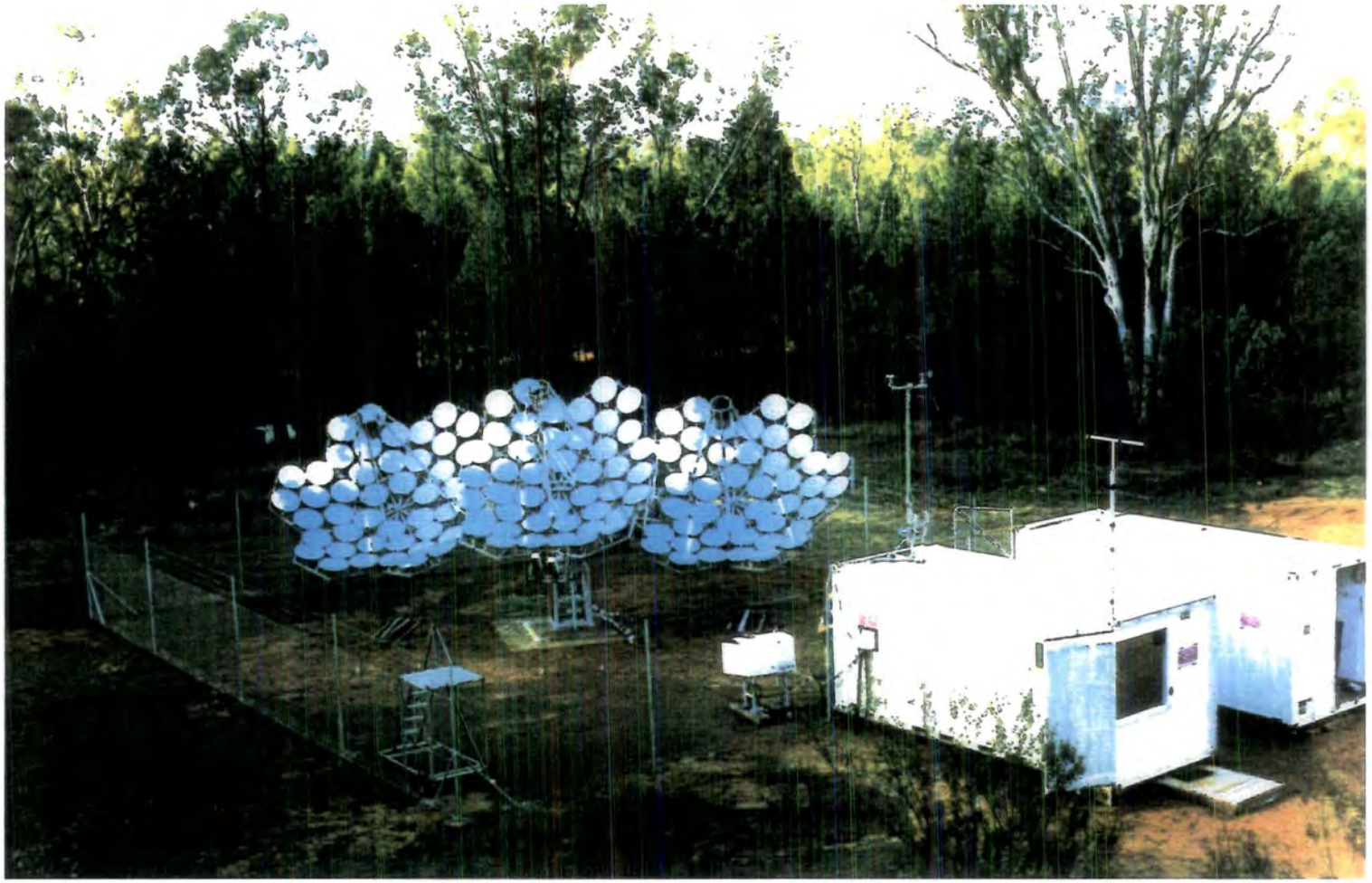

Plate 1: The Mark III γ-Ray Telescope at Narrabri

at the University of Durham telescope array at Dugway (Utah) had shown that an aperture angle ≈ 1° provides an optimum signal-to-noise ratio (see Gibson *et al.* 1982).

The method adopted for the production of the mirrors followed an extensive program of development and was similar to that employed at the Rutherford Appleton Laboratory during the construction of the antenna for the James Clerk Maxwell Millimetre-Wave Telescope. The interior of a mirror is made from aluminium honeycomb foil of wall thickness 0.04mm. The honeycomb cells are 0.8 cm in size and the depth of the honeycomb is 2.5 cm. Discs of the honeycomb material were cut and pressed against a spherical mould before the bonding of a flat plate to the rear surface and a rolled ring about the perimeter. The reflecting surface is formed from aluminium sheet of reflectivity ~ 80 % and thickness 0.5 mm; this sheet was stretched across the spherical mould and clamped into position before bonding it to the honeycomb/backplate assembly.

A total of 130 mirrors are mounted on the Mark III telescope: 44 mirrors on the central flux collector and 43 on each of the adjacent dishes. Their quality has been found to be within the bounds demanded by the design specifications; the angular size of a stellar image is < 0°.2, or approximately $^1/_5$ of the angular spread of a Cerenkov light pool. At the time of writing (1990 September), the mirrors have been in use in Australia for 4 years and have shown no appreciable degradation in performance.

3.2.3 The Focal Plane Detectors

The photomultiplier tube (PMT) is employed for the detection of optical Cerenkov light. The requirements of a PMT used with an atmospheric Cerenkov telescope are:

(i) a stable, high gain;

(ii) a fast detector response with a rise-time ~ 1 ns (comparable with the timescale of a Cerenkov pulse);

(iii) a small internal noise rate.

Each of these requirements must be met with PMT anode currents which typically approach the recommended maximum under the conditions of high photocathode illumination caused by the natural brightness of the night sky. The RCA 8575 tube offers a good combination of noise performance and gain stability when matched with the large light collecting area of the Mark III telescope.

The EHT voltage applied across an RCA 8575 PMT under dark sky conditions at the Narrabri site is normally 1850 V. This is supplied by a computer-controlled LeCroy EHT unit.

With a 50 mV discrimination threshold, a single-fold noise count-rate of ~ 30 kHz is obtained with a typical anode current of 35 μA. The anode current of a photomultiplier tube is automatically stabilised via a feedback mechanism to maintain a

constant telescope sensitivity (hence threshold γ-ray energy). This is necessary because the cathode-current/gain relationship of the RCA 8575 phototube is such that a change of illumination from complete darkness to normal sky conditions may alter the overall gain by between 5 and 10 %. The night-sky illumination may also vary over short timescales due to the passage of stars through the field of view. The result is that the PMT noise count rate can change by an amount which may be comparable with the γ-ray count rate excess expected from a typical source, i.e ~ 1 % of the cosmic ray background rate. The light from a green LED mounted in the faceplate of the PMT is used to stabilise the cathode illumination (and, therefore, the PMT gain) against the expected short-term variations. The brightness of this LED is automatically controlled with a feedback loop which keeps the anode current constant to $\leq$ 1 %. The consequent increased noise rate (by a factor ~ 1.1) is acceptable for it leads to a negligible increase in the rate of accidental three-fold coincidences. Such automatic PMT gain control routinely maintains a steady anode current throughout an observation of a source candidate.

3.2.4 The Detector Channels

The detector arrangement at the focal plane of each of the three flux collectors is shown in Figure 3.1 and comprises a symmetric arrangement of six PMTs about one central tube.

Figure 3.1

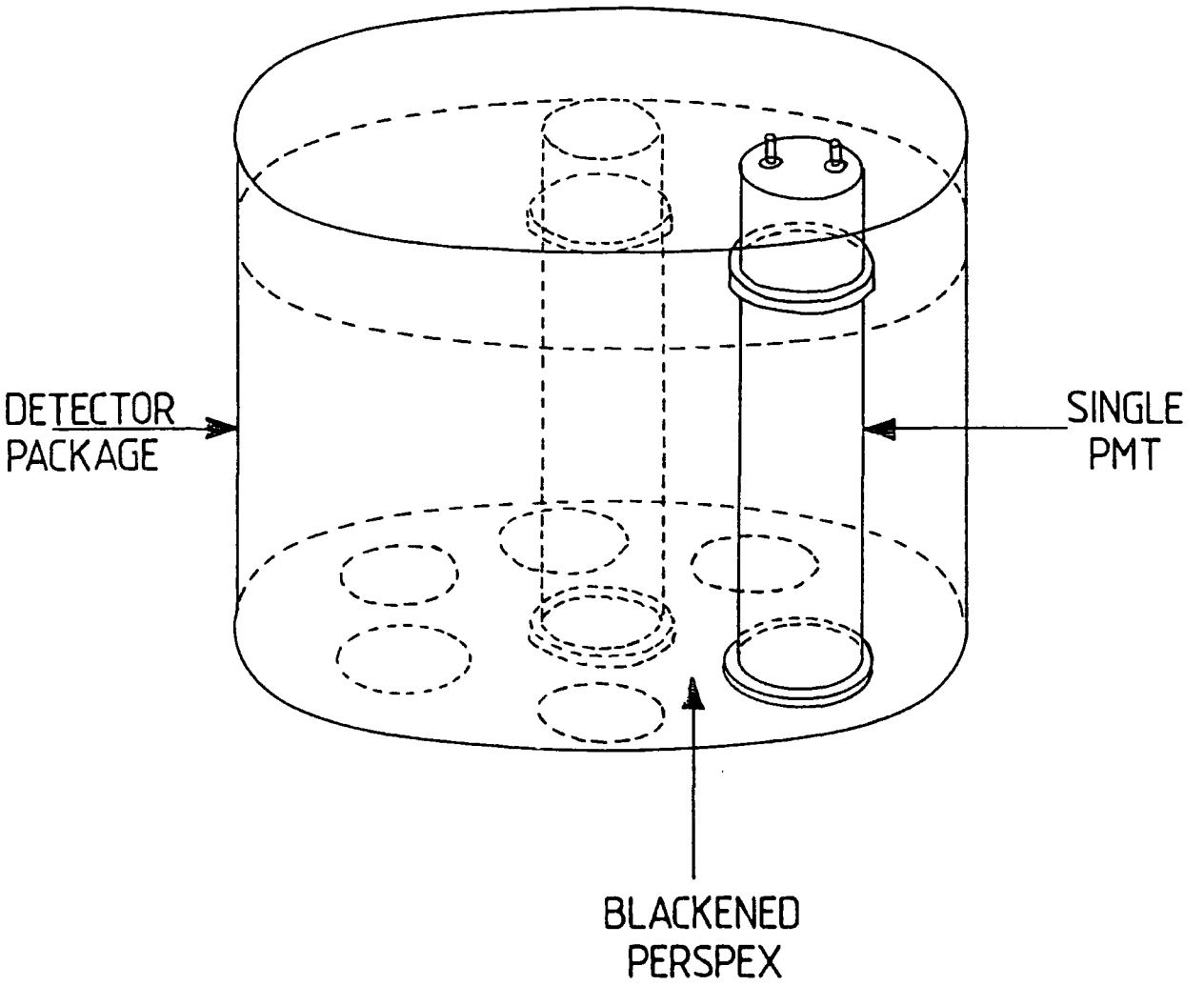

Arrangement of phototubes placed at the focus of each flux collector of the Mark III telescope

The detection of a Cerenkov event by any given channel is defined when the corresponding PMT at the focus of each of the three flux collectors registers a pulse above threshold level within a three-fold coincidence gate time of $t_g \approx 7$ ns. The accidental coincidence rate for a three-fold arrangement can be shown to be approximately $R^3 t^2_g$, where R is the typical PMT noise rate under high illumination. Thus with R ~ 30 KHz, the accidental rate is ~ 10^{-3} Hz channel^{-1}, or approximately 4 hr^{-1} channel^{-1}. This should be compared with a typical cosmic ray count rate of $\approx$ 8000 hr^{-1} channel^{-1} at the zenith.

The three groups of seven phototubes form a central on-axis coincidence channel surrounded by a "guard ring" of six off-axis channels. The centre of the $\approx 1^\circ$ field-of-view of each of the guard ring elements is displaced by an angle of 2° from the direction of the source candidate. This allows a continuous monitoring of the cosmic ray background. The off-axis channels therefore provide data which can be used as a control when evidence is found for a γ-ray signal. The guard ring data are also employed to examine the angular distribution of light in Cerenkov flashes registered by the central channel: a portion of the background cosmic ray events detected by the on-source channel, but originating away from the source direction, can be rejected, which can lead to the enhancement in the ratio of signal-to-noise. This facility will be described further in Section 3.4.6.

3.2.5 Automated Steering

The telescope is moved in azimuth and altitude by two DC servomotors. The motors drive directly onto orthogonal heavy-duty gear wheels which are secured firmly to the central telescope mount. Horizontal and vertical angles are sensed to a resolution of 5 arc minutes by absolute digital shaft encoders. The target azimuth and altitude are computed every $0^s.1$ and compared with the outputs of the encoders; the servomechanism is then completed by the transmission of appropriate error signals back to the DC motors. A second loop is created by velocity feedback in order to dampen any unwanted accelerations of the telescope which might be caused by strong winds, for example.

The drive specifications of the telescope include the ability to accelerate in 10 s to a maximum azimuthal slew rate of $1^o\ s^{-1}$. With the moment of inertia of the telescope about the central mount at $\sim 10^4$ kg m^2, the acceleration from rest to the required slew rate is accomplished with an azimuth motor of 20 N m output torque and 430 W full power.

The zeros of the azimuth and zenith shaft encoders were defined approximately during construction of the telescope; they were later refined when the telescope became fully operational. The known positions of stars were compared with the corresponding shaft encoder readings in order to compute accurately the offsets of the azimuth and zenith angles, against which all future telescope orientations could be defined. A check can be made on the pointing direction of the telescope at any time during an

observation by using a high-gain CCTV camera which is affixed to the telescope framework and which views along an axis that is parallel to those of the flux collectors. The 5°x3° field of view is regularly compared with star charts superimposed on a VDU in the telescope control room during routine observations.

3.2.6 The Local Area Network

A network of eight microcomputers provides both detailed, real time monitoring of the telescope performance and a user interface with each of the telescope drive, signal processing and data recording systems. One microcomputer permits operator access to the 68000-based data-logging computer (described below) and is used to initiate the sequence of actions performed at the beginning of the observation of each target and, should the need arise, allows real time control of the signal processing and recording systems. A second microcomputer is dedicated to the steering of the telescope and regularly updates a VDU display of both the telescope orientation and the target azimuth and zenith angles. The condition of the 21 PMTs comprising the seven detector channels is monitored by four microcomputers which receive and decode broadcasts from the 68000 data-logger at 1-second intervals. They drive displays of the anode currents and noise count rates of each of the 21 phototubes and the coincidence count rates of the tubes forming the seven channels. Also provided are graphical displays of the 3-fold coincidence

rates on all seven channels. Environmental conditions (relative humidity, ambient temperature, wind speed and direction) are continuously monitored and displayed on a VDU.

The network includes a fileserver and a workstation. Data such as weather conditions and the 3-fold coincidence rates are routinely dumped and stored on the network fileserver. Software is loaded from it in preparation for observing, e.g. the target values of the PMT EHTs required by the LeCroy EHT unit.

The various computers are programmed to alert the operator to unusual or hazardous changes in the performance of the telescope. Visual and audio alarms are activated to indicate such problems as telescope steering malfunctions, dangerously high wind speeds, or a failure to register any 3-fold coincidences during a pre-specified period of time.

The Mark III telescope control room is shown under night-time operating conditions in Plate 2.

3.2.7 γ-Ray Energy Threshold

The zenithal threshold energy of the early Mark II telescope at Dugway, Utah was estimated to be 800 GeV (Chadwick *et al.* 1985c). The threshold for the Mark III has been estimated by scaling from this value (Brazier *et al.* 1989a) and is considered to be approximately 250 GeV at the zenith. The threshold during any given observation varies with the zenith angle of the source

Plate 2: The Mark III Telescope Control Room

candidate. By measuring the zenith dependence of the cosmic ray counting rate, the threhold energy of the Mark III is estimated to rise to a value ≈ 400 GeV at zenith angles ~ 50°.

3.2.8 Observing Modes

Depending on the quality of the local atmospheric conditions and the expected characteristics of a γ-ray source candidate, the telescope can be operated in three modes:

(i) Tracking

In this mode, the orientation of the telescope is regularly adjusted so that the source candidate remains at the centre of the field of view of the central on-axis detector channel. This mode of operation is best suited to candidate γ-ray sources which are known to exhibit periodicity at lower energies.

(ii) Chopping

This technique is powerful but it can only be satisfactorily employed when the local sky conditions are very stable. Whilst tracking the source candidate, the whole telescope is periodically rotated back and forth through 2° in azimuth so that the target is alternately monitored by the central channel and an off-axis channel. A complete chop cycle is completed every four minutes. Regardless of the direction of the tracking motion of

the telescope, the chop movement is executed in a horizontal plane so that the γ-ray threshold energy is constant with respect to time throughout one cycle. The remaining five detector channels provide extensive off-source background control data in the usual way although, with the present arrangement of the three sets of seven phototubes, the guard ring of the secondary on-axis channnel is incomplete; this channel is therefore less sensitive.

The signal-chopping technique is employed in many wavebands. Here it provides a means to identify a DC γ-ray source by searching for an excess when the total number of Cerenkov events detected by a given channel on-source is compared with the number registered by the same channel off-source.

Operating the telescope in the chopping mode can demonstrate:

(a) the detection of a signal in each of two independent recording channels;

(b) the correlation of the signal with the direction of the source;

(c) the failure to register a signal with the *same* recording channels when periodically off-source.

Period analysis of the Cerenkov times series can also be performed by combining the data recorded by both channels when on-source. The search for a DC excess and the search for periodicity are two independent tests of the data, therefore the

results of a period analysis can provide independent support for the identification of a γ-ray source.

The signal-chopping mode has been employed successfully with the Mark III telescope during observations of the high-mass X-ray binaries Vela X-1 (see Carraminana *et al.* 1989a) and Centaurus X-3 (Brazier *et al.* 1989a, Carraminana *et al.* 1989b, and Brazier *et al.* 1990a), and the low-mass binary Scorpius X-1 (Brazier *et al.* 1989b).

(iii) Drift Scanning

This is the simplest of the three observing modes and has the advantage of a constant telescope threshold energy but it requires uniformly clear sky conditions with minimal variations in atmospheric transparency over long intervals of time. A drift scan is performed by fixing the orientation of the telescope at one set of values of azimuth and elevation so that a DC source candidate transits the field of view of the on-axis channel at the mid-point of the observation and, it is hoped, produces a significant rise in the rate of 3-fold coincidences. The technique is rather inefficient, for much of the observation is spent in monitoring the background count rate. Note that the automatic control of the PMT gain is now particularly important because the cathode illumination will change rapidly as star fields of varying density pass through the field of view.

The drift scan technique is only rarely employed with the Mark III: it has however been used recently to observe the extended Galactic centre region on several occasions, with each scan lasting for a time ~ 6 hours.

3.3 Signal Processing

3.3.1 Introduction

Each of the key stages of signal processing in the Mark III telescope control room will be described here, from the identification of a Cerenkov event, to the recording of the data on magnetic tape.

3.3.2 Identification of a Cerenkov Event

The high-speed signal processing electronics are housed in the air-conditioned Mark III telescope control room and are arranged into one crate of NIM modules (for amplification and PMT gain control) and one crate of CAMAC modules, the latter to provide a two-way computer interfacing system for management by the controlling 68000-based microcomputer.

Following the sampling of a Cerenkov light pool by the seven-channel array of photomultiplier tubes and the transmission of their responses into the control room, the key stages of the recognition of such an event include signal amplification, a

measure of the charge pulses from the PMTs, voltage amplitude discrimination and the test for coincidence between the three signals across any given detector channel. Each of these stages is now described in more detail.

(i) Amplification:

The analog signal arriving at the control room from an individual photomultiplier tube is first passed to the electronics in the NIM crate and through the Automatic Gain Control (AGC) unit so that a sample may be taken of the PMT anode current and a comparison made with a reference current transmitted from the controlling 68000 microcomputer. This is an important part of the servomechanism described earlier, in which a stable PMT gain is maintained under conditions of variable night-sky illumination.

Upon exit from the AGC unit, all signals from the 21 phototubes pass immediately to the NIM amplifier modules. The two modules each contain a LeCroy 12-channel linear voltage amplifier (Model 612A) and supply a fixed gain of 10.

(ii) Charge-to-Time Conversion:

The scaled representation of the size of a PMT output charge pulse is based on one of the two outputs from the NIM amplifiers and is performed with a pair of current-integrating 12-channel CAMAC analog-to-digital converters (LeCroy Model 2249A). The

conversion of the amplified input yields a digital pulse which is proportional to $\int i.dt$ and therefore offers a gauge of the charge collected over a given interval of time. This integration is routinely carried out for each of the 21 PMTs across a gate time of 30 ns; this is essentially free from error since the gate time corresponds to just ~ $^{1}/_{1000}{}^{th}$ of the average time between separate responses from a PMT operating at the typical rate of 30 kHz. The results are then stored in scalers for transmission to the 68000 microcomputer in the event that 3-fold coincidence is subsequently registered on one or more of the detector channels. Such measurements of the PMT charge have proved to be very useful for the enhancement of the signal-to-noise ratio (Section 3.4.6).

(iii) Discrimination:

The second of the two outputs from the signal amplifier modules also passes to the CAMAC crate and into the LeCroy discriminators (Model 4416B). These serve to both eliminate the lower level PMT noise responses and to convert the highly variable analog input signals to standardized pulses suitable for the subsequent logical signal processing. The input sensitivity, or discrimination threshold, is programmable and may be selected using the 68000 computer (via the CAMAC interface). It has been routinely set at a value of 50 mV.

(iv) The Test For Three-Fold Coincidence

The fixed duration logic pulses from the discriminators are fed into a LeCroy programmable CAMAC logic module (Model 4516). This unit can serve up to 16 sets of three input signals and is therefore more than adequate for the seven detection channels formed by the 21 photomultiplier tubes. Three-fold coincidence on any one detector channnel is defined by the acceptance of three corresponding input pulses at the logic module within an overlapping time window that does not exceed a width of 7 ns. Combinations of pulses which do not arrive within the time window are rejected at this stage and undergo no further processing.

Two purpose-built modules are immediately accessed following the satisfaction of the criterion for the acceptance of an event. Firstly a coincidence register records the "fire pattern" of all those detector channel responses which contribute to a set of between one and seven simultaneous three-fold coincidences at the logic unit. This pattern is also displayed on a vertical array of red LEDs mounted in the faceplate of the coincidence register to permit a simple visual check of the real time performance of the telescope. From this point forward it is taken that a single Cerenkov light pool has been detected, an event which is heralded by the master trigger module described next.

3.3.3 The Master Trigger Logic Unit

The master trigger behaves as an alarm when an event is registered and interrupts the 68000 microcomputer so that the data logging routine may be initiated. In addition it latches both the steering to establish the current telescope orientation and the CAMAC clock unit to obtain the time of the event. Should an event be accepted by the coincidence unit during the system "dead time", i.e. whilst the 68000 processor is occupied with the stream of data associated with an earlier event, then the time of the new event is latched by the master trigger and transferred to a buffer until the 68000 computer may be accessed once again. The arrival times of up to 16 such events may be buffered during the 350 μs system dead time; this therefore offers some capacity for the examination of the temporal structure of a brief, intense burst of Cerenkov events which are separated by times much less than the dead time. (The latching and buffering has the much shorter dead time of 6 μs).

The trigger unit also allows the real time inspection of the logging of Cerenkov events. Two faceplate LEDs indicate the type of event currently being logged (main/dead time). A third LED acts as a visual alarm and warns the operator should the logging system become paralysed.

3.3.4 The Clock

In contrast to astronomical observations in the lower energy wavebands, where measurements are taken of flux as a function of

time or photon energy, TeV γ-ray astronomy relies upon an ability to record the arrival times of each γ-ray and random background cosmic ray event with great precision. The specification for the Mark III telescope is a timing device which is sufficiently accurate and stable to permit separate, coherent observations of a millisecond pulsar over timescales $\sim$ 1 yr.

The Mark III telescope clock employs an Efratom model FRK-L rubidium oscillator which generates a very precise 10 MHz signal of 0.5 V r.m.s. The output signal from the clock is then scaled to provide an event time resolution of 1 μs. (Full 0.1 μs resolution is not needed and would add unnecessarily to the data storage requirements).

The rubidium oscillator was synchronised in 1987 January against an off-air signal from radio station VNG (Lyndhurst, Victoria) and has been checked almost daily during each observing sequence over a period of four years. The measured drift rate of the clock is 0.8 $\pm$ 0.02 ms month^{-1}. The relative accuracy of timings separated by one year is 0.25 ms.

3.3.5 The 68000 Microcomputer Logging System

All data are formatted and stored under the control of a versatile, high-speed 68000-based microcomputer that was constructed by the University of Durham Microprocessor Centre to the specifications of the Durham Group. Communications with the

CAMAC and NIM processing and logic electronics and with the two magnetic tape drives are facilitated by ten peripheral boards mounted above the 68000 main board. The system has no interface with the the Local Area Network fileserver; software is instead loaded to RAM in the 68000 processor from a floppy disc at the start of each observing session. The routine for the logging and broadcasting of data is programmable and is therefore highly flexible.

When a main event is registered by the master trigger unit, the 68000 processor is immediately interrupted and latched until the following data are recorded:

(i) the integrated, digitised charge pulses from the 21 PMTs

(ii) the currents at the anodes of each of the 6 PMTs forming the two prime detector channels

(iii) the arrival time of the Cerenkov light pool (to 1 μs)

(iv) the azimuth and altitude of the source candidate at the time of the event, together with the actual orientation of the telescope

(v) the "fire pattern" of those detector channels which gave a positive response at the coincidence unit

The 68000 computer then resets the master trigger in preparation for the logging of the next event.

Some 64 bytes of data are typically recorded for each event. The data on up to ~ 16,000 events may be formatted and then buffered in the 1 Mbyte of RAM available to the 68000 logger; this allows the recording of bursts of activity at rates which are greatly in excess of the usual 3-fold count rate ~ 1 to 2 Hz and in excess of the rate of data transfer from RAM to magnetic tape. The system has the capacity to record at rates of up to ~ 500 Hz.

The 68000 logger also broadcasts information on the system status and the current environmental conditions at two-second intervals to the microcomputers responsible for the monitoring of the performance of the telescope. In addition, a summary of this data is recorded once every minute to the magnetic tape and is labelled as a "housekeeping" data block. Details of the data recorded in such a block are given in Section 3.4.2 below.

3.3.6 The Tape Drives

The principal tape drive is routinely accessed by the 68000 microcomputer so that the Cerenkov event data and the housekeeping data may be transferred from RAM and recorded on magnetic tape. Both the principal drive and the back-up drive record on 67 Mbyte high density 3M DC600 portable tape cartridges; one or two such cartridges are usually sufficient for the data gathered during a single sequence of observations over a period of approximately 15 nights.

3.4 Data Processing

3.4.1 Introduction

The pre-analysis processing of the Mark III telescope data following the return of a 3M tape cartridge to the University of Durham is now described.

3.4.2 Routine Treatment of the Data

After the return of a tape cartridge to Durham, the data are processed at the Department of Physics VAX cluster (which forms the Durham node of the Starlink network). The processing sequence has three stages:

(i) All data are copied from the tape to the temporary disk space of the VAX mainframe and are then backed-up on 6250 bpi 9-track tapes, each of 20 Mbyte capacity.

(ii) The data are then grouped and translated to the readable ASCII format. The appropriate run-start file, source-start file and the datafile (described below) are combined to generate a single "source file" for each of the separate observations. This file may then be inspected directly, if required.

(iii) Analysis of the data relies primarily upon knowledge of the Cerenkov event times, the detector fire patterns, and the values of the charge pulses registered at each of the 21

phototubes. This information (together with flags to identify the on-source detector channel, in the case of a 'chopped' observation) is stripped from each source file to produce a corresponding compact file. The individual event times are also translated to the Solar System barycentre rest frame at this stage.

3.4.3 A Typical Datafile:

The data collected during a single observation are recorded in three separate files which are later combined during the data processing to produce a single source file:

(i) Run-Start File:

- a coded record of the programmable responses for the Cerenkov event, network broadcasting and housekeeping data defined for the 68000 microcomputer, together with a set of maps of the assignment of the signal processing hardware; the latter include photomultiplier tubes, charge pulse digitisers, discriminator channels, PMT EHT channels, anode current channels, and single-fold and three-fold coincidence count rate channels. Also mapped are the channels designated for weather monitoring (relative humidity, wind speed and direction, PMT temperature, mirror temperature and ambient temperature).

In addition the file contains:

a) Civil and Julian dates of the observation

b) names of the observing team

c) comments on the local observing conditions

(ii) Source-Start File:

This is a short file containing:

a) name of the source candidate

b) observing mode

c) celestial coordinates of the target

d) start time of the observing sequence

e) zenith and azimuth shaft encoder offsets

f) geographical coordinates of the observing site

g) comments on the local observing conditions

(iii) Datafile:

The word length for any Cerenkov event announced to the 68000 processor by the master trigger may be 64 or 128 bytes, depending upon the number of dead time event times appended to it at the end of the system dead time. The following is recorded for each

main event:

a) the identity of the on-source detector channel

b) the time of the event (to 1 μs resolution)

c) the digitised charge pulse at each of the 21 phototubes

d) the PMT anode currents

e) the instantaneous zenith and azimuth angles of the telescope pointing direction

f) the fire pattern of the detector channel responses above discrimination threshold.

The "housekeeping" data dumped to the datafile at 60-second intervals provides information on:

a) the time of the data sample

b) a sample of the values of each of the 21 PMT anode currents

c) the local weather conditions

d) the single-fold PMT response rates during a one-second sampling interval

e) any signal processing hardware failures.

3.4.4 Data Archives

As for the initial raw data-files copied from the 3M tape cartridge, the source files and the compact files are routinely stored on 9-track tapes to provide swift access and additional security; all tapes are housed permanently in the air-conditioned VAX machine room.

Concise versions of the compact files are transferred via a telephone link for storage and analysis at the Durham Observatory. For economy, these files contain data on only those Cerenkov events which led to a detector channel fire pattern that included a response above discrimination threshold at the on-source channel. The Observatory storage media comprise three 60 Mbyte hard discs accessed via a local area network of Acorn Cambridge Workstations, with which all data analyses are performed.

3.4.5 Routine Adjustments to Cerenkov Arrival Times

With respect to any astronomical γ-ray source, the Mark III telescope is simultaneoulsy revolving about the Earth's rotation axis once per day, the Earth-Moon barycentre approximately once per month, and the Solar System barycentre once per year. The Doppler shifting of γ-ray arrival times introduced by each of these motions can mask any periodicity which might exist in a γ-ray signal from a pulsar source.

Each of these effects must be systematically eliminated from the Cerenkov arrival time series prior to period analysis of the data. This is done by transforming the times to the rest frame of the Solar System barycentre, or centre-of-mass. In order to do this, the requirements are the geographical coordinates of the telescope site, the orbital ephemeris of the Earth, and the celestial coordinates of the γ-ray source. The latter are routinely precessed to the year 2000. Figure 3.2 shows the relevant position vectors of the site, the centre of the Earth, the Earth-Moon barycentre, the Solar System barycentre, and the source. Consider first the Doppler correction to compensate for the Earth's orbital motion. The source can be regarded as infinitley far away so that a single γ-ray pulse can be imagined as a plane wave crossing the Solar System. The Doppler correction is then simply the difference (Δt) between the arrival times of this wave at the observing site and the Solar System barycentre:

$$\Delta t = -\frac{1}{c}\,\underline{R}_{ob}.\hat{\underline{S}} \qquad (1)$$

where c is the speed of light, $\underline{R}_{ob}$ is the vector from the observing site to the barycentre, and $\hat{\underline{S}}$ is the unit vector in the direction of the source (which is identical at both the observing site and the barycentre for an infinitely distant source). The maximum Doppler correction would therefore be required if the

Figure 3.2

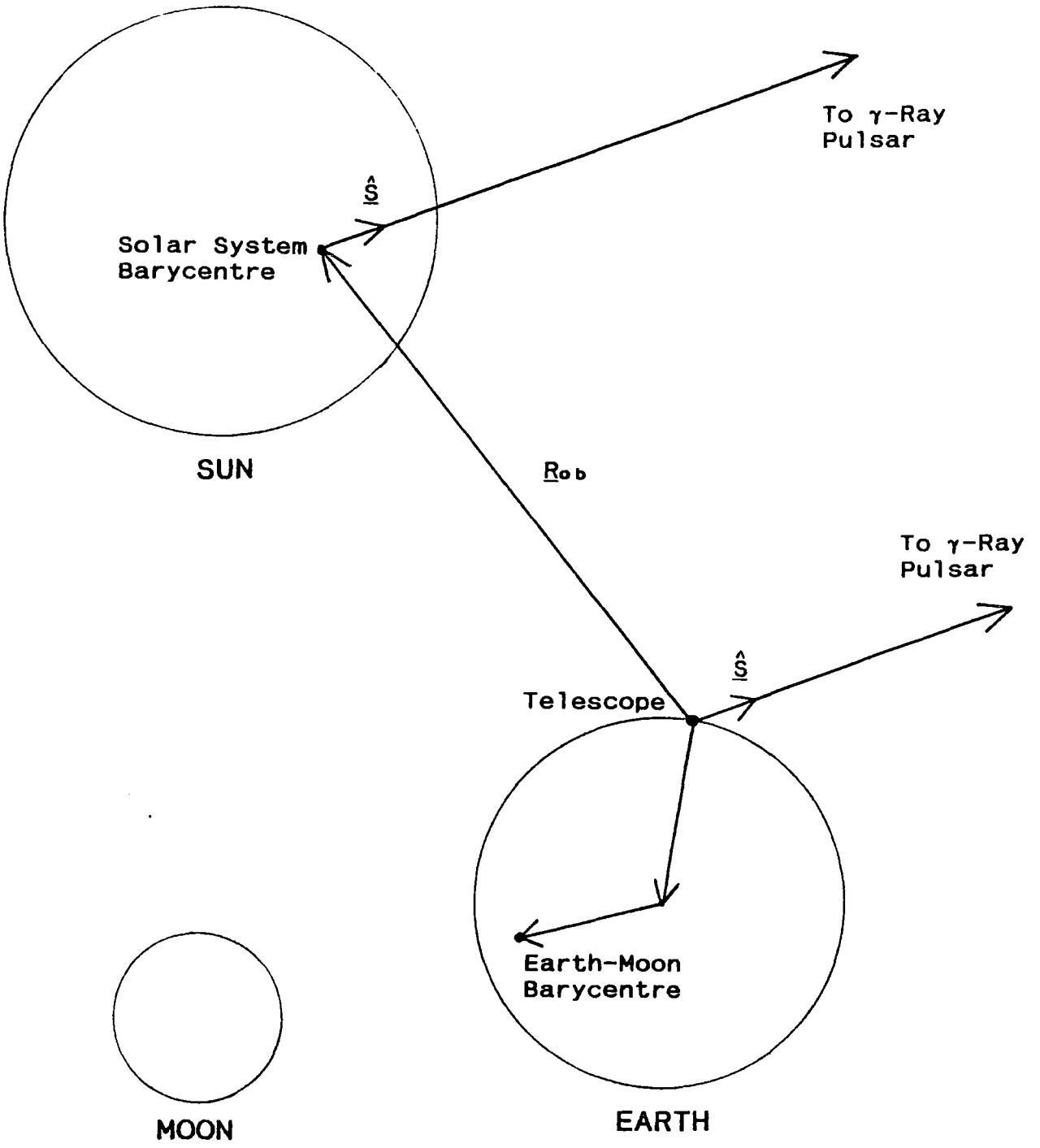

Geometry for Doppler Corrections

to Cerenkov Arrival Times

(Not to Scale)

site, barycentre and source lay upon a straight line, and would be equal to the time of flight from the Earth to the barycentre ($\Delta t \approx 500$ s). Although the Doppler shift would be instantaneously zero in such a situation, the rate of change of the shift would reach a maximum. The reverse occurs when the site, barycentre and source form a right-angled triangle. The arrival times at site and barycentre are then identical ($\Delta t = 0$), the Doppler shift is at a maximum, and the rate of change of the shift falls to zero.

The correction required for the Earth's rotation is much smaller, but it is not negligible. The radius of the Earth is approximately 0.021 light-seconds, so that the difference in arrival times over a twelve-hour period can be as high as $\approx$ 40 ms. Similarly, the Earth-Moon barycentre is located within the body of the Earth at $\approx$ 0.016 light-seconds from the centre; arrival times can therefore differ by a maximum $\approx$ 32 ms over a time interval of $\approx$ two weeks (= $^1/_2$ period of revolution), which is typical of the duration of a single dark-period (i.e. Moon-free) sequence of observations performed at the telescope site.

Finally, a general relativistic correction must be made to the arrival times. The Earth revolves in an orbit which is deep within the gravitational potential well of the Sun. Because of general relativistic time dilation, a time interval between γ-ray pulses measured at the Earth is longer than would be measured at some point displaced infinitely far from the Sun. This would be of no consequence if the Earth's orbit were circular. However,

the ellipticity of the orbit means that the difference between the near and far time intervals varies with the relative orientation of the Earth-Sun-source vectors. The peak amplitude of the corrections to the times is ≈ 3 ms. Although this is much smaller than the corrections just described, it is significant when millisecond pulsar source candidates are being studied.

All of these corrections are made by adjusting the arrival times recorded at the telescope in Coordinated Universal Time (UTC) to Barycentre Corrected Julian Ephemeris Time using the Jet Propulsion Laboratory DE200 Solar System Ephemeris (Standish 1982). This ephemeris provides the relative orientations of the Earth, Moon, and Solar System barycentre at time increments of two hours and is the standard currently adopted by the astronomical community. The accuracy of the corrections is improved by fitting a polynomial to the Earth coordinates specified for a range of times (up to one day) centred upon a given Cerenkov event time.

3.4.6 The Selection of Data for Analysis

The data recorded with the off-source guard ring detector channels are routinely processed prior to analysis in an attempt to enhance the signal-to-noise ratio. Further details of this procedure can be found in Brazier *et al.* (1989a, 1990g).

The Cerenkov light pools arising from the interaction of TeV γ-rays and cosmic rays with the atmosphere are not point-like:

they have a finite angular width $\approx 1^{o}$. First order rejection of cosmic ray background events may therefore be accomplished by restricting the acceptance angle of the telescope to a value $\approx 1^{o}$ centred upon the direction of the target. An opening angle smaller than this value would reduce the potential γ-ray detection rate, for the energy threshold of the telescope would be raised as a consequence of the reduction of the PMT cathode illumination.

The second stage of background rejection employs a quantitative assessment of the the angular distribution of a Cerenkov light pool sampled by the seven detector channels. Cosmic ray events can often occur in a direction which is just beyond the field of view of the on-source channel, but still contribute enough light to the latter to induce a response above the discrimination threshold in addition to causing a positive response at one or more of the guard ring channels. A γ-ray light pool will be centred approximately upon the target direction and will therefore be much less likely to drive a guard ring channel above threshold. In this way, the data recorded on any events which originate away from the direction of the source candidate, but nevertheless trigger the on-source channel, may be identified and eliminated prior to analysis. This rejection technique will be referred to in later chapters as the "hardware cut" since it depends upon the pre-specified setting of the PMT discrimination levels. Although approximately 60% of all events which include on-source responses above threshold are rejected, the data

analyses have indicated that few of the candidate γ-ray events appear to be lost in this process; an enhancement by a factor $\sim$ 2 in the signal-to-noise ratio is therefore obtained.

The final stage of background elimination goes beyond the simple inspection of the detector channel fire pattern and uses the individual charge pulses registered on each of the photomultiplier tubes. The threshold level for further rejection is defined by demanding the simultaneous occurrence of any off-axis response (sub-hardware threshold) which is a pre-specified fraction of the on-channel response; such a signal will be well above the sky noise, but will be of insufficient strength to exceed the hardware selection requirement for the three PMT detectors in the off-axis channel. An example might be an event which triggers the on-source channel and two of the phototubes in one of the off-axis channels, but just fails to provide a sufficient sample of light in the third tube for the channel to be included in the fire pattern. Such an event would be a strong candidate for an off-axis (cosmic ray) air shower. The threshold level for rejection has been optimised and fixed (see Brazier *et al.* 1990g) during an examination of the data recorded for the relatively strong TeV γ-ray source Centaurus X-3. This selection routinely provides a further enhancement of the signal-to-noise ratio by a factor $\sim {}^{4}/_{3}$.

3.5 Summary

An air Cerenkov telescope has been deployed and maintained by the Durham Group at a site in New South Wales, Australia. The telescope achieves a γ-ray energy threshold of 250 GeV at the zenith and has been used during almost all Moon-free periods in the four years since construction. By 1990 September it had monitored 32 Galactic and extragalactic TeV γ-ray source candidates for a total of 2660 hours.

On-site improvements in the performance of the telescope have included (i) the extension of the dynode chain in each of the photomultiplier tubes to increase the overall gain; (ii) additions to the signal processing hardware for the off-axis guard ring of detector channels to provide discrimination and tests for three-fold coincidence on all channels. An average count rate of ≥ 130 min^{-1} is currently achieved on each channel when monitoring the zenith under good observing conditions.

A smaller telescope based on the same design - the Mark IV - has been operated for two summertime observing seasons at the island of La Palma, Canary Islands during 1988 and 1989. The combined area of the three Mark IV flux collectors is approximately half that of the Mark III telescope. The acceptance angle is $\approx 1^{\circ}$, similar to that of the Mark III. A zenithal count rate of 90 min^{-1} channel^{-1} is acheived and the threshold γ-ray energy at the zenith is estimated to be $\approx$ 400 GeV. The Mark IV was shipped to Australia in early 1990 to join the Mark III telescope at Narrabri. Although the operation of

the two telescopes at the same site already offers a greatly improved monitor for the Southern Hemisphere γ-ray sources, it is hoped that they will be just the first components of an array of up to ten instruments.

Chapter 4

Techniques for the Period Analysis of Air Cerenkov Arrival Time Series

4.1 Introduction

Tests for periodicity in time series are considered here in preparation for the pulse timing analyses of the Narrabri air Cerenkov databases presented later in this work. The statistical tests employed for the analysis of unpulsed γ-ray source measurements have been discussed recently by Rayner (1989).

The majority of claims for the detection of pulsed TeV γ-rays from astronomical sources are made with signal-to-noise ratios at the $\sim$ 1 % level. A typical periodic γ-ray signal is therefore dominated by counting statistics so that it is not usually possible to recognise a regular modulation of an experimental time series simply by, for example, plotting binned counts as a function of time*. Sensitive statistical tests must instead be applied to the data in order to have any chance of successfully

*The only direct observation of periodicity is that claimed by the Potchefstroom Group (Raubenheimer *et al.* 1989) who have monitored the high-mass X-ray binary Vela X-1 at a threshold energy of 1.5 TeV; evidence is presented for the transient modulation of counts with the five-minute rotation period of the neutron star.

identifying a periodic component in the presence of the strong, random cosmic ray background.

The standard flow of operations in analysing data for periodicity is shown in Figure 4.1. The pre-analysis processing of the data includes the transformation of arrival times to the Solar System barycentre and, in the case of a γ-ray source candidate in a binary, the further transformation of times to the binary rest frame. Period analyses begin by folding, or superimposing, the transformed times onto the phase interval 0 $\longrightarrow 2\pi$ (or 0 $\longrightarrow$ 1) using candidate values for the pulse period and its time derivatives (if any). (The pulse parameters of a γ-ray source candidate are usually taken from the results of measurements at lower energies). The phase (φ_i) assigned to an event recorded at time t_i is just

$$\varphi_i = \varphi(t_o) + \frac{2\pi}{P}(t_i - t_o) \qquad (\mathrm{mod}\ 2\pi) \qquad (1)$$

where P is the pulse period being tested. Higher order terms may be included in the Taylor expansion when a source is expected to have first and second pulse period derivatives:

$$\varphi_i = \varphi(t_o) + 2\pi(t_i - t_o)\frac{1}{P} - \pi(t_i - t_o)^2\frac{\dot{P}}{P^2} + \pi(t_i - t_o)^3\frac{1}{3}\left[\frac{2\dot{P}^2}{P^3} - \frac{\ddot{P}}{P^2}\right] \qquad (2)$$

Figure 4.1

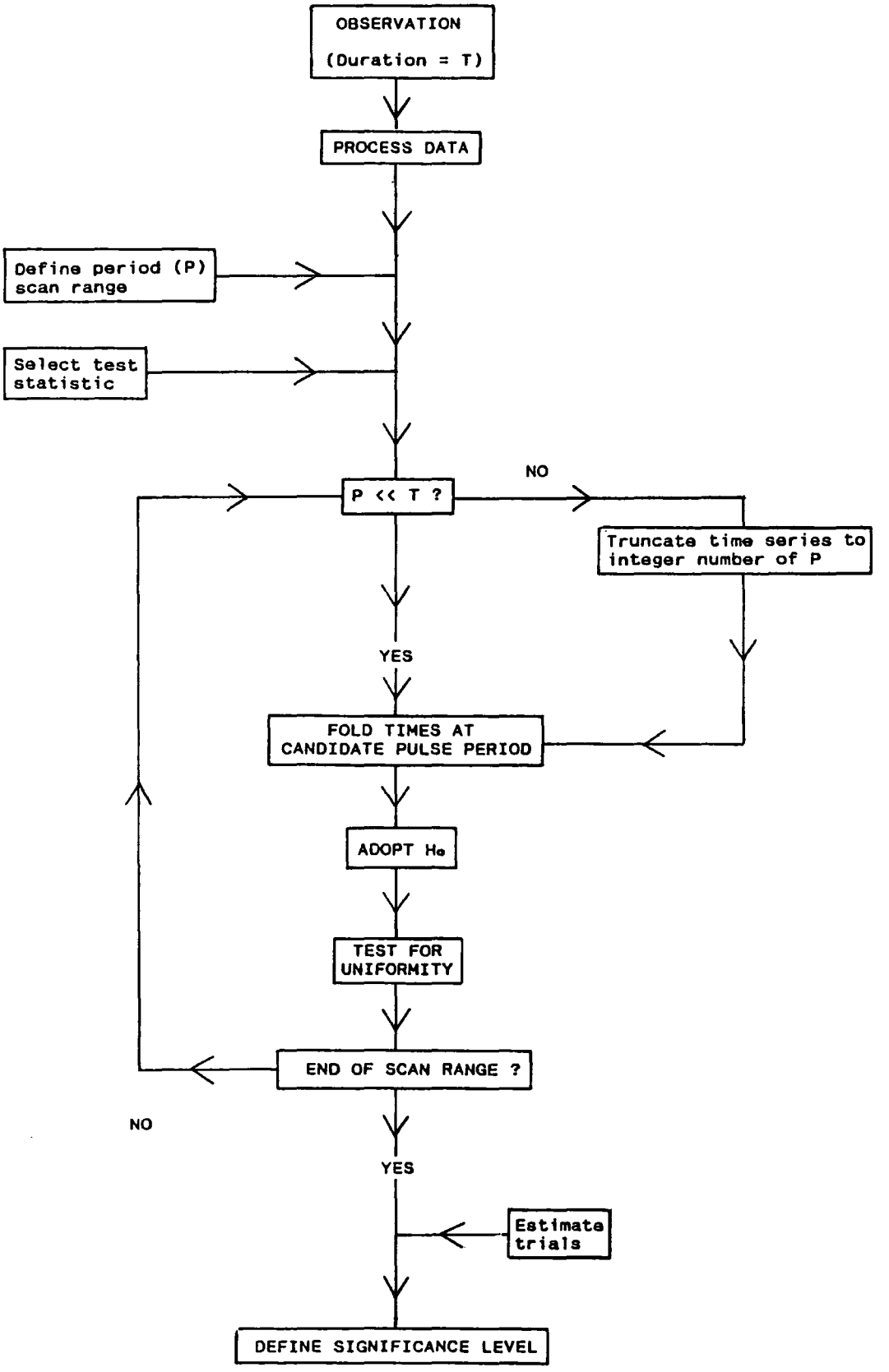

Flow of Operations for Time Series Period Analysis

Since only the relative pulse phase is usually considered, the initial phase may be set to $\varphi(t=t_0 \equiv 0) = 0$.

Periodicity is in fact searched for by testing for the absence of a signal. In other words, the null hypothesis is adopted:

> H_0: the arrival times are purely random and consequently exhibit a uniform distribution of phase at all periods

The test for periodicity is therefore performed by testing for uniformity of phase, and the statistical significance of any periodic component identified in a time series is expressed formally as the degree of confidence with which the null hypothesis may be rejected.

Note that a false rejection of the null hypothesis can occur when the value of a candidate pulse period (P) is a significant fraction of the duration (T) of a time series. The ratio T/P is not usually an integer so that, as $T/P \longrightarrow 1$, a noticeable set of residual phases is automatically built up when the time series is folded. When necessary, this problem can be easily avoided by truncating the time series to a length NP (where N is an integer) before testing for a uniform distribution of phase.

Suppose that a periodic component is in fact present in a time series: the pulse "light curve" is the name given to the resulting shape of the phase distribution. Should the periodic component be a genuine signal of γ-ray emission, then the light

curve might have a broad peak in the case of a pulsar which emits observable γ-rays during a large fraction of each rotation, and a narrow peak if the source beaming is tight. The light curve may also be multiply peaked. There are several methods for testing for uniformity in a phase distribution and the "power" of any given method is defined as the level of confidence that it will not lead to a false acceptance of the null hypothesis; unfortunately, the power varies from test to test and depends upon the shape of a light curve. The number of TeV γ-ray sources discovered is small and many of the details of the radiation production mechanisms (beaming, for example) have still to be worked out. Consequently, an *a priori* assumption concerning the shape of a pulse light curve is not possible and the optimum test for uniformity cannot be selected objectively before beginning the period analysis of a time series.

The most useful test is therefore the one which can identify periodic components with the largest variety of light curve shapes. The three most commonly used tests will be considered in this chapter. These are

(i) χ^2 test with k pulse phase bins; suffers from a bias towards light curves of phase width $\approx 2\pi/k$;

(ii) the Z^2_m-test, which involves summation of the powers at the first m harmonics of a candidate pulse frequency; the powerful Rayleigh test is a special case of this test and is obtained by taking m = 1;

(iii) the Protheroe test; this is a specialised test for very narrow light curves. It can also be used to search for modulation of time series with the orbital period of an X-ray binary source candidate in cases where the duration of the γ-ray emission might be only a small fraction of the orbital period.

These three tests are described in Section 4.2. The finite sampling intervals between independent candidate values of pulse period and pulse period derivative are defined and quantified in Section 4.3.1. When estimating the significance level, a correction must be made in order to account for the number of independent trials performed: this is considered in Section 4.3.2, together with the effect of oversampling in the values of pulse period. Section 4.4 is concerned with the procedures adopted by the Durham Group for the routine period analysis of data obtained at Narrabri.

A useful general reference is Eadie *et al* (1971); Mardia (1972) and Batschelet (1981) have examined the statistics of circular (phased) data; the application of circular statistics to data analysis in TeV and PeV γ-ray astronomy has been discussed by Gibson *et al.* (1982), de Jager (1987), de Jager *et al.* (1988), Protheroe (1988), Buccheri and de Jager (1989), de Jager, Swanepoel and Raubenheimer (1989), and Swanepoel and de Beer (1990).

4.2 Tests for Uniformity of Phase

4.2.1 χ^2 Test with k Phase Bins

Pearson's χ^2 test examines whether the expected limiting distribution of a set of experimental measurements is in agreement with the observed results of the actual experiment. In the present context, the expected distribution is the uniform distribution. The test was first applied to the analysis of Cerenkov event time series in the late 1960s (e.g. Charman *et al.* 1968 and Fazio *et al.* 1968) and was later used to search for periodicities in the data obtained during observations of lower-energy γ-rays with the satellite experiments (e.g. Leahy *et al.* 1983; Leahy, Elsner and Weisskopf 1983). Let an experimental time series corresponding to n events be folded at a candidate period P. Pearson's test is applied by approximating the phase distribution by a histogram consisting of k phase bins of equal width, such that $k\Delta\varphi = 2\pi$. For a random time series the number populating each bin will be Poisson distributed with an expected number of times $\mu = n/k$ and variance $v = \mu$. If O_i is the number of events actually observed in the i^{th} phase bin the statistic

$$S = \sum_{i=1}^{k} \frac{(O_i - n/k)^2}{n/k} \qquad (3)$$

is then distributed as χ^2; the number of degrees of freedom

is k-1 rather than k since the average has been determined from n and k. If the value of χ^2 is 0 then the agreement with the expected uniform distribution is perfect and the times are randomly distributed. More likely, in the absence of a periodic component, the individual terms in the summation on the right-hand-side of equation 3 will be ~ unity $\{O_i \approx n/k \pm \sqrt{(n/k)}\}$ so that significant deviations from uniformity correspond to

$$\chi^2 \gg k, \text{ the number of phase bins} \qquad (4)$$

The statistical significance of a periodic component recognised in the data is expressed as the probability for uniformity (≡ probability that any periodicity observed has arisen by chance):

$$Pr(H_o \text{ is true}) = Pr_d(\chi^2 > \chi_o^2) \qquad (5)$$

where d is the number of degrees of freedom, and χ_o^2 is the observed value of the statistic; Pr_d can be obtained by reference to standard tables. Note that the tabulated probabilities assume a Gaussian distribution, to which the Poissonian distribution of the discrete times within the phase bins is well approximated only when the ratio n/k is large. The lower limit to this ratio is usually taken to be around 5 (e.g. Taylor 1982); if $n/k \leq 5$ the test statistic given by equation 3 is not distributed as χ^2 and the tabulated χ^2 probabilities cannot then be used to state the confidence with which H_o is rejected.

There are two difficulties with this test for uniformity:

i) Number of Bins

The selection of the number of phase bins automatically determines the shape of the pulse light curve to which the test will be most sensitive. The value of χ^2 will deviate most from k if the majority of the residual phases are confined to a single phase bin, so that the sensitivity of the test is greatest for light curves of pulse phase width $\approx 2\pi/k$. The choice of just a few bins therefore implies a search for broad light curves whereas the use of many bins will select out only narrow or multiply peaked light curves. False acceptance of the null hypothesis can therefore occur (and a genuine pulsed γ-ray source missed) in the absence of any knowledge of the light curve shape before the number of bins is chosen. On the other hand, *a posteriori* selection of the optimum number of bins after testing with some suitably wide range of values of k must be treated with caution: the number of values of k sampled has to be remembered when making the final assessment of the statistical significance of the result.

ii) Bin Origin

Even with a fixed number of bins, the power of the test can be weakened by a poor choice of where to start the binning. For the reason noted above, the bin origin should be chosen so that as much as possible of the peak of the pulse light curve lies within a single bin. Again, care must be taken: if the bin origin is

chosen by optimisiation, then the significance of the result is less than would have been the case had the origin been selected *a priori*. Such a selection is unfortunately not often possible since the absolute pulse phase is rarely known.

4.2.2 The Z^2_m-Test

Rather than approximate the distribution of the residual phases by a histrogram - and dealing with the attendant problems introduced by binning - a better method is to inspect the magnitude of the mean phase vector constructed when a time series is folded. Imagine the pulse phase interval $0 \longrightarrow 2\pi$ on a circle of unit radius: any given event time (t_i) can then be represented by a unit vector drawn from the centre of the circle and directed according to the appropriate phase value (φ_i). See Figure 4.2. The horizontal and vertical components of this vector are just:

$$x_i = \cos\varphi_i \qquad (6a)$$

$$y_i = \sin\varphi_i \qquad (6b)$$

A time series corresponding to n events will therefore fold to give a mean vector of magnitude

$$R = \frac{1}{n}\sqrt{\left[\sum_{i=1}^{n}\cos\varphi_i\right]^2 + \left[\sum_{i=1}^{n}\sin\varphi_i\right]^2} \qquad (7)$$

Figure 4.2

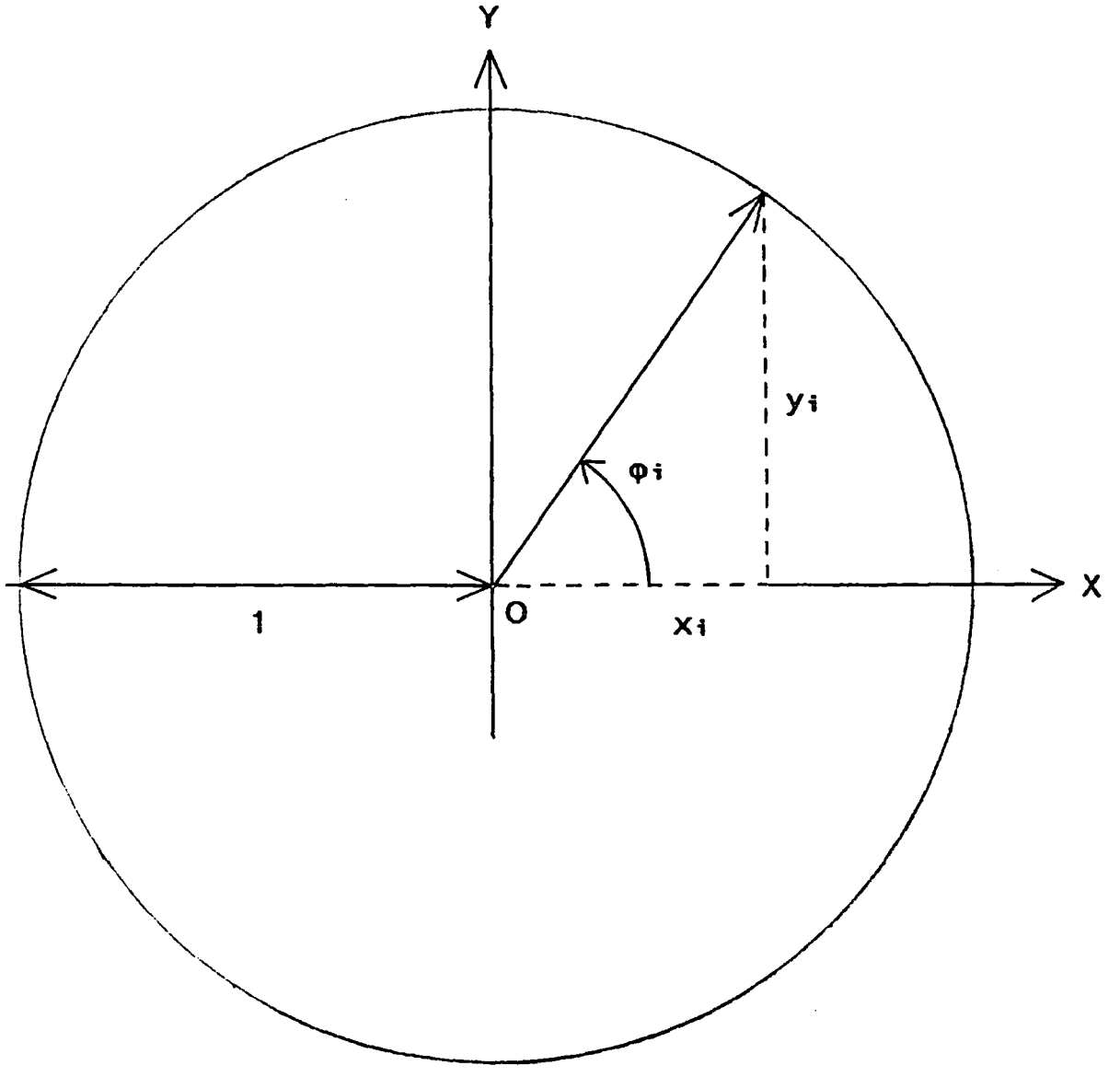

Components of Unit Vector

which will be approximately zero ($\sim 1/n$) if the times are randomly distributed. If periodicity is present then there will be a clustering of a fraction of the phases about some preferred phase, so that the value of R in equation 7 can be used to examine the data for one-sidedness, or directedness, in an effort to test the null hypothesis. The Z^2_m-test for uniformity includes the first m harmonics of the candidate pulse period and uses the test statistic

$$Z^2_m = \sum_{j=1}^{m} 2nR^2 \qquad (8)$$

$$= \frac{2}{n} \sum_{j=1}^{m} \left[\left[\sum_{i=1}^{n} \cos j\varphi_i \right]^2 + \left[\sum_{i=1}^{n} \sin j\varphi_i \right]^2 \right] \qquad (9)$$

When n is large, this statistic is distributed as χ^2 with 2m degrees of freedom, with the factor of 2 entering because the horizontal and vertical components of the unit vectors (i.e. the cosine and sine terms in the summations) follow independent Gaussian distributions. Buccheri *et al.* (1983) used this statistic to search for pulsed γ-rays from radio pulsars observed with the COS-B satellite and suggested that Z^2_2 is the optimum *a priori* choice when the shape of the pulse light curve is unknown. (de Jager *et al.* (1988) and de Jager, Swanepoel and Raubenheimer (1989) have used the Z^2_m statistic as a basis for a new test, the H_m-test, in which the value of m is optimised using the

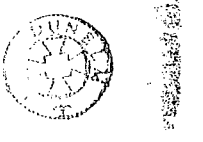

experimental data prior to performing a test for uniformity).

The Rayleigh test employs the same statistic to test for periodicity at the fundamental only and was first proposed by the Durham Group (Gibson *et al.* 1982) as a method of searching for pulsed TeV γ-rays. With m = 1, the Z^2_m statistic is distributed as χ^2 with 2 degrees of freedom and the χ^2 probabilities reduce to the exponential function:

$$\Pr(H_o \text{ is true}) = \Pr(\chi^2 > \chi^2_o) = \exp(-nR^2) \qquad (10)$$

More accurately (and necessary for $n < \sim 40$), the probability for uniformity may be computed using the result of Greenwood and Durand (1955):

$$\Pr(H_o \text{ is true}) = \exp(-z)\left[1+(2z-z^2)/4n - (24z-132z^2+76z^3-9z^4)/288n^2 - \left[1440z+1440z^2-8280z^3+4890z^4 - 870z^5+45z^6\right]/17280n^3\right] \qquad (11)$$

where $z = nR^2$.

The Rayleigh test represents an attempt to correlate an experimental time series with a sine wave that is modulated with

the candidate pulse period. It is therefore primarily sensitive to broad, uni-modal (single-peaked) light curves; false acceptance of the null hypothesis can occur when a light curve is narrow or multiply peaked. For the simple case of a light curve which displays a strong interpulse located midway between consecutive maxima, the problem may be visualised as a near cancellation of the phase vectors and the consequent suppression of the magnitude of the resultant vector, although this particular example could be rectified by performing the Rayleigh test at half the expected period.

The Rayleigh test is straight-forward and requires only moderate CPU times. Though the Z^2_2 is more powerful against narrow peaks, the Rayleigh test is superior for broad light curves. It is therefore a very useful test in the absence of *a priori* knowledge of the light curve shape and has been adopted by the Durham Group as the standard test for uniformity of phase.

4.2.3 The Protheroe Test

Protheroe (1985) has proposed another circular statistic, but one which offers a test for periodicity in cases where the light curve has a very narrow peak. The requirements of such a statistic are:

(i) that it should be sensitive to the separation of pairs of phase values in such a manner that it takes higher values when

more phase points are closer together than expected for a random series;

(ii) it should be sensitive to a grouping of several points in the same phase region;

(iii) the sensitivity to small separations between pairs of points should not be so great that the statistic is dominated by the presence of the chance proximity of a pair.

Protheroe defines the phase separation of a given pair of points i and j by

$$\Delta_{ij} = 0.5 - | (|(\varphi_i - \varphi_j)| - 0.5)| \qquad (12)$$

Taking the average of $^1/\Delta$ over *adjacent* pairs satifies requirement (i); averaging $^1/\Delta$ over *all* pairs satifies requirement (ii); the expected average separation of n random points is just $^1/_n$: obtaining the average of $(\Delta + {}^1/_n)^{-1}$ over all pairs therefore satifies requirement (iii). The statistic is then constructed using:

$$T_n = \frac{2}{n(n-1)} \sum_{i=1}^{n-1} \left[\sum_{j=i+1}^{n} (\Delta_{ij} + {}^1/_n)^{-1} \right] \qquad (13)$$

Protheroe (1985) has computed the null (random) distribution of this statistic using Monte Carlo methods for a number of events n ranging from 2 to 200. de Jager (1987) has pointed out that the T_n statistic is a special case of one first derived by Hoeffding (1948) which asymptotically approaches the χ^2 distribution when n is large; computations of the probabilitiy for uniformity may therefore be easier at larger n and de Jager suggests a lower limit of n = 300.

The Protheroe test has three disadvantages:

(i) The sensitivity diminishes rapidly as the light curve becomes broader, thereby introducing the possibility of false acceptance of the null hypothesis. (This is mirrored, though to a lesser extent, by the increasing likelihood of falsely accepting the null hypothesis when the Rayleigh test is performed on increasingly narrow light curves).

(ii) The statistic is sensitive to false phase groupings caused by the computation of phases to a finite number of significant digits (Protheroe 1988).

(iii) The number of steps which are necessary to construct T_n increases as n^2 - observe the nested summation in equation 13 - which leads to large CPU time requirements when the number of events is large.

The Protheroe test is, however, one of the most sensitive tests known for narrow-peaked light curves and has been successfully applied by PeV γ-ray astronomers. Evidence for orbitally modulated PeV emission from the high-mass binary LMC X-4 was found by Protheroe and Clay (1985) using the Protheroe test. Air shower arrival times were folded with the orbital period of the binary, after which the statistic was used to test for a uniform phase distribution. An excess in the distribution was found in the orbital phase interval 0.90 to 0.95 (where phase 0 is X-ray mid-eclipse), corresponding to entry of the neutron star into eclipse by the companion. The Protheroe test was also employed by Dingus *et al.* (1988, 1989) to discover a periodic component in two bursts of PeV air showers recorded with the CYGNUS experiment during observations of the low-mass binary Hercules X-1. The test identified narrow pulses at a period close to the contemporary value of the X-ray pulse period.

4.2.4 Other Tests for Uniformity

The χ^2 test with k phase bins, the Z^2_m-test and the Protheroe test are the most popular for period analysis in TeV and PeV γ-ray astronomy at this time. However, a number of other tests are sometimes used and these are noted briefly here. Each have been discussed by Mardia (1972) and Batschelet (1981).

The Hodges-Ajne test (Hodges 1955, Ajne 1968) can be used to search for broad, sinusoidal light curves. It consists of

binning the phases of a folded time series into two bins, each of width π, and sliding the bin orgin until the number of events in either bin reaches a minimum. Cressie (1977) proposed a modification which permits a search for narrow light curves. A narrow phase bin is selected *a priori* and has a width corresponding to the width of the proposed light curve. It is then slid across the phase distribution until it contains a maximum number of events. Watson's U^2 test (Watson 1962) employs a statistic formed by taking the sum of the squares of the deviations of the observed phase distribution from the expected distribution (which is the random distribution here); since it uses the full 2π range in phase, it is better suited to searches for broad light curves. In Kuiper's test (Kuiper 1960), the maximum and minimum deviations of two distributions are searched for, so that this test is more powerful for light curves with narrow peaks. The V-test is a modified Rayleigh test and may be used when absolute pulse phase is known. This test was introduced by Greenwood and Durand (1955) and is designed to decide whether an observed phase distribution tends to cluster about a hypothetical direction specified *a priori*. In the present application, the mean phase vector produced by folding a time series can be projected onto a hypothetical unit vector predicted using an accurate pulsar ephemeris; the closer is the projection to +1 or -1, the greater is the clustering of phases about the expected direction.

4.3 Independent Sampling Intervals and Corrections for the Number of Trials Performed

4.3.1 Sampling Intervals for P and $\dot{P}$

A short range of candidate values of pulse period is often employed when testing a time series for periodicity. This may be done in order to allow for uncertainties (δP, $\delta \dot{P}$) in a radio or X-ray pulsar ephemeris. In the case of binary source candidates, uncertainties may also be introduced when using a published set of orbital parameters to compensate for the Doppler shift of the pulse period caused by the orbital motion of the source.

The question addressed here is the number of values of period across any given range, say P_1 to P_2, which should be sampled when performing a test for periodicity. Associated with any time series of finite length is a non-zero interval between period values, within which candidate periods are indistinguisable. To see this, return to the pulse phase relation of equation 1. Let the phase interval here be 0 ——> 1 so that for a candidate pulse period P the phase number at some time t is

$$\varphi_i = \varphi_o + \frac{t-t_o}{P} \qquad (14)$$

Allow the time series to begin at time t_i and let it end at time

t_f. The difference between the final and initial phase numbers is then

$$\varphi_f - \varphi_i = \frac{1}{P}(t_f - t_i) \qquad (15)$$

Keeping t_i and t_f fixed and altering the value of P to some value P*, it is clear that the increment required to significantly change P is that which sends the initial and final values of φ to φ'_i and φ'_f such that

$$(\varphi'_f - \varphi'_i) - (\varphi_f - \varphi_i) = 1 \qquad (16)$$

Equations 15 and 16 give

$$(t_f - t_i)\frac{(P - P^*)}{PP^*} = 1 \qquad (17)$$

or

$$\Delta P = \frac{PP^*}{\Delta t} \approx \frac{P^2}{\Delta t} \qquad (18)$$

The increment ΔP is therefore the interval between independent candidate values of the pulse period. Thus, even if the expected value of the period is well known, there remains a finite range $P-\Delta P \leq P \leq P+\Delta P$ which must be sampled in order to recover the full pulsed signal strength. A simple approach to this result is

just to compute the nearest integer number of period cycles within the duration of the time series, i.e. $\Delta t/P$, and to multiply this by the fractional increment in P, $\Delta P/P$, required to provide an accumulated phase error of one cycle:

$$\frac{\Delta P}{P} \frac{\Delta t}{P} = 1$$

which is equivalent to equation 18.

If a pulsar ephemeris includes a non-zero value of pulse period derivative $\dot{P}$, the independent sampling interval $\Delta\dot{P}$ can be found by expanding the phase relation in equation 14:

$$\varphi = \varphi_o + \frac{t-t_o}{P} - \frac{\dot{P}}{2}\frac{(t-t_o)^2}{P^2} \qquad (19a)$$

and

$$\varphi' = \varphi_o + \frac{t-t_o}{P} - \frac{\dot{P}^*}{2}\frac{(t-t_o)^2}{P^2} \qquad (19b)$$

where the value of P is held constant. Substitution from equations 19a and 19b for the two sets of initial and final pulse phase numbers in equation 16 gives

$$\dot{\Delta P} = 2 \left[\frac{P}{\Delta t} \right]^2 \qquad (20)$$

So, athough the signal-to-noise ratio for persistent sources improves as $\sqrt{\Delta t}$, the sensitivity to errors (δP, $\delta \dot{P}$) in the pulse ephemeris increases much more rapidly: directly with Δt in the case of P, and with $(\Delta t)^2$ for $\dot{P}$.

4.3.2 Number of Trials

If candidate values of pulse period are sampled across a range P_1 to P_2 then the number of independent values of period within this range is equal to the number (N) of independent trials made. This must be taken into account when stating the confidence with which the null hypothesis is rejected: in other words, the probability (Pr) for uniformity must be multiplied by the number of trials. This is not the complete truth, however, if the chosen test statistic has been evaluated more than once within each of the period sampling intervals. The product NPr must then be multiplied by a further factor $r > 1$. Orford (1990) has quantified the variation of the value of r with increasing values of the Rayleigh statistic (see also Section 4.2.2 earlier) and finds that a value ≈ 3 is approached asymptotically. A

conservative value of r = 3 will be taken during the analyses described in the present thesis.

4.4 Routine Period Analyses of the Narrabri Database

The χ^2 test is used by the Durham Group to test for uniformity in the rare case when absolute pulse phase is known (e.g. the Crab pulsar). The Rayleigh test is employed for the remainder of the radio and X-ray pulsar source candidates.

Often the outcome of separate period analyses of independent time series are directly combined. During a typical dark period T ~ 2 weeks, a given γ-ray source candidate is usually monitored from Narrabri on ~ 10 occasions, each lasting for a time $\Delta t \approx 3$ hours. The value of the secular pulse period derivative is, for most of the source candidates observed to date, insufficient to change the value of the expected pulse period (P) significantly during a single dark period; i.e. it is usually the case that $T\dot{P} < P^2/\Delta t$. Each time series may then be tested across a fixed set of trial pulse periods and the independent probabilities for uniformity at a given candidate period combined. Let there be N time series: the combination of probabilities (Pr) at some test period P_i is obtained by taking their product and constructing the statistic

$$C_i = -2 \log_e \prod_{j=1}^{N} Pr_j(P_i) \qquad (21)$$

which, under the null hypothesis, is distributed as χ^2 with 2N degrees of freedom (Eadie *et al.* 1971). So, by evaluating the combined probability

$$\text{Pr (null hypothesis is true)} = \text{Pr} \left({}_{2N}\chi^2 > C_i \right) \qquad (22)$$

an overall statement of the result of the test for phase uniformity in the N time series can be made.

Chapter 5

Accreting Neutron Stars in X-Ray Binary Systems

5.1 Introduction

Of the X-ray binary systems which are believed to contain an accreting neutron star, approximately 10 % have now been claimed to be sources of TeV γ-ray emission; they constitute the dominant category of known high-energy γ-ray sources at this time.

Chapters 7 to 10 of this thesis will be concerned with the analysis of the Narrabri databases accumulated for the high-mass X-ray binary SMC X-1 and the low-mass binaries X0021.8-7221 and GX 1+4. A comparison of the observed characteristics of TeV γ-ray emission from X-ray binaries in general will then be made in Chapter 11, together with a discussion of the restrictions imposed on models of production mechanisms. Before presenting these new results, it will be useful to consider some of the basic properties of X-ray binary systems. Section 2 of the present chapter provides a brief description of their classification and general features. A concise treatment of the energetics of mass transfer in binaries is given in Section 5.3.

5.2 The Two Populations of X-Ray Binaries

5.2.1 Introduction

Recent reviews of X-ray binaries are provided by Nagase (1989), Ogelman (1989), van Paradijs (1989), and White (1989).

The high-mass and the low-mass X-ray binary systems (HMXRB and LMXRB) form two distinct Galactic populations. The differences in the properties exhibited at X-ray energies by these two populations are believed to be a direct result of the great differences in the ages and, therefore, the magnetic field strengths of the neutron star components. Approximately 100 X-ray sources thought to contain accreting neutron stars in binary systems have been observed. Half of these sources have known binary periods and one third have been found to contain X-ray modulation which is attributed to neutron star rotation. The X-ray luminosities range from $\sim 10^{33}$ to $\sim 10^{39}$ ergs s^{-1}. The lifetimes of the X-ray sources in the high-mass and the low-mass systems are believed to be $\sim 10^4$ - 10^5 yr and $\sim 10^8$ - 10^9 yr, respectively. Given that approximately equal numbers of sources are seen in both populations, the formation rate of the high-mass X-ray binaries must be $\sim 10^4$ times that of the low-mass systems. The low-mass stars outnumber the high-mass stars by a factor $\sim 10^2$, so that the likelihood for the formation of an X-ray binary in the high-mass systems must be $\sim 10^6$ that for the low-mass binaries.

The locations of the optically identified HMXRB and LMXRB are plotted in Galactic coordinates in Figure 5.1. The massive binaries (upper diagram) are distributed almost uniformly along the Galactic plane and are restricted to a very narrow band in latitude. (Also shown are the several HMXRB observed in the Magellanic Clouds). In contrast, the low-mass binaries (lower diagram) are more concentrated in the general direction of the Galactic bulge and populate a much wider spread in latitude. These distributions are consistent with the idea that the optical counterparts of the HMXRB and LMXRB are, respectively, just small subsets of the young disk Population I stars and the much older Population II stars found in both the Galactic bulge and the disk.

5.2.2 The High-Mass X-Ray Binaries

The high-mass binary systems may be sub-divided into two groups according to the optical luminosity class of the companion star. See White (1989). The two groups comprise:

i) Supergiant X-ray binaries. Here the spectral type of the optical companion is earlier than B2 and the luminosity class lies in the range I to III. Such stars have evolved off the main sequence and either fill, or are close to filling, their Roche lobes.

ii) Massive Be binaries. The primary is a B-emission (Be) star located close to the main sequence in the Hertzsprung-Russell

Figure 5.1

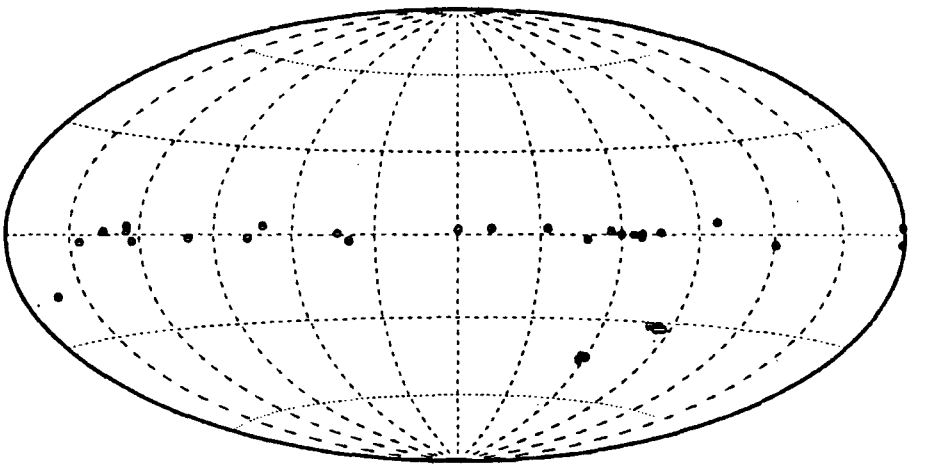

HIGH-MASS X-RAY BINARIES

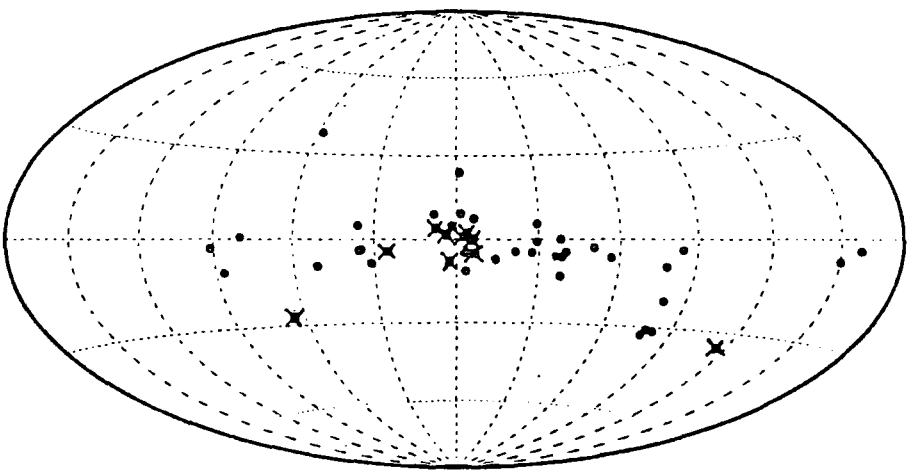

LOW-MASS X-RAY BINARIES

(Globular cluster sources indicated by crosses)

Sky-Maps (Galactic Coordinates) of the Optically Identified X-Ray Binaries

(From van Paradijs 1989)

diagram. The orbits of Be binaries tend to be eccentric and have long periods; the primary stars do not fill their Roche lobes.

(i) Supergiant X-Ray Binary Systems

Ten of the twelve known SXRB systems have been found to contain X-ray pulsars, including the SMC X-1 binary studied in the present work. The parameters of these binaries are listed in Table 5.1. For each entry, the Table includes Galactic coordinates, the X-ray pulse period and, where known, the distance to the source and the X-ray luminosity. Orbital elements and details of the optical counterparts are also listed.

At optical wavelengths, almost all of the SXRBs show a double-peaked orbital light curve with generally equal maxima at the orbital nodes (X-ray phases 0.25 and 0.75), a minimum at inferior conjunction (phase 0.5) and a second, deeper minimum at X-ray eclipse (phase 0). Such variations are the result of rotational and tidal distortion of the shape of the primary and a non-uniform surface brightness distribution. The amplitudes of the emission near phases 0 and 0.5 provide information on the relative contributions from optical emission generated by X-ray heating of the surface of the primary, and, if present, that arising from X-ray heating of an accretion disk about the neutron star.

Table 5.1

Name	Galactic Coordinates		X-Ray Pulse Period	Distance	L_x	Orbital Parameters				Optical Component			Remarks
	l (°)	b (°)	(s)	(kpc)	(ergs s^{-1})	P (d)	$a_x \sin i$ (ls)	e	i (°)	Name	Spectral Type	Luminosity Class	
1E1024-5732	284.5	-00.2	0.0693	< 3	10^{34}-10^{36}	-	-	-	-	Wack 2154	O5	-	Wolf-Rayet Primary ?
SMC X-1	300.4	-43.6	0.7105	65	0.5-3 10^{39}	3.893	53.46	<0.007	64.5 ± 4.5	Sk 160	B0	I	High & low X-ray states (P-60 d)
Cen X-3	292.1	+00.3	4.823	8	10^{38}	2.09	39.8	<0.0008	82-85	Krz V779 Cen	O6-8f	II-III	QPO source
LMC X-4	276.3	-32.5	13.49	50	6 10^{38}	1.408	26	<0.02	68^{+11}_{-9}		O7	III-V	30.4-d X-ray & optical cycles
OAO 1657-415	344.4	+00.3	38.2	1-5	0.3-6 10^{38}	-	-	-	-	-	-	-	
Vela X-1	263.r	+03.9	283	2	5 10^{36}	8.97	113	0.089	83±6	HD 77581	B0.5	Ib	
4U1145-614	295.5	00.0	297	8	3 10^{34}	5.6?	-	-	-	-	B1	I	
4U1907+097	43.7	+00.5	438	7	4 10^{37}	8.38	83±3	0.22±0.05	-	-	OB	I	
4U1538-522	327.4	+02.1	529.8	7	4 10^{36}	3.7283	52.8±1.8	-	71^{+13}_{-11}	QV Nor	B0	I	
GX 301-2	300.1	-2.0	696	1.8	3 10^{36}	41.508	371.2±3.3	0.472±0.011	-	Wray 977	B1.5	Ia	

Pulsars in Supergiant X-Ray Binary Systems

The X-ray luminosities of the SXRBs are observed in the range $\sim 10^{36}$ to $\sim 10^{39}$ ergs s^{-1}. The neutron star component of these systems orbits typically within a few stellar radii of the OB supergiant companion and is therefore often deeply embedded within the strong stellar wind of the massive primary. The gravitational capture of a fraction of this high velocity wind by the neutron star would be sufficient to power the lower luminosity systems. An enhanced mass flow to the neutron star is required to drive the highest luminosity SXRBs, which may indicate that the supergiant primary has begun to fill its Roche lobe. Adequate mass flow could also be provided by a focusing of the wind in the direction of the neutron star from a supergiant that is just close to filling its Roche lobe.

The X-ray pulse periods of the highest luminosity systems are in the range 1-15 s, whereas those pulsars with periods in excess of ~ three minutes tend to have lower X-ray luminosities. (1E1024-5732, currently the shortest period XRB pulsar known, is an exception). The higher luminosity pulsars exhibit a long-term decrease in the value of the X-ray period. This is attributed to a spin-up of the neutron star and is thought to be due to a sustained accretion torque which orginates in a disk of material about the neutron star. The disk is fed by Roche lobe overflow from the massive primary. Stellar wind-driven binaries display no long-term trend. Instead, they undergo a random walk in the value of the pulsar period, possibly as a consequence of time-dependent fluctuations in the stellar wind flowing past the neutron star.

(ii) **Be X-Ray Binaries**

The massive B-emission stars rotate very rapidly. The centrifugal acceleration at their surfaces almost balances the acceleration due to gravity. Such stars are therefore close to disruption. Mass transfer to the neutron star occurs as a result of the anisotropic ejection of matter from the equatorial region of the primary.

Table 5.2 provides details of the thirteen known Be X-ray binary pulsars. The Be XRBs fall into two classes: transient and persistent X-ray sources.

i) Transient: examples of this class are 4U0115+634, 4U1553-542 and EXO2030+375 (White 1989 and references therein). Orbital periods of a few tens of days are observed, together with moderate orbital eccentricities $e \sim 0.3$. Most of the transients show a rapid decrease in the value of the X-ray pulse period, suggesting the presence of an accretion disk. The outbursts of X-ray emission are thought to be a consequence of episodes of mass ejection from the massive primary. Some of the transients show regular (Type I) outbursts which repeat with the period of the orbit and which entail an increase in the X-ray luminosity by a factor > 100. The variable accretion rate is a reflection of the motion of the neutron star in an eccentric orbit through regions of varying matter density around the Be primary. Others show aperiodic (Type II) outbursts lasting for tens of days, with luminosity increases $\sim 10^2 - 10^3$. Such outbursts may be due to

Table 5.2

Name	Galactic Coordinates		X-Ray Pulse Period	Distance	L_x	Orbital Parameters				Optical Component			Remarks
	l (°)	b (°)	(s)	(kpc)	(ergs s^{-1})	P (d)	$a_x \sin i$ (ls)	e	i (°)	Name	Spectral Type	Luminosity Class	
A0538-668	-	-	0.069	50	10^{39}	16.66	-	0.4	-	-	B2	III-Ve	Type I (periodic) X-ray outbursts
4U0115+634	125.9	+01.0	3.61	3.5	10^{37}	24.31	140.13	0.34	-	-	O-Be	-	Transient. Type I & II outbursts
V0331+530	-	-	4.37	2-4	$4\ 10^{35}$	34.25	48	0.31	-	-	Be	-	
1E1048.1-5937	-	-	6.44	3	$3\ 10^{34}$	-	-	-	-	-	Be	-	
1E2259+586	109.1	-01.0	6.98	4-5	$2\ 10^{35}$	-	-	-	-	-	-	-	Identity is disputed
4U1553-542	327.9	-00.9	9.26	-	-	30.6	164	0.09	-	-	-	-	Transient
2S1417-624	313.0	-01.6	17.6	-	-	> 15	-	-	-	-	Be ?	-	
EXO 2030+375	-	-	41.8	≈5	$\approx 10^{38}$	≈46.5	-	-	-	-	Be	-	Transient
A0535+262	181.4	-02.6	104	2.4	$2\ 10^{37}$	111	500	0.3	-	HDE 245770	B0	III-Ve	
GX 304-1	304.1	-01.2	272	2.4	10^{36}	133	500	-	-	-	B2	Ve	
4U1145-619	295.8	-00.2	292	1.5	10^{35}	187.57	600	-	-	HD 162567	B0-1	Ve	Persistent
A1118-616	292.5	-00.9	405	5	$5\ 10^{36}$	-	-	-	-	HEN 3-640	O9.5	IV-Ve	
X Per	163.1	-17.1	835	0.35	$4\ 10^{33}$	580 ?	-	-	-	X Per	O9.5	III-Ve	Persistent

Pulsars in Be X-Ray Binary Systems

a sudden enhancement of the rate of mass loss from the Be star. The Be transient V0331+534 has displayed both types of X-ray outburst.

ii) Persistent: the X-ray luminosities of the persistent Be XRBs are generally low and have values ~ 10^{33} - 10^{35} ergs s^{-1}. Most of the persistent Be X-ray pulsars have X-ray periods longer than 200 s. Their orbital X-ray light curves reveal erratic behaviour. X-ray flares are observed on timescales ~ 100 s, when the intensity can increase by a factor of 10; the outbursts last for a time typically ~ 5 % of the orbital period. They are thought to be due to enhanced accretion at the time of periastron passage.

5.2.3 Low-Mass X-Ray Binary Systems

The low-mass X-ray binaries form a much older population of X-ray sources than the massive systems. The presence of the low-mass (~ 1 $M_\odot$) companion stars in these binaries implies that the average age of a LMXRB is a factor ~100 greater than that of a HMXRB, i.e. $> 10^9$ yr compared with $\leq 10^7$ yr. Such extreme ages may have allowed the magnetic field strengths at the surfaces of the neutron stars to decay to values much less than the 10^{12}-10^{13} G fields believed to prevail in the HMXRBs. This is supported by the fact that only very few of the LMXRBs show X-ray pulsations, by which it is inferred that weak fields permit the deposition of

accreted material over a fraction of the neutron star surface that is much greater than in the case of the HMXRBs. The parameters of the four known LMXRB pulsars are listed in Table 5.3. (These include GX 1+4 and X0021.8-7221, the subjects of Chapter 10). Low surface magnetic field strengths may permit a neutron star to be eventually spun up to rotation periods ~ 1 ms by the torque supplied by accretion. The millisecond radio pulsars are believed to have been produced in this way. The possible progenitors of some of the observed millisecond radio pulsars may therefore have been low-mass X-ray binaries with evolved companion stars.

The optical light from the LMXRBs is dominated by emission from the accretion disk rather than the late-type companion star. (The reverse is observed for the high-mass binaries). The disk radiates mainly through the reprocessing of incident X-rays into optical and UV photons. Only rarely may optical emission from the companion star be identified.

The highest luminosity LMXRBs tend to be situated in the central bulge of the Galaxy and show very few X-ray bursts compared with the fainter systems. The ten brightest sources (eight of which are bulge sources) have X-ray luminosities close to the Eddington limit of $L_x \sim 10^{38}$ ergs s^{-1}. The spectral type of the companion star in a LMXRB may have a direct influence upon the average X-ray luminosity. Main sequence companions would provide low rates of mass transfer through Roche lobe overflow. Companions which have evolved away from the main sequence towards

Table 5.3

Name	Galactic Coordinates		X-Ray Pulse Period	Distance	L_x	Orbital Parameters				Optical Component			Remarks
	l (°)	b (°)	(s)	(kpc)	(ergs s^{-1})	P (d)	$a_x \sin i$ (ls)	e	i (°)	Name	Spectral Type	Luminosity Class	
Her X-1	85.2	+37.5	1.24	5	$2\ 10^{37}$	1.70	13.18	<0.0002	80^{+8}_{-5}	HZ Her	A9-B	-	35-d X-ray cycles
4U1626-673	321.8	-13.1	7.68	≈6	$\approx 10^{37}$	0.0228	< 0.01	-	< 16	Kz Tra	A	-	Associated with SNR
GX 1+4	1.9	+04.8	113.626	10	10^{36}-10^{38}	304 ?	≈600 ?	≈0.25 ?	-	V2216 Oph	M6	III	Rapid spin-down & spin-up states
X0021.8-7221 (in 47 Tuc)	305.0	-45.0	120.2	4.6	10^{34}	-	-	-	-	-	-	-	Transient

Pulsars in Low-Mass X-Ray Binary Systems

the giant branch could offer high mass transfer rates by their evolutionary expansion and so lead to high X-ray luminosities at the neutron star. The brightest sources are therefore expected by necessity to have longer orbital periods.

The orbital periods of approximately 25 LMXRBs have recently been determined by observations of regular dips in the X-ray intensity and by optical photometry of the companion stars (White 1989). The majority contain main sequence companions and have periods in the range 2.9 to 9 hr, athough periods as short as 11 minutes and as long as 9 days have been measured. The brightest sources do not usually show X-ray dips and, since most cannot be observed optically due to their location in the Galactic bulge, their orbital periods are often unknown. Two exceptions are Sco X-1 and Cygnus X-2. These are observed away from the bulge and have been found to display optical periods of 19 hr and 235 hr, respectively.

The strong magnetic fields of the neutron stars in the high-mass systems limit the radius of the inner edge of an accretion disk to values ~ 100 neutron star radii. In contrast, the weak fields at the LMXRB neutron star may allow the disk to extend much further down. An inner region of the disk may form which is dominated by radiation pressure. X-ray luminosities close to the Eddington limit may cause an expansion of the inner disk region to produce a dense accretion torus. For binary systems with high angles of inclination, the disk completely obscures the central region of X-ray emission at all orbital phases. Such

binaries may still be observed because an accretion disk corona, formed by X-ray heating of the disk, permits X-rays to be scattered in all directions. The observed X-ray luminosity may then only be a small fraction of the power generated at the central X-ray source.

5.3 Mass Transfer in X-Ray Binaries

5.3.1 Introduction

The energetics of accretion onto neutron stars are quickly explored and quantified in order to establish a backdrop for the results of the TeV γ-ray observations of X-ray binary systems. Accretion phenomena are broadly described by making some simple approximations and by performing a few of the relevant back-of-the-envelope calculations. Useful sources are Lewin and van den Heuvel (1983), Frank, King and Raine (1985), Katz (1987), and Ogelman (1989).

5.3.2 Roche Lobe Overflow

Observe the sequence of events depicted in Figure 5.2. The top diagram shows some of the lines of gravitational equipotential drawn in a plane which includes the centre-of-mass of a binary system. The innermost contour drawn around the two stars and through L_1 is the critical Roche potential which defines the

Figure 5.2

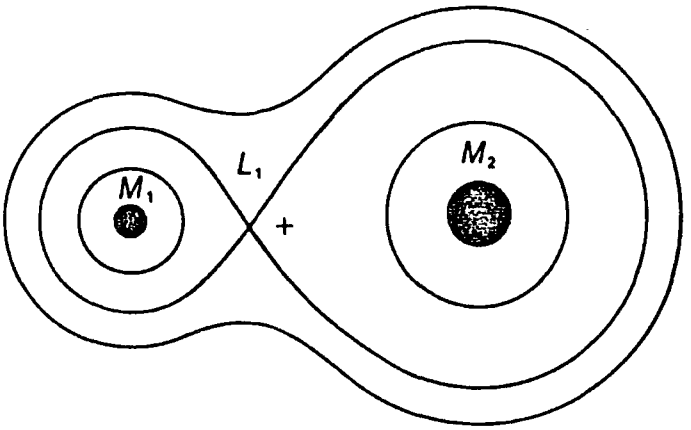

Equipotential contours on a plane through the centre-of-mass (+) of a binary system. L_1 is the inner Lagrangian point.

(From Petterson 1983)

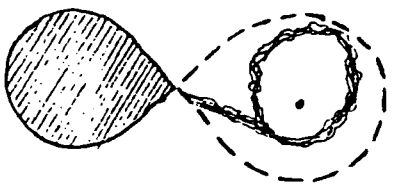

(a)

Initial ring

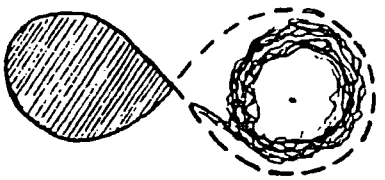

(b)

Spreading due to viscosity

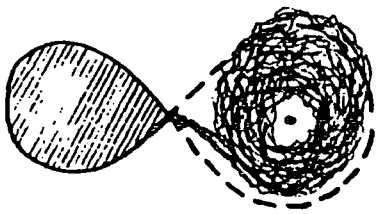

(c)

Full-size steady-state disk

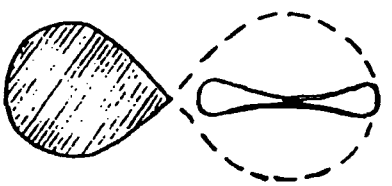

(d)

Side view (cross-section)

Formation of an Accretion Disk by Roche Lobe Overflow

boundaries of their Roche lobes. If the companion star fills or is close to filling its Roche lobe then pressure forces in the gas will cause a flow from the envelope through L_1. The gas will therefore enter the Roche lobe of the neutron star.

5.3.3 The Formation of an Accretion Disk

From the rest frame of the neutron star, the gas flowing through L_1 appears as though it has been squirted through a nozzle which is rotating in the plane of the binary. The gas stream therefore has a relative motion which is almost orthogonal to the line joining the centres of the two stars and will, in the first instance, form a ring of material about the neutron star. See the lower set of sketches in Figure 5.2. Viscous energy-dissipating interactions within the stream cause the gas to approach the neutron star and so form a flat accretion disk. Material at the inner edge of the disk is eventually channelled along the field lines of the pulsar magnetosphere and down to the surface of the neutron star.

5.3.4 Accretion Onto the Neutron Star

Consider the power generated at the pulsar by the conversion of the gravitational potential energy of the disk plasma to radiation. Let the neutron star mass and radius be M_{ns} and R_{ns}, respectively: the gravitational potential energy gained by a

mass m falling to the neutron star from rest at a distance r >> R_{ns} is just

$$E = \frac{GM_{ns}m}{R_{ns}} \qquad (1)$$

so that the power ($\dot{E}$) generated at the pulsar surface by accretion is

$$L_{acc} \sim \frac{GM_{ns}}{R_{ns}} \dot{m} \qquad (2)$$

The accretion luminosity reaches a maximum when there is a balance between the forces acting on the plasma due to radiation and gravitation. The momentum (p) absorbed by a particle scattered by a photon of energy E_{ph} is $p = E_{ph}/c$. If σ_T is the Thomson scattering cross-section of the particle, then the radiation force ($\dot{p}$) at distance r is just

$$F_{rad} = \frac{L_{acc}}{c} \frac{\sigma_T}{4\pi r^2} \qquad (3)$$

This force is exerted mainly on electrons rather than protons, since σ_T is inversely proportional to the square of the particle mass and $m_e/m_p \sim 5 \times 10^{-4}$. However, the Coulomb force between electrons and protons in the plasma means that the protons are

dragged with the electrons as the latter are accelerated by the radiation force.

With $m_e + m_p \approx m_p$, the gravitational force on the electron-proton pair is

$$F_{grav} \approx \frac{GM_{ns}m_p}{r^2} \qquad (4)$$

so that the limit on the accretion luminosity is, by balancing equations 3 and 4,

$$L_{max} = \frac{4\pi GM_{ns}m_p c}{\sigma_T(e^-)} \approx 1.3 \times 10^{38} \frac{M_{ns}}{M_\odot} \text{ ergs s}^{-1} \qquad (5)$$

This is the Eddington luminosity. With M_{ns} typically $\approx 1.4\ M_\odot$, many of the X-ray sources discussed earlier are seen to be radiating at luminosities close to their Eddington limits. An upper bound on the mass accretion rate is obtained by substituting for L_{acc} in equation 2 from equation 5,

$$\dot{m}_{Edd} = \frac{4\pi m_p R_{ns} c}{\sigma_T} \approx 10^{-8} \frac{M_{ns}}{M_\odot} M_\odot \text{ yr}^{-1} \qquad (6)$$

The maximum inward radial drift speed (v_r) of the gas can be found by equating this accretion rate to the rate at which matter

crosses the surface area of an annulus in the disk at radius r:

$$v_r(r) = \frac{\dot{m}_{Edd}}{2\pi r h \rho(r)} \qquad (7)$$

where h is the thickness of the disk and ρ is the matter density.

5.3.5 Interaction of Disk and Pulsar Magnetosphere

Neutron star surface magnetic fields of up to ~ 10^{12} G are sufficiently strong to disrupt and dominate the flow of plasma within the inner regions of an accretion disk. The size of the region dominated by the pulsar magnetosphere may be estimated by balancing the magnetic pressure and the ram pressure (inertia) of the plasma. If B is the field strength, the magnetic pressure at r is

$$P_B = \frac{B^2(r)}{8\pi} \qquad (8)$$

Using equation 7, the rate of mass transfer across an area A for a plasma of speed v is $\dot{m} = \rho(r)v(r)A$, so that the ram pressure is just

$$P_{ram} = \frac{1}{A}\frac{d(mv)}{dt} = \frac{1}{A}\dot{m}v = \rho(r)v^2(r) \qquad (9)$$

The Keplerian velocity of the plasma is simply

$$v(r) = \sqrt{(GM_{ns}/r)} \qquad (10)$$

The magnetic field strength varies with the cube of the radial distance: if μ is the magnetic dipole moment,

$$B \approx \frac{\mu}{r^3}, \quad \mu = B_{ns}R_{ns}^3 \ (\sim 10^{30}\ G\ cm^3) = \text{constant} \qquad (11)$$

So, by balancing the pressures given by equations 8 and 9, and substituting for $\rho(r)$, $v(r)$ and $B(r)$ from equations 7, 10 and 11, the magnetosphere begins to dominate the plasma flow at a radius

$$r \sim \mu^{4/7}(GM_{ns})^{-1/7}\dot{M}^{-2/7} \qquad (12)$$

(where, for simplicity, spherical accretion is assumed in equation 7 when substituting for ρ). This distance is called the Alfven radius. For $B \sim 10^{12}$ G, a neutron star radiating near the Eddington limit will have an Alfven radius $r_A \sim 10^2 R_{ns}$.

Another important distance scale is the corotation radius (r_{co}) at which the Keplerian orbital period is equal to the rotation period (P_{rot}) of the neutron star (and, therefore, of the magnetosphere):

$$P_{rot} = \frac{2\pi r_{co}}{v(r_{co})} \qquad (13)$$

from which

$$r_{co} = (GM_{ns})^{1/3} (P_{rot}/2\pi)^{2/3}$$

$$\sim 2 \times 10^{3} R_{ns} (P_{rot})^{2/3} \qquad (14)$$

In the case $r_A < r_{co}$, a stable flow of plasma can be maintained along the field lines to the magnetic polar caps and, assuming that the neutron star rotates in the same sense as its motion about the companion star, a spin-up torque is exerted by the transfer of angular momentum from the infalling matter to the neutron star. Spin-down torques can result for faster rotators due to the drag exerted by the disk upon the field lines and the consequent transfer of angular momentum from the neutron star to the disk plasma.

5.3.6 Accretion From A Stellar Wind

Even if a companion star does not fill its Roche lobe, accretion onto the neutron star may still take place in the high-mass binary systems, where the strong winds driven by radiation pressure from the hot atmospheres of the primaries may remove ~ 10^{-6} to 10^{-4} $M_\odot$ yr^{-1}. The Eddington limit on the mass accretion rate in equation 6 indicates that such wind losses would be more than sufficient to drive the HMXRBs even if the neutron star captured just ~ 0.01 to 1 % of the material driven from the surface of the primary. A simple estimate of the mass accretion rate by the neutron star may be made by assuming that all wind material which exists within a radius r_{acc} of the neutron star will be accreted if its kinetic energy is less than the gravitational potential energy at that distance, i.e.

$$r_{acc} \leq \frac{2GM_{ns}}{v^2} \qquad (15)$$

where v is the speed of the wind with respect to the neutron star If gas is blown from the surface of the primary star at a rate $\dot{M}_w$, then the fraction entering the target area is

$$\dot{M}_{acc} = \dot{M}_w \frac{\pi r_{acc}^2}{4\pi a^2} \qquad (16)$$

where a is the separation of the two stars. Taking the equality in equation 15 for r_{acc} and substituting into 16,

$$\dot{M}_{acc} \approx \dot{M}_{w} \left[\frac{GM_{ns}}{av^2} \right]^2 \qquad (17)$$

For example, the HMXRB Vela X-1 has $v \approx 900$ km s^{-1} and $a \sim 10^2$ lt-sec. Equation 17 implies that a fraction $\sim 4 \times 10^{-5}$ of the wind is captured. The X-ray luminosity of Vela X-1 is $\sim 10^{36}$ ergs s^{-1}, which requires $\dot{M}_{acc} \sim 10^{-10}$ M_o yr^{-1} (equation 2) and, by equation 17, $\dot{M}_w \sim 3 \times 10^{-6}$ M_o yr^{-1}; the $\sim$ 20 M_o supergiant primary star in the Vela X-1 binary is capable of providing such a wind (Ogelman 1989).

Chapter 6

Previous Observations of TeV γ-Ray Emission From X-Ray Binaries

6.1 Introduction

By 1990 September, claims had been made for the detection of TeV γ-rays from a total of ten X-ray binary systems. Emission at TeV and PeV energies had not been predicted (e.g. Harding 1989) and the binaries were thought to be powered only by accretion onto the surface of a neutron star. Since the temperature at the base of an accretion column is approximately nine orders of magnitude below that required for thermal emission of the high-energy γ-rays - Chapter 1 - the successful observations immediately suggest that other highly energetic processes must also be operating in X-ray binaries. Therein lies the importance of the γ-ray observations to a better understanding of these systems.

TeV γ-rays have been detected from examples of each of the three categories of binary: supergiant, Be, and low-mass. The previous observations are quickly summarised here and are grouped according to the binary class. The properties of these γ-ray sources will be compared in Chapter 11 after the presentation of the new results.

6.2 Supergiant X-Ray Binaries

Pulsed TeV γ-ray emission has been detected from four of the ten SXRB pulsars.

(i) Vela X-1

The Potchefstroom Group (North *et al.* 1987) made the first discovery of TeV γ-ray emission from a supergiant binary when they found the wind-driven pulsar Vela X-1 (P_x=283 s, P_{orb}=8.96 d) to be radiating pulsed γ-rays with the relatively weak but steady time-averaged luminosity of (2.4±1.1) x 10^{34} ergs s^{-1} ($E \geq 1.5$ TeV). In addition to the stable pulsed flux recorded at many phases in the orbit, enhancements (also periodic) lasting for times $\approx$ 2 to 4 pulsar rotations have been witnessed near X-ray eclipse ingress and during eclipse. This suggests that both the immediate environment of the neutron star and the limb of the primary star may be sites for the production of TeV γ-rays; the duration of γ-ray eclipse by the optical companion may be at most just half that measured at X-ray energies (Raubenheimer *et al.* 1989).

The Durham group (Carraminana *et al.* 1989a) have confirmed that Vela X-1 is a source of γ-rays and estimate the time-averaged luminosity to be (3.6±0.7) x 10^{34} ergs s^{-1} ($E > 0.3$ TeV), which is consistent with the value measured at discovery. No γ-ray outbursts have been identified.

(ii) Centaurus X-3

Centaurus X-3 (P_x=4.82 s, P_{orb}=2.09 d) was discovered by the Durham group to be a source of pulsed TeV γ-rays with a peak luminosity of $\approx$ 6 x 10^{36} ergs s^{-1} (E > 0.25 TeV). See Carraminana *et al.* (1989b) and Brazier *et al.* (1989b, 1990a). The γ-ray emission appears to be observable only when the neutron star is in the vicinity of the ascending node of the orbit (X-ray phase 0.75). North *et al.* (1989) have also claimed the detection of pulsed TeV γ-rays from Cen X-3 at similar orbital phases.

(iii) LMC X-4

The only evidence for pulsed TeV emission from LMC X-4 (P_x=13.49 s, P_{orb}=1.408 d) was found by the Durham group in early 1987. Subsequent observations do not confirm the result (Brazier *et al.* 1990e). The time-averaged luminosity of LMC X-4 during the 1987 observations is estimated to be 2.0 x 10^{37} ergs s^{-1} (E > 0.4 TeV). It may be that opportunities to observe γ-ray emission from this binary are governed in part by a 30.4-day cycle which has been measured at optical and X-ray wavelengths.

(iv) SMC X-1

See Chapters 7 to 9 of the present work for the analysis of the Narrabri database.

6.3 Be X-Ray Binaries

One of the thirteen known X-ray pulsars in Be binary systems has been found to be a TeV γ-ray emitter; there is some evidence for a second γ-ray source.

(i) 4U0115+634

4U0115+634 (P_x=3.61 s, P_{orb}=24.315 d, e=0.34) was the first binary in this class to be detected at TeV energies. It was discovered by the Durham group in 1984 using an array of γ-ray telescopes at Dugway, Utah. See Chadwick *et al.* (1985b). The time-averaged luminosity at discovery was ~ 6 x 10^{35} ergs s^{-1} (E > 1 TeV). No significant variation in the strength of the pulsed emission was detected over the nine days of the observations, although 4U0115+634 is known to be a transient X-ray source. The discovery was confirmed by Lamb *et al.* (1987) and Resvanis *et al.* (1987) using the Whipple and Haleakala experiments, respectively. Observations by the Durham group in 1988 using the Mark IV γ-ray telescope at La Palma again provided evidence for steady emission at the X-ray period (Brazier *et al.* 1989c and 1990d); the average luminosity at E > 0.4 TeV was ~ 2 x 10^{36} ergs s^{-1}.

(ii) 1E2259+586

Evidence for TeV γ-ray radiation from 1E2259+586 (P_x=6.979 s; the orbital parameters are unknown) was discovered by the Durham Group with the Mark IV telescope during observations in 1988.

See Brazier *et al.* (1989c and 1990d). A periodic component was found in the data close to the second harmonic of the X-ray pulse period. The implied average luminosity was (5.3±2.1) x 10^{35} ergs s^{-1} (E > 0.4 TeV). Observations made with the same instrument one year after the discovery show no evidence for pulsed γ-ray emission.

(Note that the inclusion of 1E2259+586 in this class of X-ray sources is tentative; on the basis of IR photometry, Davies *et al.* (1989) have recently questioned both the identity of the optical counterpart and the evidence for the binary nature of the source).

6.4 Low-Mass X-Ray Binaries

Four low-mass X-ray binary systems have been found to be TeV γ-ray sources, including two of the four known LMXRB pulsars.

(i) Cygnus X-3

The nature of Cygnus X-3 (d ≈ 11 kpc) remains a mystery even though it has been investigated for 23 years in the radio, IR and X-ray wavebands, and at GeV, TeV and Pev γ-ray energies. Stanev (1987) and Weekes (1988) have reviewed the research on this source and provide copious references to the literature.

Cygnus X-3 is a strong radio source and exhibits sequences of violent outbursts, during which the radio flux density can

increase by a factor of ~ 10^4 above the quiescent level of ~ 20 mJ at 20 cm. The most recent outburst occurred on 1990 August 15 and reached a level of 8 Jy at 3.6 cm (Waltman, Fiedlar and Johnston 1990). The radio luminosity can be as high as 10^{35} ergs s^{-1}. Extended radio lobes on a scale ~ 1 light yr have been discovered (Achterberg, 1989; Strom, van Paradijs and van der Klis, 1989). These may be bubbles that have been blown into the local interstellar medium by the combined energy of the bursts.

Only moderate changes in the IR emission have been witnessed. The peak luminosity at 2.2 μm is ~ 10^{36} ergs s^{-1}. Cygnus X-3 has not been identified in the optical waveband. At X-ray energies, the luminosity varies only within a factor of 2 of ~ 10^{37} ergs s^{-1} (e.g. Ghosh *et al.* 1981).

Lamb *et al.* (1977) claimed the detection of a 0.1 GeV flux from Cygnus X-3 using the SAS II satellite, though this was not confirmed by COS B. A TeV luminosity of 2 x 10^{37} ergs s^{-1} was estimated by Vladimirsky, Stepanian and Fomin (1973) when they reported the first identification of an astronomical source of TeV γ-ray radiation. The detection of PeV γ-rays from Cygnus X-3 during the late 1970s and early 1980s has been described in Chapter 1.

With the exception of the radio emission, the radiation at all other energies displays a periodicity of 4.8 hr. This is assumed to be the orbital period of a binary system. Such a short period would suggest that the source is a low-mass binary system which

may be quite closely packed. If the companion is taken to be a main sequence star (for example) that is filling its Roche lobe then, for a standard neutron star mass of ≈ 1.4 $M_\odot$, the mass of the companion would be ≈ 0.55 $M_\odot$ and the separation of the two stars would be ≈ 4 lt-sec.

The IR and X-ray emissions are observed at all orbital phases and have broad maxima. In contrast, the signal at TeV energies is detected across only short orbital phase-bands. Neshpor *et al.* (1979) in the Crimea reported emission at E > 2 TeV from X-ray phases 0.15 to 0.20 and 0.78 to 0.83 during the interval 1972-1977. The Whipple Collaboration (Danaher *et al.* 1981) observed γ-rays at the same threshold energy during 1980 in the phase band 0.6 to 0.8. The narrower band of 0.625-0.655 was reported by the Durham Group following observations from Utah at E > 1.3 TeV in 1981-1983 (Dowthwaite *et al.* 1983).

An outburst lasting for 7 minutes was witnessed at Utah by the Durham Group in 1983 September around the phase of X-ray maximum (0.625). See Brazier *et al.* (1990c) and references therein. This burst was subsequently found to provide evidence for pulsed γ-ray radiation from Cygnus X-3 at a period of 12.5908 ms. More evidence for periodic emission at 12.59 ms was found in data taken at Utah both before and after the 1983 September outburst. Periodicity was again identified using measurements taken with a Mark II telescope at Durham in 1985. Taken together, the pulsed γ-ray signals indicated a secular period derivative of $(2.8\pm0.4) \times 10^{-14}$ ss^{-1} during the interval 1981-

1985. Confirmation of the existence of a rapid pulsar in the Cygnus X-3 binary was provided when the system was monitored by the Durham Group with the Mark IV telescope ($E > 0.4$ TeV) at La Palma during the summer observing seasons of 1988 and 1989. Independent confirmation of the presence of a 12.59 ms pulsar in Cygnus X-3 has recently been announced by the Adelaide Group (Gregory *et al.* 1990) following observations from Woomera at $E > 100$ TeV using the low-elevation air Cerenkov technique.

(ii) Scorpius X-1

Scorpius X-1 ($d \approx 1.5$ kpc) shares with Cygnus X-3 both the breadth of investigation that has been conducted during the past ~ 20 years and the paucity of hard facts gleaned about it. Like Cygnus X-3, it is a highly luminous X-ray source radiating close to the Eddington limit and it is believed to be a low-mass binary system comprising a neutron star and a main sequence star that is filling its Roche lobe. Photometry of the optical counterpart (V818 Scorpii) has revealed a periodicity of 18.9 hr, which is assumed to be the orbital period of the binary.

The Potchefstroom Group were the first to announce the detection of TeV γ-rays from Sco X-1 (de Jager *et al.* 1986). The Durham Group have reported the detection of TeV γ-ray emission following observations during 1988 and 1989. These were made at Narrabri using the Mark III telescope in the signal-chopping mode. See Brazier *et al.* (1990b). Persistent unpulsed γ-ray emission was observed and the luminosity was estimated at

$(2.3\pm0.7) \times 10^{34}$ ergs s^{-1} ($E > 0.3$ TeV).

(iii) Hercules X-1

Hercules X-1 (P_x=1.24 s, P_{orb}=1.70 d) comprises an A9 companion star and a neutron star in a circular orbit of $a_x \sin i$ = 13.18 ls. It was the first LMXRB pulsar to be identified as a TeV γ-ray emitter. The discovery was made by the Durham Group in 1983 April with the Utah experiment when a burst of events lasting for $\approx$ 3 minutes was recorded (Dowthwaite *et al.* 1984c). This burst was found to contain a periodic component at the contemporary X-ray pulse period. Recent re-analysis of the data taken during the 1983 July and October Utah observations (Brazier *et al.* 1990f) indicates a time-averaged luminosity of 1.3×10^{36} ergs s^{-1} ($E > 1$ TeV).

Subsequent TeV γ-ray observations of Hercules X-1 were made at the Whipple Observatory (e.g. Gorham *et al.* 1986, Lamb *et al.* 1988, and Reynolds *et al.* 1990) and by the Haleakala Collaboration (e.g. Resvanis *et al.* 1988); both collaborations found evidence for pulsed γ-rays at periods which were significantly different from the expected value of the contemporary X-ray pulse period. (Slane and Fry (1989) have reviewed the claims for pulsed γ-ray signals from Her X-1 at anomalous periods in order to examine the implications for models of the emission site).

In addition to the 1.24-s and 1.70-d X-ray periodicities, Hercules X-1 displays a modulation in the X-ray intensity with a period of 35 d. The X-ray light curve is composed of a high-intensity state which lasts for 11 days, followed by an intermediate high state (at 40 % of the high state intensity) for 5 days and a 19-day low-intensity state. This modulation may be caused by free precession of the neutron star, or by a precession of an inclined accretion disk. Thus the 19-d low state may occur when the view to the pulsar is obscured by the disk and the 11-day high state occurs when the view is unobstructed. The 5-d intermediate high state is then the result of the line-of-sight passing close to the plane of the precessing disk and cutting through an accretion disk corona. See Eichler and Vestrand (1985) and references therein. Resvanis *et al.* (1988) have reviewed the observations of γ-rays from Her X-1: no reports of γ-ray emission have been made during the low states of the 35-d cycle. The TeV γ-ray outburst observed at Utah in 1983 occurred at the expected time for the onset of the 11-d high-intensity state, when the line-of-sight to the pulsar was grazing the accretion disk; the neutron star was near to the ascending node of the orbit. Hercules X-1 was again monitored by the Durham group in 1988 and 1989 at La Palma (Brazier *et al.* 1989c, 1990d, and 1990f). A 3.3-minute outburst was detected in 1988 July with a signal which was pulsed at the X-ray period. The orbital phase was once more near the ascending node and the expected 35-d phase was again at the start of the high X-ray intensity state.

(iv) X0021.8-7221

A transient 2-minute X-ray pulsar has been identified in the nearby globular cluster NGC 104 (47 Tucanae) by Auriere, Koch-Miramond and Ortolani (1989). None of the orbital elements have been determined. The X-ray luminosity is ~ 10^{34} ergs s^{-1}. The Potchefstroom Group observed the cluster during 1989 and have reported the detection of TeV γ-ray radiation which is pulsed at the X-ray period (de Jager *et al.* 1989 and 1990). The peak luminosity is $\approx 10^{36}$ ergs s^{-1} ($E > 5$ TeV) or 2 orders of magnitude greater than the X-ray power. de Jager *et al.* (1990) speculate that the relatively low X-ray luminosity may be in consequence of the observation of the binary at a high angle of inclination, so that a fraction of the X-rays are absorbed along the line-of-sight through an accretion disk. At the same time, the absorber could act as a target for collisions of high-energy particles, followed by π^0 decay to γ-rays. See also Chapter 10 of the present work for details of the analysis of the Narrabri database.

Chapter 7

The High-Mass X-Ray Binary SMC X-1

7.1 Introduction

The supergiant X-ray binary system SMC X-1 has been monitored for a total of 316 hours with the Mark III γ-ray telescope at Narrabri, New South Wales during eleven separate sequences of tracking observations over the period 1986 October to 1989 December. The SMC X-1 data comprise the largest set taken with the telecope to date. There are no published reports of previous observations of SMC X-1 at TeV energies.

Although SMC X-1 is the most distant stellar source candidate yet selected for observation ($d \approx 65$ kpc), there are good reasons to propose that a detectable flux of TeV γ-rays might exist. The SMC X-1 system is amongst the most powerful X-ray binaries known and has been recorded with high-state X-ray luminosities in excess of 10^{39} ergs s^{-1}. Several successful attempts to detect high-energy γ-rays from X-ray binaries have already been made. The binary is a good candidate for practical reasons also: the values of the X-ray pulse period and the secular period derivative are well established, as are the values of the orbital elements. Such knowledge permits a test of the simple hypothesis that a time series recorded at Narrabri might contain a component which is pulsed at the expected period of the X-ray

pulsar. The analysis of the Narrabri data is presented in Chapters 8 and 9. This has been greatly assisted by the availability of contemporary values of the SMC X-1 X-ray pulse period and the epoch of X-ray mid-eclipse. These were determined from the measurements performed in 1987 May with the Japanese satellite *Ginga* (Takeshima 1987) and in 1989 March with the Roentgen X-ray observatory aboard the *Kvant* module of the Soviet *Mir* space station (Gilfanov *et al.* 1989).

The results of the X-ray and optical measurements of SMC X-1 are described in this chapter and the X-ray pulse period history is presented. Details of the Narrabri database are provided in Section 7.3. Chapter 8 is concerned with the pulse timing analysis of the data. Further analysis of the database is presented in Chapter 9, together with a concluding discussion of the implications of the results.

7.2 Properties of the SMC X-1 Binary

7.2.1 Introduction

The Small Magellanic Cloud is an irregular satellite galaxy of diameter 10 kpc. It possesses a mass of approximately 1 % that of the Galaxy and it is at a distance of 63 kpc (≈ 10 % of the distance to the Andromeda Nebula). The composition of the SMC resembles the arms of spiral galaxies, for it contains relatively few representatives of the old, red (Population II) stars

associated with elliptical galaxies and the nuclei of spirals. Almost one third of the mass of the SMC is in the form of interstellar hydrogen gas; both this proportion and the ratio of gas to dust are higher than the corresponding values found for the Galaxy. A further indication that the SMC is at a less advanced stage of chemical evolution than the Galaxy is provided by evidence of a relative underabundance of heavy elements (Clark *et al.* 1978 and references therein). The Cloud is therefore young and may have an age of just ~ 2 x 10^9 yr, which is approximately one fifth of the age of the Galaxy.

The regions of the most active contemporary star formation in the SMC were mapped by Azzopardi and Vigneau (1977) in a survey of luminous O-B2 supergiants. As with SMC X-1, two X-ray binary sources discovered by Clark *et al.* (1978) are found to be located just beyond the edges of these star formation regions. The creation of a high-mass X-ray binary involves the interaction of two initially bright, blue Population I stars and requires a time $\geq$ the duration of the pre-collapse stage of whichever component was originally the more massive. The current positions of the X-ray sources observed in the SMC may therefore indicate that the locations of regions where star formation occurs are time-dependent. Stars may be born during sporadic bursts which spread out through sections of the SMC and leave behind X-ray sources as evidence of their passage.

7.2.2 X-Ray Emission From SMC X-1: The First Results

The first detection of X-rays from the direction of the Small Magellanic Cloud was reported by Price *et al.* (1971) following brief observations at energies of 5-75 keV using sets of proportional counters and scintillation counters carried aboard a Thor missile in 1970. Although the fields of view of the instruments were large (≈ 22-28 sq deg), it was suggested that the observed flux could be due to a small number of strong sources in the SMC which were radiating at X-ray luminosities ~ 10^{38} ergs s^{-1}.

Measurements at 2-7 keV (Leong *et al.* 1971) were made with the *Uhuru* satellite shortly after the Thor flight and revealed the presence of a discrete source of high X-ray luminosity and variable intensity located at the southeast edge of the SMC. Designated SMC X-1, it was the first stellar X-ray source to be recognised in an external galaxy. The peak luminosity integrated across the detector bandpass was determined to be 1.2 x 10^{38} ergs s^{-1}, assuming isotropic emission at a distance of 63 kpc.

SMC X-1 was the subject of further investigation when it was found that several of the variable X-ray sources observed from *Uhuru* are short-period binaries (e.g. Centaurus X-3 and Hercules X-1: Schreier *et al.* 1972a, Tananbaum *et al.* 1972). New *Uhuru* data were analysed by Schreier *et al.* (1972b), who discovered that SMC X-1 is indeed a binary system and that much of the reported X-ray variability could be accounted for by periodic occultations of the X-ray source by a companion star. The

orbital period of this eclipsing binary was determined to be approximately $3^d.9$, with an eclipse duration of approximately $0^d.6$. The derived peak 2-6 keV luminosity was in excess of 10^{38} ergs s^{-1}, in agreement with the earlier results. A low-energy cut-off at the edge of an otherwise flat spectrum was tentatively attributed to absorption by material in the plane of a highly inclined orbit (the latter being implied by the observation of X-ray eclipses); both the cut-off and the possibility that the maximum X-ray power was close to or above the limiting Eddington luminosity were offered as support for the identification of the X-ray production mechanism with non-spherical accretion onto a compact object following mass transfer from a companion star, as postulated for other X-ray binary sources discovered at this time (Schreier *et al.* 1971, Schreier *et al.* 1972a, and Giacconi *et al.* 1972).

7.2.3 High and Low X-Ray States

A very important characteristic of the SMC X-1 X-ray emission is a pronounced variability of intensity which is apparently irregular. It was first noted by Schreier *et al.* (1972b) who found fluctuations in X-ray intensity which were in addition to those caused by the periodic eclipsing by the companion star.

In 1976 the COS-B satellite recorded a transition from a low X-ray state to a high X-ray state during a set of 2-12 keV measurements spanning 38 days. Bonnet-Bidaud and van der Klis

(1981) found that this transition in X-ray intensity had a timescale of 4 to 8 days, or 1 to 2 binary cycles. SMC X-1 was also monitored at 13-180 keV by HEAO 1 during three ~ 80-day periods in 1977 and 1978. Gruber and Rothschild (1984) eliminated the periods of binary eclipse and measured the detector count rate as a function of time. The strong temporal variation in X-ray intensity is illustrated in Figure 7.1. Although the timescale between two high states or two low states appears to be ≈ 60 days during each of the 3 sets of observations, Gruber and Rothschild were unable to fit a constant period that holds phase between all measurements. Instead they found that the X-ray variability is consistent with a random walk process and suggested the possibility of the irregular transfer of material from the companion star, or the inner edge of an accretion disk, over a timescale of tens of days. As an alternative explanation, Gruber and Rothschild postulate the existence of a tilted, precessing disc which periodically crosses the line of sight to the neutron star and eclipses the X-ray emitting region. Such a model has been suggested to account for the 35-day X-ray intensity cycle of Her X-1 (Boynton, Crosa and Deeter 1980) and the $30^{d}.5$ cycle of LMC X-4 (Lang *et al.* 1981), although the variation in the "period" of the cycles for SMC X-1 (≈ 15 %) is a factor ~ 3 greater than the period instabilities found for the other two binaries.

A search for regular long-term variations in the orbital light curve of SMC X-1 at optical wavelengths has revealed no

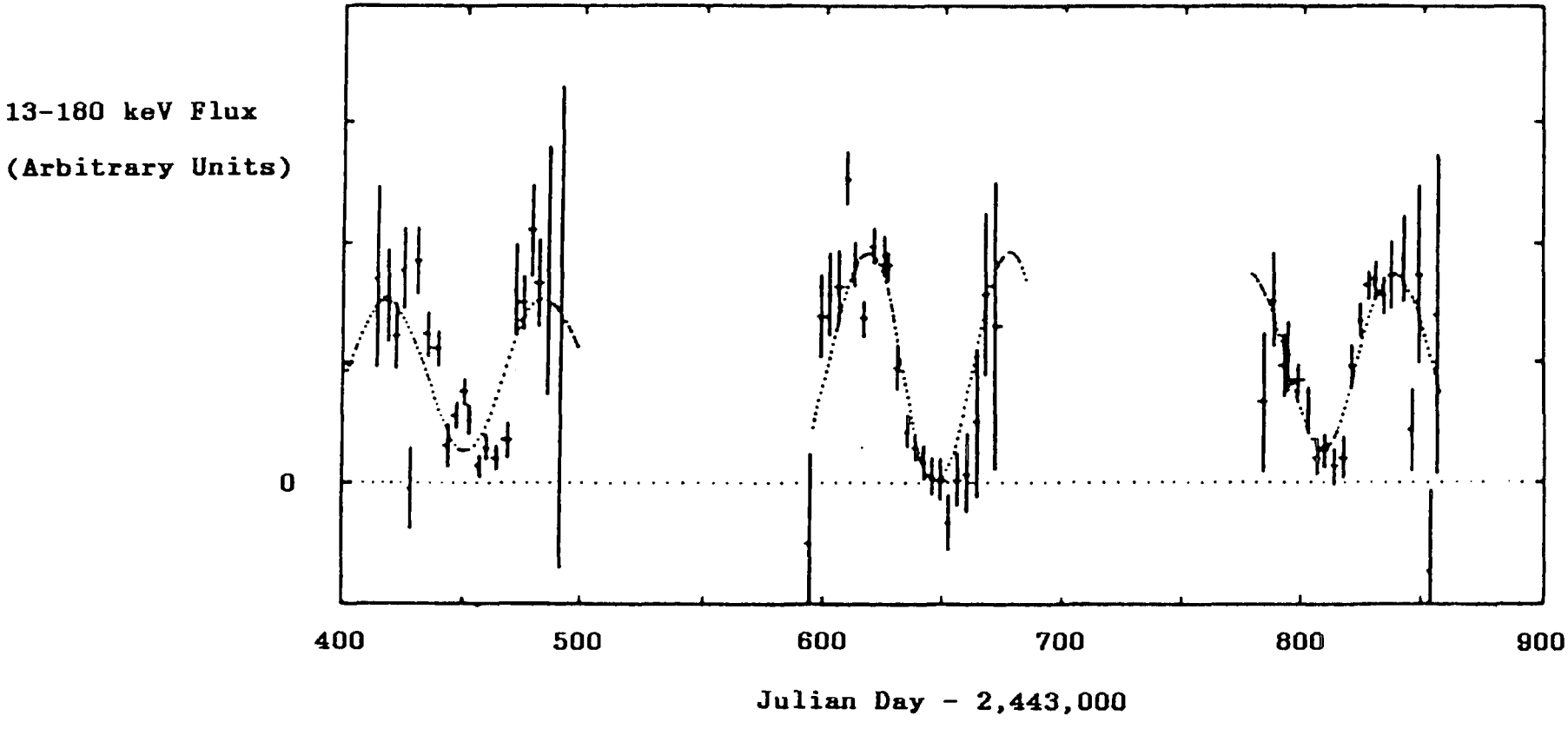

Figure 7.1

Long-Term SMC X-1 X-Ray Light Curve

(Periods of binary eclipse are excluded)

From Gruber and Rothschild (1984)

evidence for periodic modulation with amplitudes in excess of $0^m.015$ (upper limit) at periods between 15 and 150 days. See van Paradijs *et al.* 1983; van Paradijs and Kuiper 1984.

7.2.4 The X-Ray Spectrum

Figure 7.2 shows a 2-60 keV spectrum obtained with the *Ariel V* satellite in 1975 (Coe *et al.* 1981). The solid line is the best fit power law spectrum (spectral index $\alpha = 1.35 \pm 0.1$) for the 2-10 keV measurements. A change to a steeper slope is required near 40 keV in order to pass beneath the 2σ upper limits on flux above 60 keV. Coe *et al.* abandoned the fitting of power law spectra to the data and instead proposed a model which incorporates Thomson scattering of the X-ray photons at the emission region. The dashed curve in Figure 7.2 shows the model spectrum fitted to the *Ariel V* measurements.

From the position of the high-energy cut-off in the observed spectrum, Coe *et al.* employed the model to deduce a magnetic field strength of 1.0×10^{13} G at the region of X-ray emission. An expected characteristic of the X-ray spectrum is the presence of either cyclotron emission lines or cyclotron absorption dips. These features have not been observed in the X-ray spectra of SMC X-1, although they have been reported for Her X-1 (Coe *et al.* 1977 and Trumper *et al.* 1978) and the Be binary 4U0115+634 (Wheaton *et al.* 1979); possible cyclotron lines have also been reported recently for the Be binary 1E2259+586 and the supergiant

Figure 7.2

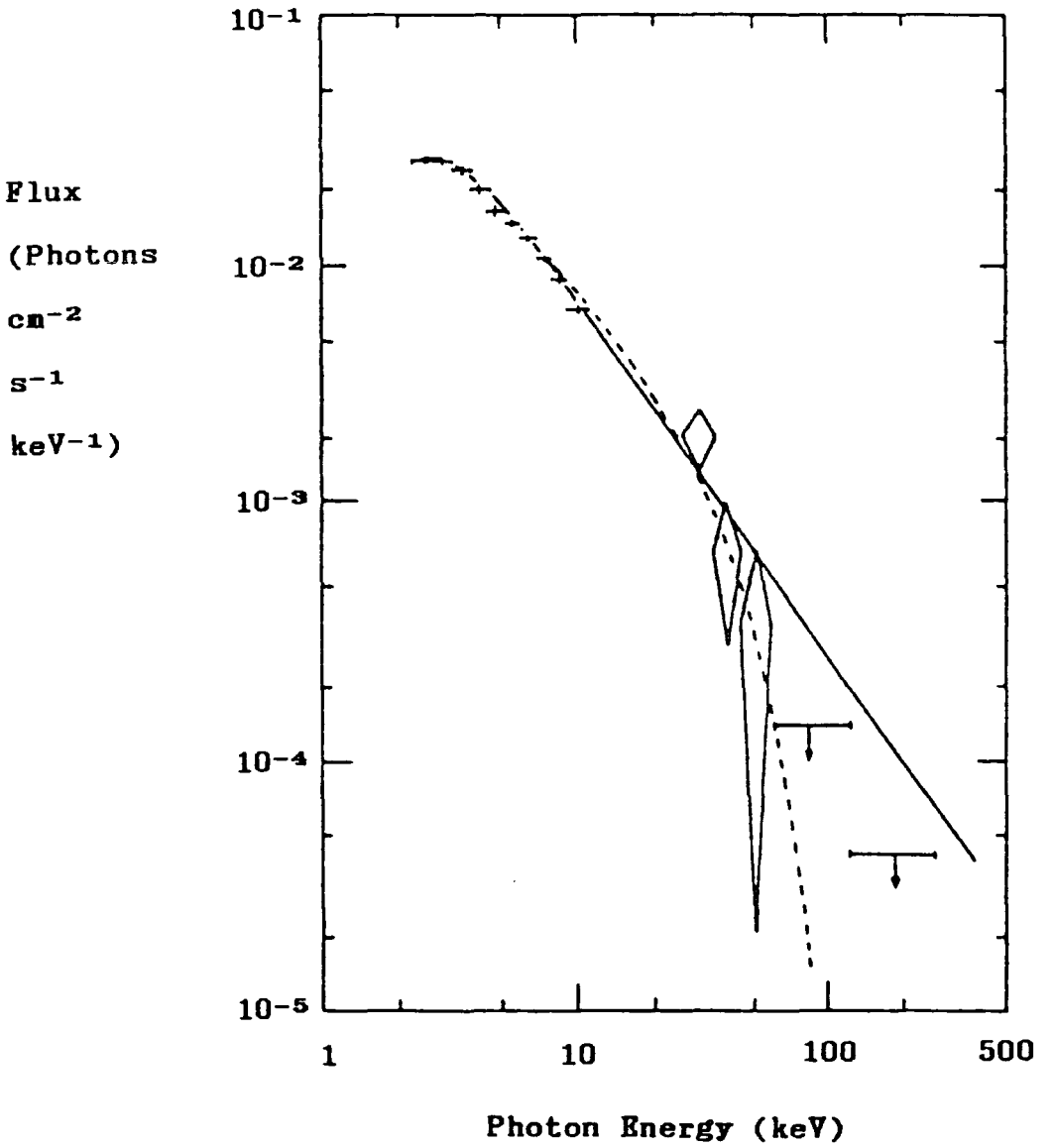

X-Ray Spectrum of SMC X-1

(From Coe *et al.* 1981)

——— Power law fit to ≤ 10 keV measurements

------ Thomson scattering fit

binary 4U1538-52 (Nagase 1989).

7.2.5 X-Ray Pulse Period History

In their study of the orbital modulation of the X-ray signal from SMC X-1, Schreier *et al.* (1972b) found a superficial resemblance of the source to the X-ray binaries Cen X-3 and Her X-1. These binaries show orbital periods of approximately $2^{d}.1$ and $1^{d}.7$, respectively. However their analysis revealed no evidence in the *Uhuru* data for pulsed emission at periods comparable with the (then) $4^{s}.84$ period of Cen X-3 and the $1^{s}.24$ period of Her X-1. The first announcement of the existence of a pulsed component in the SMC X-1 X-ray emission was made by Lucke *et al.* (1976) following 1.6-10 keV observations from an *Aerobee 170* sounding rocket launched at Woomera, Australia in 1973, and a second experiment which was operated during the *Apollo-Soyuz* mission of 1975. X-ray pulse period values of $0^{s}.7164 \pm 0^{s}.0002$ and $0^{s}.7151 \pm 0^{s}.0002$ were later reported by Yentis *et al.* (1977) using the *Aerobee* and *Apollo-Soyuz* data, respectively.

A total of nine reports of measurements of the SMC X-1 X-ray pulse period have been made since the discovery of the X-ray source in 1970. The values of the periods are plotted against epoch of observation in Figure 7.3a. Table 7.1 provides a list of the individual epochs and period determinations. Over timescales of the order of the average separation of the observations, the pulse period decreases at a mean rate $\sim 10^{-11}$

Figure 7.3a

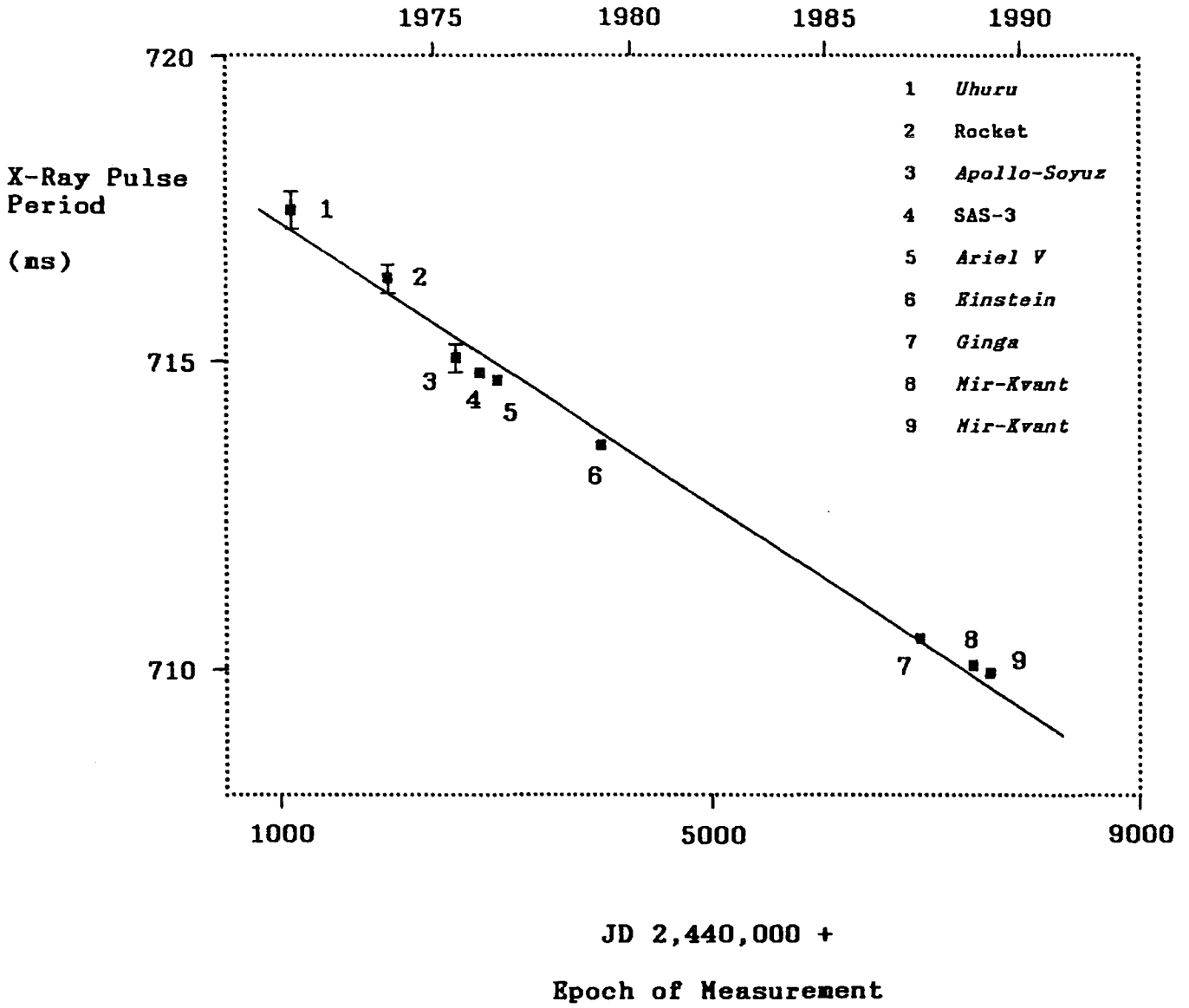

SMC X-1: X-Ray Pulse Period History

Epoch of Measurement (JD 2,440,000+)	Period (ms)	Reference
1114.7 (1971 Jun 11)	717.48 ± 0.26	Henry & Schreier (1977) *Uhuru*
2000.1 (1973 Nov 12)	716.4 ± 0.2	Yentis *et al.* (1977) *Aerobee* rocket
2614.3 (1975 Jul 20)	715.1 ± 0.2	Yentis *et al.* (1977) *Apollo-Soyuz*
2836.6823 (1976 Feb 28)	714.88585 ± 0.00004	Primini, Rappaport & Joss (1977) SAS-3
3000.1562 (1976 Aug 10)	714.7337 ± 0.0012	Davison (1977) *Ariel V*
3986.407 (1979 Apr 22)	713.684 ± 0.032	Darbro *et al.* (1981) *Einstein*
6942.02676 (1987 May 26)	710.551 ± 0.005	Takeshima (1987) *Ginga*
7452 (1988 Oct 17)	710.0972	Gilfanov *et al.* (1989) *Mir-Kvant*
7591 (1989 Mar 05)	709.9830	Gilfanov *et al.* (1989) *Mir-Kvant*

Table 7.1 SMC X-1 X-Ray Pulse Period History

Figure 7.3b

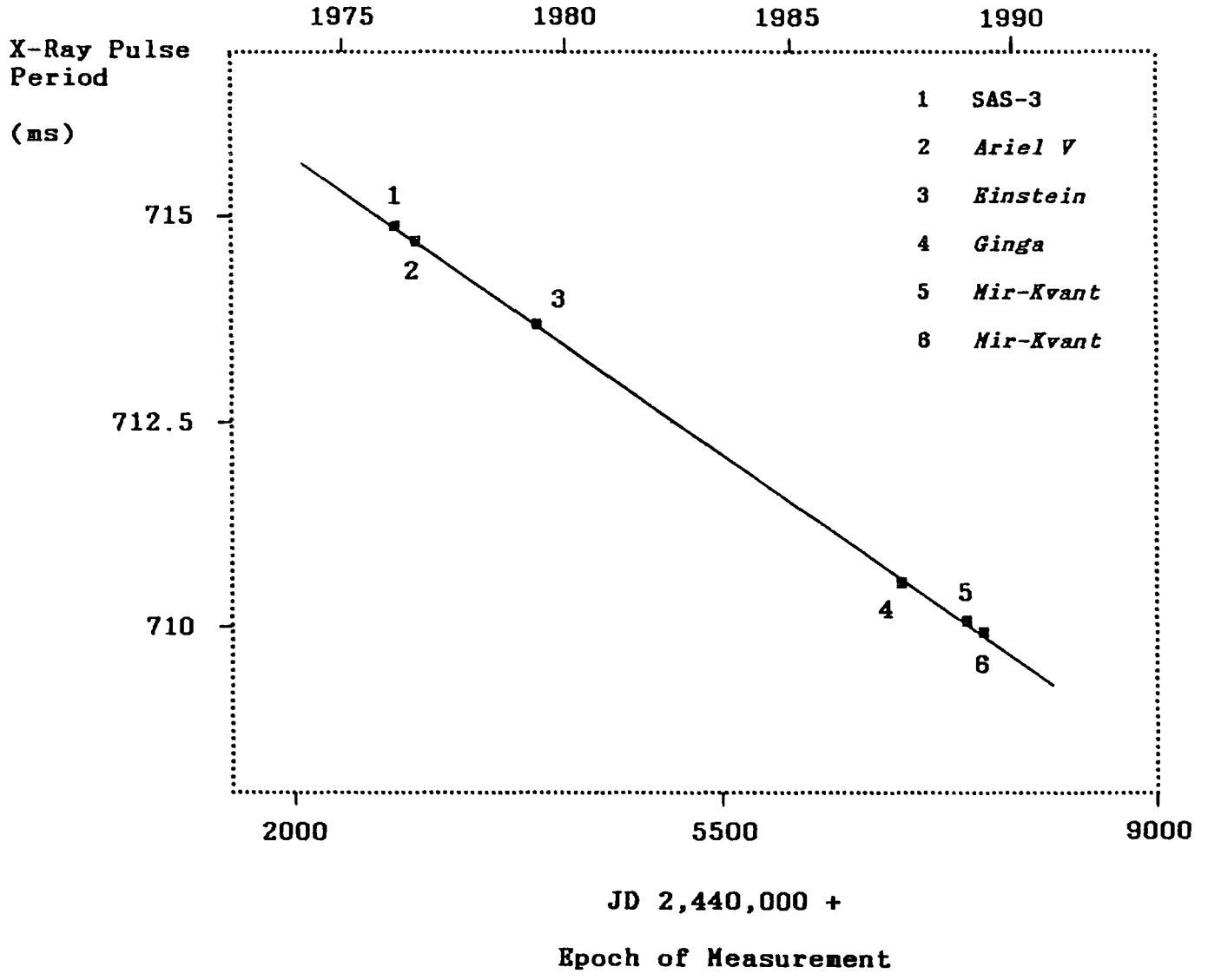

SMC X-1: X-Ray Pulse Period History

Measured by the Later Space Experiments

s/s. With the assumption that the period change is a linear function of time, a least squares fit to the nine measurements suggests an average value for the secular period derivative of $\dot{P} = -(1.299 \pm 0.057) \times 10^{-11}$ s/s.

A much better fit is obtained after omitting the considerably less precise period values determined from the early *Uhuru* *Aerobee*, and *Apollo-Soyuz* observations. The values of the X-ray period measured by the SAS-3, *Ariel V*, *Einstein*, *Ginga* and *Mir-Kvant* experiments are plotted in Figure 7.3b, together with the line of least squares fit; the errors on these measurements are smaller than the symbols used to represent them. The decrease in the X-ray period (average value of $\dot{P} = -(1.205 \pm 0.014) \times 10^{-11}$ s/s) is seen to be very uniform over an interval of approximately 15 years. This is of particular importance to the present work, for it allows a confident prediction to be made for the value of the pulse period at the epoch of a given sequence of Narrabri observations.

7.2.6 SMC X-1 at Optical Wavelengths

The star Sk 160 (Sanduleak 1968) was proposed as the optical counterpart to the X-ray source by Webster *et al.* (1972). This identification was confirmed by Liller (1973) after the measurement of optical intensity variations which displayed the orbital period of SMC X-1. The primary is of spectral type B0.5 and luminosity class I and has an average V-band apparent

magnitude of ≈ 13.25. Stars of this class have typical lifetimes of just ~ 10^7 years. The location of the supergiant on the Hertzsprung-Russell diagram is shown in Figure 7.4, where the positions of the optical components of other high-mass X-ray binaries are included for comparison.

van Paradijs and Kuiper (1984) conducted photometric observations of Sk 160 at the European Southern Observatory between 1979 and 1982 and obtained the average light curve shown in Figure 7.5, where V-band magnitude is plotted against orbital phase, ø. (Optical light curves for several high-mass binaries, including SMC X-1, are provided by Tjemkes, Zuiderwijk and van Paradijs 1986). Two peaks are found. They occur near ø = 0.25 and ø = 0.75 and are interpreted as the result of tidal distortion of the shape of the primary star by the neutron star companion. The deeper of the two minima occurs at the phase of X-ray eclipse, an effect which indicates that the observed optical brightness of the primary star may at times include a component which is due to heating of the surface by X-rays emitted at the neutron star. A similar analysis was performed earlier by Howarth (1982), who suggests that X-ray heating increases the observed optical flux significantly only between orbital phases $0.2 < ø < 0.8$. It is claimed that in order to account for the observed excess at ø ≈ 0.1-0.15 and 0.85-0.9, a third source of optical flux is required, one which is periodically co-eclipsed with the X-ray source. Such excess flux is attributed to an accretion disc about the neutron star which contributes ≈ 5 % of the total V-band optical luminosity of the

Figure 7.4

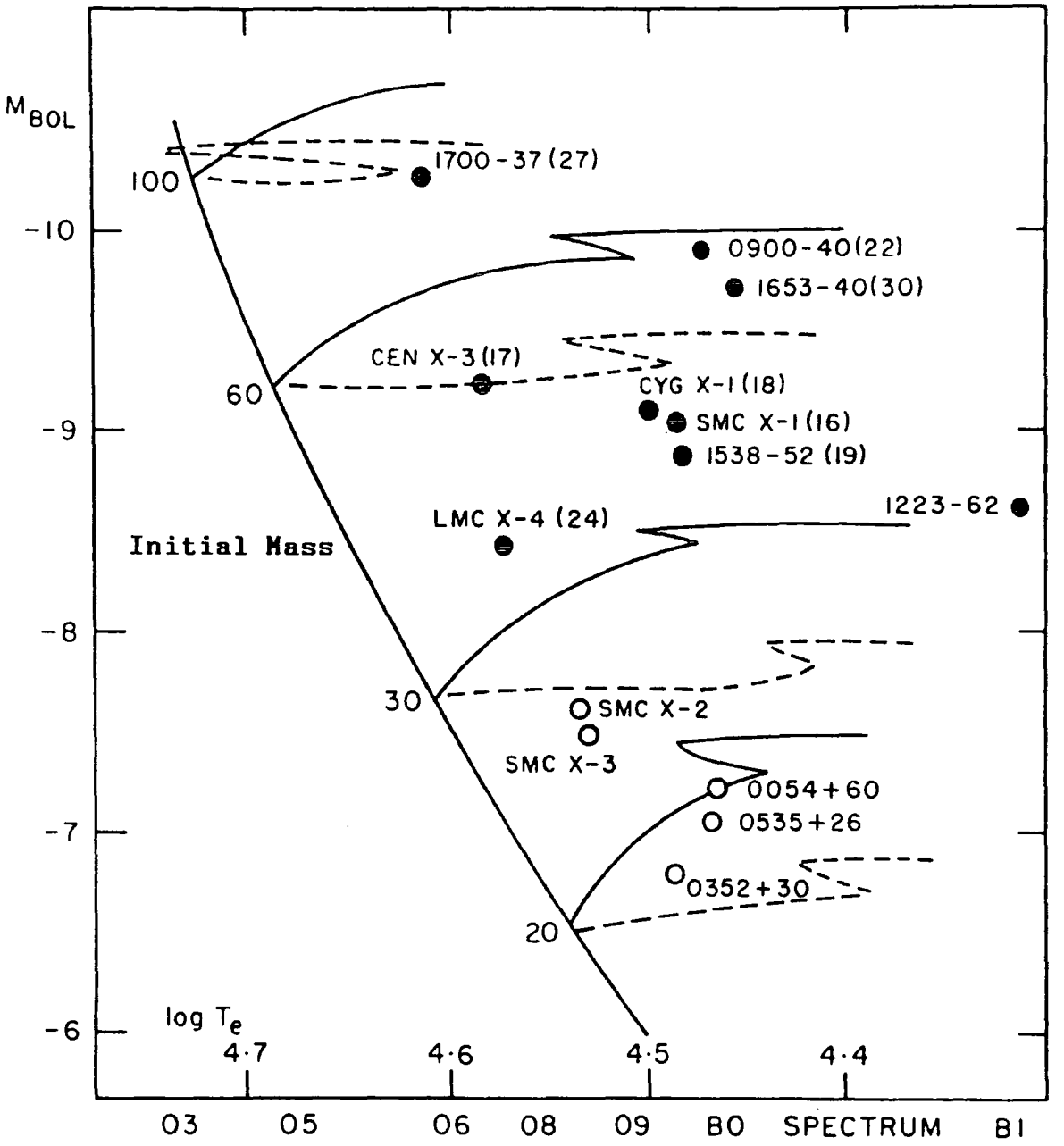

H-R diagram with positions of HMXRB primaries.

Filled circles: supergiant primaries

Open circles: Be primaries

Masses in $M_\odot$ given in parentheses

Solid and dashed lines: possible evolution tracks leading from line of initial mass (in $M_\odot$)

(From Hutchings 1982)

Figure 7.5

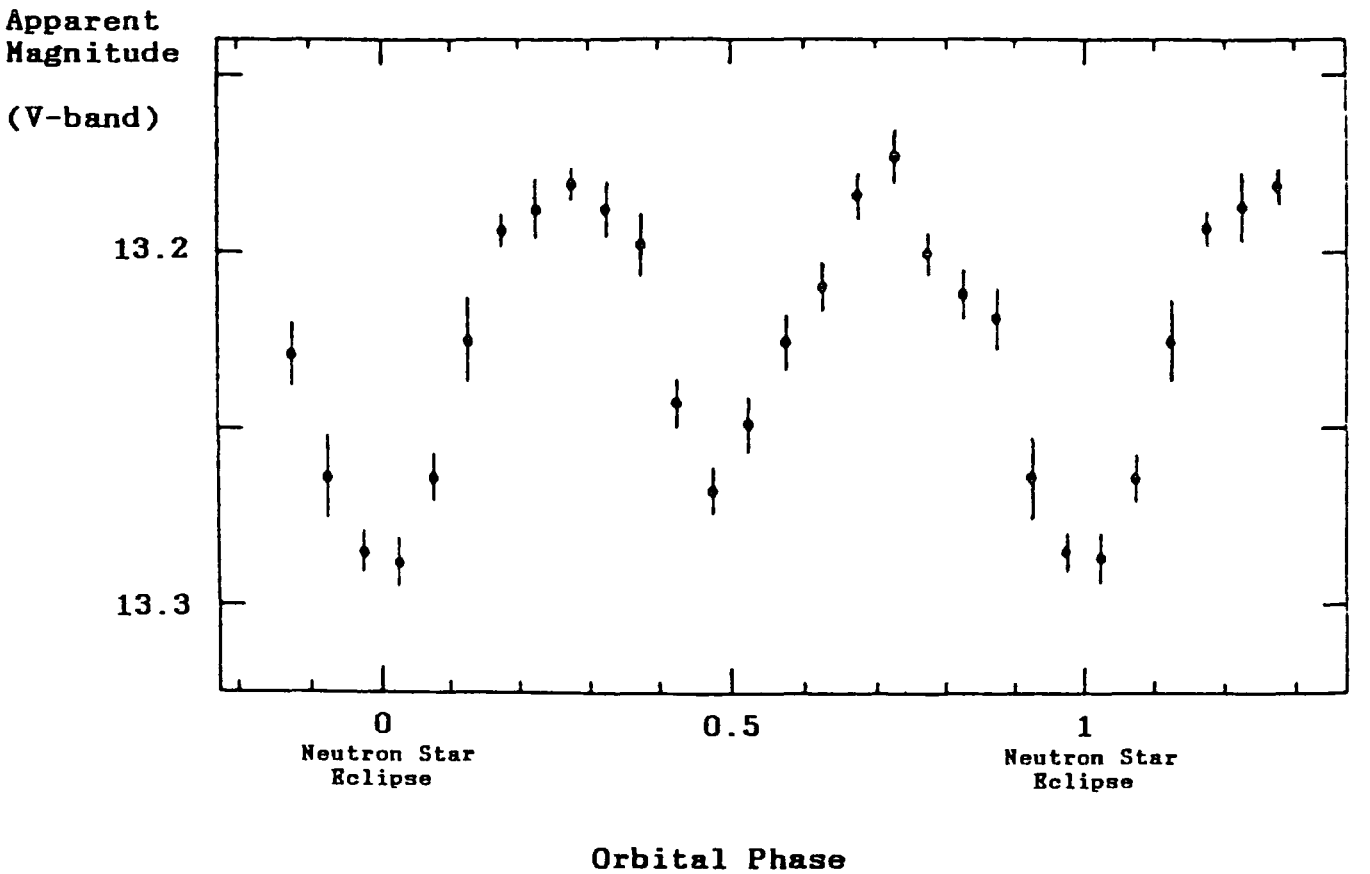

SMC X-1: Average Optical Light Curve

(From van Paradijs and Kuiper 1984)

binary.

7.2.7 Orbital and Stellar Parameters of the SMC X-1 Binary

Primini *et al.* (1976) were the first to publish a full set of values for the binary parameters of SMC X-1. This followed a study of the variation of the X-ray pulse period with orbital phase using SAS-3 2-6 keV data obtained over the course of one binary cycle. The results of a refined analysis were presented by Primini, Rappaport and Joss (1977) and are listed in Table 7.2.

SMC X-1 has a circular orbit ($e < 0.0007$) which is inclined to the plane of the sky at an angle of $i = 53^{\circ}-73^{\circ}$. The projected semi-major axis has a value of 53.46 ± 0.05 ls. Tuohy and Rapley (1975) used X-ray measurements performed with the *Copernicus* Observatory to determine a value for the orbital period. Since that time, five observations of the epoch of X-ray mid-eclipse have been made using the SAS-3, *Ariel V*, *Einstein*, *Ginga*, and *Mir-Kvant* experiments. Binary cycle number is plotted against all six measurements of epoch (including the *Copernicus* value) in Figure 7.6; they are listed, with references, in Table 7.3. A least squares fit to these measurements provides a value of orbital period of $P_{orb} = 3^{d}.89212 \pm 0^{d}.00010$, which is consistent with the value of $3^{d}.89217 \pm 0^{d}.00012$ reported by Tuohy and Rapley (1975).

Parameter	Value	Reference
Projected semi-major axis	53.46 ± 0.05 ls	Primini, Rappaport and Joss (1977)
Eccentricity	< 0.0007	" " "
Inclination to plane of sky	53° - 73°	" " "
Eclipse 1/2-angle	28°.2 ± 0°.9	" " "
Orbital period	$3^d.89217 \pm 0^d.00012$	Tuohy and Rapley (1975)
Orbital period	$3^d.89212 \pm 0^d.00010$	This work
Epoch of X-ray mid-Eclipse	MJD 7534.59 ±0.01	Gilfanov *et al.* (1989)

Table 7.2 Orbital Parameters of the SMC X-1 Binary

Figure 7.6

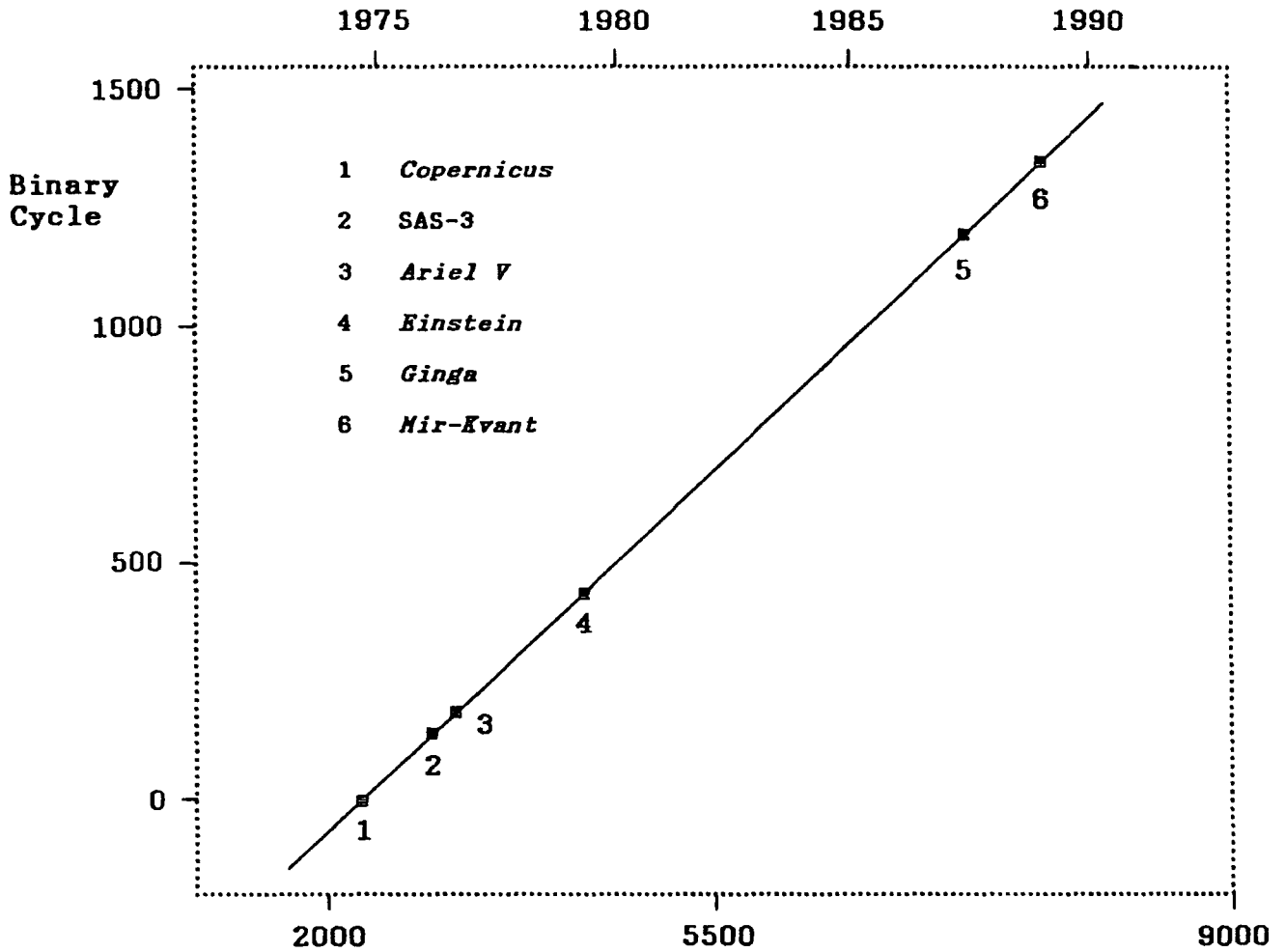

SMC X-1: Least Squares Fit to Measurements of Epoch of X-Ray Mid-Eclipse

Experiment	Epoch of X-ray Mid-Eclipse (MJD)	Binary Cycle
Copernicus (Tuohy and Rapley 1975)	2276.15 ± 0.04	0
SAS-3 (Primimi, Rappaport and Joss 1977)	2836.6823 ± 0.0002	144
Ariel V Davison (1977)	3000.1562 ± 0.0016	186
Einstein (Darbro *et al.* 1981)	3986.407	439
Ginga (Takeshima 1987)	6942.94 ± 0.01	1199
Mir-Kvant (Gilfanov *et al.* 1989)	7534.59 ± 0.01	1351

Table 7.3 SMC X-1: Measurements of Epoch of X-Ray Mid-Eclipse

Parameter	Value
Mass of primary ($M_{vis}/M_{\odot}$)	16.7 ± 1.8
Mass of neutron star ($M_x/M_{\odot}$)	1.41 ± 0.49
Radius of primary (ls)	38.3 ± 4.4
Radius of accretion disc (ls)	12.1 ± 2.8
Max. radius of neutron star Roche lobe (ls)	16.9 ± 2.6
Separation of components (ls)	63.3 ± 1.6
Orbital inclination (deg)	64.5 ± 4.5
Visual disc luminosity (ergs s^{-1})	(2.7 ± 1.8) x 10^{35}
Visual luminosity of primary (ergs s^{-1})	~ 6 x 10^{38}

Table 7.4 Parameters of the SMC X-1 Binary

(From the results of Khruzina and Cherepashchuk 1987)

Figure 7.7

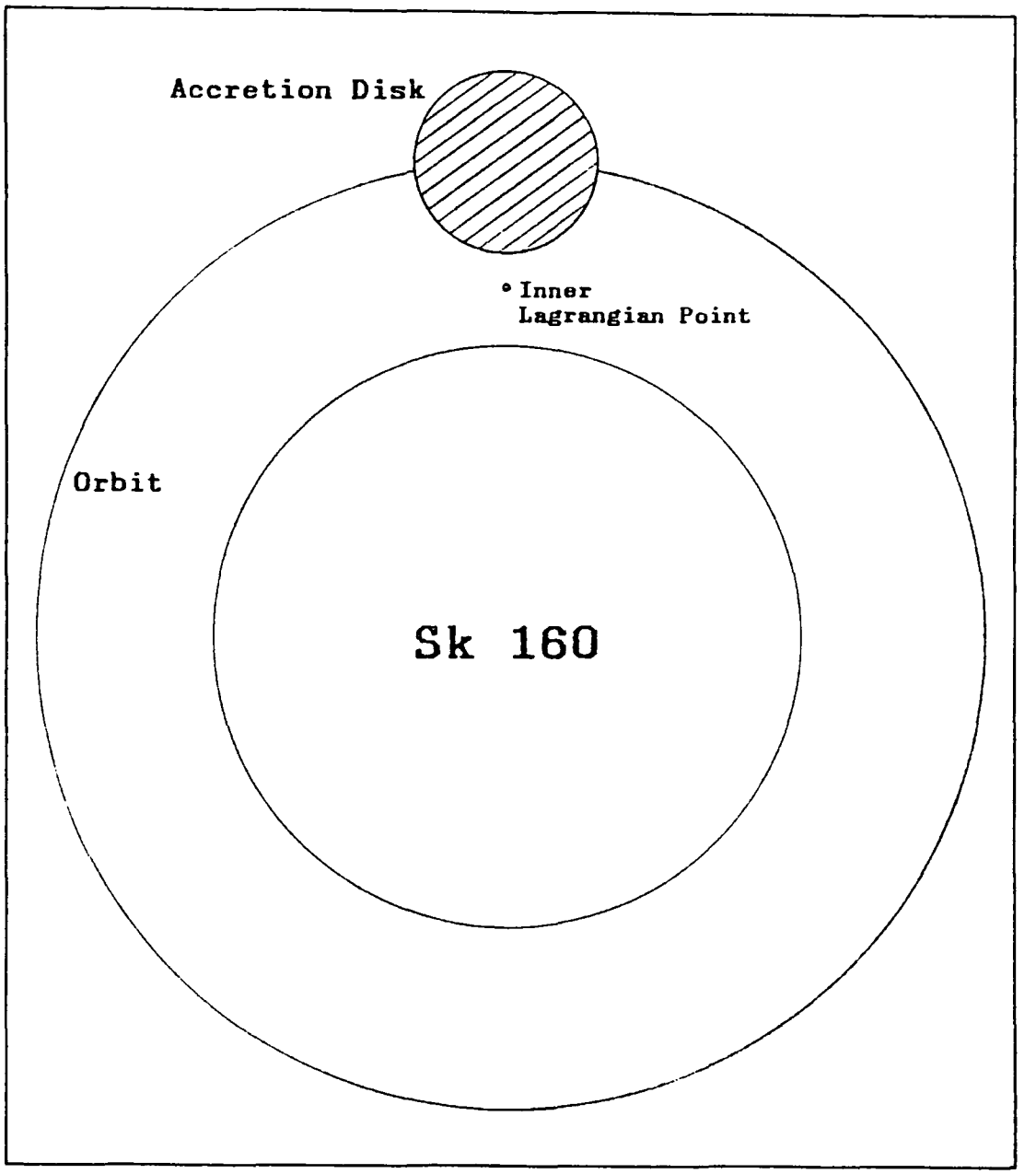

SMC X-1 Viewed Into Orbital Plane

(To Scale)

The parameters of the SMC X-1 binary have also been studied by Khruzina and Cherepashchuck (1987) using the results of the optical and X-ray observations. The optical light curve was investigated using a model of the binary in which the visible star is heated by isotropic X-ray flux emitted at a point source; the X-ray source is assumed to be encircled by a thin, flat, optically opaque, luminous accretion disk orientated within the orbital plane. The stellar and orbital parameters obtained from this analysis are listed in Table 7.4. The values claimed for inclination angle and the separation of the components are consistent with the value of the projected semi-major axis reported by Primini, Rappaport and Joss (1977).

A sketch of the SMC X-1 binary is shown in Figure 7.7 for a line-of-sight which is normal to the plane of the orbit.

7.3 The Narrabri Database

7.3.1 Observation Log

SMC X-1 has been observed from Narrabri at an energy threshold $E = 0.4$ TeV on 94 nights during the interval 1986 October 24 to 1989 December 01. The telescope was operated in the tracking mode at all times. An observation log is given in Table 7.5; it includes for each night the duration of the observation, the number of Cerenkov events selected during routine pre-analysis data processing (Section 7.3.2), the value of UT at the middle

	DATE	DURATION (hr)	NUMBER OF EVENTS	UT AT MID-POINT	ZENITH ANGLES	CHANNELS OPERATING
1)	241086	2.0	2954	13:15	43°-41°	1000
	251086	2.5	2909	12:30		1234
	261086	3.4	3880	12:20		1200
	271086	3.8	2675	12:00		1234
	281086	1.6	1859	12:40		1234
	301086	2.1	2252	12:55		1234
	011186	3.5	8500	12:00		1000
	021186	2.7	6174	11:40		1000
	031186	3.3	7542	11:50		1000
	041186	2.4	4610	12:20		1000
2)	210787	2.9	1767	17:35	57°-41°	1234567
	220787	3.4	2113	17:25		1234567
	230787	4.3	5556	17:40		1234567
	240787	4.1	4974	17:20		1234567
	250787	3.3	1423	16:40		1234567
	260787	1.4	1716	17:15		1234567
	280787	2.8	3077	17:00		1234567
	290787	4.3	1998	16:55		1234567
	310787	5.0	5216	17:05		1234567
3)	200887	2.8	2270	15:35	52°-41°	1234567
	210887	2.7	3123	15:35		1234567
	220887	2.9	3367	15:30		1234567
	230887	2.7	3388	13:35		1234567
	240887	3.2	2860	15:20		1234567
	250887	3.2	3869	15:20		1234567
	260887	3.2	4075	15:20		1234567
	280887	3.3	2947	15:15		1234567
4)	140987	2.3	1993	14:10	54°-41°	1234567
	150987	3.3	4136	13:45		1234567
	160987	3.3	3624	13:20		1234567
	170987	2.1	1517	14:20		1234567
	180987	3.7	3911	13:35		1234567
	190987	3.8	3291	13:35		1234567
	200987	1.6	1213	13:35		1234567
	210987	3.8	3297	13:35		1234567
	220987	3.8	3084	13:35		1234567
	230987	2.8	2441	14:05		1234567
	240987	3.3	1352	13:55		1234567
	250987	3.3	2370	13:50		1234567
	260987	2.0	1309	15:25		1234567
	270987	4.3	2839	17:10		1234567

Table 7.5 SMC X-1: Narrabri Observation Log

	DATE	DURATION (hr)	NUMBER OF EVENTS	UT AT MID-POINT	ZENITH ANGLES	CHANNELS OPERATING
5)	101087	1.7	1468	10:45	55°-41°	1234567
	111087	2.9	1780	11:20		1234567
	121087	3.9	2621	11:55		1034567
	141087	4.1	3326	11:45		1234567
	161087	2.1	1386	14:35		1234567
	171087	4.0	3984	11:55		1234567
	181087	4.0	3693	11:55		1234567
	221087	2.9	3828	11:25		1234567
	231087	1.8	1870	12:00		1034567
	251087	2.0	2864	11:50		1234567
6)	131187	1.9	1772	12:00	41°-43°	1234560
	151187	2.6	1003	12:15		1234560
	171187	3.1	1748	11:55		1234560
	181187	3.1	3604	12:10		1234560
	191187	3.1	3648	11:55		1234560
7)	140788	3.3	4960	18:05	50°-41°	1234000
	160788	3.4	4737	18:00		1234000
	170788	3.4	5309	18:00		1234000
	180788	3.4	5500	18:00		1234000
	200788	3.3	1175	18:05		1234000
8)	040988	3.8	1016	14:55	53°-41°	1234567
	070988	4.0	4244	14:30		1234567
	090988	4.5	5014	13:50		1234567
	100988	6.4	8617	15:15		1234567
	120988	5.7	6892	15:40		1234567
	130988	5.2	13395	13:55		1234567
	140988	4.0	9601	14:15		1234567
	160988	5.2	6059	15:55		1234567
9)	220989	5.3	7377	12:50	60°-41°	1234567
	230989	3.8	4132	13:24		1234567
	240989	4.0	4976	14:01		1234567
	260989	4.9	4131	13:38		1234567
	280989	3.6	6321	13:04		1234567
	290989	4.0	6369	13:30		1234567
	300989	5.1	2477	13:11		1234567
	011089	4.7	7650	13:07		1234567
	021089	5.6	8709	12:44		1234567
	031089	4.3	5845	12:42		1234567
	041089	3.3	3255	14:34		1234567

Table 7.5 SMC X-1: Narrabri Observation Log (Cont.)

	DATE	DURATION (hr)	NUMBER OF EVENTS	UT AT MID-POINT	ZENITH ANGLES	CHANNELS OPERATING
10)	201089	1.0	726	13:55	50°-41°	1234567
	221089	5.8	1343	12:37		1234567
	231089	2.3	864	10:53		1234567
	251089	3.8	1638	11:36		1234567
	291089	2.8	1061	13:37		1234567
	301089	2.8	840	13:54		1234567
	021189	1.7	545	12:33		1234567
11)	181189	3.3	1750	11:53	41°-44°	1234567
	191189	4.1	2434	12:11		1234567
	231189	3.3	1808	11:53		1234567
	241189	2.9	500	11:36		1234567
	251189	3.4	1262	11:52		1234567
	291189	3.0	1404	12:28		1234567
	011289	1.8	1122	12:15		1234567

Table 7.5 SMC X-1: Narrabri Observation Log (Cont.)

Total nights:	94
Total hours:	315.6
Total events:	327,124
Average duration:	3.4 hr
Average count rate:	$\approx$ 1000 hr^{-1}

of the observation, the zenith angles at which SMC X-1 was monitored, and the telescope detector channels in operation.

From an aggregate of 327,124 Cerenkov events logged during a total of 315.6 hours, a mean count rate of 1037 events hr^{-1} was recorded during an average observation spanning 3.4 hr. Most of the data (1987 July 21 to 1989 December 01) were taken using an on-axis detector channel located at the centre of a "guard-ring" of six off-axis channels. The observations after 1988 July had the additional benefit of being made with upgraded performance (higher gain) from the photomultiplier tubes.

7.3.2 The Selection of Data for Analysis

Two levels of selection are routinely employed, both of which are systematically applied to all data prior to analysis. Further details are given in Chapter 3.

Consider a file of data recorded during a single observation. From the full set of Cerenkov events in which single-fold and multiple-fold responses are registered across permutations of 1 through 7 detector channels, a subset is initially extracted in which only the central on-axis channel has recorded an event at a level above the hardware discrimination threshold. This selection rejects those events which, though they were registered at the on-axis channel, were also detected by the off-axis channels. Such events do not usually correspond to Cerenkov radiation from air showers in a direction which is

coincident with that of a source candidate.

A second selection is made to further enhance the ratio of a possible γ-ray signal to the strong cosmic ray background. In this selection, the low-level (sub-threshold) photomultiplier tube responses at the off-axis channels are compared with the on-axis channel response. The criterion for rejection is the presence of a "guard ring" signal on any one (or more) of the channels which has a value $\geq$ 60 % of that registered by the central channel alone.

CHAPTER 8

Pulse Timing Analysis of the SMC X-1 Database

8.1 Introduction

All Cerenkov arrival time series recorded during the observations of SMC X-1 are to be tested for pulse periodicity.

Before the period analysis can be conducted, the time series must first be transformed to the rest frame of the SMC X-1 binary. This is performed in order to eliminate the Doppler shift of the value of the pulse period caused by the orbital motion of the neutron star.

SMC X-1 has one of the shortest pulse periods of all X-ray pulsars measured to date. It is also one of the largest supergiant X-ray binaries discovered so far. It will be seen that these properties combine to demand a relatively accurate knowledge of the orientation of the SMC X-1 binary at any given time so that the Doppler corrections will be adequate to maintain pulse phase coherence. In contrast, it is a comparatively simple task to recover periodic components from time series recorded during observations of the X-ray binaries Vela X-1, Cen X-3 and LMC X-4; Doppler corrections of sufficient accuracy could be made for these source candidates even in the absence of a good orbital ephemeris.

However, the SMC X-1 orbital ephemeris is well measured at X-ray energies so that this problem can be turned to advantage. Spatial information on the site of γ-ray production can, assuming that a γ-ray signal is present, be extracted by the very fact that the period analysis of the SMC X-1 data will be particularly sensitive to the configuration of the binary. In principle, therefore, the transformation of arrival times can be used as a probe to investigate whether a γ-ray emission site is co-located with the SMC X-1 neutron star or if it is displaced to some point on or beyond the accretion disk. This possibility is explored in the present chapter.

The method employed for the period analysis of the data is descibed in Sections 8.2 to 8.7. The results of the work are presented in Sections 8.8 to 8.11. The chapter concludes with a discussion of the results.

8.2 The Strategy for Analysis of the Database

When there is a possibility that high-energy γ-ray emission might be pulsed at a known frequency, the period analysis of a recorded time series offers the most powerful test for evidence of an enhancement in the number of Cerenkov events observed in the direction of a source candidate. It is postulated in the present analysis that, should it exist, TeV γ-ray emission from SMC X-1 will be detected as a sequence of pulses with a frequency which is identical to that of the contemporary pulsed X-ray emission.

The null hypothesis is adopted and tested. In other words, it is first postulated that a recorded Cerenkov arrival time series is distributed randomly and contains no evidence for pulsed γ-ray emission. If the null hypothesis is true then the unfolding of a time series at any given period must reveal a uniform distribution of phase. Since there is no *a priori* knowledge of the shape of the SMC X-1 pulsar light-curve at TeV γ-ray energies, the Rayleigh test is selected - as the uniformly most powerful - in order to inspect the data for such uniformity in phase. The probability that any observed non-uniformity is due entirely to chance is then used to decide whether to accept or to reject the null hypothesis.

8.3 Transformation of Event Times to the SMC X-1 Rest Frame

The neutron star in the SMC X-1 binary revolves about its supergiant companion with a speed = $2\pi a_x / P_{orb} \approx 350$ km s^{-1}, where a_x is the semi-major axis of the orbit.

The binary is viewed at a high angle of inclination, so that the speed of the neutron star is sufficient to produce a measurable sinusoidal Doppler variation in the observed frequency of pulsed emission. If P' is the pulse period measured in the rest frame of the observer, then

$$P' = P_o \left[1 - \frac{v}{c} \sin(\varphi_o + \varphi) \right] \qquad (1)$$

where P_o is the pulse period in the rest frame of the binary and v and φ are the speed and orbital phase of the neutron star, respectively.

The observed peak amplitude of the variation of the SMC X-1 X-ray pulsar period with orbital phase represents a change by 0.1 % of the binary rest frame period (e.g. Takeshima 1987).

The upper panel in Figure 8.1 shows the maximum duration of an observation of SMC X-1, as a function of orbital phase, for which pulse phase coherence can be maintained across the full length of a recorded time series without making corrections for Doppler shifting. At any given orbital phase, a pulsed component *can* be recovered from a time series if the duration is shorter than this critical length though it will of course be observed at the Doppler shifted period rather than at the binary rest frame value.

Consider the sensitivity of pulse phase coherence to the orbital phase of the neutron star. The definition of zero phase is taken here from the convention adopted in X-ray astronomy and corresponds to the instant when the neutron star is located at the position of mid-eclipse behind the companion. Another name for this phase is superior conjunction. Inferior conjunction corresponds to anti-eclipse, which is therefore orbital phase 0.5. The descending node of the orbit is at phase 0.25 and is the point at which the neutron star has a maximum velocity of approach to the observer; the ascending node is at phase 0.75 and is therefore the point at which the neutron star recedes

Figure 8.1

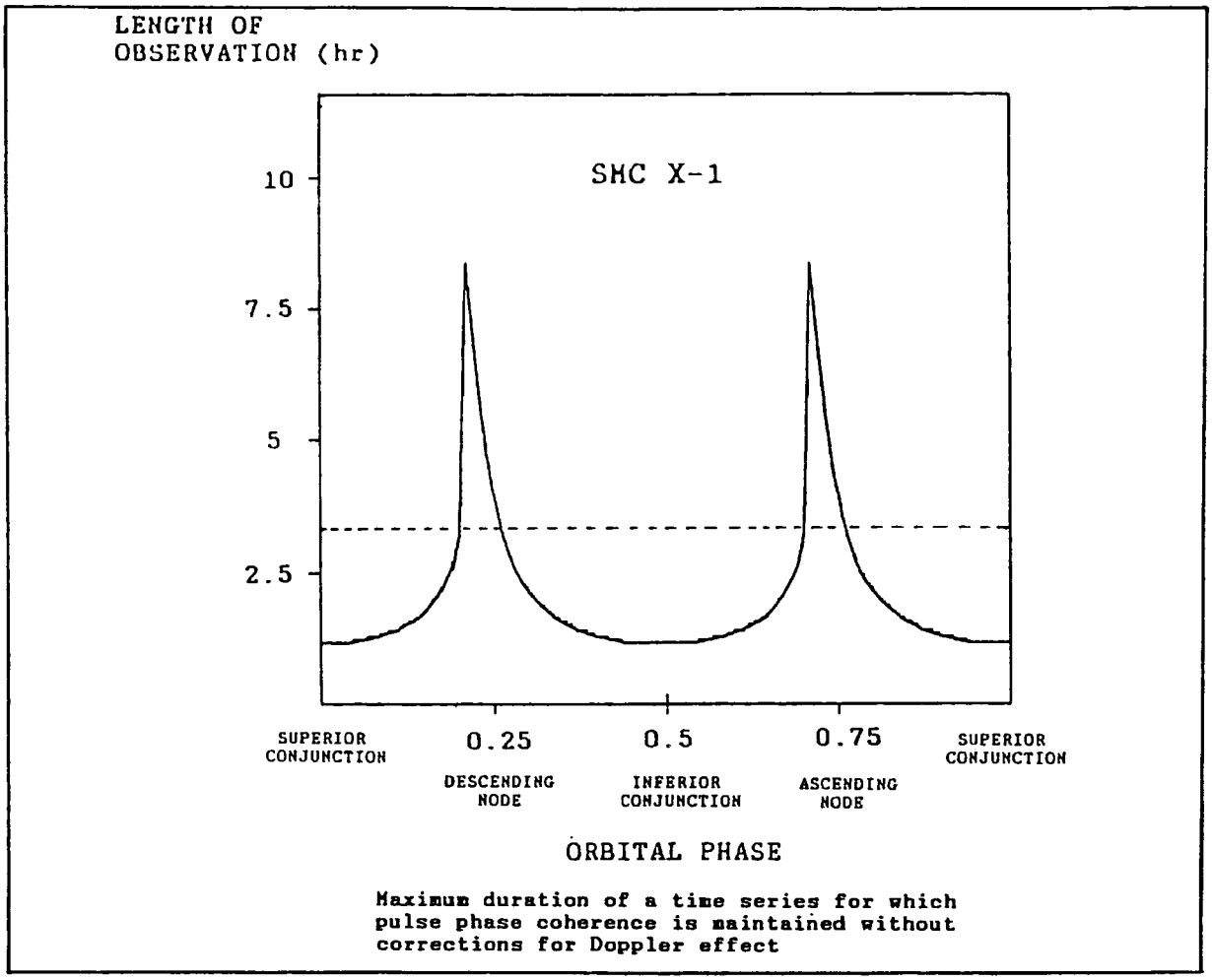
LENGTH OF
OBSERVATION (hr)
SMC X-1
10
7.5
5
2.5
SUPERIOR
CONJUNCTION
0.25
DESCENDING
NODE
0.5
INFERIOR
CONJUNCTION
0.75
ASCENDING
NODE
SUPERIOR
CONJUNCTION
ORBITAL PHASE
Maximum duration of a time series for which
pulse phase coherence is maintained without
corrections for Doppler effect

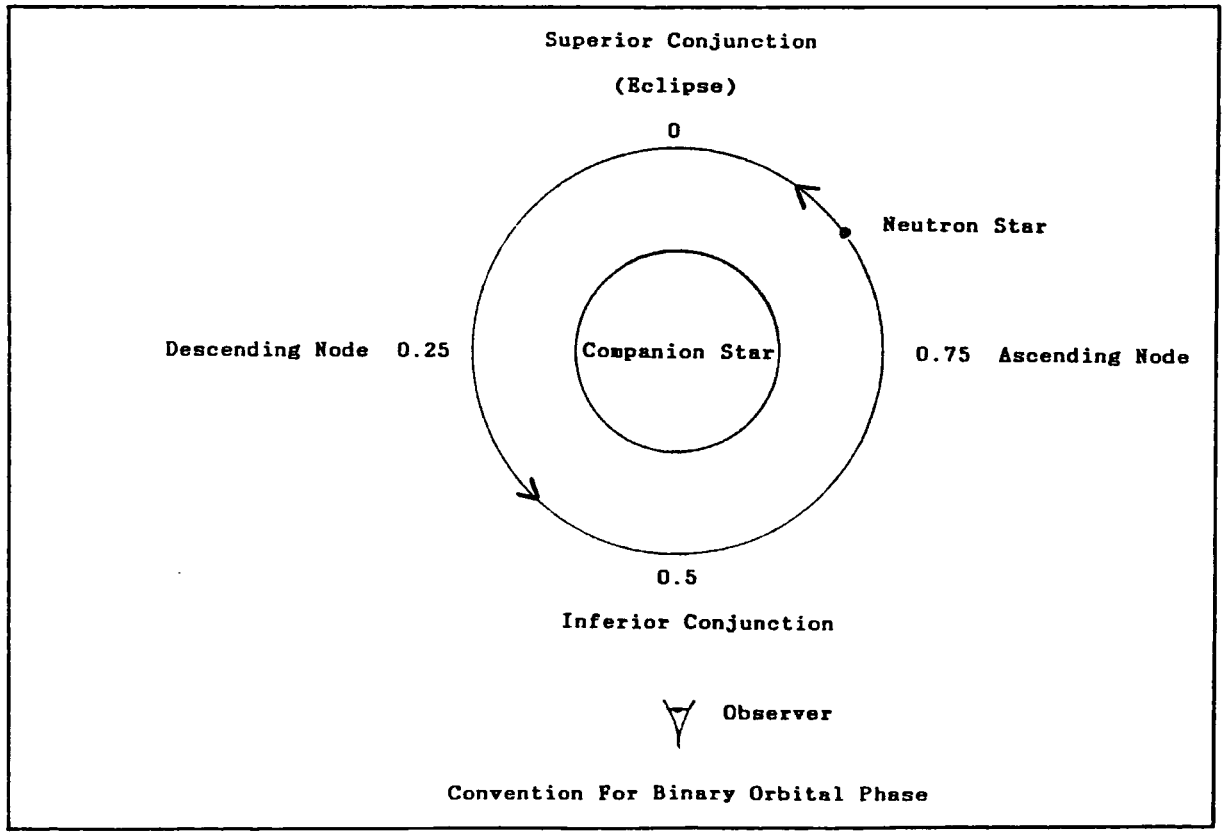
Superior Conjunction
(Eclipse)
0
Neutron Star
Descending Node
0.25
Companion Star
0.75
Ascending Node
0.5
Inferior Conjunction
Observer
Convention For Binary Orbital Phase

with maximum velocity. The orbital phase nomenclature is summarised in the lower panel of Figure 8.1. Without corrections for Doppler shifting, pulse phase coherence is soon lost for a time series which is recorded when the neutron star is at inferior or superior conjunction. This is because the rate of change of the radial velocity component is greatest at these orbital phases. Conversely, relatively long observations are tolerated in the vicinity of the ascending and descending nodes. Although the Doppler shift reaches a maximum at the nodes, the rate of change of the radial velocity component drops rapidly and falls to zero for an instant as the nodes are crossed.

It can be seen in the upper panel of Figure 8.1 that pulse phase coherence is maintained at any orbital phase for observations of SMC X-1 which are shorter than 1.2 hours. The horizontal dashed line drawn at 3.4 hr corresponds to the average duration of the observations performed at Narrabri. Corrections for Doppler shifting are necessary for observations of this length when the neutron star is within the phase ranges 0.3 to 0.7 and 0.8 to 0.2, i.e. Doppler corrections are required here for the majority of orbital phases.

All the time series recorded at Narrabri during observations of SMC X-1 will be transformed to the rest frame of the SMC X-1 binary irrespective of the orbital phase and the duration of the observation. A search will then be made for a periodic component at the expected rest frame value of the X-ray pulse period. To consider how the Doppler corrections are made, see Figure 8.2,

Figure 8.2

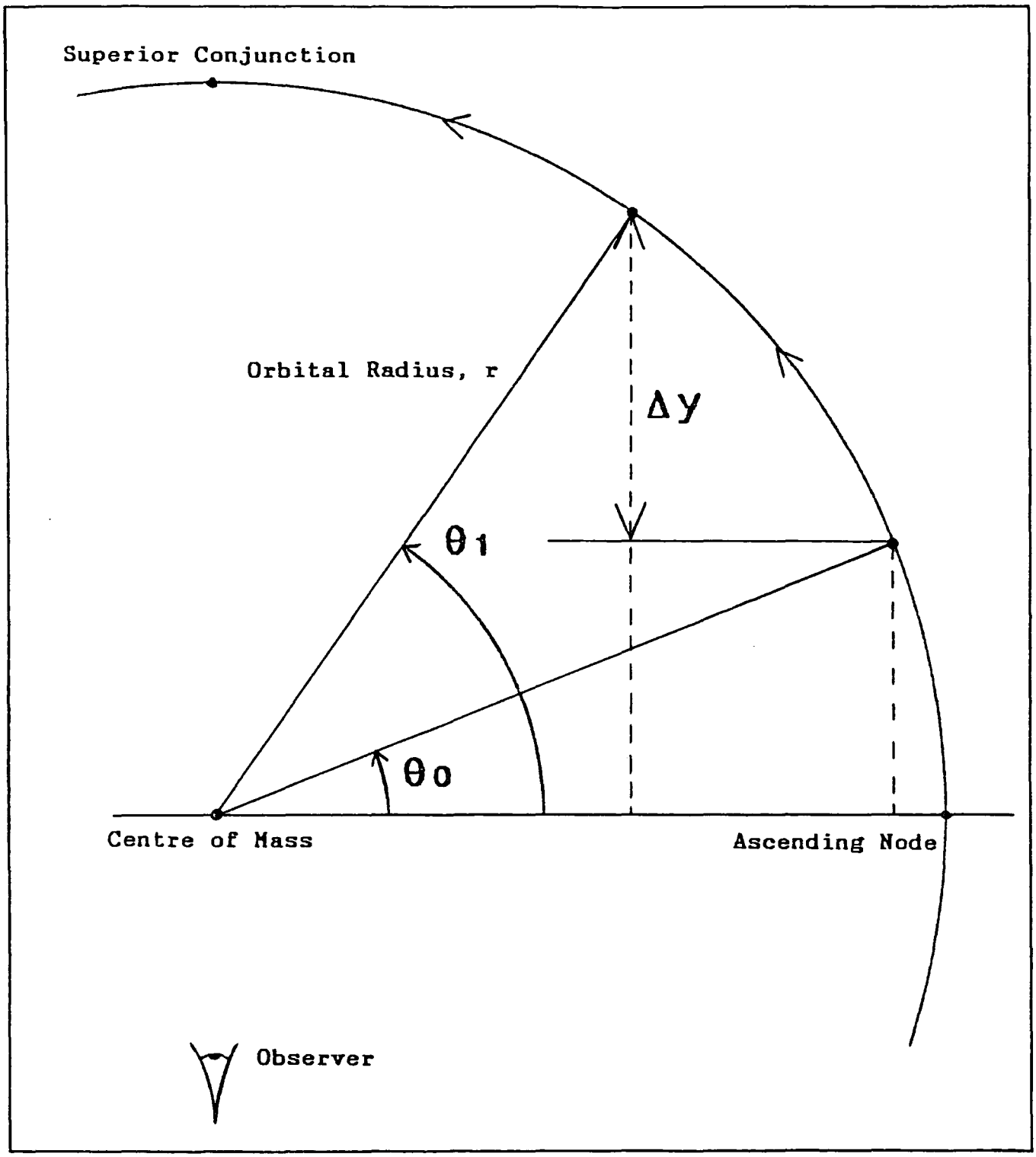

Orbital Geometry for Computation

of Correction for Doppler Shifting

where the observer is taken to be in the orbital plane of the binary. The orbital phase is here measured anticlockwise from the ascending node. Let a photon be emitted at pulsar phase φ_0 when the neutron star is at orbital phase θ_0. In the pulsar rest frame, a second photon emitted after an interval of time t will have a pulse phase φ given simply by

$$\varphi(t) = \varphi_0 + ft \qquad (2)$$

where f is the pulsar rotation frequency. However the neutron star has moved to orbital phase θ_1 by the time this second photon leaves the pulsar (Figure 8.2); the photon therefore travels an extra distance Δy *en route* to the observer, so that the time t' at which the second photon is registered by the observer is increased to

$$t' = t + \frac{r}{c}(\sin\theta_1 - \sin\theta_0) \qquad (3)$$

where a circular orbit has been assumed. Substituting for t on the right-hand-side of equation 2,

$$\varphi(t) = \varphi_0 + f\left[t' - \frac{r}{c}(\sin\theta_1 - \sin\theta_0)\right] \qquad (4)$$

The correct relative pulse phase is therefore obtained simply by adjusting the time (t') recorded at the telescope by the extra time of flight within the binary system. Since the value of θ_0 is arbitrary, it can be set to zero. The general expression for t is then

$$t = t' - \frac{r}{c} \sin\theta \qquad (5)$$

Or, setting $r = a_x \sin i$ and expressing the orbital radius in units of light-travel time,

$$t = t' - a_x \sin i \sin\theta \qquad (6)$$

If t' is set to zero at the time of a measurement of the epoch of X-ray mid-eclipse then equation 6 becomes

$$t = t' - a_x \sin i \sin \pi\left[\frac{1}{2} + \frac{2t'}{P_{orb}} \right] \qquad (7)$$

where P_{orb} is the binary period. Doppler corrections to all times (t') of Cerenkov events registered at the telescope are made using equation 7.

8.4 Temporal and Spatial Resolution of the Period Analysis

It is well known that if a time series is tested for periodicity across some range of candidate values of pulse period P_1 to P_2, it is not necessary that the data should be analysed at the infinite number of period values within this interval. Instead, the test needs to be performed only at periods separated by an amount which is governed by the magnitude of the trial period (P) and the total duration (Δt) of the time series. In Chapter 4 it was shown that the separation - the sampling interval - of independent values of period is just $P^2/\Delta t$. Therefore if a time series is modulated at a given period, then most or all of the periodic component will be recovered as long as it is analysed within one sampling interval of this period.

In the same way, there are finite sampling intervals in the values of the orbital elements, so that a very precise knowledge of the location of a γ-ray emission site in an X-ray binary is not required in order to make an adequate compensation for the Doppler shift of a γ-ray pulse period. There is a finite 'error box', within which the Doppler corrections will be indistinguishable: the γ-ray periodicity will be recovered from a time series if the emission site is known to be inside this box during a given observation. The size of the box is determined by the separations between independent values of the orbital elements. These in turn, depend upon the values of the orbital elements themselves, the duration of the time series, the orbital phase of the emission site during the observation, and

the magnitude of the expected γ-ray pulse period.

Consider two extreme examples:

(1) Take the case when the statistical errors reported on the values of the orbital elements of a binary system greatly exceed the sampling intervals appropriate to the γ-ray period analysis. A problem then arises. It is then highly unlikely that the full γ-ray signal strength will be recovered if an attempt has been made to transform the event times to the binary rest frame by naively selecting only the reported values of the orbital elements. A failure to take samples of the orbital elements will often lead to a false acceptance of the null hypothesis.

(2) Conversely, when the independent sampling intervals are very much larger than the measurement errors, there is a good chance that the transformation of a time series using the reported values of the orbital elements will allow the recovery of most of the periodic component, although a small amount of sampling within the interval will still be required in order to be sure of recognising the full signal strength.

The period analysis of the SMC X-1 database is an example of case (2). It will be seen, however, that the particular values of the X-ray pulsar period and the orbital elements, coupled with the typical length of an observation performed at Narrabri, lead to sampling intervals which are *small* when compared with those of other X-ray binary pulsars.

Therein lies the potential of the pulse timing analysis. The SMC X-1 orbital ephemeris has been well measured using the X-ray observations so that, in principle, the location of a γ-ray source at SMC X-1 can be investigated using the good spatial resolution offered by the test for periodicity. Indeed, it is already known that the γ-ray emission region in an X-ray binary is not necessarily co-located with the neutron star X-ray source. Both Hercules X-1 and Vela X-1 have been detected at TeV γ-ray energies during the predicted time of X-ray eclipse, indicating that the origin of the observed γ-ray emission can be displaced considerably from the neutron star and is possibly located at the limb of the companion. See Gorham *et al.* (1986), North et al. (1987), and Raubenheimer *et al.* (1989). Protheroe and Stanev (1987) have modelled the observed Cygnus X-3 γ-ray orbital light curve using an emission site which is positioned at a bulge towards the edge of the neutron star accretion disk. The Centaurus X-3 high-mass binary is detected at TeV energies only when the neutron star is in the vicinity of the ascending node of the orbit. See Carraminana *et al.* (1989b), Brazier *et al.* (1989b, 1990a), and North *et al.* (1989). The present author has considered the Centaurus X-3 orbital light curve (Chapter 12) in terms of ultrahigh energy protons which originate at the neutron star and interact with an accretion wake.

The identification of γ-ray emission regions in each of these binary systems was indirect and was inferred from a knowledge of the orbital phase of the neutron star at the time when γ-ray emission was detected. In the case of SMC X-1 it may be

possible, for the first time, to identify directly the position of a γ-ray emission site in an X-ray binary.

8.5 Sampling Intervals for the Orbital Elements

Consider which of the SMC X-1 binary parameters should be examined. Primini, Rappaport and Joss (1977) reported an upper limit for the eccentricity of the binary orbit of e = 0.007. The orbit will be assumed to be circular here. The value of the orbital period is accurately known from a least squares fit to the measurements of the epoch of X-ray mid-eclipse ($P = 3^d.89212 \pm 0^d.00010$; Chapter 7).

If a γ-ray emission site is co-moving with the SMC X-1 neutron star about the primary then only two quantities need to be inspected in order to identify its location. These are

i) Projected semi-major axis, or $a_x \sin i$, where a_x is the semi-major axis of the orbit and i is the angle of inclination of the orbital plane to the plane of the sky. This quantity is just the projected radial displacement from the centre-of-mass of the binary which, in the case of SMC X-1, can be considered to be coincident with the centre of the giant companion star.

ii) Orbital phase. This will be examined using the known phase of the neutron star as a reference value, the zero of which is

defined at the epoch of X-ray mid-eclipse. An investigation of the value of this epoch is therefore identical to probing the value of orbital phase.

Both these quantities appeared directly as variables in the expression derived earlier for the transformation of times to the binary frame:

$$t = t' - a_x \sin i \sin \pi \left[\frac{1}{2} + \frac{2t'}{P_{orb}} \right]$$

where the observed time t' is measured from the epoch of mid-eclipse. The recovery of a periodic component in a given time series will therefore be tested as a function of $a_x \sin i$ and epoch by simply employing a matrix of candidate pairs of values of these two quantities directly with this expression.

The computation of the intervals between independent values of $a_x \sin i$ and epoch is described in an appendix to this thesis. Expressions are derived which may be used for any pulse period, observation length, orbital phase, and radial displacement from the companion star.

The LMC X-4, Cen X-3 and SMC X-1 X-ray binaries are drawn to scale in Figure 8.3. The limits of the boxes drawn on each sketch represent the approximate spacing between independent values of $a_x \sin i$ and epoch, radiating from the position of the

Figure 8.3

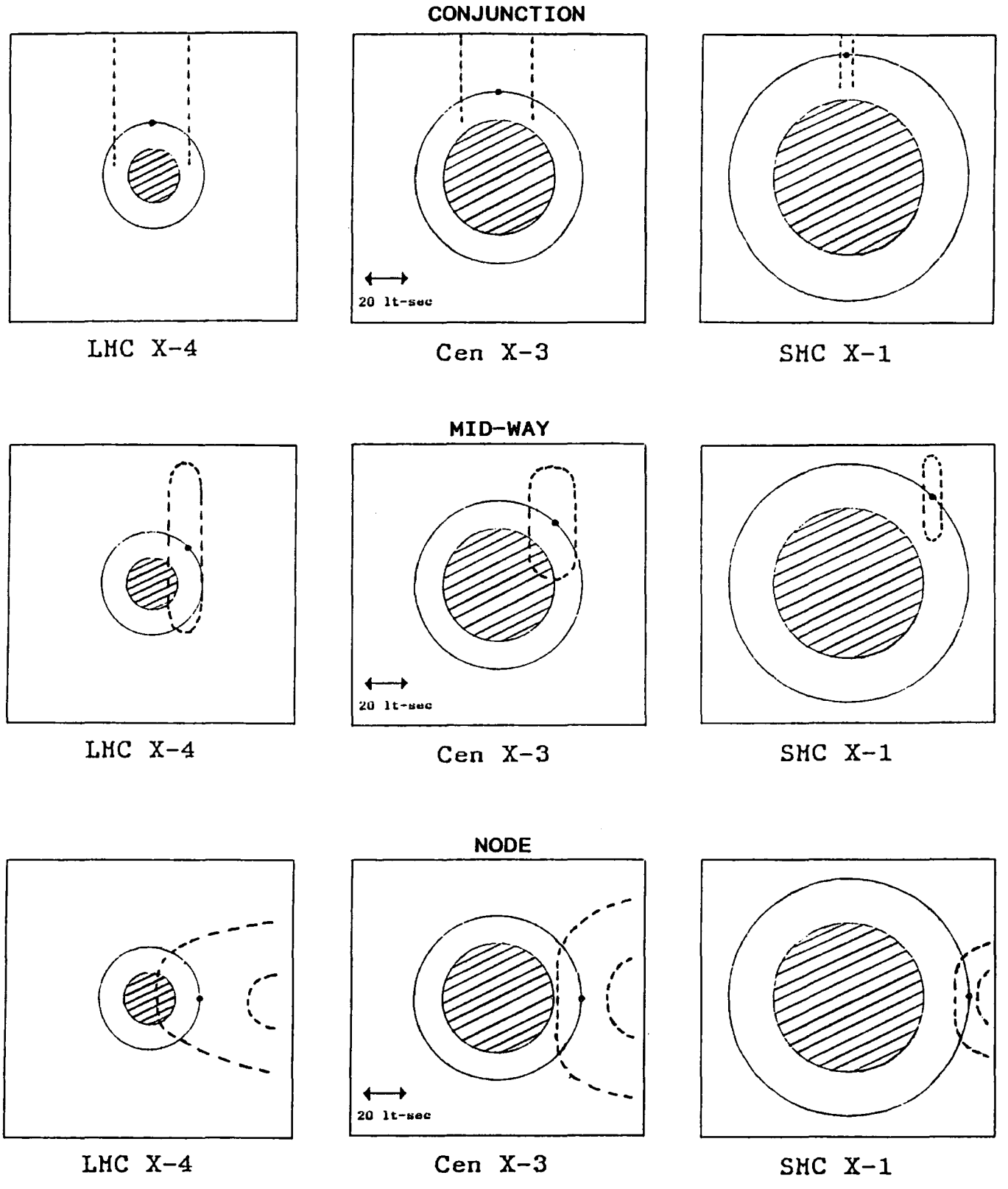

Sampling intervals for $a_x \sin i$ and epoch of mid-eclipse

Solid circle: neutron star orbit

Disk: companion star

Dashed line: Sampling interval 'error box' about position of neutron star

neutron star. Since the size and shape of such a box for a given binary will vary depending upon the observation length and the orbital phase, the example shown here for all three binaries is of an observation with fixed duration. This is set at 3.4 hours, the average length of the observations of SMC X-1 performed at Narrabri. The sampling intervals have been computed for observations of this length which are centred upon neutron star orbital phases of 0 (superior conjunction), 0.75 (ascending node), and 0.875. Compare the narrow error boxes of SMC X-1 with those for LMC X-4 and Cen X-3:

i) The giant X-ray binary LMC X-4 consists of a 13.5-second X-ray pulsar in an orbit of radius 26 lt-sec. The orbital period is 1.4 d. It is evident that adequate Doppler corrections may be made, and pulse phase coherence maintained, using very wide ranges of values of $a_x \sin i$ and mid-eclipse epoch.

ii) The supergiant X-ray binary Cen X-3 has a pulsar period of 4.8 s. The orbital radius is 39.8 lt-sec and the binary period is 2.1 d. The corrections for Doppler shifting are more exacting here but, as with LMC X-4, they are indistinguishable over distances which are large compared with those for SMC X-1.

8.6 Technique for the Period Analysis of the SMC X-1 Database

A typical observing sequence performed at Narrabri comprises ~ 10 short observations spread over an interval of time ~ 10 days. If T is the typical duration of an observation (≈ 3.4 hours) and P_X is the expected value of the X-ray pulsar period (≈ 0.710 ms) at the epoch of a set of γ-ray observations, then the spacing between independent values of candidate pulse periods is $\Delta P_I \approx P_X^2/T = 0.041$ ms. The expected decrease in the value of the X-ray period due to the spin-up of the SMC X-1 neutron star is ≈ 0.010 ms over 10 days, or approximately $\Delta P_I/4$, so that the value of P_X can be regarded as constant during a single observing sequence. This allows the data to be combined and tested for periodicity at a unique value of the X-ray period. The minimum separation of two adjacent observing sequences is ≈ 10 days; since the observations will then be spread over a time ≈ 40 days, the expected secular change in the value of P_X will be comparable with ΔP_I. The data from each of the eleven sets of observations made during 1986-1989 must therefore be analysed separately.

Suppose N separate time series are recorded during one observing sequence. These will be analysed in combination using the following steps:

i) all times are transformed using a candidate pair of values of $a_x \sin i$ and epoch;

ii) the Rayleigh test is applied separately to each time series at successive candidate period values drawn from the range $P_X - \Delta P_I$

$\leq P \leq P_X + \Delta P_I$; at each value the probability for periodicity arising by chance is determined;

iii) at each candidate period (P), the product of the chance probabilities obtained from the N time series is taken in order to construct the statistic:

$$C = -2 \log_e \prod_{j=1}^{N} Pr_j(P) \qquad (8)$$

Under the null hypothesis, this statistic is distributed as χ^2 with 2N degrees of freedom. Thus:

$$Pr(\text{null hypothesis is true}) = Pr(\chi^2_{2N} > C) \qquad (9)$$

(Chapter 4 provides further details of this method).

8.7 Scheme for the Presentation of Results

The results of the period analysis of a time series are usually presented by constructing a periodogram, so that the distribution of chance probabilities may be displayed against candidate values of the pulse period. The present data have been tested for periodicity at the expected X-ray pulse period (P_X), following successive attempts to correct the times for Doppler shifting

using a range of values for the projected semi-major axis and the epoch of mid-eclipse. So, rather than build a periodogram, the aim here is to observe how the chance probabilities at P_x are distributed with candidate values of $a_x \sin i$ and epoch.

The scheme for the presentation of results is illustrated in Figure 8.4. Contours of combined chance probability (equation 8 above) will be drawn in the [epoch,$a_x \sin i$] plane. The ranges of candidate values of these two parameters are chosen to include the full extent of the neutron star accretion disk. Khruzina and Cherepashchuk (1987) have determined a disk radius of r_d = 12.1 ± 2.8 lt-sec, which translates to a range ≈ $P_{orb} r_d/(2\pi a_x \sin i)$ = $0^d.14$ in the value of the epoch of mid-eclipse. The test ranges selected will be slightly in excess of these values in order to explore the possibility that γ-ray emission may arise near the edge of the disk. The expected coordinates of the neutron star will be at the centre of all the probability contour plots: the value of $a_x \sin i$ adopted for the neutron star is that determined by Primini, Rappaport and Joss (1977); the epoch of X-ray mid-eclipse reported by Takeshima (1987) is used as the reference value for the 1986-1987 Narrabri data, while for the 1988-1989 data the contemporary value measured by Gilfanov *et al.* (1989) is taken.

A scale of colours will be used to represent decades of chance probability. The colours will vary from violet for probabilities near to unity, across to deep red for probabilities down to the 10^{-6} level.

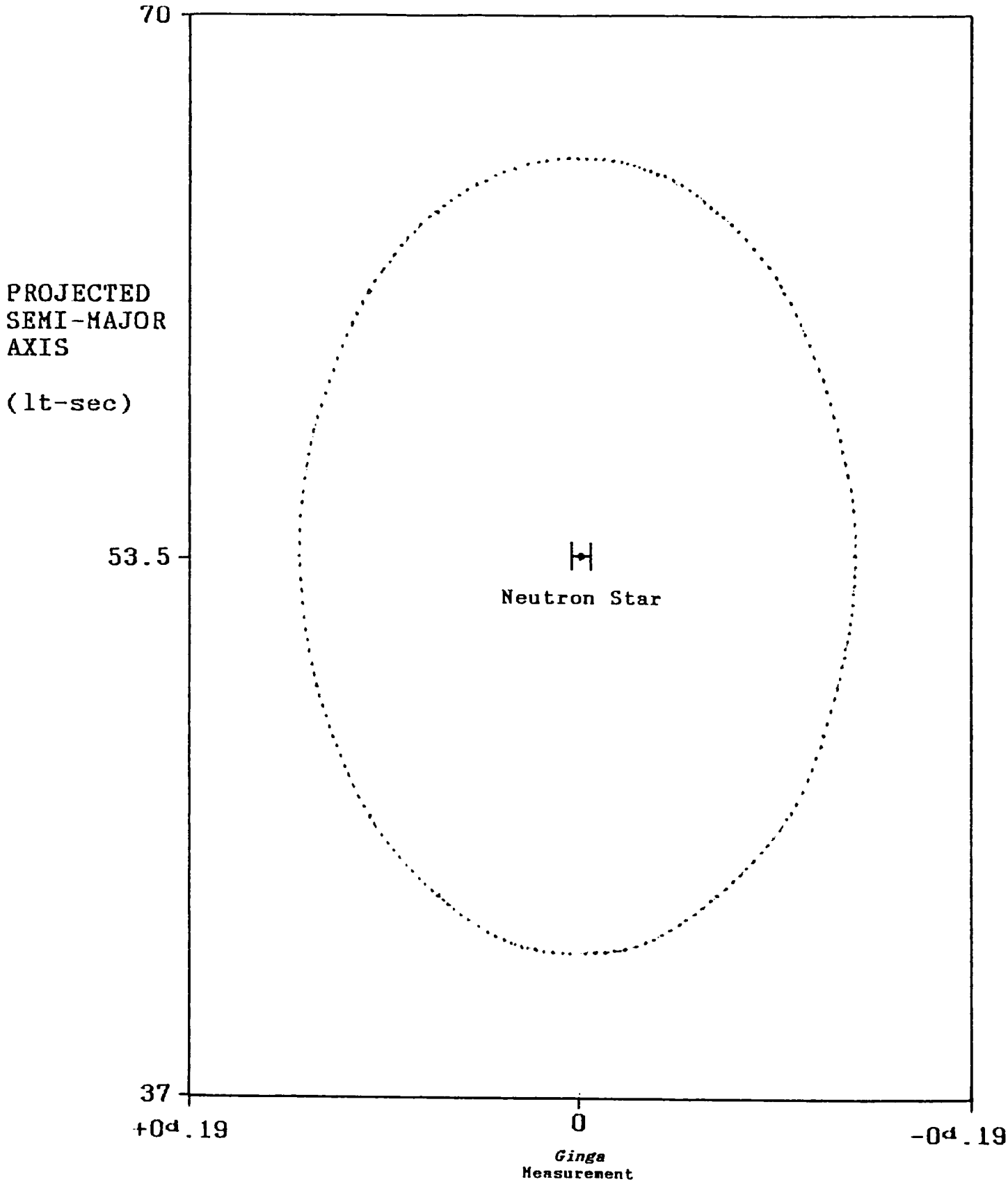

Figure 8.4

[Epoch, $a_x \sin i$] plane in which contours of chance probability will be drawn

..... Boundary of accretion disk

8.8 Results of the Analysis

Contours of chance probability are drawn in Figure 8.5 for the data from each of the eleven observing sequences. The results are consistent with those expected from the analysis of randomly distributed arrival times, with the possible exception of those observed for the two datasets of 1987 July 21-31 and 1989 September 22 - October 04. The contour plots for both these observing sequences display two interesting features:

i) minimum chance probabilities of 5.0×10^{-6} (1987 July) and 5.4×10^{-5} (1989 September-October) are found for periodicity within one period sampling interval of the contemporary value of P_X;

ii) by inspection, the coordinates of the probability minima are near to those of the the SMC X-1 neutron star;

These two datasets will next be examined further. The statistical significance of the results observed here will be assessed following both quality checks and control tests of the data.

Figure 8.5

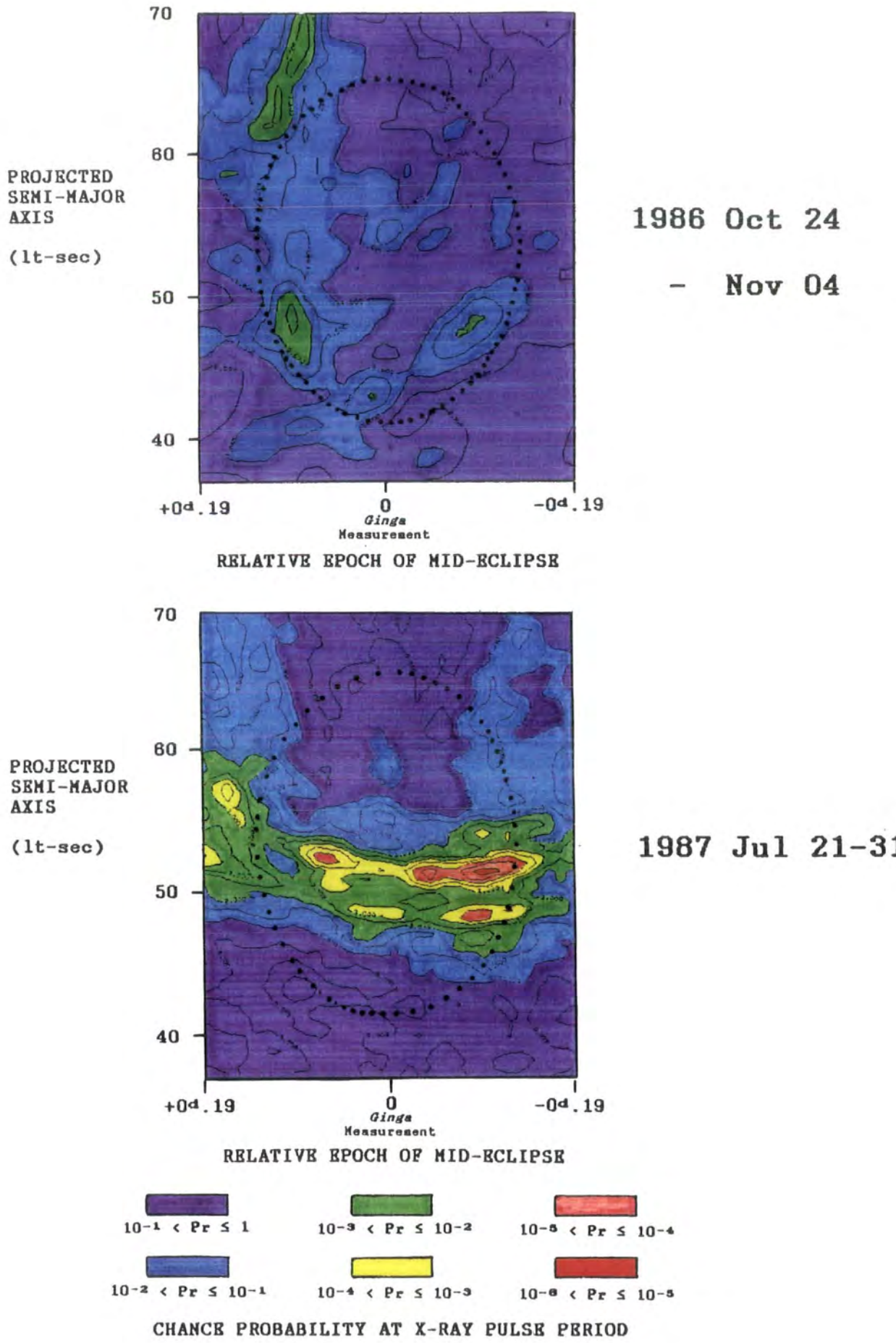
70
60
50
40
PROJECTED SEMI-MAJOR AXIS
(lt-sec)
+0d.19
0
-0d.19
Ginga Measurement
RELATIVE EPOCH OF MID-ECLIPSE
1986 Oct 24
- Nov 04
70
60
50
40
PROJECTED SEMI-MAJOR AXIS
(lt-sec)
+0d.19
0
-0d.19
Ginga Measurement
RELATIVE EPOCH OF MID-ECLIPSE
1987 Jul 21-31
10-1 < Pr ≤ 1
10-2 < Pr ≤ 10-1
10-3 < Pr ≤ 10-2
10-4 < Pr ≤ 10-3
10-5 < Pr ≤ 10-4
10-6 < Pr ≤ 10-5
CHANCE PROBABILITY AT X-RAY PULSE PERIOD

Figure 8.5 (cont.)

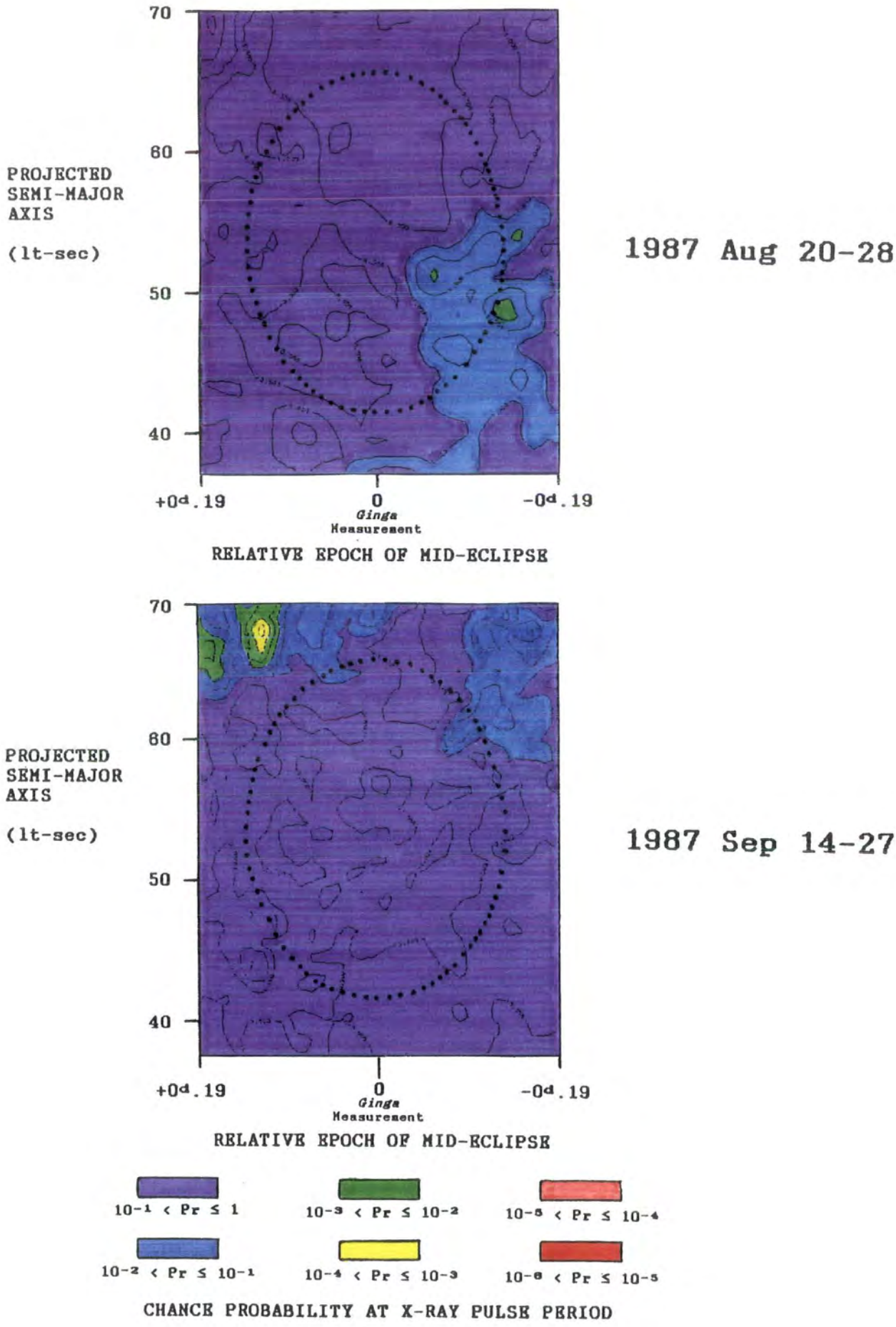

Figure 8.5 (cont.)

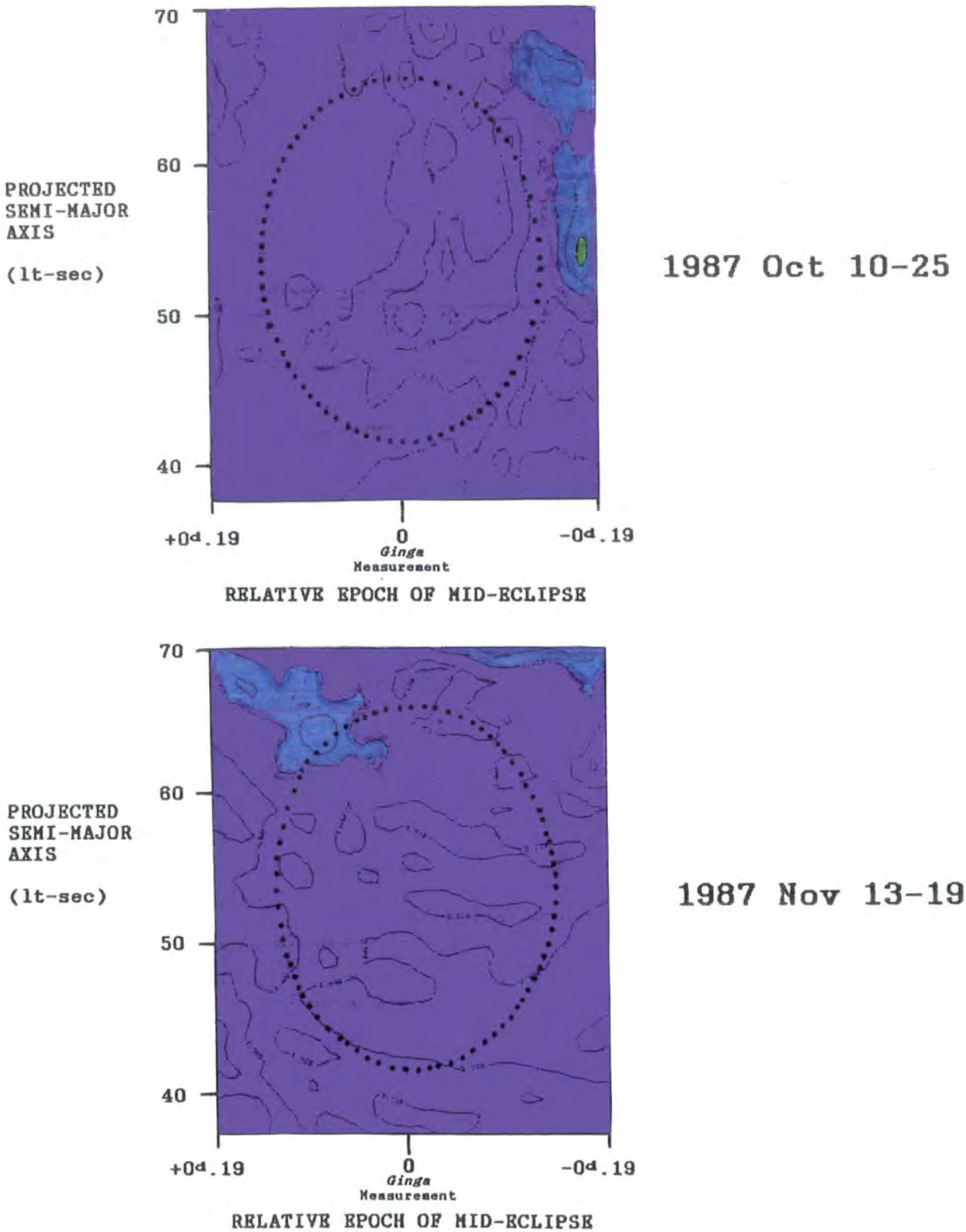

Figure 8.5 (cont.)

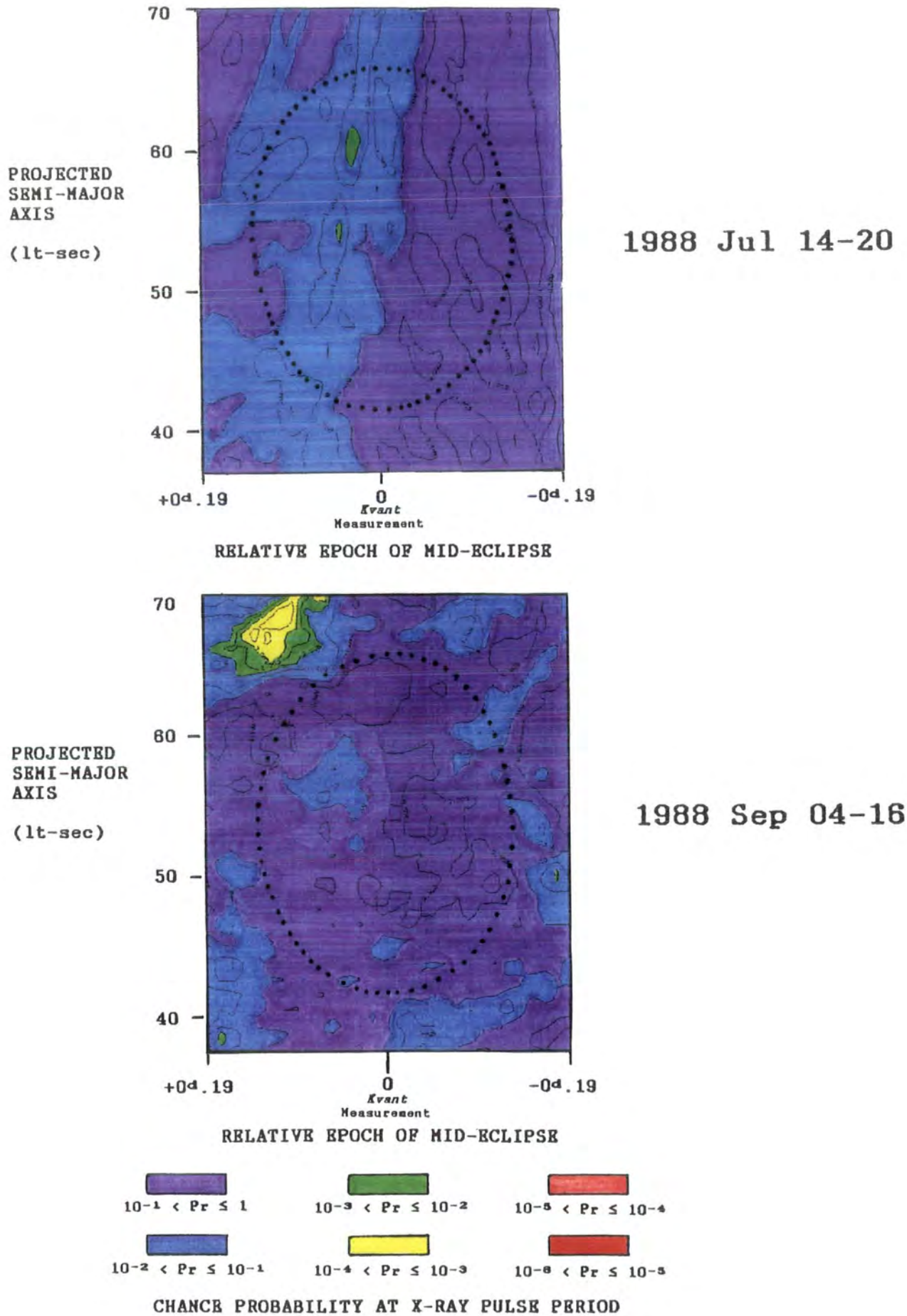

Figure 8.5 (cont.)

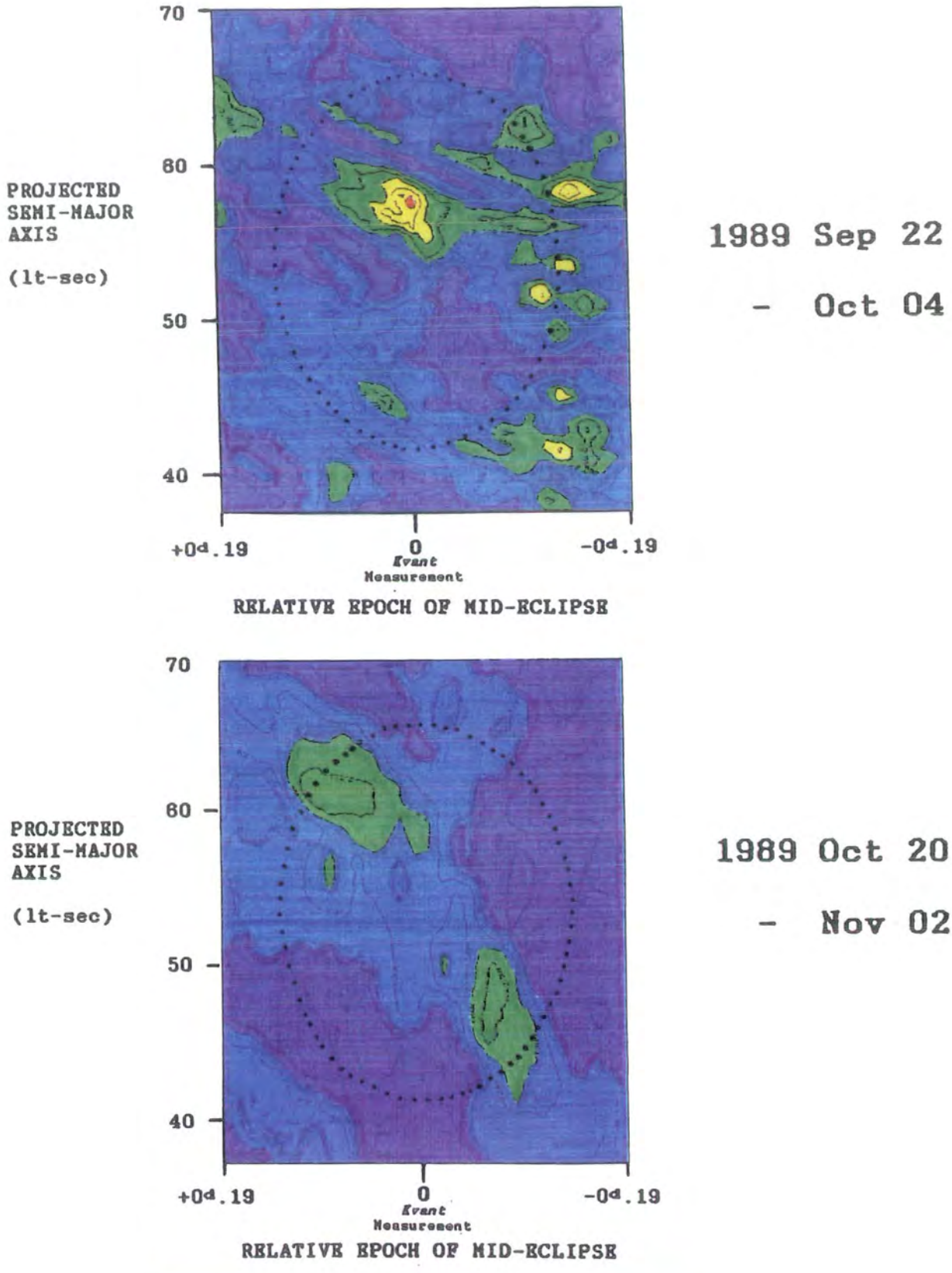

Figure 8.5 (cont.)

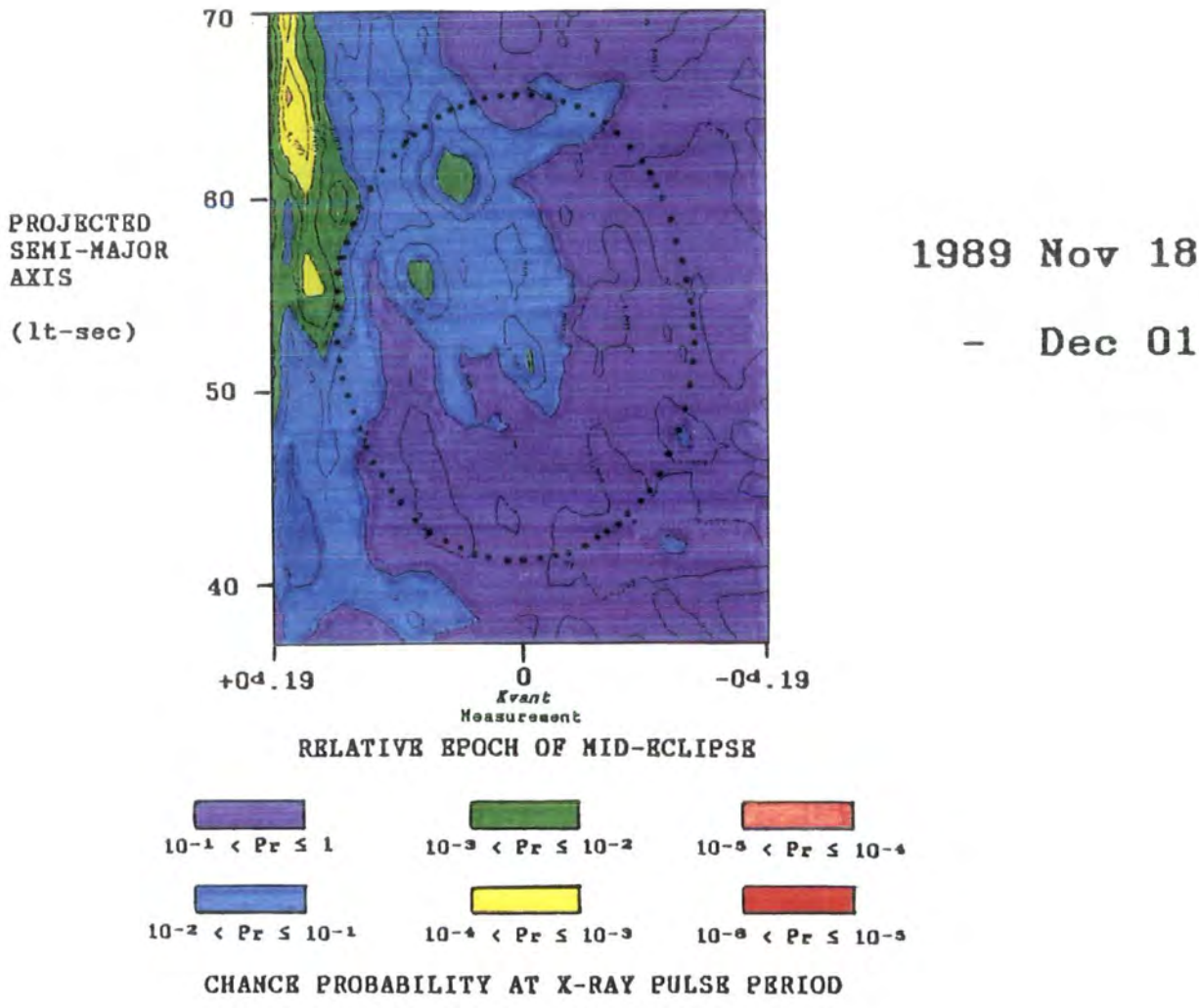

8.9 Quality of the Data

Setting aside the periodic component observed at the X-ray period, do the chance probabilities found at other test periods follow the distribution expected of random time series ?

The periodograms in Figures 8.6a and 8.6b show the values of the chance probabilities determined for the two datasets using a wide range of candidate periods both below and above the expected contemporary value of the X-ray period. The total number of independent periods tested is ~ 20,000 in each case. Times have been reduced to the SMC X-1 rest frame using the values of epoch and $a_x \sin i$ at the minima of the probability contour plots in Figure 8.5.

The distribution of the chance probabilities is plotted in Figures 8.7a and 8.7b, after exclusion of the periodic effect at P_x. The binomial distribution is the expected distribution for random time series, since the aim is to observe what fraction (≡ number of successes) of the population of probabilities lies below a given probability threshold. The observed distribution is seen to be consistent with that expected for randomly distributed times in both datasets.

Figure 8.6a

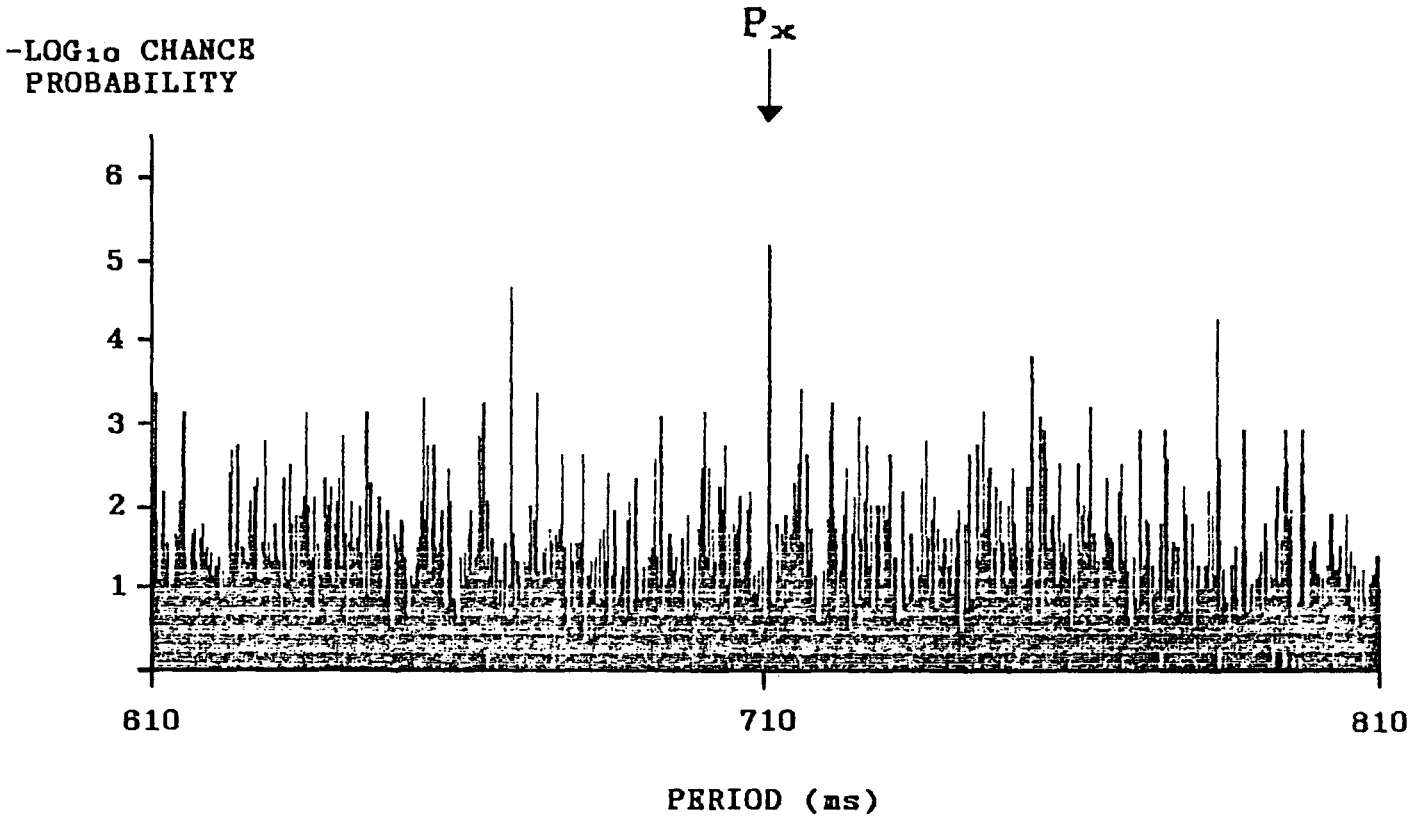

SMC X-1: Period Analysis of the

1987 July 21-31 Data

Figure 8.6b

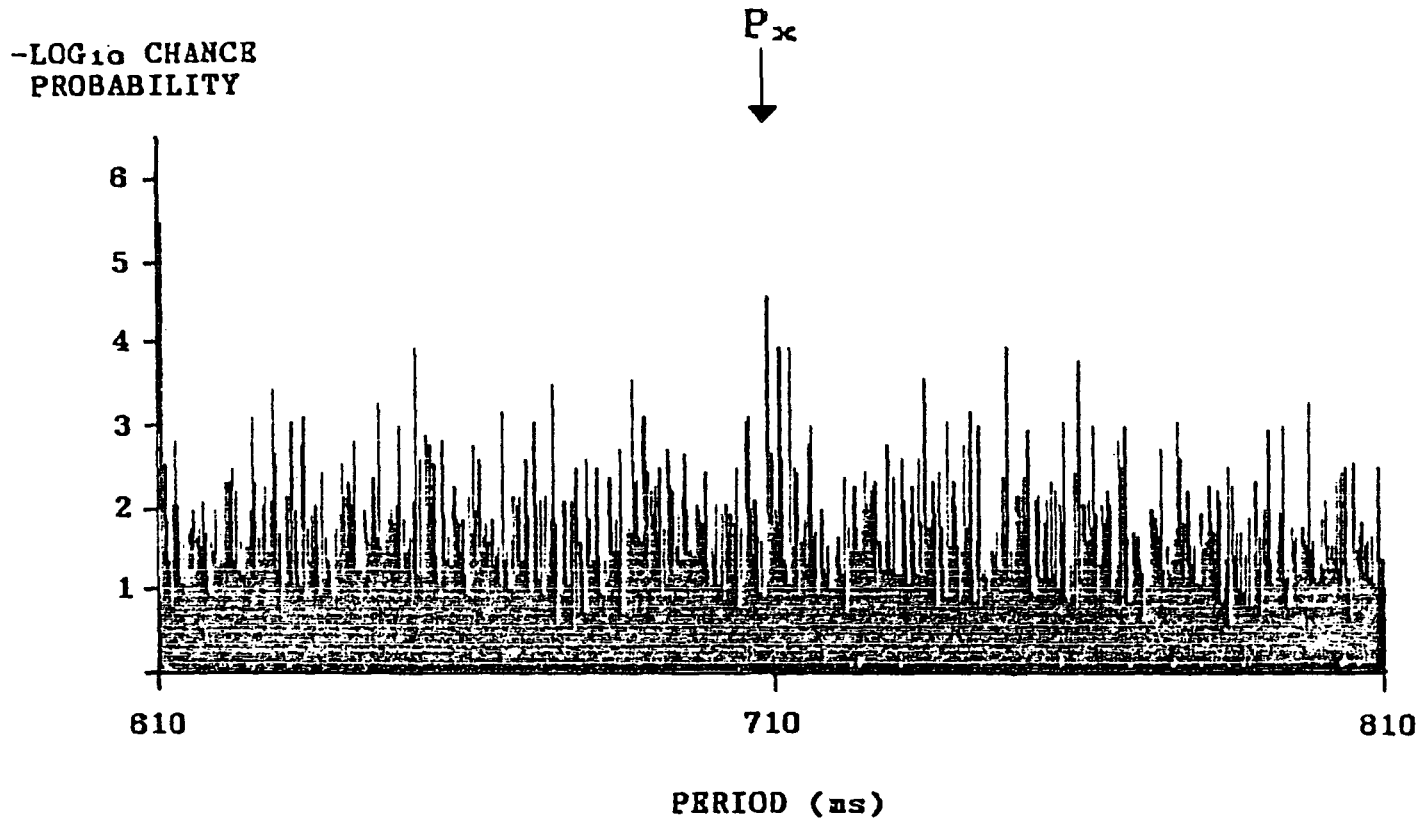

SMC X-1: Period Analysis of the

1989 September 22 -

October 04 Data

Figure 8.7a

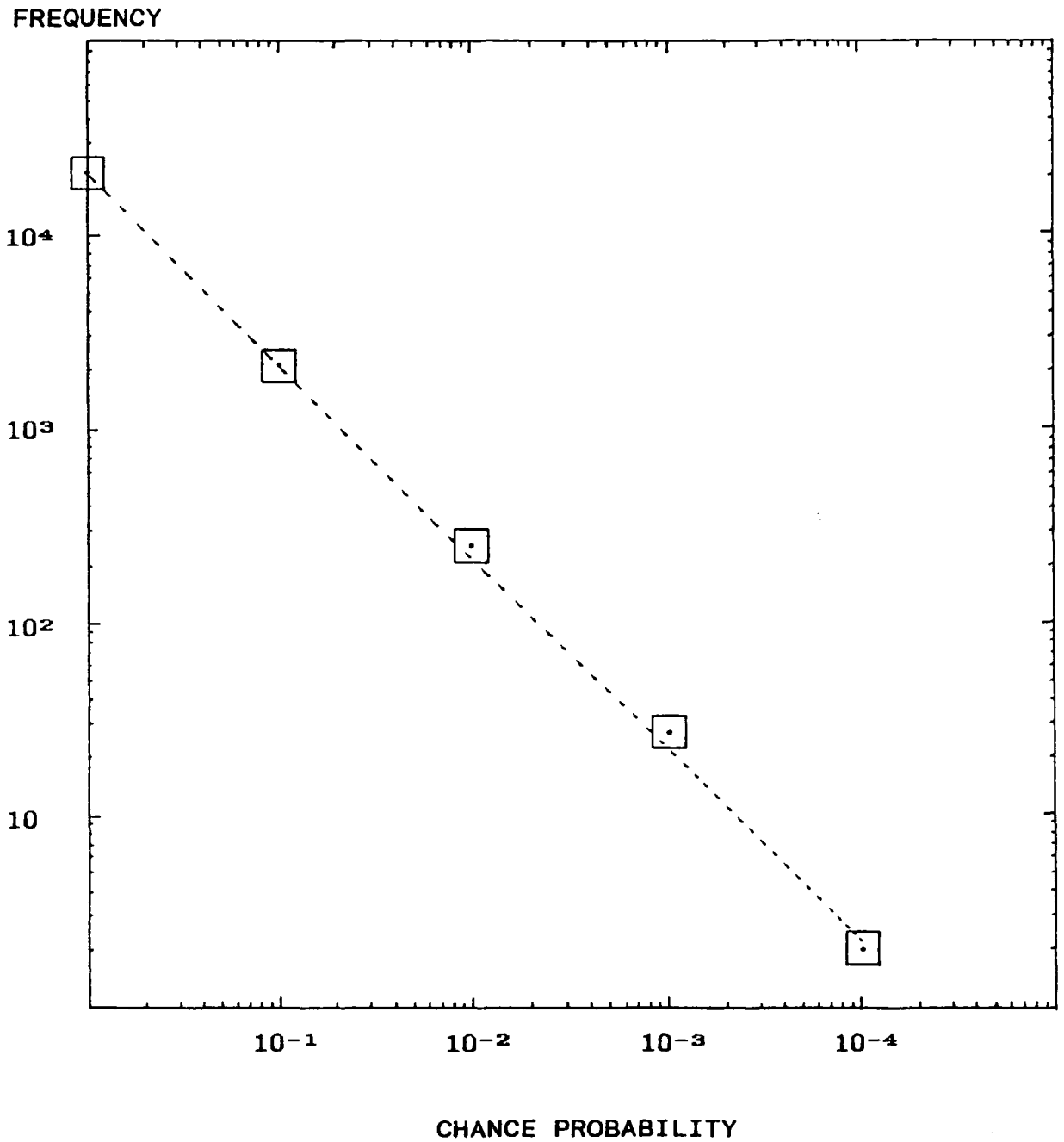

SMC X-1: Period analysis of 1987 July 21-31 data.

Distribution of chance probabilities
across period range 610 to 810 ms.
Periodic component at P_x excluded.

⊡ Total observed below indicated probability

----- Total expected for random time series

Figure 8.7b

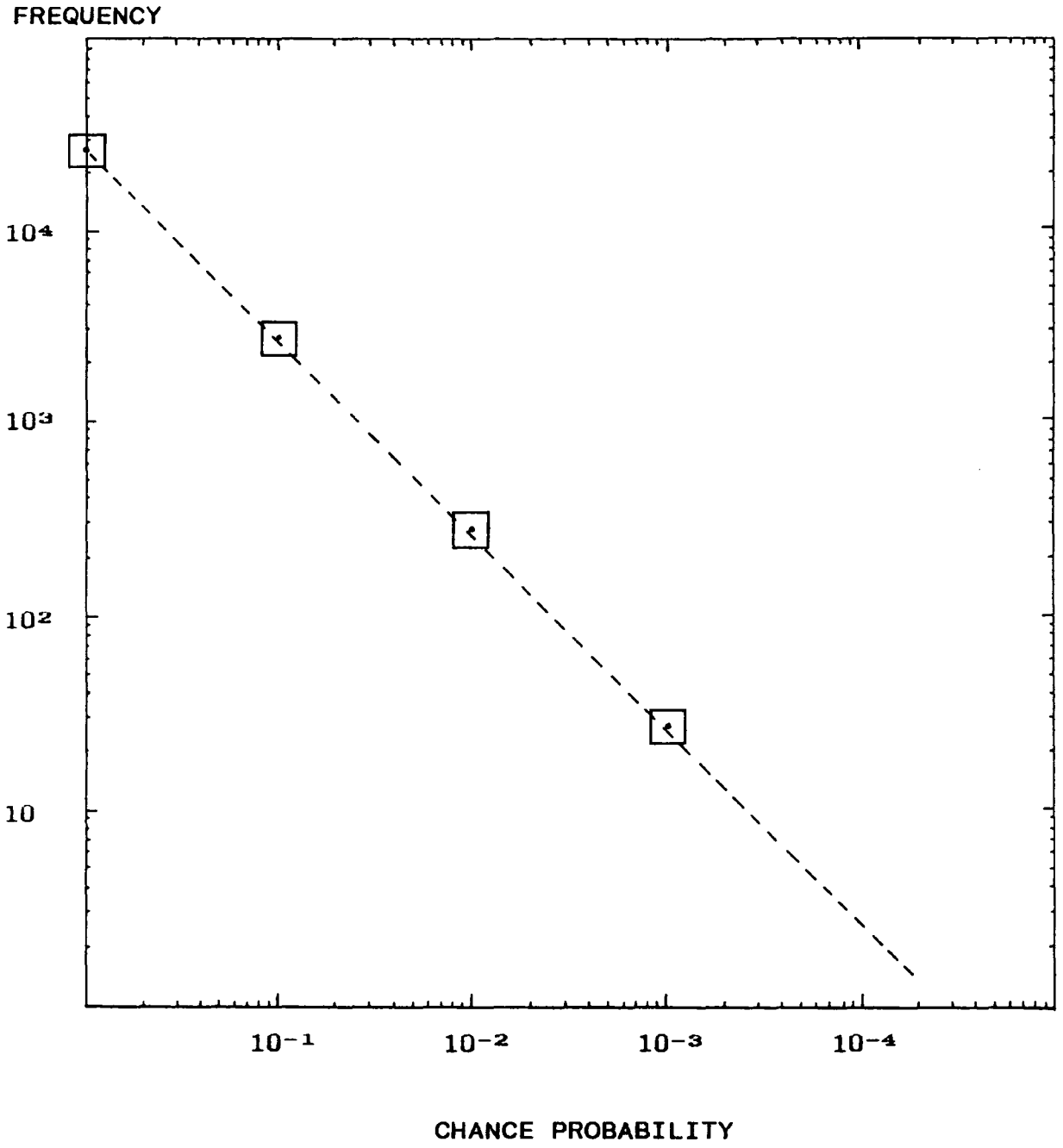

SMC X-1: Period analysis of 1989 September 22 - October 04 data.

Distribution of chance probabilities across period range 610 to 810 ms. Periodic component at P_x excluded.

⊡ Total observed below indicated probability

----- Total expected for random time series

8.10 Control Tests

Off-source data collected simultaneously during the SMC X-1 observations of 1987 July and 1989 September-October have been analysed for periodicity.

In Chapter 3 it was seen that seven fast three-fold coincidence detector channels are formed by clusters of photomultiplier tubes located at the focal planes of the three Mark III telescope flux collectors. When the telescope is operated in the tracking mode, the central detector channel, labelled channel # 1, monitors the target whilst an encircling "guard ring" of six channels provides continuous coverage of the sky at an angular separation of 2° from the source candidate. The Mark III signal-processing hardware was upgraded in 1990 January to permit discrimination on the full complement of guard ring channels. Before this time, discrimination was performed on the responses from a symmetric arrangement of three of the guard ring channels; the data recorded with these channels (# 2, 3 and 4) will therefore be considered here.

8.10.1 1987 July 21-31

All off-source arrival times recorded during 1987 July 21-31 have been reduced to the rest frame of the SMC X-1 binary using the values for epoch and $a_x \sin i$ at the minimum of the probability contour plot in Figure 8.5. Periodograms are shown in Figure 8.8a for channels 1, 2, 3 and 4. It can be seen that evidence

Figure 8.8a

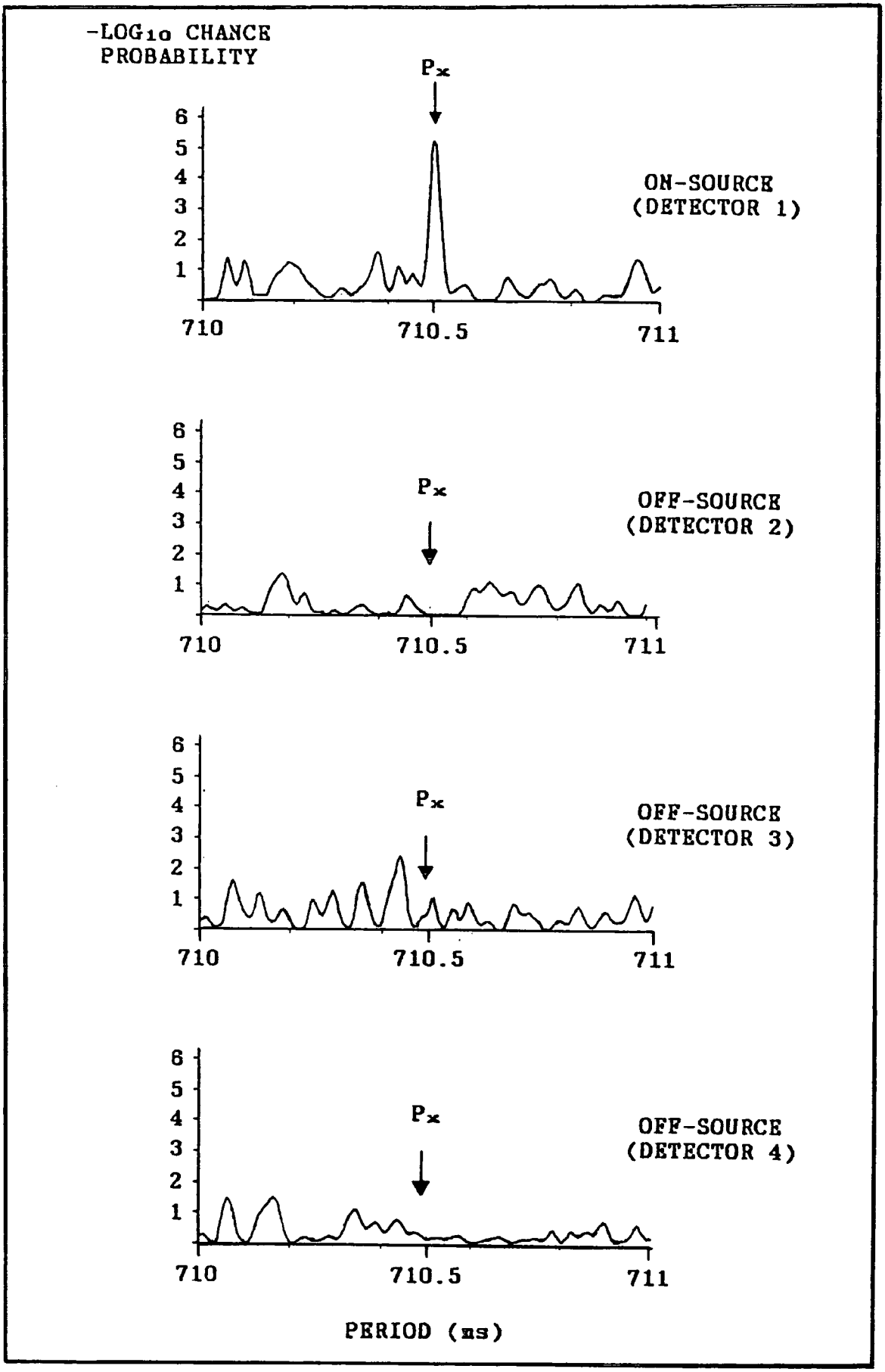

SMC X-1: Control Tests on the 1987 July 21-31 Data

Figure 8.8b

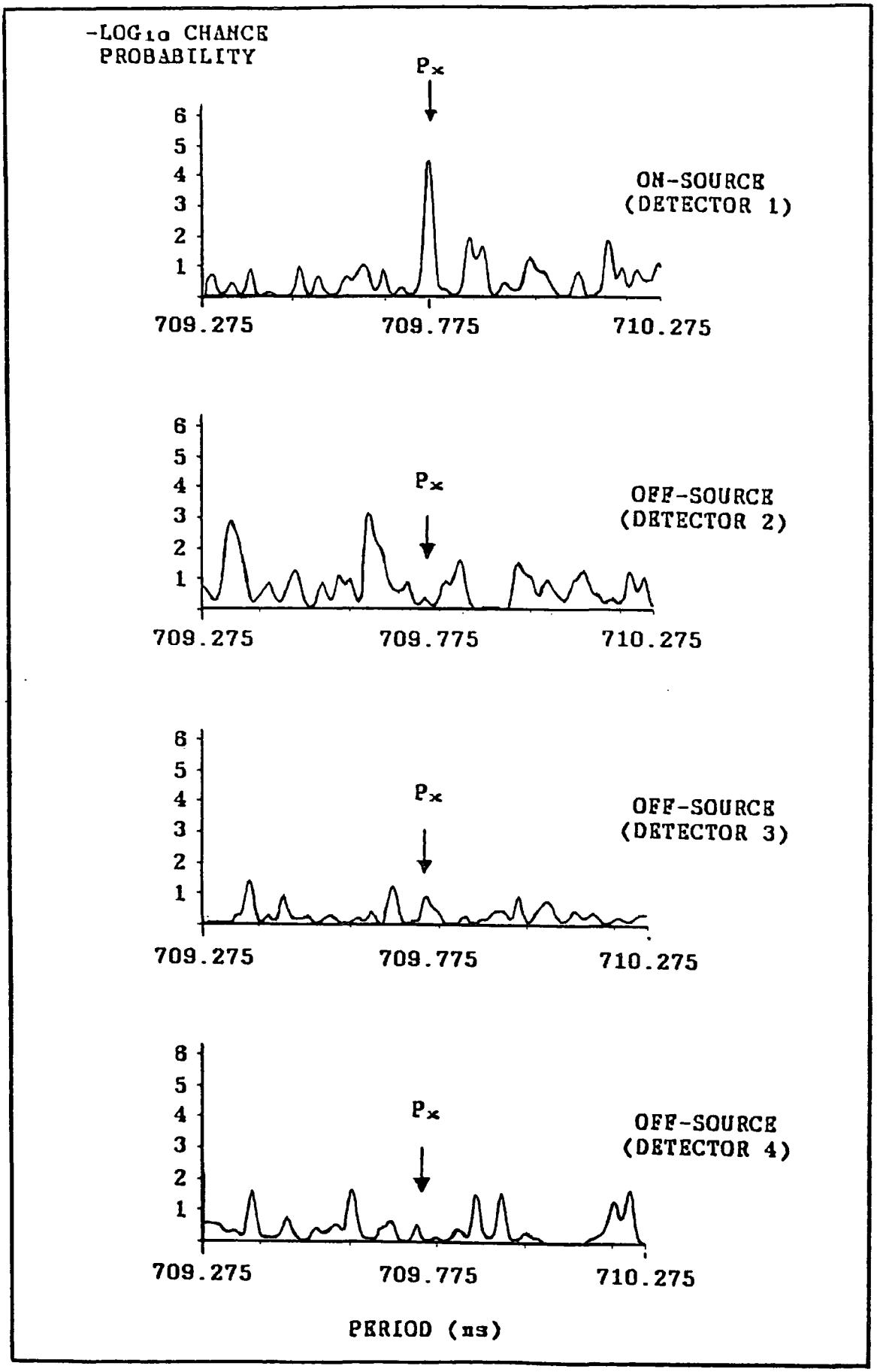

SMC X-1: Control Tests on the 1989 Sep 22 - Oct 04 Data

for a pulsed component at the X-ray period is confined to the data collected by the on-source detector channel.

8.10.2 1989 September 22 - October 04

Periodograms are shown in Figure 8.8b for the data from the four detector channels. Again it is seen that only the time series recorded with the on-source detector channel includes a component which is pulsed at the contemporary X-ray period.

8.11 Statistical Significance of the Results

The minimum chance probabilities found earlier for periodicity within one independent period sampling interval of P_x were:

	Probability
1987 July 21-31	5.0×10^{-6}
1989 September 22 - October 04	5.4×10^{-5}

Although these probabilities are small, they were observed using a three-dimensional matrix of candidate values of epoch of mid-eclipse, $a_x \sin i$, and γ-ray pulse period. The number of independent trials performed during the search for periodicity

must therefore be considered in order to see whether there is sufficient evidence to justify rejection of the null hypothesis. Equivalently: what is the likelihood that the above results have arisen by chance ? This has been examined by generating randomly distributed time series which were matched in duration, average Cerenkov count rate, and X-ray phase to those recorded during the 1987 July 21-31 observations at Narrabri. The procedure was:

(i) simulate the 1987 July dataset using random arrival times;

(ii) search for periodicity at P_X; period range: $P_X - \Delta P_I \leq P \leq P_X + \Delta P_I$; ranges of epoch and $a_X \sin i$: those which encompass the estimated dimensions of the neutron star accretion disk;

(iii) observe the minimum value of chance probability.

Each search required $\approx$ 20 hr of computing time; with this restriction, the number of simulations was limited to 200.

Figure 8.9a shows a histogram of the minimum chance probabilities obtained during the 200 random simulations. Note the strong tail of points at low values of probability. If N is the number of points observed below a given probability (Pr) in a population totalling some N_{tot} points, then the likelihood L of observing Pr is

$$L = \frac{N\ (< Pr)}{N_{tot}} \qquad (10)$$

Figure 8.9a

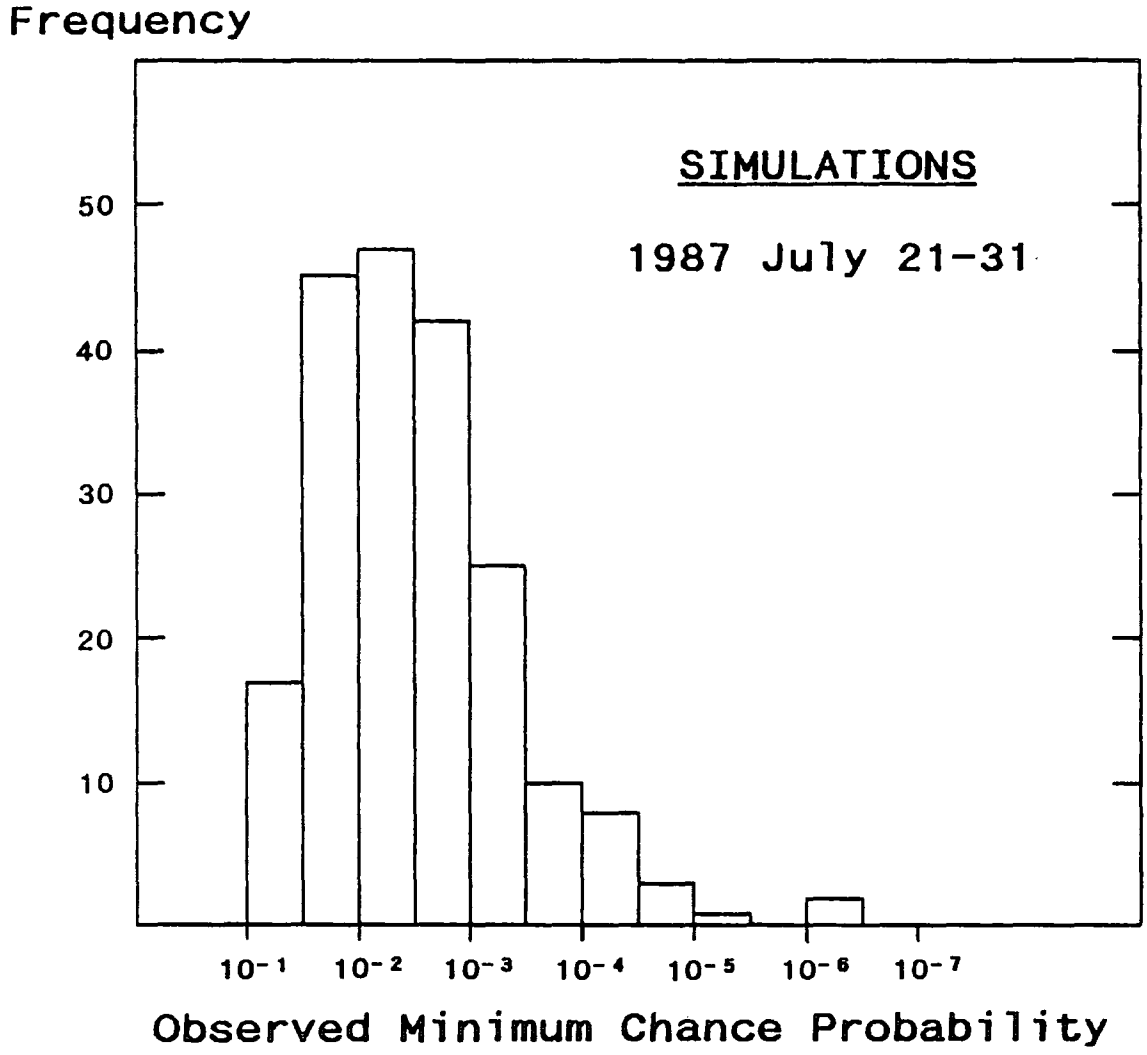

Histogram of minimum chance probabilities obtained by period analyses of 200 sets of random arrival time series.

Figure 8.9b displays values of L against Pr. Although the number of simulations is small, it can be seen that it is sufficient to reveal the trend in the values of L over the range of interest here. An estimate of the likelihood of obtaining the result found earlier during the analysis of the Narrabri data of 1987 July can therefore be made by reading directly from this plot, and it is seen to be at the 10^{-2} level. This must be multiplied by the total number of observing sequences (11), raising the chance probability to ≈ 0.1. On the basis of this test for periodicity, the null hypothesis must therefore be accepted.

Consider now the data of 1989 September 22 - October 04. The number of Cerenkov events recorded during these observations is more than double that obtained in 1987 July: a repeat of the above procedure of simulation and period analysis would require a time $\approx 10^5$ hours, which is not practicable. The probability calibration plot shown in Figure 8.9b for 1987 July can, however, be used to calibrate the result obtained from the period analysis of the 1989 September-October dataset in the following way. The average duration of the observations made during the 1989 sequence is $\approx$ 40 % greater than for those made in 1987 July: since the samples of SMC X-1 orbital phases were similar during the two sequences, the greater average duration of the observations of 1989 September-October means that the independent sampling intervals in the values of epoch and $a_x \sin i$ are smaller. The effect of this can be seen by inspecting the probability contour plots shown earlier in Figure 8.5. The dimensions of

Figure 8.9b

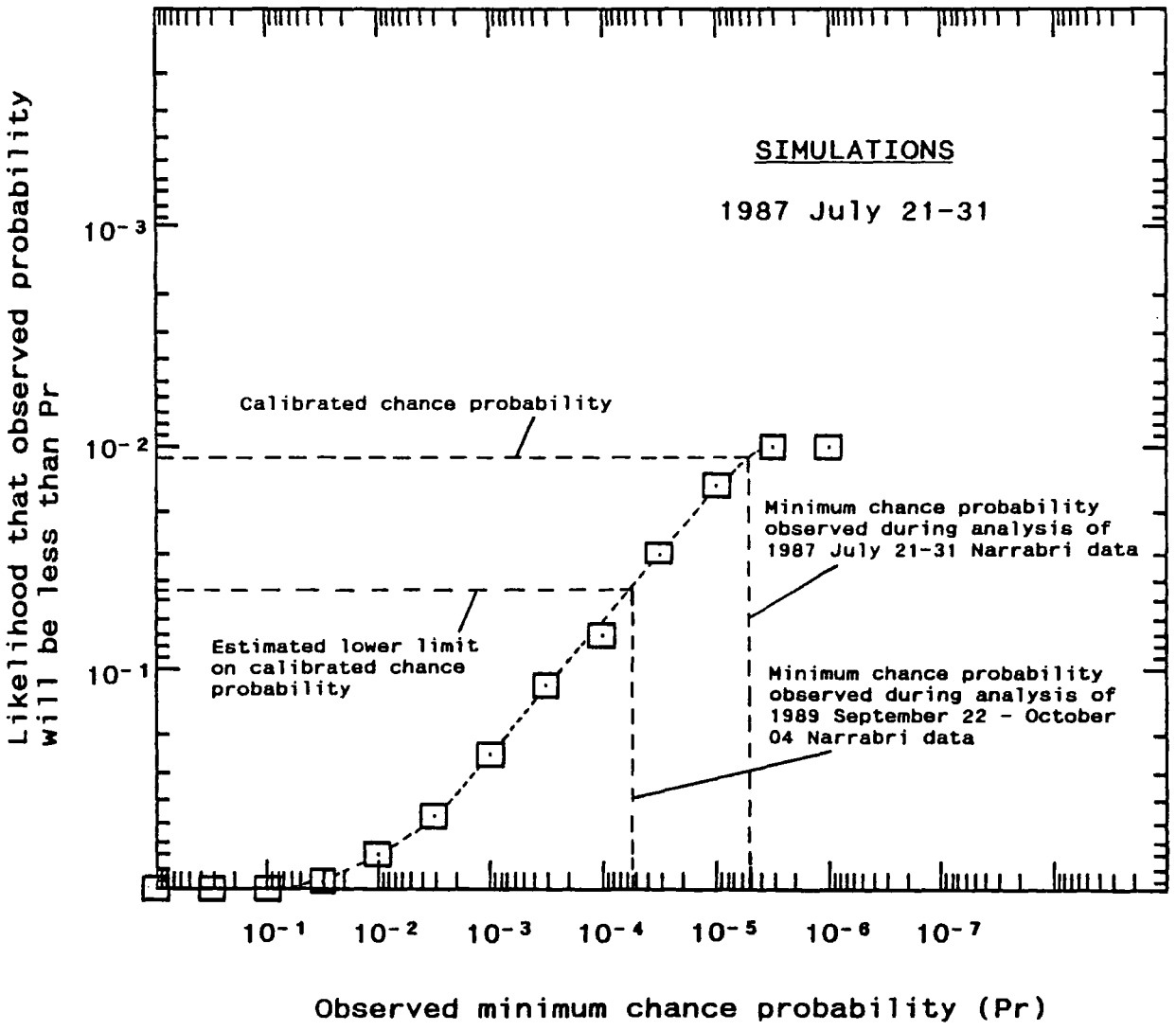

Calibration of the minimum chance probabilities obtained during period analyses of 200 sets of random arrival time series.

the probability minimum for the 1989 September-October data are appreciably smaller than those for 1987 July. The number of independent trials performed during the period analysis of the 1989 September-October data is therefore greater than for the 1987 July data, hence the calibration plot in Figure 8.9b can be used to place a *lower* bound on the probability of a chance origin for the observed periodicity: from the plot is can be seen that an observed probability of 5.4×10^{-5} corresponds to a chance probability of 5×10^{-2}. The null hypothesis must therefore again be accepted

8.12 Discussion

SMC X-1 was observed during eleven sequences of observations. The time series recorded within each sequence have been combined and tested for periodicity at the contemporary value of the X-ray pulse period. These tests were made using broad ranges of values of $a_x \sin i$ and mid-eclipse epoch in order to explore a range of possible locations of γ-ray emission in the neighbourhood of the SMC X-1 X-ray pulsar.

The results of these tests have shown that two of the eleven datasets include strong periodic components at the X-ray pulse period. These components are observed when tranformations of the arrival times are made using values of $a_x \sin i$ and epoch which are close to those determined for the SMC X-1 neutron star from the X-ray measurements. However, calibration of the period analysis

has revealed that the confidence levels of these results are low and are consistent with a chance origin.

The simultaneous search for information on both the periodicity of γ-ray emission from SMC X-1 and the location of an emission site is potentially very powerful. However, a strong signal-to-noise ratio is required for there is a trade-off between the extraction of such information and the number of trials which must be performed during the period analysis of the data. The conclusion to the present chapter must therefore be that either

a) the Narrabri data contain no evidence for γ-ray pulses from SMC X-1

or

b) the sensitivity of the present test for periodicity is too low.

The second possibility will be examined in the next chapter.

CHAPTER 9

Further Analysis of the SMC X-1 Database

9.1 Introduction

In Chapter 8 it was found that the data obtained during observations of SMC X-1 from Narrabri in 1987 July 21-31 and 1989 September 22 - October 04 included components which were strongly pulsed at a period consistent with the contemporary X-ray pulse period. However, calibration of the analysis technique used to identify these pulsations, together with allowance for the fact that eleven datasets had been analysed, revealed that the strengths of these periodic components were insufficient for a claim to be made that evidence had been found for pulsed emission from SMC X-1. These data will now be examined more closely.

The distribution of the periodic component in the two datasets will be explored in Section 9.2. A test for pulse phase coherence between periodic components identified in the separate Cerenkov arrival time series is presented in Section 9.3. The chapter concludes with a discussion of the results of the analysis of the SMC X-1 database.

9.2 Temporal Distribution of the Periodic Components

9.2.1 Introduction

The two datasets are first divided into the separate time series recorded during the individual observations of SMC X-1. The Rayleigh test is then used to search for evidence of a pulsed component at the predicted X-ray pulsar period in each time series. Those time series which are observed to include such a pulsed component are subjected to further analysis in order to explore two possibilities:

i) the putative γ-ray emission is detected continuously throughout a given observation;

ii) flux arriving at the telescope exceeds the limiting detector sensitivity only for short intervals of time.

As discussed in Chapter 8, the expected sinusoidal variation in the observed value of the pulse period due to the orbital motion of the neutron star is eliminated prior to the period analysis by transforming all times to the rest frame of the SMC X-1 binary. The results of this process are again explored by taking a range of values of the projected semi-major axis and the epoch of mid-eclipse.

9.2.2 Analysis of the 1987 July 21-31 Data

Figure 9.1 shows the results of performing the Rayleigh test on each of the nine time series. The colour scale represents the chance probability of periodicity within one independent sampling interval of the predicted X-ray pulse period, following the transformation of times using the indicated values of $a_x \sin i$ and mid-eclipse epoch. The dotted outline represents the boundary of the neutron star accretion disk determined by Khruzina and Cherepashchuk (1987).

On the basis of this test, it appears that possible evidence for pulsed γ-ray emission from SMC X-1 is confined to the time series recorded during two of the observations, namely those of 1987 July 23 and 29.

The chance probabilities for periodicity at the X-ray period are 7.8×10^{-4} and 2.1×10^{-4} for July 23 and 29, respectively. The reported values of $a_x \sin i$ (Primini, Rappaport and Joss, 1977) and epoch of X-ray mid-eclipse (Takeshima 1987) correspond to the centre of each of the diagrams in Figure 9.1. It can be seen that the pulsed components are identified only after transforming the arrival times using values of epoch and $a_x \sin i$ which are within one sampling interval of the reported values.

The data of 1987 July 23 and 29 were next analysed using a greater range of values of $a_x \sin i$ and epoch so that more of the pattern of chance probability contours could be studied. The results are shown in Figures 9.2a and 9.2b. The consistency of

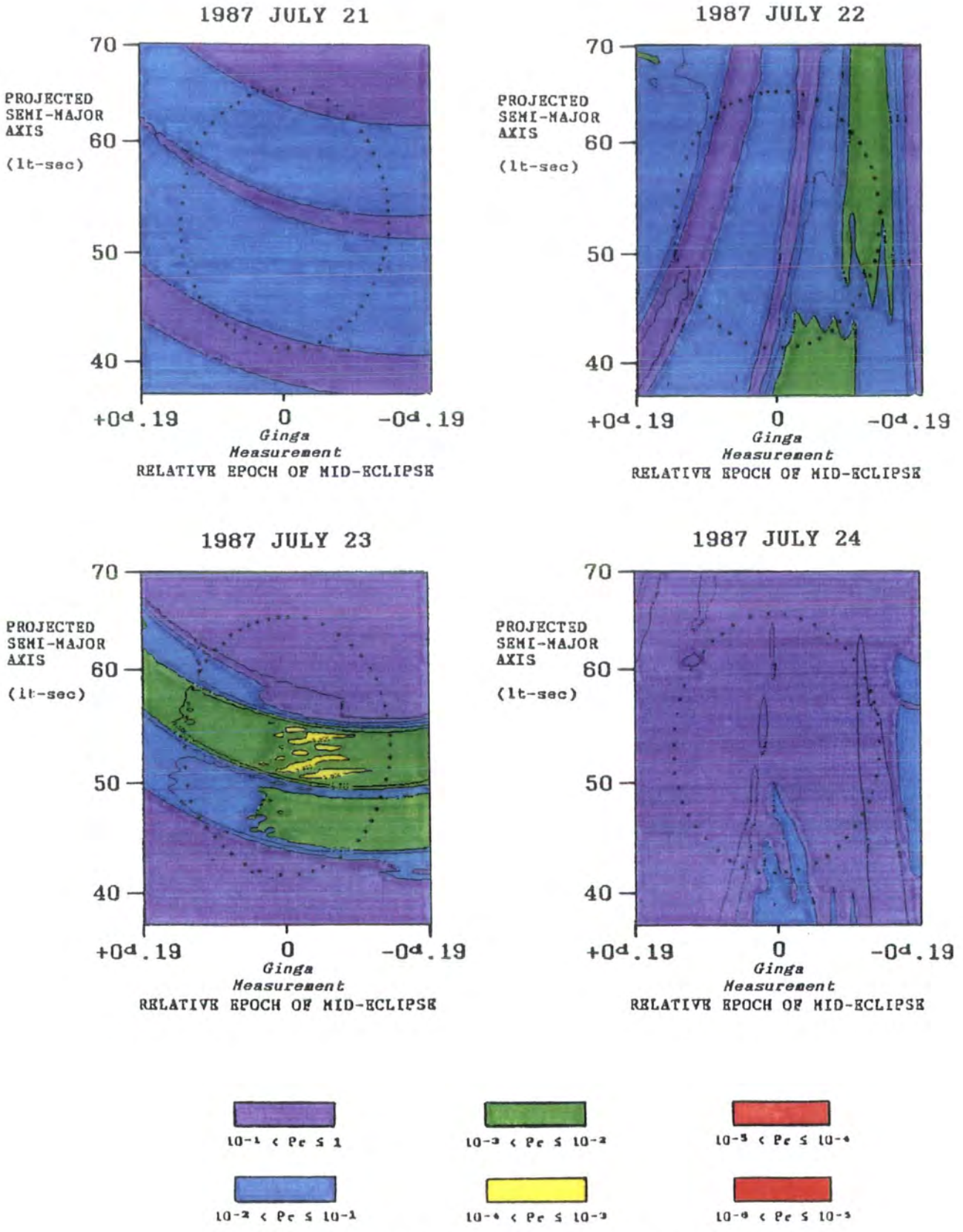
1987 JULY 21
1987 JULY 22
1987 JULY 23
1987 JULY 24
PROJECTED SEMI-MAJOR AXIS (lt-sec)
70
60
50
40
+0d.19
0
-0d.19
Ginga Measurement
RELATIVE EPOCH OF MID-ECLIPSE
10-1 < Pe ≤ 1
10-2 < Pe ≤ 10-1
10-3 < Pe ≤ 10-2
10-4 < Pe ≤ 10-3
10-5 < Pe ≤ 10-4
10-6 < Pe ≤ 10-5
CHANCE PROBABILITY AT X-RAY PULSE PERIOD

FIGURE 9.1

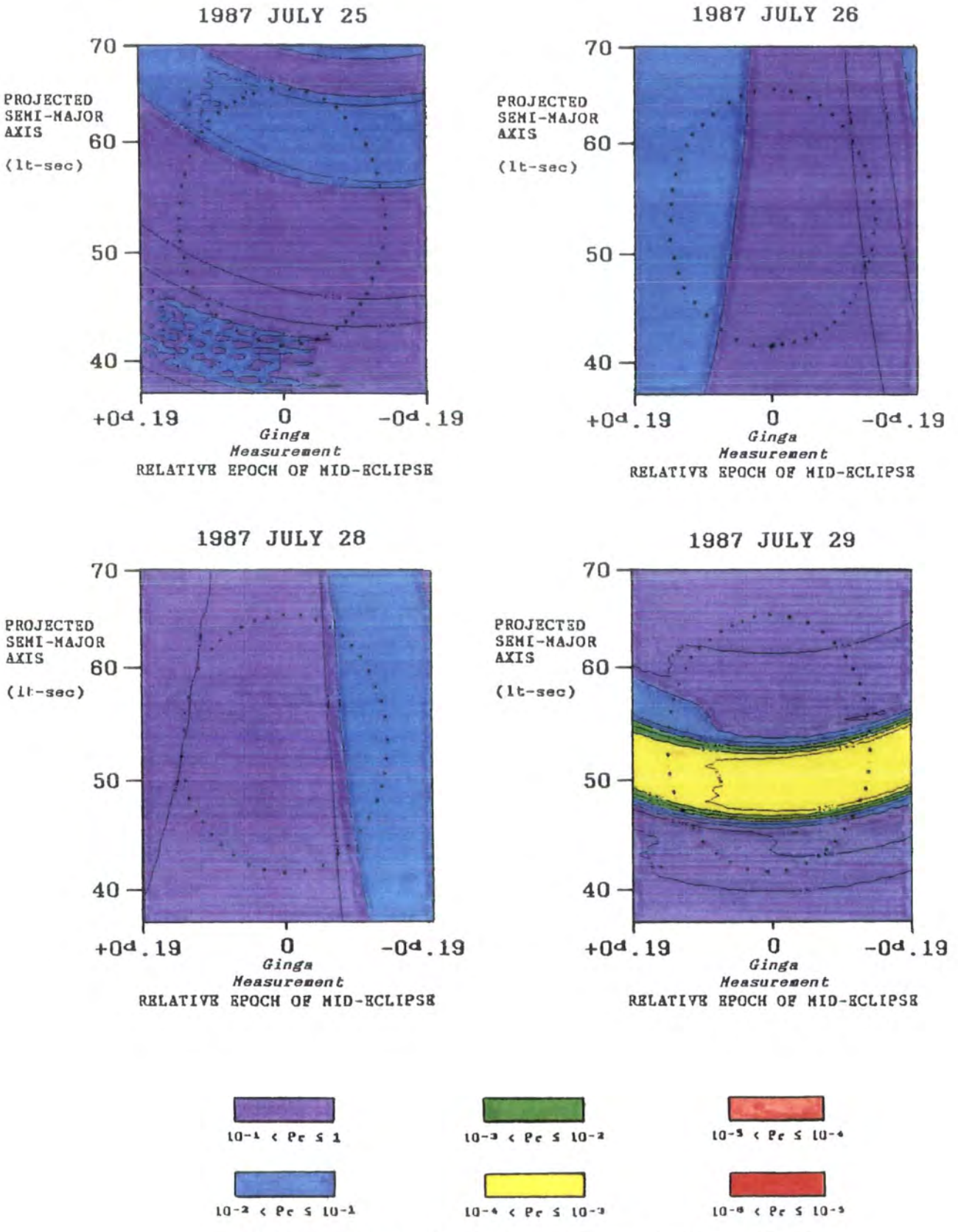

FIGURE 9.1 (cont.)

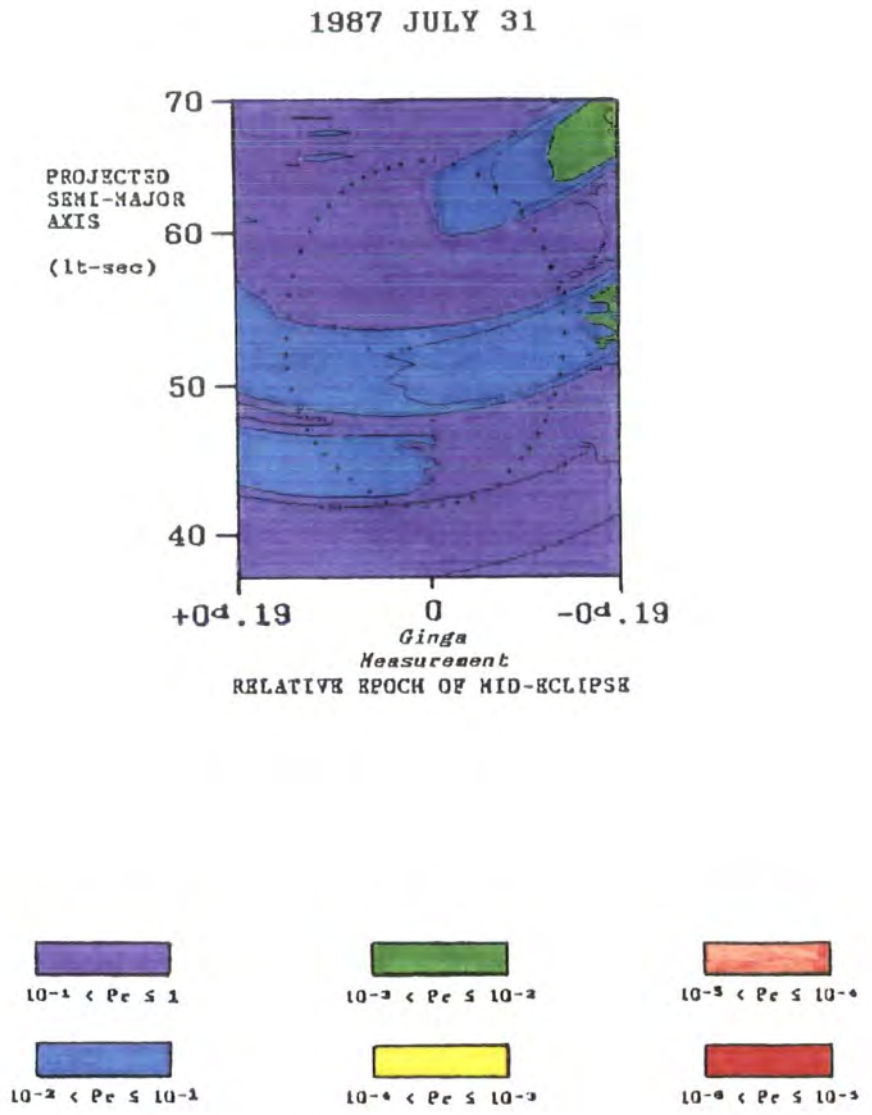

FIGURE 9.1 (cont.)

Figure 9.2a

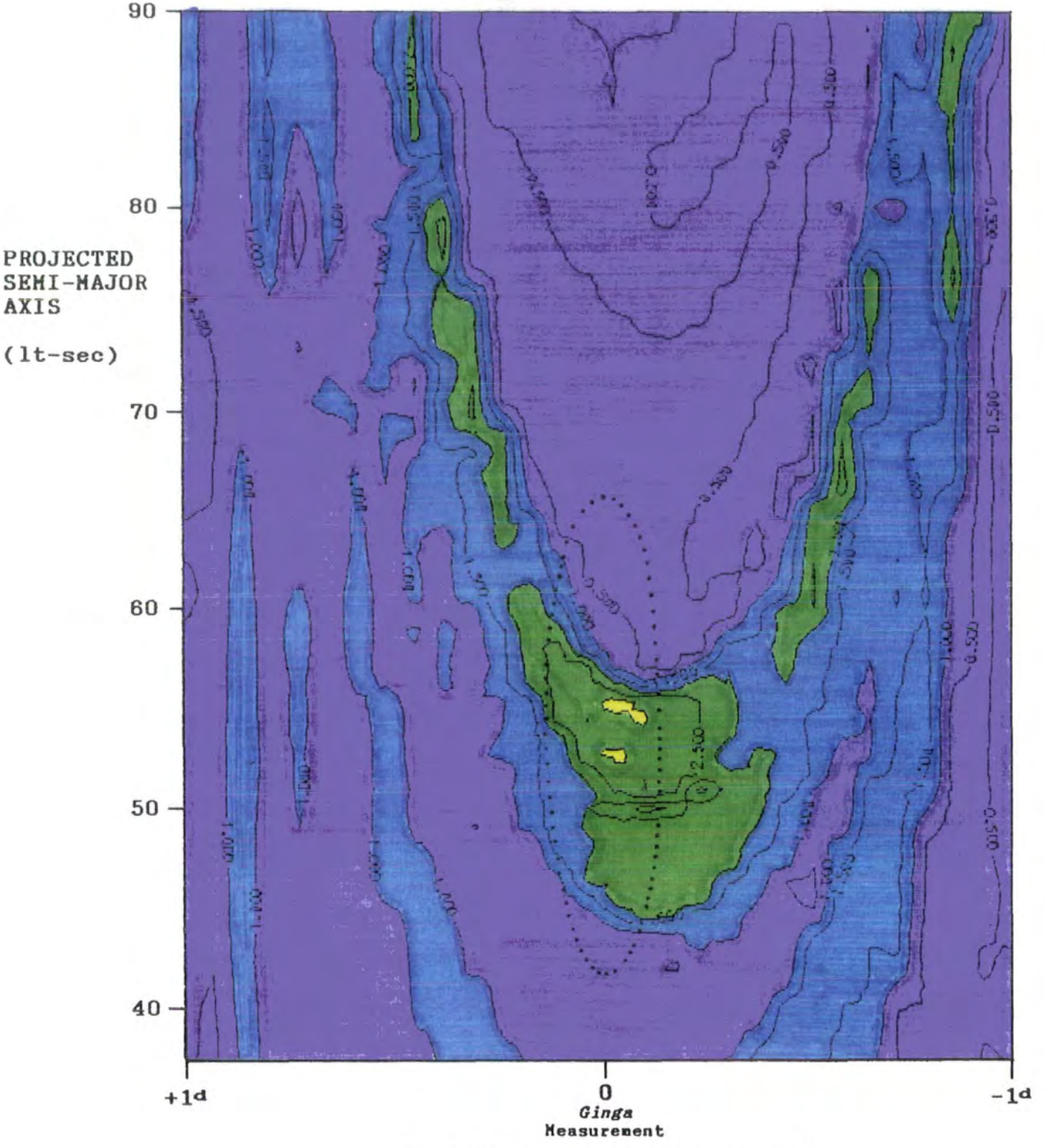

SMC X-1: Analysis of 1987 July 23 Data

Figure 9.2b

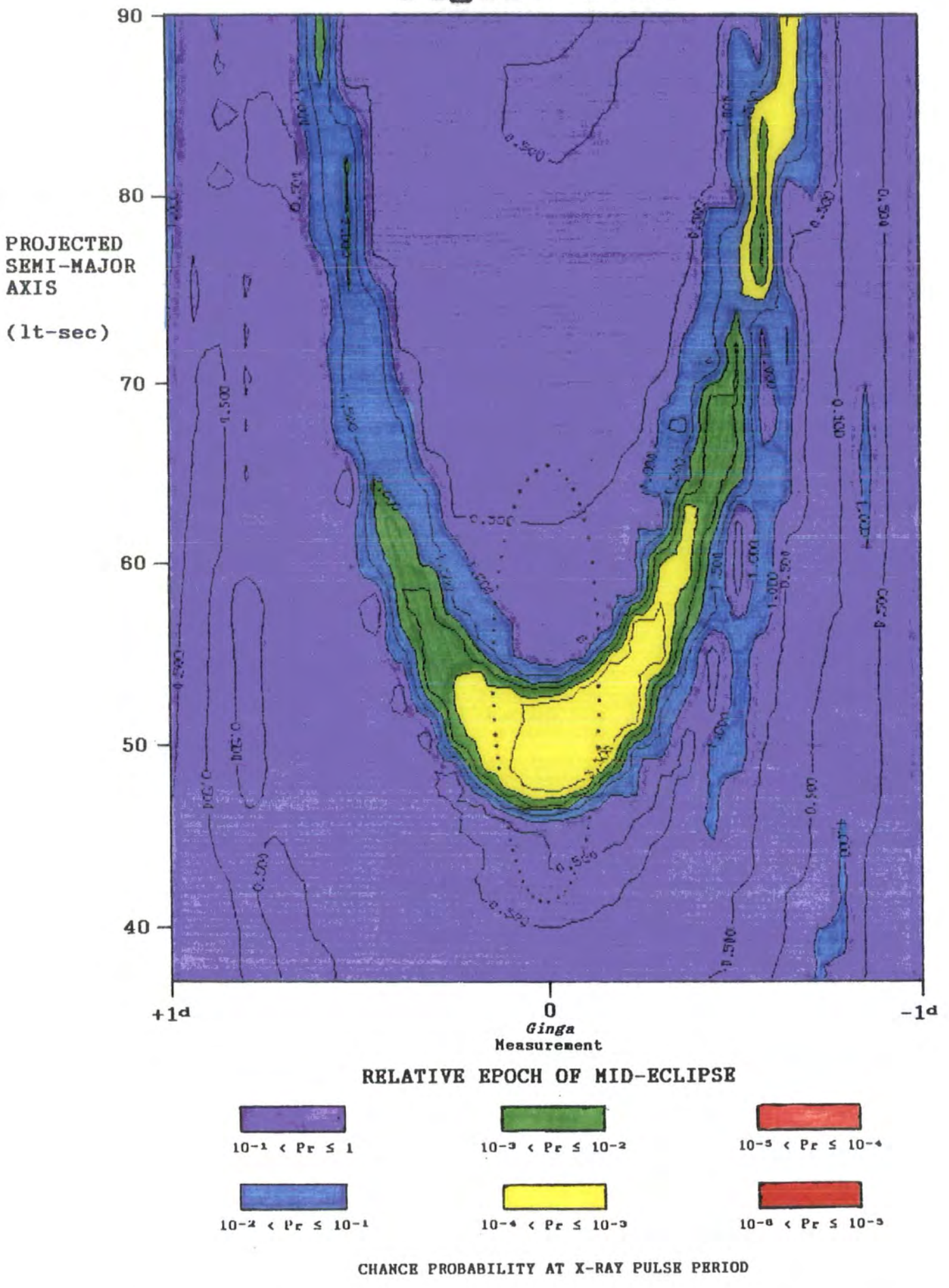

SMC X-1: Analysis of 1987 July 29 Data

the coordinates of the chance probability minima with the location of the neutron star is now particularly striking. The similarity of the two contour patterns and their symmetry about a vertical axis drawn through the *Ginga* measurement of the epoch can be explained by the fact that the two observations were of equal duration (T = 4.3 hr) and were each made when the SMC X-1 neutron star was within the vicinity of one of the orbital nodes. To explain this further, the convention of defining the zero of orbital phase (φ) as the epoch of X-ray mid-eclipse will be adopted. The descending node is then equivalent to φ = 0.25 and the ascending node is φ= 0.75. Phase ranges sampled during the two observations were:

Date	Start Phase	End Phase
1987 July 23	0.697	0.743
1987 July 29	0.232	0.277

Since the value of the binary orbital period has been fixed at that determined from a least squares fit to the epoch measurements (Chapter 7), there is a trade-off between the values of epoch and $a_x \sin i$ which provide an adequate correction for the Doppler shift of the pulse period and which permit the rest-frame period value to be observed. See the sketch in Figure 9.2c, where the region of the orbit at the ascending node is shown. If the neutron star and the putative γ-ray emission site are co-

Figure 9.2c

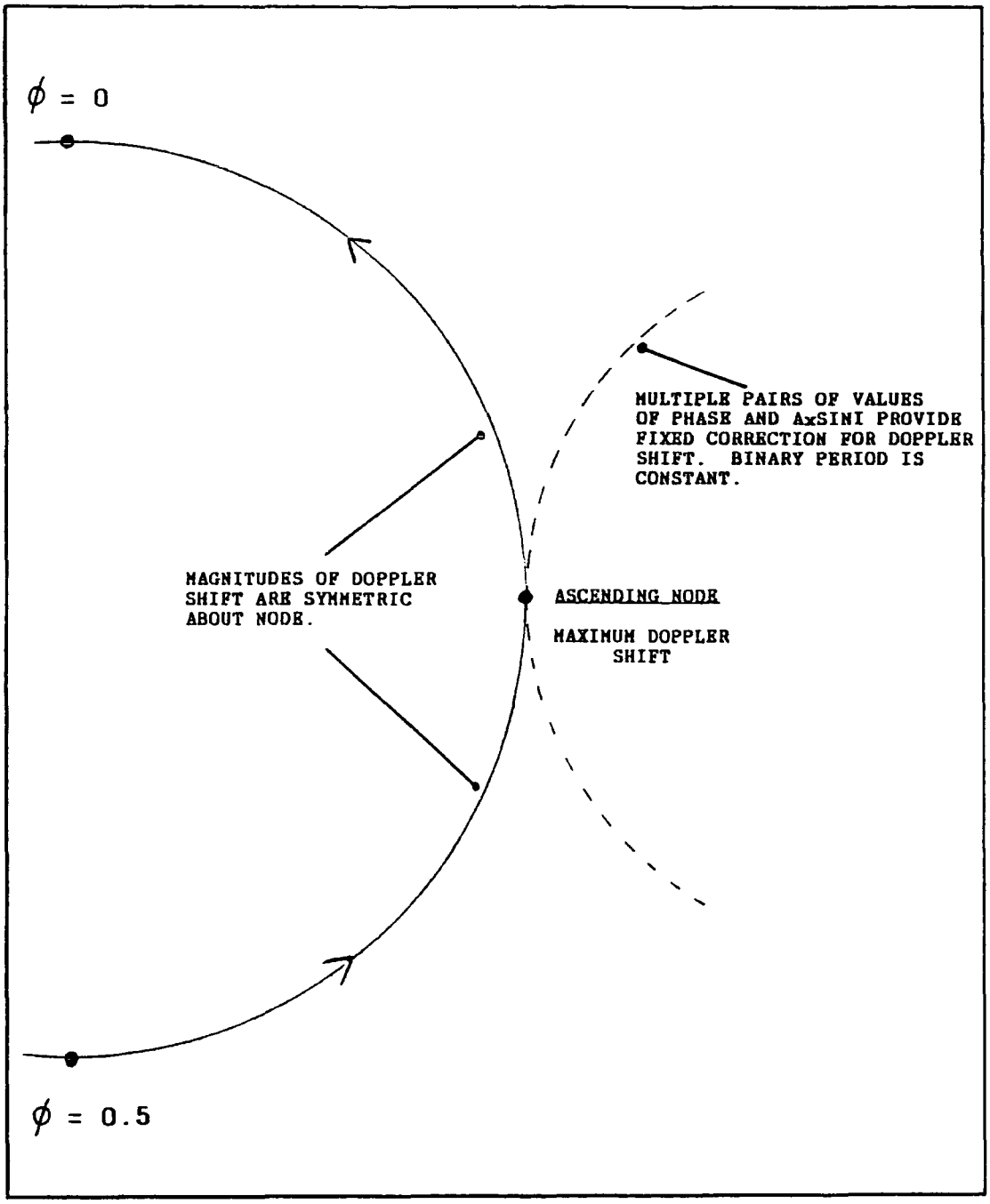

Elimination of Doppler Shift to Obtain Rest Frame Pulse Period.

located then, at either orbital node, the required pair of values of epoch and $a_x \sin i$ is of course those pertaining to the neutron star itself. Now consider the effect of increasing the value of $a_x \sin i$ whilst keeping the orbital period constant. This would imply an increase in the velocity of the neutron star and, consequently, a greater degree of Doppler shifting. To compensate for this, the neutron star orbital phase (≡ epoch of mid-eclipse) can be adjusted until the Doppler shift is reduced back to the previous level. By the symmetry of the magnitude and sign of the Doppler shift about an orbital node, this alteration in the neutron star phase can be positive or negative. This accounts for the U-shaped contour patterns in Figures 9.2a and 9.2b. In these two diagrams there are two values of epoch, approximately symmetric about epoch=0, for each value of $a_x \sin i + \Delta a_x \sin i$, where $\Delta a_x \sin i$ is positive. (When $\Delta a_x \sin i$ is negative the neutron star would be required to move more slowly in order to keep the orbital period fixed: there is then no alteration in orbital phase which can restore the Doppler shift to the required value, hence the lack of symmetry about a horizontal axis through the X-ray measurement of $a_x \sin i$). It is interesting that the U-shaped patterns in both diagrams extend from the expected position of the SMC X-1 neutron star. These results are consistent with the pulsed component at the X-ray pulse period in the two times series being due to pulsed emission from SMC X-1.

Consider now the distribution of the pulsed component within these two time series. Short-term bursts of γ-ray emission have been reported for Her X-1, Cygnus X-3 and Vela X-1. For Her

X-1, see Dowthwaite *et al.* (1984c) and Brazier *et al.* (1990d); Cygnus X-3: Brazier *et al.* (1990c) and Gregory *et al.* (1990); Vela X-1: North *et al.* (1987) and Raubenheimer *et al.* (1989). See also Chapter 12 of the present work. The timescale of these events was typically ~ 5 to 10 minutes. A search will be made for evidence of bursts of pulsed γ-ray emission from SMC X-1 on timescales of this order of magnitude.

Two methods will be employed to investigate how the pulsed components are distributed within the time series of 1987 July 23 and 29:

1) matching time series will be simulated and the test for periodicity repeated;

2) the search for periodicity will be performed over short sub-divisions of the two recorded time series.

1) **Simulation**

A γ-ray burst which lasted for a time ~ 10 minutes would correspond to ~ 5 % of the average duration of the SMC X-1 observations. The independent sampling interval, ΔP, in the values of candidate pulse periods is inversely proportional to the duration, T, of a time series ($\Delta P \approx P^2/T$); therefore, if significant enhancements occur in the strength of a pulsed component during intervals of time which are short compared with the total duration of an observation, then the effective

independent sampling interval would be greater than that for the full length of the time series. Similarly, the effective sampling intervals in the values of $a_x \sin i$ and epoch used to correct for Doppler shifting would be larger. A comparison of the observed magnitude of the sampling intervals with those expected can therefore provide information on the distribution of the pulsed component.

Two time series have been generated which match the duration, orbital phase, and average count rate of those recorded on 1987 July 23 and 29. A strong signal which is pulsed at the X-ray period has been injected and spread *uniformly* through the two series. Using the values of epoch and $a_x \sin i$ for the SMC X-1 neutron star, all times have been adjusted from the binary rest frame to the rest frame of the observer, so that the independent sampling intervals in the values of these two orbital elements can be assessed directly. The Rayleigh test has been performed at candidate periods within one independent period sampling interval of the X-ray period.

Figure 9.3a shows the results for the time series simulated for 1987 July 23. A scale of colours is not used for the chance probabilities here. Instead, the contour pattern is discerned by examining the shape and density of the probability contours. Compare this diagram with the results of the analysis of the real data of 1987 July 23 shown earlier in Figure 9.2a. The similarity of the contour patterns in both diagrams indicates that the pulsed signal identified in the data of 1987 July 23 is

Figure 9.3a

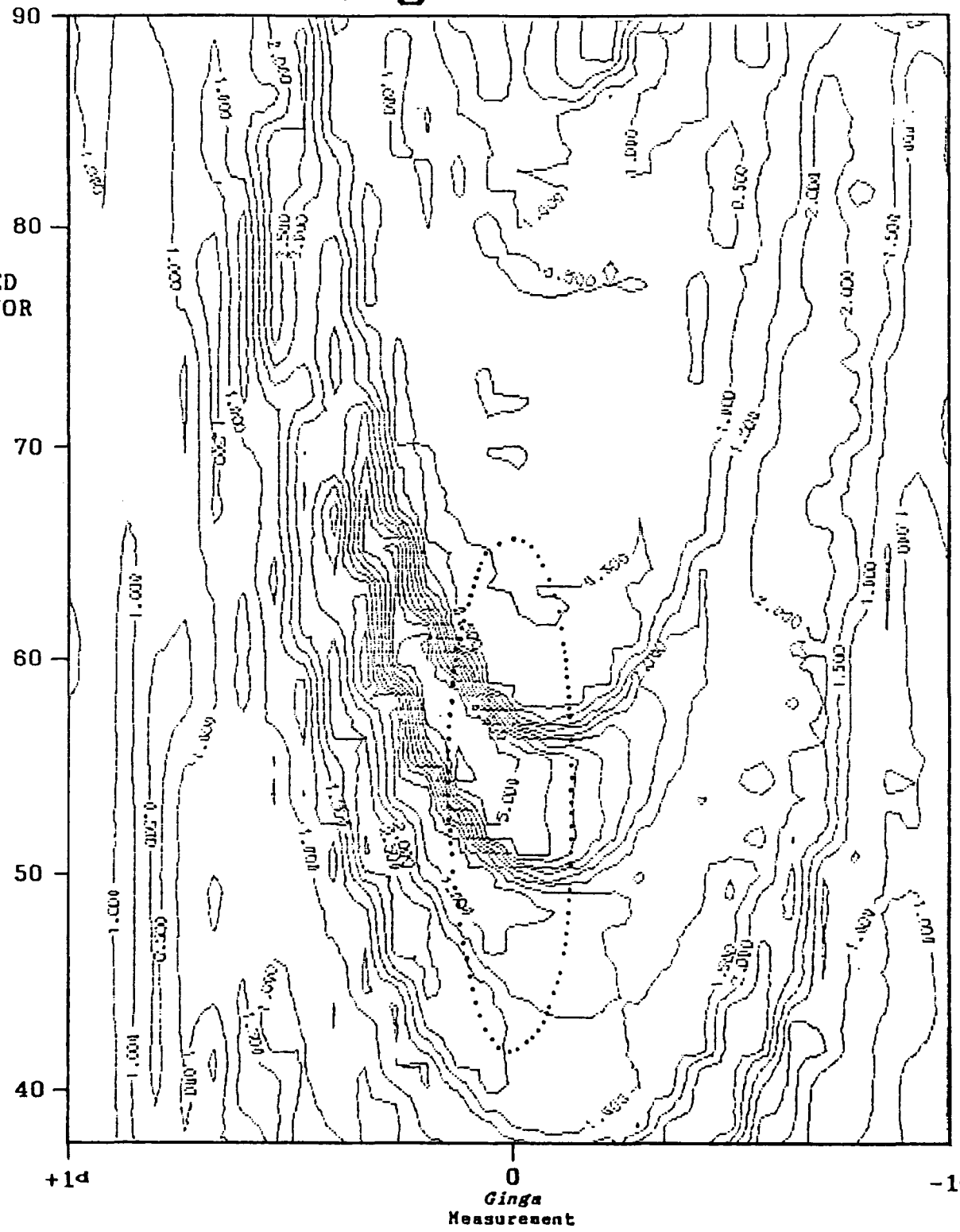

SMC X-1: SIMULATION of 1987 July 23 Data

with uniform pulsed signal

Figure 9.3b

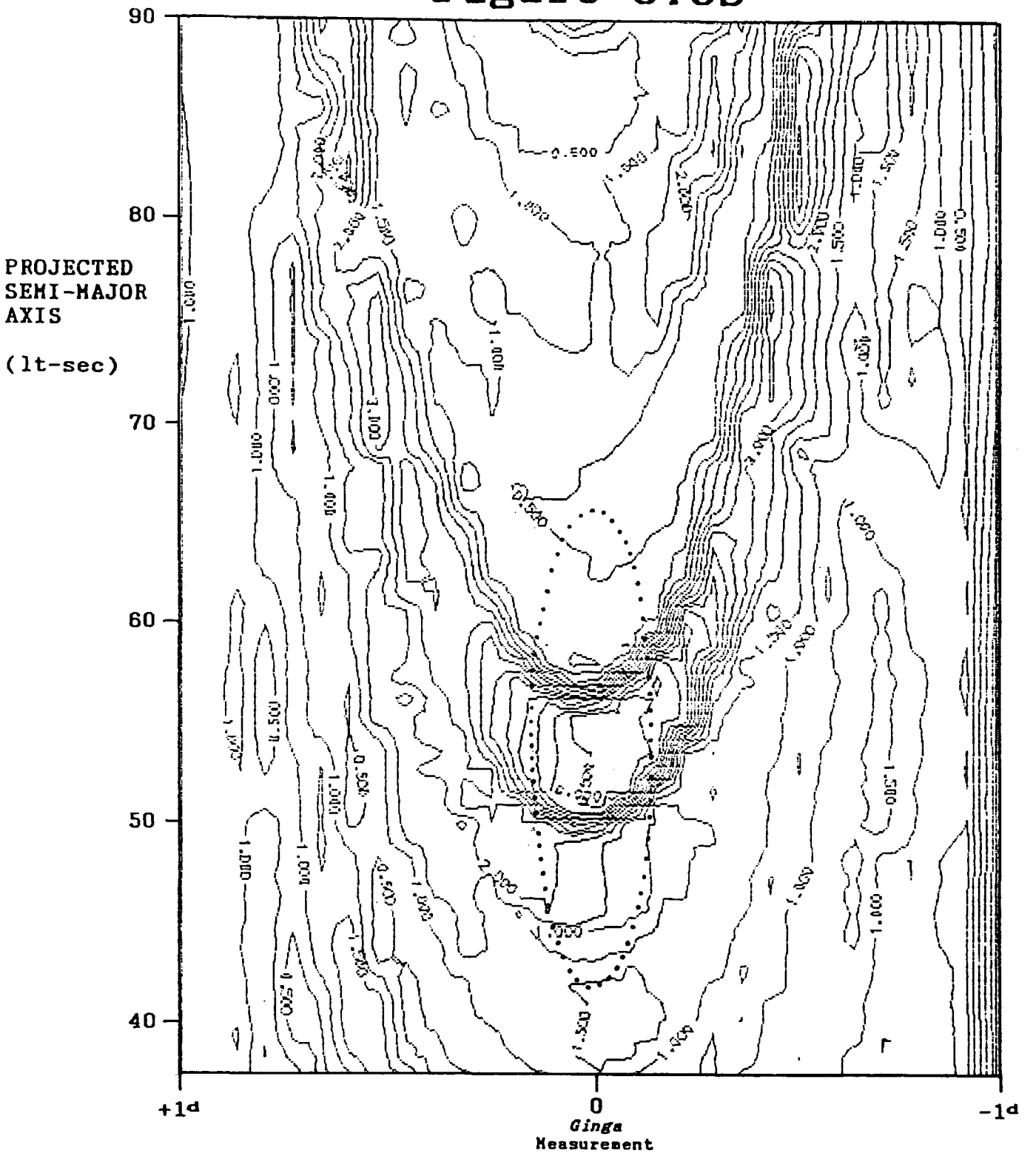

SMC X-1: SIMULATION of 1987 July 29 Data

with uniform pulsed signal

distributed throughout the time series and is not restricted to small sections of it. The same conclusion is made for the data of 1987 July 29 by comparison of the two contour plots in Figures 9.2b and 9.3b.

2) Period Analysis of Sub-Divisions of the Data

The two recorded time series were first transformed using the values of epoch and $a_x \sin i$ at the probability minima displayed in Figures 9.2a and 9.2b. The distributions of the pulsed components were then investigated by applying the Rayleigh test at the X-ray pulse period across successive short sections of the data. In the absence of *a priori* knowledge of the time of the start of a γ-ray burst, the data were analysed in overlapping sections, each separated by 10 % of the section length.

No evidence was found for a significant enhancement in the strength of the pulsed component in either time series on timescales ~ 5 to 10 minutes, which is consistent with the results of the simulations described above.

9.2.3 Analysis of the 1989 September 22 - October 04 Data

The Roentgen X-ray observatory aboard the Kvant module of the Soviet Mir space station measured X-ray pulsations from SMC X-1 at a period of 709.983 ms during 1989 March. See Gilfanov *et al.* (1989). (The error on this period value is not stated).

Extrapolation to the epoch of the Narrabri observations predicts a value of 709.775 ms for the X-ray pulse period. Figure 9.4 shows the chance probability contours obtained using the Rayleigh test on each of the eleven time series using a range of candidate values of pulse period within one independent sampling interval of the predicted value.

Evidence for periodicity is revealed only by the data obtained on 1989 October 02. The chance probability is 3.5×10^{-5} and, again, the effect is observed only when the times are transformed using values of epoch and $a_x \sin i$ which are within one sampling interval of the position of the neutron star. The remainder of the time series show no significant modulation at the expected X-ray period.

Figure 9.5a shows the results of the period analysis of the data of 1989 October 02 using larger ranges of values of epoch and $a_x \sin i$. Note the familiar U-shaped pattern in the probability contours, once again extending from the coordinates of the SMC X-1 neutron star. This observation of SMC X-1 was made when the neutron star was approaching the ascending node of the orbit, so that the results shown here can be compared directly with those from the analysis of the 1987 July 23 and 29 data. The range in orbital phase sampled on 1989 October 02 was φ = 0.682 to 0.721. At 5.6 hours, the duration of this observation of SMC X-1 is one of the longest performed with the Mark III telescope. It was 30 % longer than the two 1987 July observations, which explains why the dimensions of the

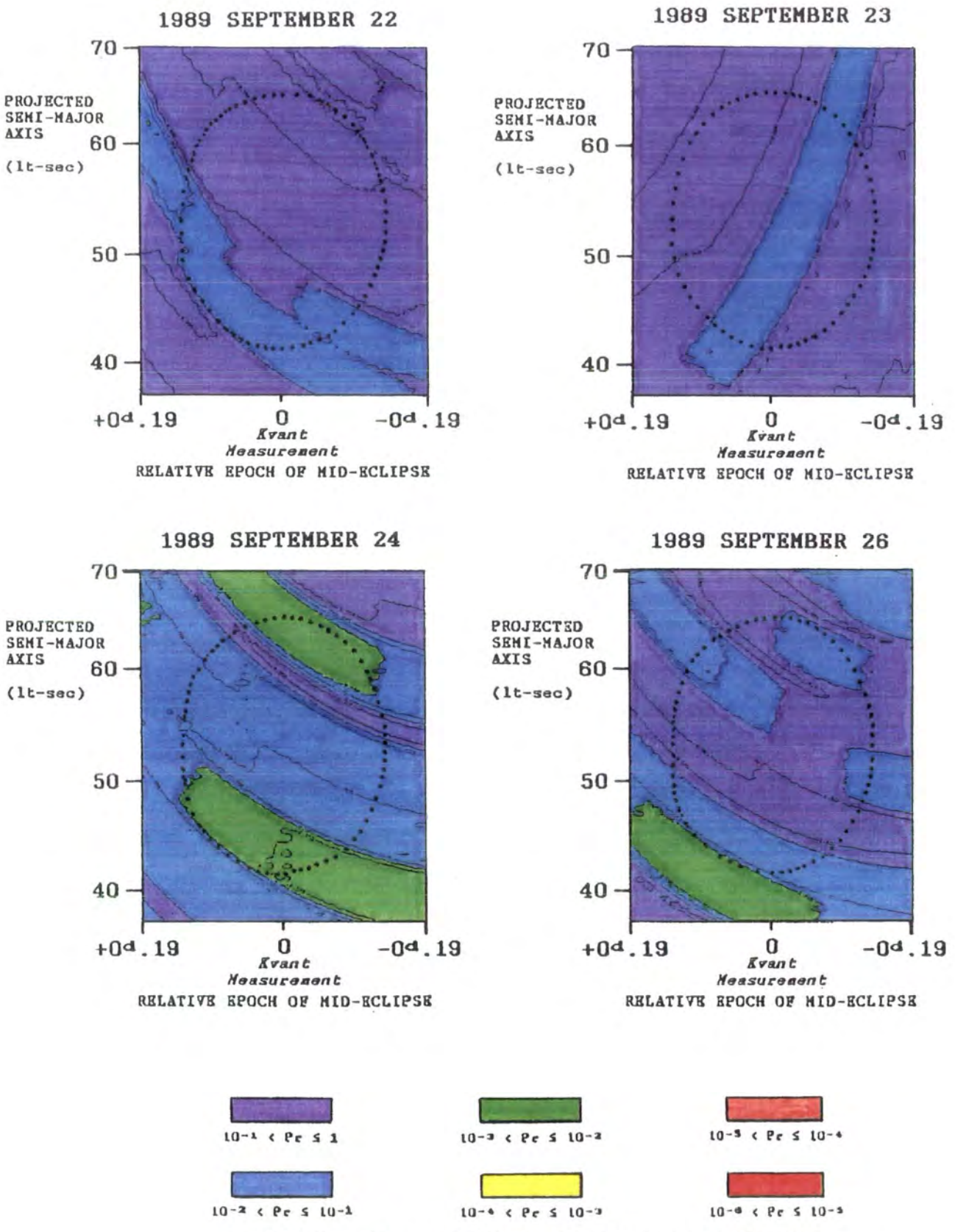
1989 SEPTEMBER 22
1989 SEPTEMBER 23
1989 SEPTEMBER 24
1989 SEPTEMBER 26
PROJECTED SEMI-MAJOR AXIS (lt-sec)
70
60
50
40
+0d.19
0
-0d.19
Kvant Measurement
RELATIVE EPOCH OF MID-ECLIPSE
10-1 < Pc ≤ 1
10-2 < Pc ≤ 10-1
10-3 < Pc ≤ 10-2
10-4 < Pc ≤ 10-3
10-5 < Pc ≤ 10-4
10-6 < Pc ≤ 10-5
CHANCE PROBABILITY AT X-RAY PULSE PERIOD

FIGURE 9.4

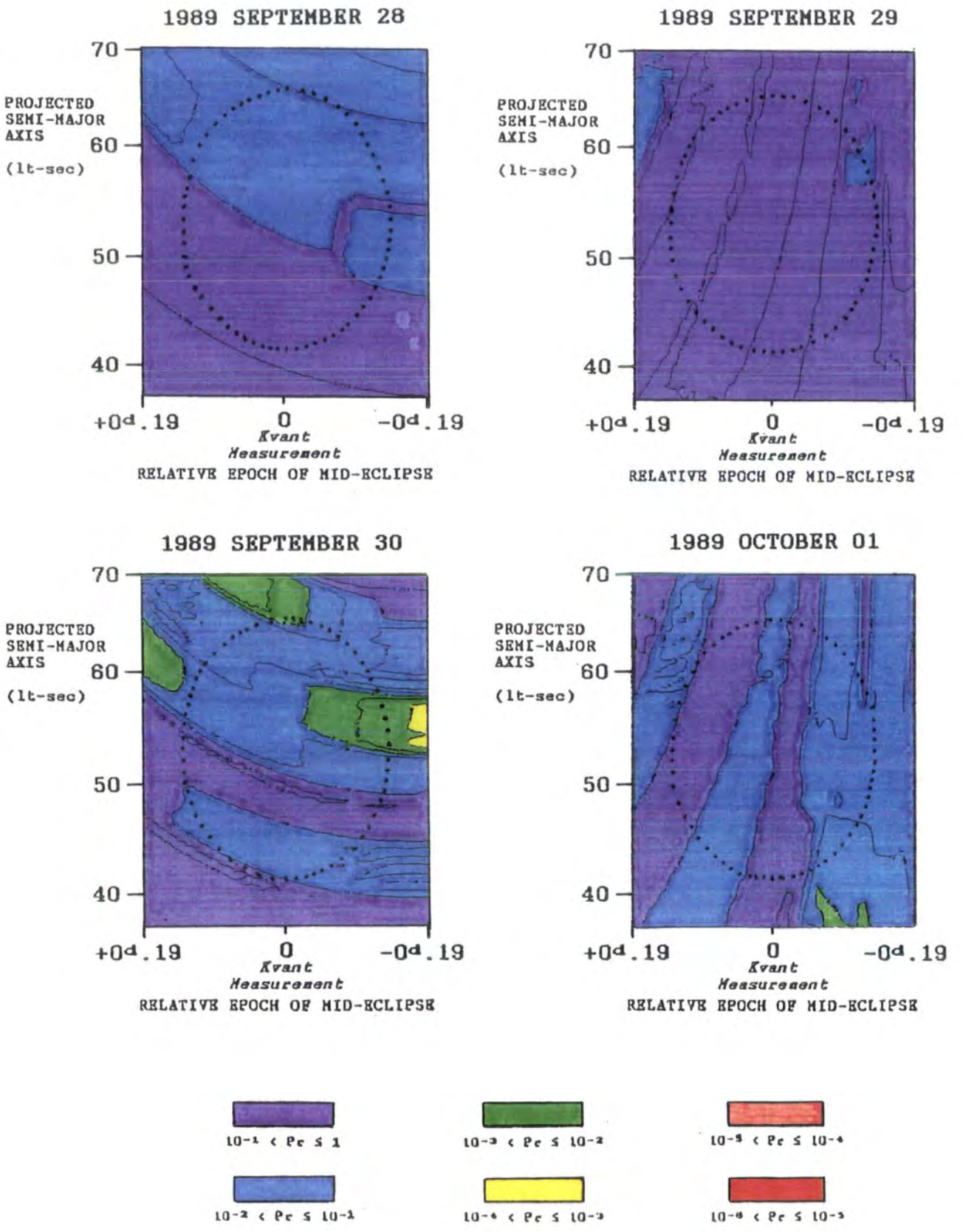

FIGURE 9.4 (cont.)

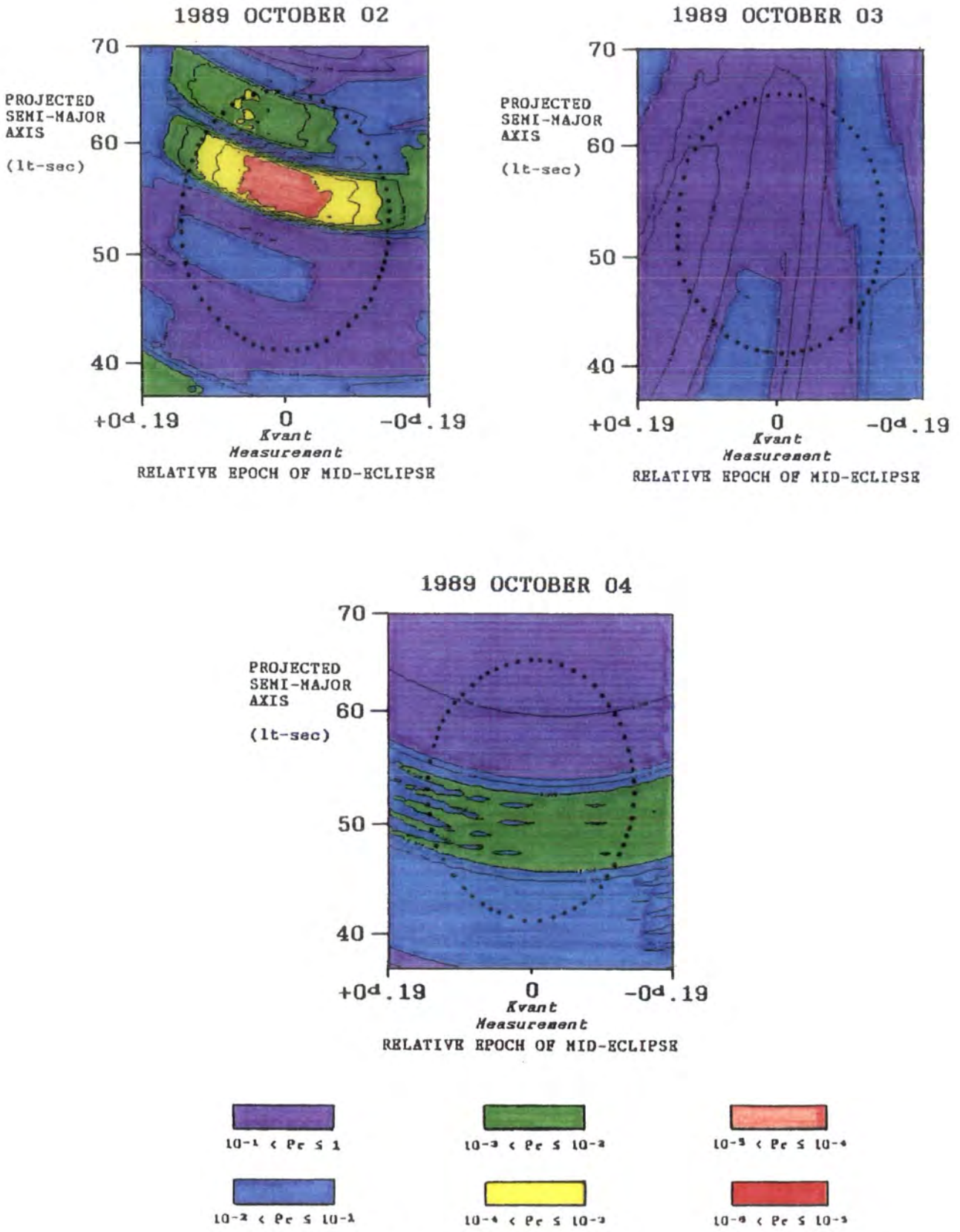

FIGURE 9.4 (cont.)

Figure 9.5a

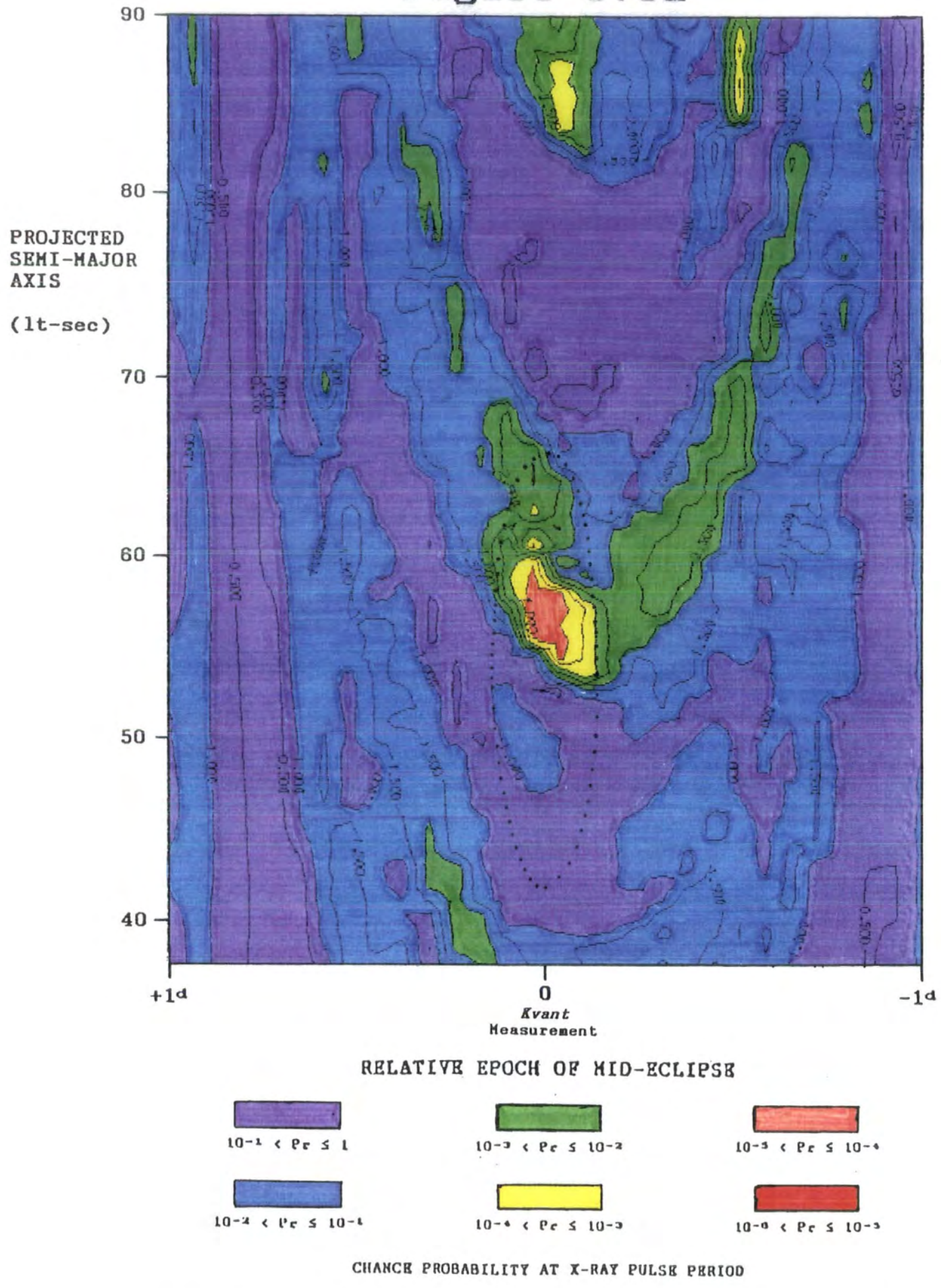

SMC X-1: Analysis of 1989 October 02 Data

Figure 9.5b

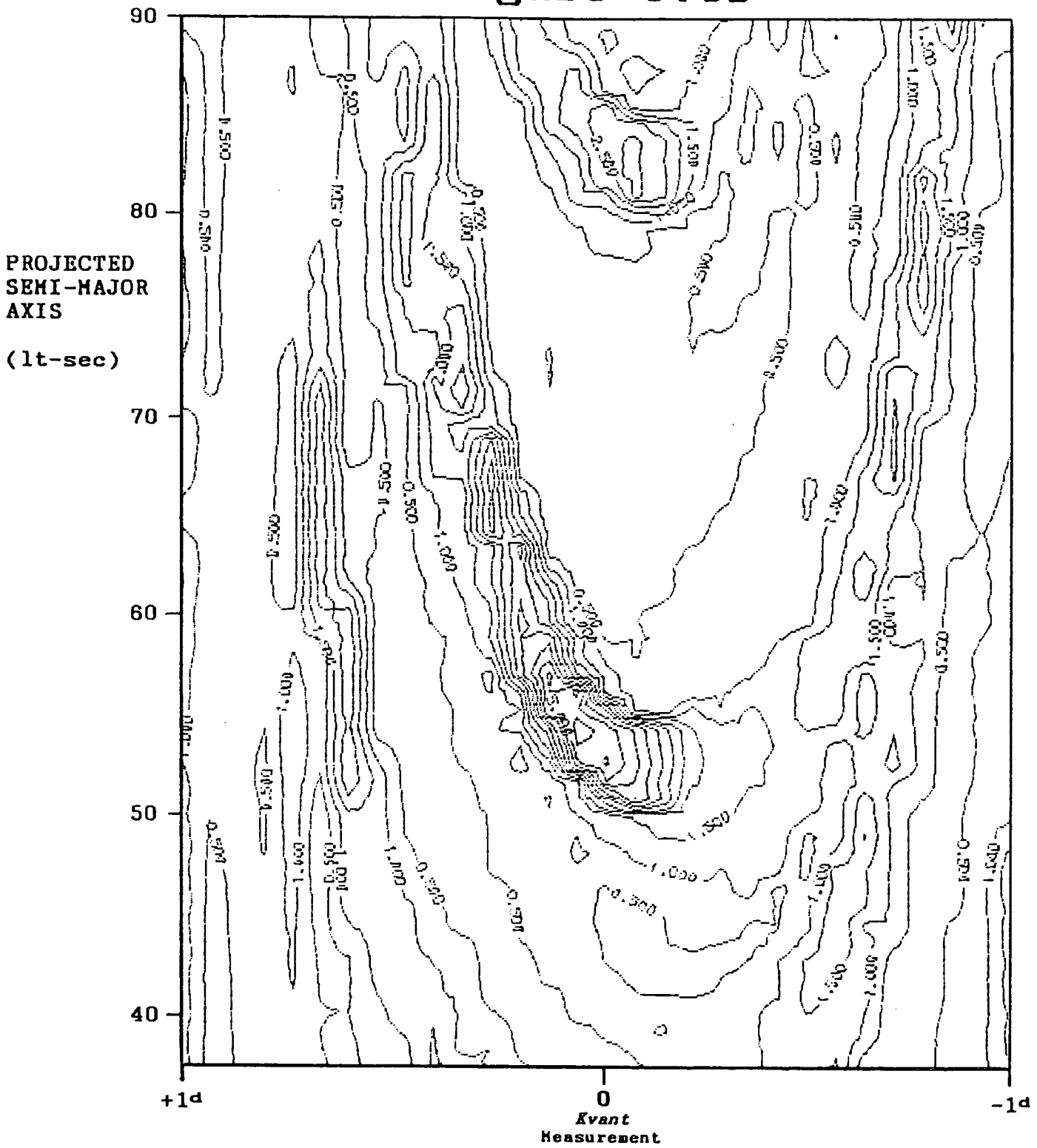

SMC X-1: SIMULATION of 1989 October 02 Data

with uniform pulsed signal

probability minimum in Figure 9.5a are smaller than those of the minima observed earlier in Figures 9.2a and 9.2b if it is assumed that the pulsed component is again spread throughout the time series.

The distribution of the pulsed component is investigated using the two methods described above.

1) A time series has been created with duration, orbital phase and average count rate equal to those of the real data of 1989 October 02. A strong pulsed component has been included at the X-ray period. Figure 9.5b shows the results obtained using the Rayleigh test. Compare with Figure 9.5a. These results are consistent with the periodicity being spread approximately evenly throughout the recorded time series.

2) The data have been tested for periodicity at the X-ray period in overlapping sections of five and ten minutes. Again, no evidence is found for significant enhancements in the strength of the pulsations in sub-divisions of the data on these timescales.

9.2.4 Summary

Separate analyses of the twenty time series recorded during observations of SMC X-1 in 1987 July and 1989 September-October indicate that three contain a component which is strongly pulsed

at the X-ray pulse period. No evidence is found for short (~ 5 - 10 minutes) episodes of enhanced pulsed emission.

The overall chance probability is determined in the following way. Allowance must be made for:

a) the number of period sampling intervals tested (2);

b) the number of sampling intervals in epoch and $a_x \sin i$: this will be assumed to be 1 for each quantity, since the locations of the probability minima are consistent with the coordinates of the neutron star;

c) oversampling within the independent sampling intervals for period, epoch, and $a_x \sin i$: a correction factor of 3 will be taken for each quantity

d) the number of ways in which the two subsets of time series may be selected from their parent datasets;

e) the total number of datasets (11).

i) <u>1987 July 21-31</u>

The chance probabilities (Pr) observed for the time series of 1987 July 23 and 29 are 7.8×10^{-4} and 2.1×10^{-4}, respectively. The combined chance probability is determined from

$$\chi^2_4 = \prod_{i=1}^{2} (Pr_i \times 2 \times 3^3) \qquad (1)$$

where the factor of 54 on the right-hand-side is from points a, b, and c above. The probability that χ^2 is greater than the value given by equation 1 is 4.1×10^{-3}. There are 36 unique ways in which 2 time series may be selected from a total of 9: points d and e above therefore introduce a further correction factor of 396. Accordingly, the two pulsed components identified in the data of 1987 July must be said to be consistent with a chance origin.

ii) <u>1989 September 22 - October 04</u>

A strong periodic component was found in one time series from a total of eleven, with chance probability 3.5×10^{-5}. This value must be multiplied by a factor of 54 x 11 x 11, which raises the chance probability to 0.23. This result is therefore again consistent with a chance origin

Formally, the results of the above tests demand acceptance of the null hypothesis that the SMC X-1 database provides no evidence for pulsed γ-ray emission. However it is interesting that, nevertheless, the three *strongest* periodic components in the twenty time series are each identified *only* when the Cerenkov arrival times are transformed using values of epoch and $a_x \sin i$ which are consistent with those of the SMC X-1 neutron star. Such qualitative evidence for pulsed γ-rays is sufficient to encourage further observations of this source candidate.

9.3 A Test For Pulse Phase Coherence Between γ-Ray Signals

9.3.1 Introduction

The aim of this section is to take the data from a sequence of observations of SMC X-1 and to establish whether phase coherence exists between pulsed components identified in the separate time series.

The potential reward of the discovery of such coherence goes beyond the support it would offer for the validity of a claim that pulsed γ-ray emission from SMC X-1 has been detected. The ability to identify the location of the source of the emission within the SMC X-1 binary would also be greatly improved. Once coherence between γ-ray signals in separate time series has been recognised, all the pulses may be regarded as constituting just one signal which has an *effective* duration equal to the time separating the first and last observations. The total signal-to-noise ratio is of course unchanged and is governed by the duty cycle of the observations themselves. A typical observing sequence lasts for ~ 10 d and the average length of observations is ≈ 3.4 hr: the duration of the signal is therefore effectively increased by a factor ~ 10^2. The spacing of independent candidate values of the pulse period is inversely proportional to the length of a time series, so that the effective increase in the duration of the γ-ray signal here provides much better resolution in the value of the pulse period and, in the same way, leads to a reduction in the separation of

the independent values of $a_x \sin i$ and mid-eclipse epoch which must be used to transform the time series. In principle, therefore, the γ-ray pulse period and the emission region may be recognised with great accuracy.

Phase coherence will be searched for in the data of 1987 July and 1989 September-October using the Rayleigh test. To do this, the separate time series within each dataset are first transformed and are then linked in phase according to the particular value of the candidate period being tested.

In linking the phases of the Cerenkov event times, allowance must be made for both the intervals of time separating the observations and for the anticipated secular decrease in the value of the pulse period due to the spin-up of the SMC X-1 neutron star. The importance of the pulse period derivative may be gauged by taking the third term of the pulse phase equation,

$$\varphi(t) = \varphi_o + \frac{t}{P} - \frac{\dot{P}t^2}{2P^2} + \frac{t^3}{3!}\left[\frac{2(\dot{P})^2}{P^3} - \frac{\ddot{P}}{P^2}\right] + \ldots\ldots \qquad (2)$$

The observed value of the SMC X-1 X-ray period derivative is $\dot{P} = -(1.205 \pm 0.014) \times 10^{-11}$ s/s and is therefore sufficient to change the relative phases of pulses by 2π after a time $t = \sqrt{(2P^2/|\dot{P}|)} \approx 3.4$ days. Both datasets exceed this duration. In fact, the use of $\dot{P}$ is more important than this since, with a

dataset duration (T) typically ~ 10 d, the expected change in the value of the pulse period equals the value of the period sampling interval after a time $t = P^2/(T\dot{P}) \approx 0.5$ d. Consequently, if it is postulated that γ-ray emission from SMC X-1 is not only pulsed at the expected X-ray period but that the value of the period of the γ-ray pulses decreases at the same rate observed at X-ray energies, then an extra test is being made when the time series are linked and tested for phase coherence: such coherence can only be recognised if the pulse period is decreasing at the expected rate.

9.3.2 Analysis of the 1987 July 21-31 Data

The nine time series in this dataset have been linked coherently and tested for periodicity. Contours of chance probability for periodicity at the X-ray period are drawn in Figure 9.6 against candidate values of epoch and $a_x \sin i$. The smallest chance probabilities occur at the centres of the elliptical probability minima in this diagram; the background to the contour pattern is formed by probabilities ~ unity. Arrows indicate the coordinates of the overall minimum value of chance probability. Evidence is found for a coherent signal which is pulsed at the X-ray period. The probability is $\approx 1.5 \times 10^{-9}$ that this periodicity has arisen by chance. This corresponds to a pulsed signal strength of approximately 2.7 % of the cosmic ray background. Two consequences of this test for phase coherence

Figure 9.6

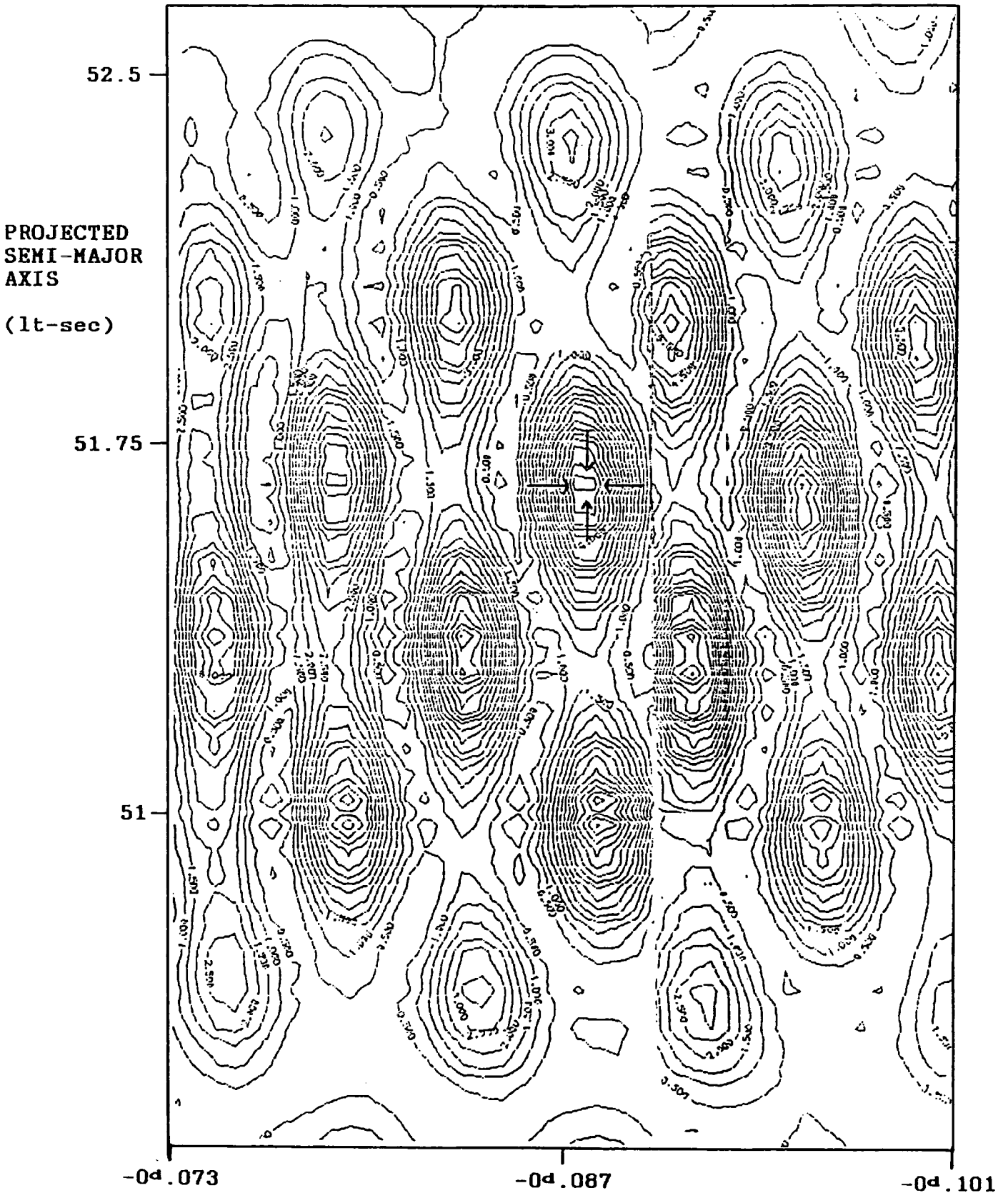

SMC X-1: Test for phase coherence in 1987 July data. Chance probability contours are drawn at X-ray period

are apparent in Figure 9.6:

1) There is a large set of pairs of values of epoch and $a_x \sin i$ with which adequate corrections for Doppler shifting may be made and a coherent signal recovered at the X-ray period. Such aliassing of the true pair of values is caused by the fact that the time series is not continuous but is instead formed by the linking of separate time series, each of which have a short duty cycle ($\approx$ 14 %).

2) the improved resolution in the values of epoch and $a_x \sin i$ automatically implies an increase in the number of independent trials which must be performed when *a priori* knowledge of the precise location of the emission region is unavailable.

The overall statistical significance is estimated as follows. The number (N) of independent candidate values of epoch and $a_x \sin i$ which were sampled during the test for phase coherence can be measured directly by inspecting the dimensions of the probability minima in the contour plot in Figure 9.6. For the horizontal and vertical ranges of epoch and $a_x \sin i$ indicated in this diagram, the value of N is ~ $6 \times 3.5 \times 3^2 = 189$, where a factor of three has been included for oversampling in each quantity.

However, the ranges of values of these orbital elements were selected using the results of the test for periodicity presented earlier in Chapter 8. The ranges employed during both tests are

shown in Figure 9.7; the ranges used in the present test for phase coherence is indicated by the hashed box. Dividing the full area in this diagram by the area of the hashed region [(0.38x33)/0.028x2.32] = 193], the value of N must be increased to $N \approx 3.65 \times 10^4$.

The uncertainty in the predicted value of the X-ray period for the epoch of the γ-ray observations is $\Delta P_x \approx 0.006$ ms. Independent candidate values of the pulse period are separated by an amount $P_x^2/T \approx (0.710493)^2/8.64 \times 10^5 = 5.8 \times 10^{-4}$ ms. The number of period trials made was therefore $(2 \times \Delta P_x \times T/P_x^2) \times 3 = 62$, where a factor of three is again included to correct for oversampling. The final factor which must be included is the total number of sequences of SMC X-1 observations which were performed at Narrabri: N therefore becomes $11 \times 62 \times 3.65 \times 10^4$, or $N = 2.5 \times 10^7$

Accordingly, the chance probability for a coherent pulsed signal in the data of 1987 July must be raised to the value $2.5 \times 10^7 \times 1.5 \times 10^{-9} = 4 \times 10^{-2}$. A very strong coherent periodic signal has been identified but, formally, the significance level is equivalent to that of a $\approx 2\sigma$ fluctuation above the mean noise level: it cannot therefore support rejection of the null hypothesis that the times are randomly distributed.

Figure 9.7

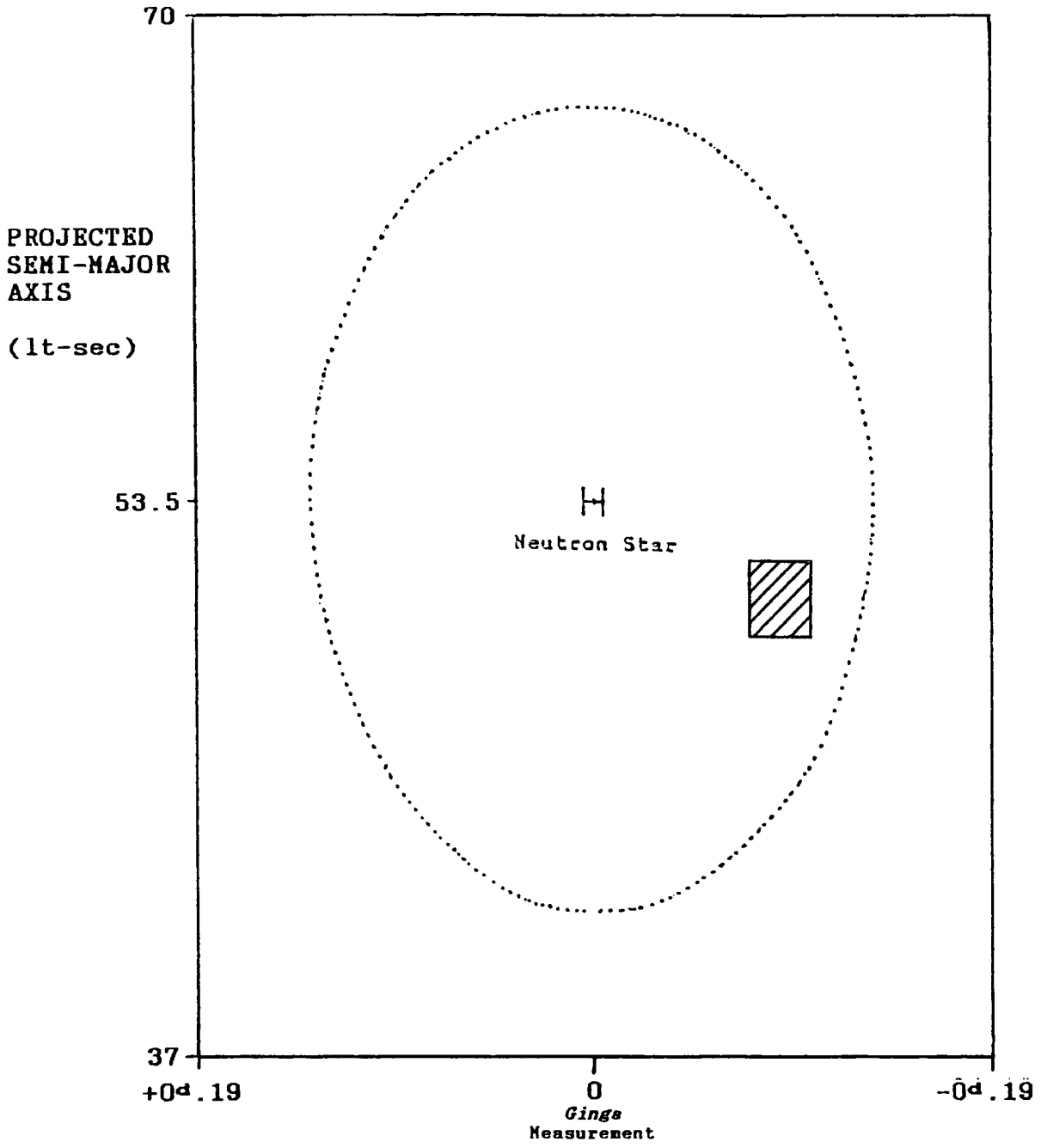

Region of [τ, $a_x \sin i$] plane shown in Figure 9.6

9.3.3 Analysis of the 1989 September 22 - October 04 Data

The eleven time series in this dataset have been linked in phase and tested for periodicity using the Rayleigh test. Chance probability contours for periodicity at the X-ray pulse period are drawn against values of epoch and $a_x \sin i$ in Figure 9.8. Arrows indicate the overall value of minimum chance probability, which is at the 2×10^{-6} level. The number of independent trials performed in this test is estimated using the method described in Section 9.3.2 and has the value

$$[(0.38\times33)/(0.057\times4.5)] \times (10.5\times12\times3^2) \times 3[1.2\times10^{-5}/((0.709775)^2/1.04\times10^6)] \sim 4 \times 10^6 .$$

The result of this test for a coherent pulsed signal is therefore once again consistent with randomness.

9.3.4 Discussion

The test for pulse phase coherence is potentially very powerful and offers fine resolution in the values of pulse period, mid-eclipse epoch and $a_x \sin i$; however, by its very nature, it requires a strong signal-to-noise ratio if this potential is to be fully realised in the absence of accurate *a priori* knowledge of the position of the emission region.

Figure 9.8

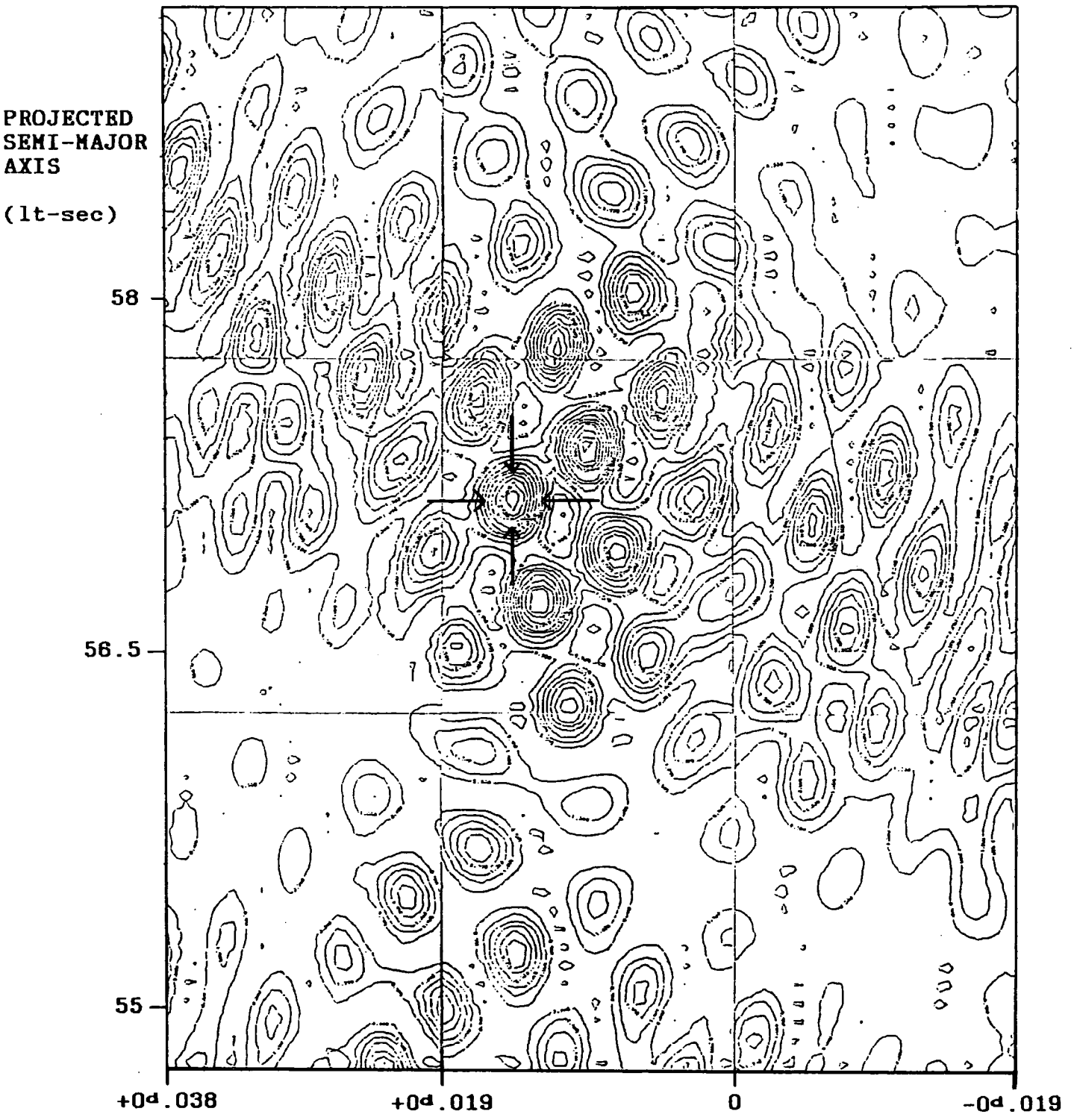

SMC X-1: Test for phase coherence in data of 1989 September 22 - October 04. Chance probability contours are drawn at X-ray period.

It is interesting to consider the possible consequences had the coherent periodic signal in the data of 1987 July been of sufficient strength to provide firm evidence of pulsed γ-ray emission from SMC X-1: i.e. what spatial information might have been extracted from this result ? How might knowledge of the position of the site of γ-ray emission been improved by the good spatial resolution of the test for phase coherence ?

To explore this, the ranges in the values of epoch and $a_x \sin i$ displayed earlier in Figure 9.6 have been extended until they include the coordinates of the SMC X-1 neutron star. See Figure 9.9. The position of the neutron star is indicated in the top left-hand corner of this diagram and the overall chance probability minimum is shown to the right of centre. Observe the pattern of the probability minima due to the aliassing introduced by the discrete nature of the observations. These aliases extend across the *Ginga* X-ray measurement of the mid-eclipse epoch, so that the value of epoch at the coordinates of the overall minimum is consistent with this measurement. However, the aliases decay quickly to probabilities ~ unity in the vertical direction. The value of $a_x \sin i$ at the probability minimum is inconsistent with the value of 53.46 ± 0.05 lt-sec determined from the X-ray measurements (Primini, Rappaport and Joss 1977); the upper boundary of the contour pattern in Figure 9.9 occurs at approximately one light-second below this value. Khruzina and Cherepashchuck (1987) find the radius of the SMC X-1 accretion disk to be r_{disc} = 12.1 ± 2.8 lt-sec. A distance of of ≈ 1 lt-sec therefore amounts to just ~ 10 % of this value so

Figure 9.9

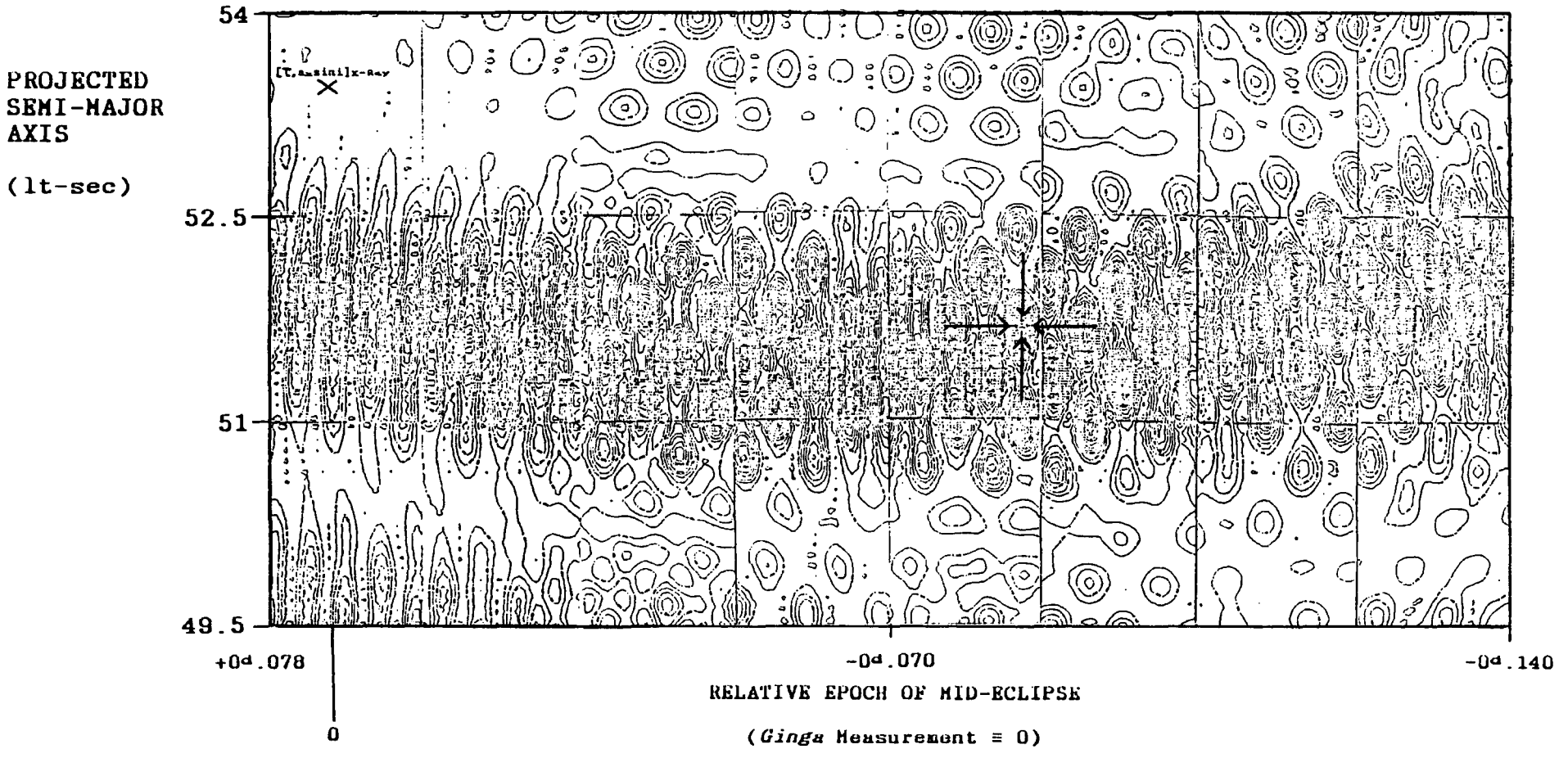

SMC X-1: Test for phase coherence in 1987 July data.
Chance probability contours are drawn at X-ray period

that the site of emission would be placed well within the boundary of the accretion disk. Such unprecedented spatial resolution would be of great benefit to the modelling of TeV γ-ray emission mechanisms. For example, the SMC X-1 pulsar light cylinder - which limits the maximum radial extent of the pulsar magnetosphere - has a radius $r_c = c/2\pi f \approx 0.1$ lt-sec (where f is the rotation frequency of the neutron star). Therefore, although the site of emission could be narrowed down to the disk it could, in principle, be found to be considerably beyond the direct influence of the magnetosphere of the pulsar. The spatial resolution would be adequate to allow such important distinctions to be made.

Various models of TeV γ-ray emission from X-ray binary systems are discussed in detail in Chapter 11. They each postulate the acceleration of charged particles to ultrahigh energies in the pulsar magnetospheres. This is followed by the transport of beams of protons to various possible sites within the binary, and the emission of high-energy γ-rays from the decay of neutral pions formed in collisions. If detections of γ-ray emission from SMC X-1 are in future made with improved signal-to-noise ratios, it is possible that one of these models could be adapted to fit firm constraints which might be deduced for the location of the γ-ray emission site.

9.4 Conclusion

SMC X-1 has been monitored from Narrabri at a threshold γ-ray energy of 0.4 TeV during 11 separate sequences of observations in the interval 1986 October to 1989 December. Results were presented in Chapter 8 from the period analysis of the Cerenkov arrival time series recorded during each of these observing sequences. Although strong components pulsed at periods consistent with the contemporary X-ray pulse period were identified in the data of 1987 July and 1989 September-October, calibration of the analysis indicates that no quantitative evidence can be claimed for pulsed γ-ray emission from SMC X-1. The twenty time series which form these two datasets were each analysed separately in the present chapter: three of the time series were found to contain a signal which is strongly pulsed at the X-ray period. Even though the significance level of these periodic components is consistent with a chance origin, qualitative evidence for the detection of pulsed emission from SMC X-1 is provided by the fact that *each* of the components was identified *only* when the arrival times were transformed using values of mid-eclipse epoch and $a_x \sin i$ which are consistent with the values determined for the neutron star from the X-ray measurements.

No evidence was found for short-term enhancements in the strength of the periodic component within each of the three time series.

Strong pulsed signals were identified by a test for pulse phase coherence within the 1987 July and 1989 September-October datasets but, once again, the number of independent trials carried out precludes a claim for evidence of the detection of periodic emission from SMC X-1.

Upper limits on the time-averaged value of the pulsed γ-ray luminosity of SMC X-1 ($E > 0.4$ TeV) during each of the eleven observing sequences have been estimated. These were determined by seeking the value which would have led to a detection significant at the 99.7 % (3σ) level, which corresponds to a chance probability of 3×10^{-3}. The computations have been made conservatively by taking into account the matrix of candidate values of pulse period, mid-eclipse epoch, and $a_x \sin i$ which is employed by the analysis technique described in Chapter 8. Calibration of the period analysis of the 1987 July 21-31 data indicated that this matrix corresponds to $\sim 2 \times 10^3$ trials, therefore the chance probability required for a detection significant at the 3σ level is

$$\Pr\left(\chi^2 \geq {}_{2N}\chi^2\right) \approx 1.5 \times 10^{-6} \qquad (3)$$

where N is the number of nights in a given observing sequence. The value of ${}_{2N}\chi^2$ was computed in Chapter 8 using

$$\chi^2 = -2 \log_e \prod_{j=1}^{N} \Pr_j(P) \qquad (4)$$

where $Pr_j(P)$ is the chance probability observed at period P after searching for periodicity in a single time series. Let the flux of γ-rays arriving at the top of the atmosphere be R % of the cosmic ray background. This γ-ray flux is assumed here to be steady throughout each observing sequence. If the number of Cerenkov arrival times in any given time series is n_i then the chance probability for periodicity at candidate period P is $\exp(-n_i R^2)$; see Chapter 4. Rearrangement of equation 4 then gives

$$R = \left[\frac{1}{2} \chi^2_{2N} \left(\sum_{i=1}^{N} n_i \right)^{-1} \right]^{1/2} \qquad (5)$$

SMC X-1 was observed from Narrabri at zenith angles ranging between $\approx 40^\circ$ to 60°, at which the cosmic ray background flux recorded by the Mark III telescope is estimated to be $\approx 3 \times 10^{-9}$ cm^{-2} s^{-1} with a threshold energy ≈ 0.4 TeV (Brazier *et al.* 1989a). The 3σ upper limits to the time-averaged pulsed γ-ray fluxes were estimated using this value of the cosmic ray flux together with equations 3 and 5. They are listed in Table 9.1. These flux limits have been converted to 3σ upper limits on luminosity by making the following assumptions:

1) SMC X-1 is at a distance of 63 kpc.

2) No attenuation of γ-ray flux occurs *en route* to the detector.

Table 9.1

Observing Sequence	Flux 3σ Upper Limit (10^{-11} cm^{-2} s^{-1})	Luminosity* 3σ Upper Limit (10^{37} ergs s^{-1})
1986 Oct 24 - Nov 04	8.2	1.9
1987 Jul 21 - 31	9.9	2.4
1987 Aug 20 - 28	10.0	2.4
1987 Sep 14 - 27	9.8	2.3
1987 Oct 10 - 25	10.4	2.5
1987 Nov 13 - 19	13.2	3.1
1988 Jul 14 - 20	9.8	2.3
1988 Sep 04 - 16	6.8	1.6
1989 Sep 22 - Oct 04	7.1	1.7
1989 Oct 20 - Nov 02	18.5	4.4
1989 Nov 18 - Dec 01	15.3	3.6

Upper limits on time-averaged flux and luminosity of γ-rays from SMC X-1 pulsed at the X-ray pulse period ($E > 0.4$ TeV)

*Estimated to be correct to better than one order of magnitude.

3) The differential photon energy spectrum index is equal to the cosmic ray proton index of -2.6.

4) γ-rays are emitted isotropically.

See Table 9.1. Each of the upper limits on the pulsed γ-ray luminosity is found to be at a level ~ 10^{37} ergs s^{-1}, which is comparable with the pulsed γ-ray luminosities observed at similar threshold energies during outburst from the low-mass binaries Cygnus X-3 (Brazier *et al.* 1990c) and Hercules X-1 (Brazier *et al.* 1990d). This emphasises the difficulty of detecting γ-rays from such a distant source candidate: in order to be measured with marginal statistical significance during a typical sequence ~ 10 observations at Narrabri, the time-averaged luminosity of SMC X-1 would need to be at the level of the outburst luminosity of the two most powerful stellar TeV γ-ray sources discovered to date.

A 3σ upper limit of ~ 1.5 x 10^{37} ergs s^{-1} is placed on the time-averaged pulsed luminosity of SMC X-1 over the three years during which the observations were made. For comparison with other high-mass X-ray binaries, this is about a factor of 3 higher than the peak TeV γ-ray luminosity measured for Centaurus X-3 (Brazier *et al.* 1990a) and a factor ~ 400 higher than the steady γ-ray power of Vela X-1 (Carraminana *et al.* 1989a).

A firm detection of γ-rays from SMC X-1 therefore demands a high intrinsic luminosity. However, the level required is not unreasonably high and there are grounds to believe that such

luminosities may possibly be attained. SMC X-1 is a very powerful X-ray source and has been observed at X-ray luminosities ~ 10 times greater than the Eddington limit (e.g. Coe *et al.* 1981). In Chapter 11 it will be seen that the observed TeV γ-ray luminosities of Cen X-3, Vela X-1 and LMC X-4 correspond to ~ 1 % their X-ray luminosities. If this pattern is continued with SMC X-1 then a TeV γ-ray luminosity ~ 10^{37} ergs s^{-1} is feasible. SMC X-1 exhibits X-ray high states which persist for times $\approx$ 30 days FWHM and are separated by intervals $\approx$ 60 days (Gruber and Rothschild 1984 and Chapter 7). If the power of γ-ray emission at SMC X-1 were to be (a) variable on similar timescales and (b) at or in excess of the limits determined above, then the duration of the typical Narrabri observation sequence is well matched. The qualitative evidence for pulsed γ-ray emission provided by the periodic components identified in three of the twenty time series of 1987 July and 1989 September-October strongly suggests that further observations of SMC X-1 using improved flux sensitivity would be of great interest. If these components are due to the detection of a pulsed γ-ray signal, then the signal-to-noise ratio is currently too low to compensate for the number of independent trials which must be performed during the analysis in order to recover the periodicity. A second air Cerenkov telescope (the Mark IV) was installed at the Narrabri site during early 1990. A concentrated programme of observations with the two telescopes during one or two Moon-free periods could be sufficient to provide conclusive evidence for the detection of pulsed γ-rays from SMC X-1.

Chapter 10

Observations of Two Low-Mass X-Ray Binary Systems

10.1 Introduction

This chapter is concerned with the results of period analyses of databases accumulated during observations from Narrabri of two low-mass binaries containing X-ray pulsars. Upper limits are determined for the time-averaged luminosity of pulsed TeV γ-rays.

The discovery of transient X-ray pulsations at a period of 120.2 s from the source X0021.8-7221 near the core of the nearby globular cluster 47 Tucanae has been reported by Auriere, Koch-Miramond and Ortolani (1989). This followed analysis of X-ray data from the *Einstein* archives of 1979 November. The Potchefstroom Group observed 47 Tucanae at a threshold γ-ray energy of 3 TeV during 1989 and have reported evidence for transient emission which is pulsed at the above X-ray pulse period (de Jager *et al.* 1990). The reported time-averaged luminosity is $\approx 2 \times 10^{35}$ ergs s^{-1} ($E > 2.8$ TeV). Period analysis of data taken at Narrabri during the interval 1988 July to 1990 September does not confirm this result and places a 3σ upper limit on the pulsed γ-ray luminosity of $\approx 7 \times 10^{34}$ ergs s^{-1} ($E > 0.4$ TeV) averaged over the entire sequence of observations.

The Galactic centre low-mass X-ray binary GX 1+4 comprises an X-ray pulsar ($P_x \approx$ two minutes) in a very wide orbit about an M6 III symbiotic red giant. Observations of this source candidate have been made from Narrabri on 5 occasions during 1988 July. No evidence for emission which is pulsed at the contemporary X-ray pulse period is revealed by period analysis of the data. A 3σ upper limit is determined for the time-averaged pulsed γ-ray luminosity.

10.2 X0021.8-7221 in 47 Tucanae

10.2.1 Introduction

The position of the globular cluster 47 Tucanae (NGC 104) offers a number of advantages to observers. It is a relatively nearby cluster and is at a distance of just 4.6 kpc. In addition, it is observed well away from the obscuring interstellar dust lanes found in the plane of the Galaxy; it is in fact viewed in projection close to the north-eastern edge of the Small Magellanic Cloud. 47 Tucanae is an unusual globular cluster. The proportion of heavy elements is a factor of ~ 10 higher than that observed in other clusters. It may be that it is a relatively young cluster and was formed out of interstellar gas that had already been enriched with heavy elements released by numerous supernova explosions early in the history of the Galaxy. 47 Tucanae may be between 10 and 13 billion years old, in contrast to the 15 to 20 billion-year ages

ascribed to the majority of globular clusters.

A faint X-ray source was discovered in the core of 47 Tucanae during an X-ray survey with the *Einstein* observatory of more than half of the known globular clusters associated with the Galaxy. See Hertz and Grindlay (1983a,b). Designated X0021.8-7221, the source is located at just 0.36 core radius from the centre of the cluster. The X-ray luminosity at discovery was ~ 10^{34} ergs s^{-1} (0.5 - 4.5 keV). Comparatively little is known about X0021.8-7221. Recently, Auriere, Koch-Miramond and Ortolani (1989: henceforth referred to as AKO) studied the *Einstein* Imaging Proportional Counter data archives of 1979 November 19-22. The luminosity of X0021.8-7221 at 0.1 to 8 keV was found to be $\approx 10^{34}$ ergs s^{-1}. X-ray variability in this source was first suggested by Hertz and Grindlay (1983a). AKO discovered variability on timescales of days, hours and tens of minutes. The 0.5-2.5 keV flux was found to vary by a factor $\approx$ 2.5 to 3 in 2.6 days and by a factor ~ 2 in 13 h. Variations over t $\approx$ $^1/_4$ hr to $^1/_2$ hr were also found. Of most interest to the present work is the evidence for transient X-ray pulse periodicity. The *Einstein* data of 1979 November 19 reveal pulsations at a period P = 120.200 s. (No errors are given for this value). The X-ray pulses were detected only during a 2.2-hr interval, when the (decreasing) luminosity of the source was L_X ~ 8 x 10^{33} ergs s^{-1}. Classification of the source is difficult. No optical counterpart has been identified, due to the high density of field stars. The most massive of the evolving stars in 47 Tucanae have masses $\approx$ 0.8 $M_\odot$, therefore

excluding the possibility that X0021.8-7221 is a high-mass X-ray binary. The X-ray luminosity is $L_X \sim 7 \times 10^{33}$ to 2×10^{34} ergs s^{-1} in the 0.2 to 4 keV energy range, which is a factor of 4 higher than that of the brightest Galactic cataclysmic variable but a factor of 10 to 100 times lower than that of the faintest known low-mass X-ray binary. Verbunt, van Paradijs and Elson (1984) have suggested that the brightest of the globular cluster X-ray sources identified with cataclysmic variables (with luminosity $L_X \sim 10^{33}$ ergs s^{-1}) could in fact be low-mass X-ray binaries (LMXRB). Also, the location of X0021.8-7221 very close to the centre of 47 Tucanae is at the average location of the *bright* globular cluster X-ray sources (Grindlay *et al.* 1984), therefore supporting the idea that X0021.8-7221 is a LMXRB.

10.2.2 Observations of 47 Tucanae by the Potchefstroom Group

de Jager *et al.* (1990) observed 47 Tucanae at a threshold γ-ray energy of 2.8 TeV for a total of 66.2 hours on 27 nights between 1989 July 7 and October 23. On the basis of these observations, they make the first claim for the detection of TeV γ-ray emission from a globular cluster. A Rayleigh test was performed on each of the 27 time series in a search for periodicity at the X-ray pulse period of X0021.8-7221. A strong pulsed component was identified in the data from just one of the nights, that of 1989 August 10. Periodicity was found at P = 120.1 ± 0.2 s, consistent with the X-ray period, with a chance probability of 1.37×10^{-5}. This probability is increased to 3.7

x 10^{-4} after multiplication by the total number of observations. The results of the separate time series analyses were next combined in order to determine whether data from other nights have weak periodic components at P_x. This was carried out in the manner described in Chapter 8 for the analysis of the Narrabri SMC X-1 database:

i) establish a range of trial periods centred upon the candidate pulse period and use a fixed set of period values in this range for each of the time series.

ii) at each trial period (P) compute the statistic:

$$C = -2 \log_e \prod_{j=1}^{27} Pr_j(P) \qquad (1)$$

which, under the null hypothesis, is distributed as χ^2 with 2x27 degrees of freedom.

The results of this test are shown in the upper panel of Figure 10.1, together with that for the night of 1989 August 10. If the only contribution were that from the August 10 data, then the expected combined chance probability at $P = P_x$ would be $\approx 3 \times 10^{-2}$. With this value being a factor of ten greater than that actually observed, de Jager *et al.* (1990) claim that data from some of the remaining 26 observations also include a weak component pulsed at the X-ray period. Two intervals of possible activity separated by three weeks are identified during the $3\frac{1}{2}$-month sequence of observations, both lasting for a time $\approx$ 5 days.

Figure 10.1

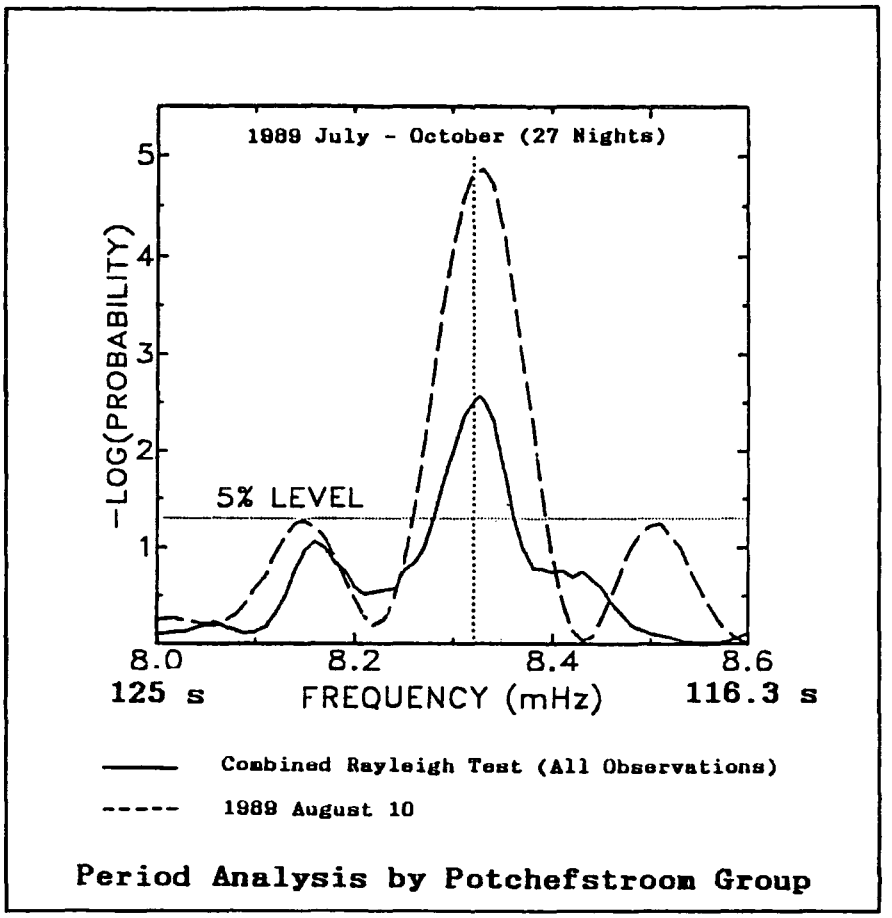

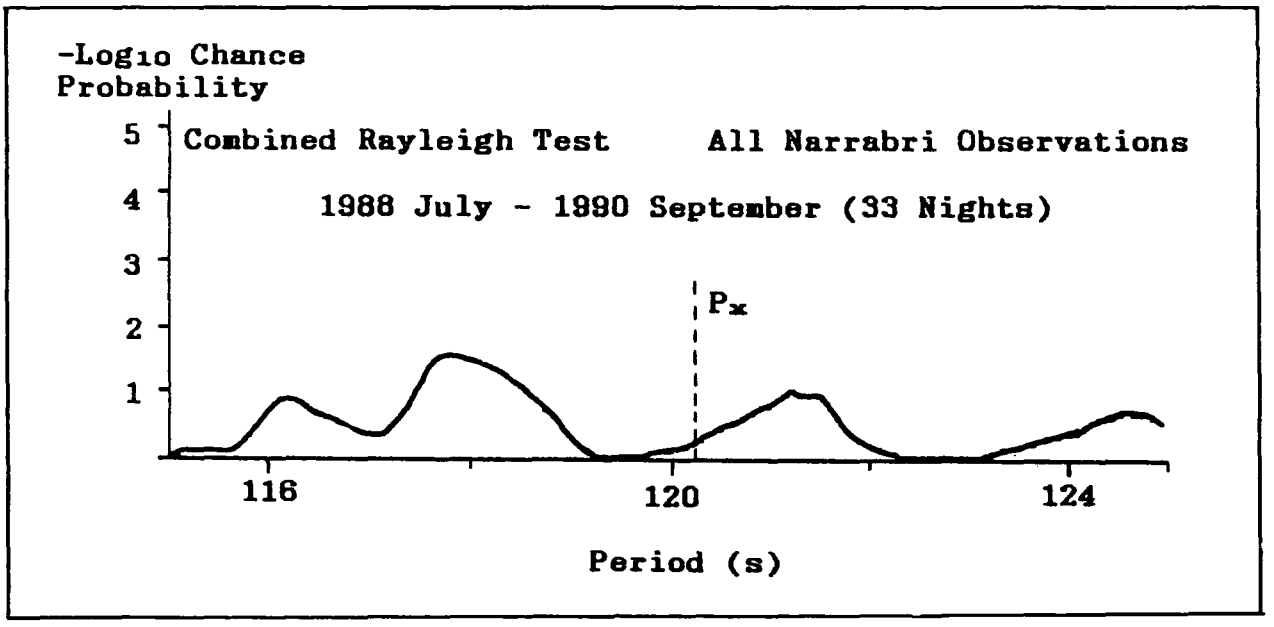

47 Tucanae: Period Analyses by Potchefstroom and Durham Groups

A search for pulse phase coherence between the separate time series using the Rayleigh test yielded a null result.

The luminosity estimated for 1989 August 10 is $L \approx 9 \times 10^{35}$ ergs s^{-1} ($E > 2.8$ TeV). The time-averaged value over the 109 day span of the observations is $\approx 2 \times 10^{35}$ ergs s^{-1} ($E > 2.8$ TeV) assuming a differential spectral index of -2.6, equal to that of the cosmic ray proton index. This luminosity is a factor ~ 10 greater than the X-ray luminosity noted above. De Jager *et al.* (1990) suggest that if the claimed γ-ray source is identified with the X-ray source X0021.8-7221, such a high γ-ray luminosity would favour classification as a low-mass X-ray binary rather than a cataclysmic variable. The low luminosity observed at X-ray energies may be the result of absorption of X-rays in the line-of-sight to a binary viewed at high inclination. The proposed absorbing medium is a flared region at the outer edge of an accretion disk which simultaneously acts as a beam target for particles accelerated near the neutron star. High-energy γ-rays then arise through the decay of neutral pions produced in the particle collisions.

10.2.3 The Narrabri 47 Tucanae Database

47 Tucanae was observed from Narrabri at zenith angles $\approx 40^{\circ}$-50° and at a threshold γ-ray energy of 0.4 TeV on 33 nights during 5 separate sequences of observations between 1988 July 09 and 1990 September 17. Two of these sequences occurred in late

1989, the first starting around the date of the final observation by the Potchefstroom Group. The Mark III telescope was operated in the tracking mode on each occasion. A total of 112 hours of data were logged, during which approximately 168,000 air Cerenkov events were recorded. The average count rate over all observations is ≈ 1500 hr^{-1} and the average duration of a single observation is 3.4 hr. The date and UT of each observation is listed in Table 10.1, together with duration, zenith angles, and the focal plane detector channels in operation

10.2.4 Analysis of the 47 Tucanae Database

An hypothesis is provided by the previous X-ray and TeV γ-ray observations of this globular cluster which can easily be tested. The simple prediction is that the Narrabri 47 Tucanae data include a periodic component at a period ≈ 120 s. A search will be made for such periodicity using the Rayleigh test, which is powerful for broad pulse light curves (Chapter 4) and which was also the test used by the Potchefstroom Group to obtain the positive result described above; the X0021.8-7221 X-ray pulse light curve is broad (AKO) therefore if the putative TeV γ-ray light curve is similarly shaped, then the Rayleigh test will be the most sensitive.

The orbital parameters of the X0021.8-7221 binary have not been measured, therefore the Cerenkov arrival times cannot be transformed to the binary rest frame before period analysis.

Table 10.1

	DATE	DURATION (hr)	NUMBER OF EVENTS	TIME (UT)	ZENITH ANGLES	CHANNELS OPERATING
(1)	090788	3.1	3585	14:23-17:30	56°-42°	1234567
	100788	2.0	2158	16:45-18:45		1234567
	110788	3.4	4057	16:25-19:46		1234000
	120788	3.4	3203	16:28-19:48		1204000
	130788	3.7	3294	16:04-19:48		1204000
	190788	3.1	5348	16:37-19:45		1234000
(2)	021088	2.8	2574	09:41-12:30	48°-42°	1234567
	031088	5.4	6154	10:45-16:09		1234567
	041088	5.8	9465	10:54-16:42		1234567
	071088	3.3	7207	11:11-14:30		1234567
	081088	3.6	5846	10:52-14:30		1234567
	091088	3.5	9934	11:03-14:30		1234567
	101088	3.4	8290	11:04-14:30		1234567
	111088	3.3	8687	10:55-14:14		1234567
	121088	3.5	7647	10:46-14:19		1234567
	131088	3.6	6441	10:23-14:10		1234567
	141088	2.1	3248	11:27-13:30		1234567
(3)	211089	5.2	7853	09:49-14:59	41°-49°	1234567
	271089	4.0	4435	09:59-14:00		1234567
	281089	3.0	3969	10:28-13:48		1234567
	301089	2.5	1790	09:45-12:15		1234567
	011189	4.5	6063	10:31-15:00		1234567
(4)	201189	2.0	3290	10:39-12:39	41°-50°	1234567
	211189	3.9	6100	10:09-14:00		1234567
	221189	2.8	4436	10:13-13:00		1234567
	271189	2.8	2668	10:35-13:20		1234567
	281189	3.0	4173	10:15-13:15		1234567
	301189	2.8	3970	10:33-13:21		1234567
(5)	110990	1.4	1851	13:27-14:51	47°-42°	1234567
	140990	5.2	5992	12:19-17:30		1234567
	150990	3.4	3713	12:36-16:00		1234567
	160990	3.3	5306	12:40-16:00		1234567
	170990	3.2	5108	12:41-15:50		1234567

47 Tucanae: Narrabri Observing Log

Total nights	33
Total hours	112
Total events	167,855

However, this should not cause difficulty. Orbital speeds of neutron stars are typically $v \sim 10^2$ km s^{-1} in close low-mass binaries, where the masses of the two stars are comparable ($\sim$ 1 $M_\odot$) and the orbital periods are usually $\sim$ 1 day or less. Let θ be orbital phase measured from superior conjunction: then, if P_o and P_{max} are the binary rest frame pulsar period ($\approx$ 120 s here) and the maximum value of the Doppler shifted period, respectively, $P_o - P_{max} = P_o(v/c)\sin\theta = P_o v/c \approx 0.04$ s. The spacing between independent values of candidate pulse period for a single observation is $\Delta P_I = 120^2/(3.4 \times 60^2) \approx 1.2$ s, which is a factor of 30 greater than the smearing anticipated by orbital motions.

There is also no known secular pulse period derivative for X0021.8-7221. The first of the tests described below simply takes the full 47 Tucanae database and tests for periodicity at the candidate X-ray pulse period. The data were obtained over an interval $T \sim 2$ years, so that the critical value of the long term-pulse period derivative is $\dot{P} \sim \Delta P_I/T \sim 2 \times 10^{-8}$ s s^{-1}. However, if the X-ray pulse period were decreasing/increasing uniformly with time at this rate, then it would have changed by up to 6 seconds between the 1979 X-ray measurement and the epoch of the TeV γ-ray observations by the Potchefstroom Group. This is at variance with the claim by de Jager *et al.* (1990) that the X-ray and TeV γ-ray pulse periods were consistent. It will therefore be assumed here that a fixed candidate γ-ray pulse period is appropriate to analysis of the full database, of the

data from within each observing sequence, and of the data from individual nights.

The periodogram in the lower panel of Figure 10.1 shows the result of analysis of all data obtained at Narrabri during observations of 47 Tucanae. Each of the 33 time series were tested for periodicity and the chance probabilities at each candidate period combined according to equation 1. No evidence is found for a periodic component at the X-ray pulse period. Similarly, separate period analyses of the data from each of the sequences of observations, and from each of the observations themselves, yielded results which are consistent with randomness. On the basis of these tests, the hypothesis that the data include a periodic component at P = 120.1 s is rejected.

10.2.5 Discussion

An upper limit to the time-averaged pulsed γ-ray luminosity is determined by seeking the value which would have led to a detection significant at the 99.7 % (3σ) level. The method for obtaining such an upper limit has been described in Chapter 9. The limit is obtained here by first assuming that a search for periodicity is made across the range $P_X - \Delta P_I \leq P \leq P_X + \Delta P_I$ which, allowing a factor of 3 for oversampling, would effectively introduce 6 independent trials. The value of chance probability then required is:

$$Pr\ (\chi^2 \geq {}_{2N}\chi^2) \approx 5 \times 10^{-4} \qquad (2)$$

where N = 33 is the total number of nights during which 47 Tucanae was observed from Narrabri. Let the flux of γ-rays arriving at the top of the atmosphere be R % of the cosmic ray background. The γ-ray flux is assumed here to be steady throughout the full observing period. From Chapter 9:

$$R = \left[\frac{1}{2}^{2N} \chi^2 \left(\sum_{i=1}^{N} n_i \right)^{-1} \right]^{1/2} \qquad (3)$$

where n_i is the number of Cerenkov arrival times constituting the i^{th} time series. Equations 2 and 3 provide R = 1.81 % using the full 47 Tucanae database. The cosmic ray flux detected by the Mark III telescope at the zenith angles 40° to 50° is estimated to be $\approx 3 \times 10^{-9}$ cm^{-2} s^{-1} (E > 0.4 TeV). The 3σ upper limit on the time-averaged flux of pulsed γ-rays is therefore 5.4×10^{-11} cm^{-2} s^{-1} (E > 0.4 TeV). With 47 Tucanae at a distance d $\approx$ 4.6 kpc, this converts to a luminosity of γ-rays pulsed at the X-ray pulse period of X0021.8-7221 $\approx 7 \times 10^{34}$ ergs s^{-1} (E > 0.4 TeV) using all observations of 47 Tucanae made from Narrabri in the interval 1988 July to 1990 September. This value is estimated to be correct to within one order of magnitude and assumes a differential spectral index equal to the cosmic ray proton index of -2.6, together with isotropic emission and no attenuation of γ-ray flux.

Recall that the time-averaged luminosity reported by the Potchefstroom Group for the interval 1989 July - October was $\approx$ 2 x 10^{35} ergs s^{-1} (E > 2.8 TeV) using the same value of spectral slope. Extrapolated to the threshold γ-ray energy of the Mark III telescope this would predict an observed luminosity 2 x $(2.8/0.4)^{0.6}$ x $10^{35} \approx 6 \times 10^{35}$ ergs s^{-1}, or a factor of ~ 9 higher than the upper limit determined here from the Narrabri observations. This discrepancy does not indicate a flattening of the γ-ray spectrum at these energies: similar differences between γ-ray flux measurements reported by the Durham and Potchefstroom Groups have been noted and discussed before by Chadwick *et al.* (1988) and Turver (1990a) in connection with observations of SN1987a and Vela X-1 and may be due to different methods of estimating the effective collecting areas achieved by the two experiments.

Observations of the 47 Tucanae globular cluster from Narrabri are a regular component of the Durham Group observing programme so that measurements can be made of three millisecond radio pulsars (Manchester *et al.* 1990 and references therein). It will be of interest to routinely test the new data for periodicity at a pulse period of two minutes and either find support for the Potchefstroom claim or reduce the upper limit on the average luminosity of pulsed TeV γ-rays.

10.3 GX 1+4

10.3.1 Introduction

GX 1+4 is a low-mass X-ray binary located close to the Galactic centre. There have been no published reports of TeV γ-ray emission from this binary. GX 1+4 was first identified by Lewin, Ricker and McClintock (1971) following observations with a high energy X-ray balloon-borne detector flown from Australia on 1970 October 16. Variability in the X-ray flux was observed on a timescale of minutes and a period of approximately 140 s was proposed.

Davidsen, Malina and Bowyer (1977) performed spectrophotometry of an optical counterpart first suggested by Glass and Feast (1973) and discovered that GX 1+4 is an unusual X-ray binary. The classification of the optical component is M6 III (red giant). The optical spectrum is that of a symbiotic star, i.e. one which displays both low-temperature absorption lines and high-excitation emission features. The strengths of the emission lines indicate the existence of a cocoon of gas around the binary system, with a radius ~ 2×10^3 lt-sec and a number density ~ 10^9 cm^{-3}. Column densities along a line-of-sight through this cocoon to the potential neutron star TeV γ-ray emission site would then be ~ 0.06 g cm^{-2}, or ~ 0.1 % of the radiation length of TeV γ-rays in matter. The cocoon is therefore essentially transparent at the energies of interest here.

The radius of the red giant is approximately 400 lt-sec. If the gas is modelled as a spherically symmetric wind originating at the red giant then, for an assumed velocity of ~ 10 km s^{-1} (which is typical of stars of this class), the above figures suggest a mass-loss rate ~ 10^{-6} $M_{\odot}$ yr^{-1}. This is sufficient to power an X-ray source via accretion by a neutron star companion (Chapter 5).

10.3.2 X-Ray Pulse Period History

Measurements of the X-ray pulse period are plotted against epoch of observation in Figure 10.2, which is taken from Gilfanov *et al.* (1989). Until 1980, the pulsar in GX 1+4 was spinning up at the very high rate of $\approx 8 \times 10^{-8}$ s s^{-1}. The spin-up timescale ($P/\dot{P}$) was just 40 yrs, one of the shortest observed so far. GX 1+4 was a bright X-ray source at this time and had a luminosity L_X ~ 10^{37} to 10^{38} ergs s^{-1}. However, *EXOSAT* observations in 1983 recorded a flux $\leq 1/25$ of that detected previously and subsequent observations showed that the X-ray luminosity had fallen further to $\leq 10^{36}$ ergs s^{-1}. The X-ray source had entered an extended low-state, although the hard X-ray flux may have remained approximately constant. See Makishima *et al.* (1988) and references therein. A period of extremely rapid pulsar spin-down during the X-ray low-state is indicated by the results of a low-energy γ-ray (E ~ 342 keV) balloon-borne experiment flown in 1982 (Jayanthi, Jablonski and Braga 1987). Compared with a period of 109.7 s measured using 1-50 keV X-ray

Figure 10.2

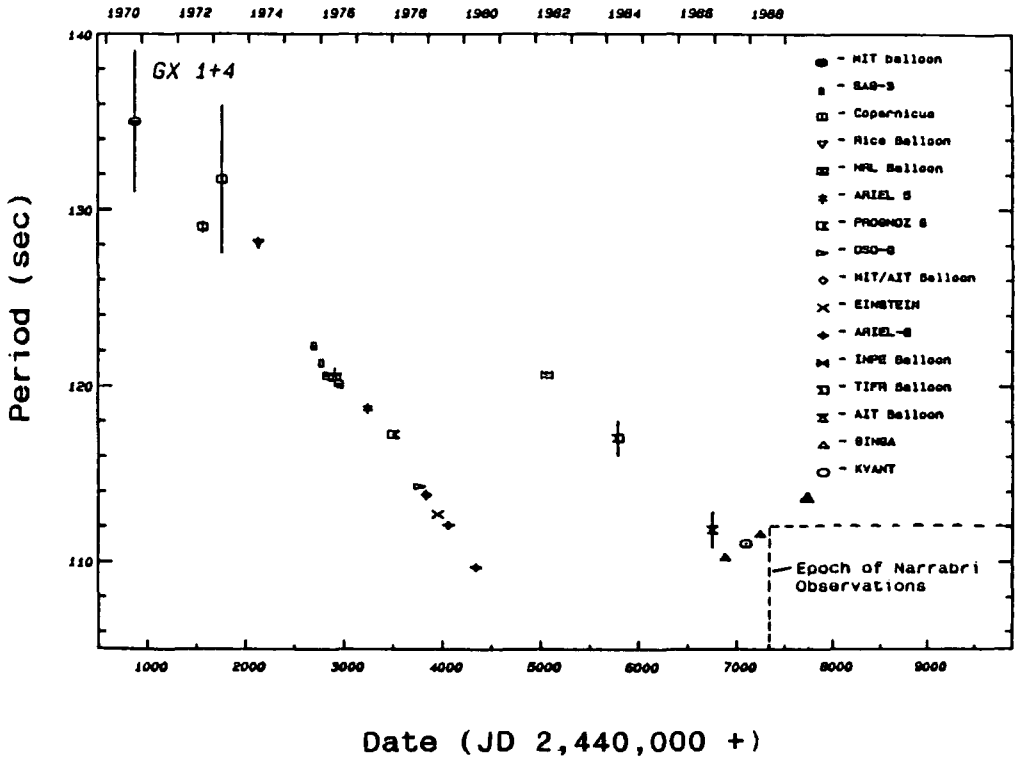

GX 1+4: X-Ray Pulse Period History

(From Gilfanov *et al.* 1989)

data obtained with *Ariel* 6 in 1980 (Ricketts *et al.* 1982), the period had increased by almost 11 seconds. The implied average period derivative at this time was therefore $\approx +2 \times 10^{-7}$ s s^{-1}. This was apparently followed by a further episode of spin-up lasting until 1987. Recent X-ray measurements with *Ginga* (Nagase 1989) and *Mir-Kvant* (Gilfanov *et al.* 1989) show that GX 1+4 is currently spinning down once again at an average rate of approximately 4×10^{-8} s s^{-1}.

On the basis of the X-ray pulse period history, McClintock and Leventhal (1989) have made a tentative identification of GX 1+4 with an intense 511-keV electron-positron annihilation line source detected during the 1970s in the direction of the Galactic centre. The γ-ray source was not detected during the early 1980s and apparently remained in a low state until at least 1984. Leventhal *et al.* (1989) detected 511 keV line flux with a balloon-borne experiment in 1988 May and again in 1988 October. The source had therefore re-emerged at some time between 1984 and 1988. Identification with GX 1+4 is suggested on the grounds of the similarity of the long-term X-ray and LE γ-ray behaviour and the unusual nature of the GX 1+4 binary. No LE γ-ray pulsations at $\approx$ 2 minutes have been reported.

10.3.3 Orbital Elements

None of the parameters of the GX 1+4 binary orbit have been determined. Cutler, Dennis and Dolan (1986) have constructed an

elliptical binary orbit model for the system and supply a set of estimates of the values of the orbital elements. Of particular interest is their analysis of short-term variations in the rate of spin-up of the of the X-ray pulsar during the 1970s. Evidence is found for regular enhancements in the spin-up rate, with consecutive episodes of increased spin-up separated in time by approximately 300 days. The authors do not give the errors on this period but it is noted here that the FWHM of the episodes of increased X-ray $\dot{P}$ considered by Cutler, Dennis and Dolan is around three months. The following ephemeris is provided for the occurrence of such episodes:

$$T = JD\ 2,441,574.5 \pm 304n$$

where n is any integer. They propose that the neutron star is in an eccentric orbit ($e \approx 0.25$) with a period of 304 days and suggest that the enhanced spin-up is the direct result of an increase in the rate of accretion by the X-ray pulsar around the time of periastron. They also speculate that a gradual long-term increase which was observed in the magnitude of the pulse period derivative during the high spin-up phase of the 1970s may have been due to an increase in the mass accretion rate caused either by expansion of the red giant primary star, or by an increase in the time spent by the neutron star in the periastron region of the orbit as the latter was being circularized by tidal friction.

If the mass of the red giant is taken as $M \approx 1.5\ M_{\odot}$, then the semimajor axis of a binary orbit of period T = 304 days is approximately 600 lt-sec; this is 50 % larger than the 400 lt-sec radius suggested for the red giant component by Davidsen, Malina and Bowyer (1977), but is well within the ~ 2000 lt-sec radius of the cocoon of gas noted earlier.

10.3.4 The Narrabri GX 1+4 Database

GX 1+4 was monitored from Narrabri for a total of 31.3 hours during 5 nights between 1988 July 9 to 18. The Mark III telescope was operated in the tracking mode at all times. The Narrabri telescope site is well located for observations of the Galactic centre and the X-ray binary passes within 6° of the zenith at culmination. Table 10.2 provides details of each of the observations.

10.3.5 Analysis of the GX 1+4 Database

The epoch of the Narrabri observations is indicated on the X-ray pulse period history in Figure 10.2. Interpolation predicts a contemporary value of P_X of approximately 112 s.

A semi-major axis of 600 ls and an orbital period of 304 d implies a typical neutron star orbital speed v ~ 40 km s^{-1}. If ΔP_I is the spacing between independent candidate values of γ-ray pulse period for a time series of duration T then the maximum

Table 10.2

DATE	DURATION (hr)	NUMBER OF EVENTS	TIME (UT)	ZENITH ANGLES	CHANNELS OPERATING
090788	5.2	11598	08:50-14:00	56^{o}-05^{o}	1234567
110788	7.2	13313	08:46-16:00		1234000
120788	7.2	9888	08:49-16:00		1234000
130788	7.0	11960	08:36-15:36		1234000
180788	4.7	9805	11:20-16:00		1234000

GX 1+4: Narrabri Observing Log

Total nights	5
Total hours	31.3
Total events	56,564

fractional Doppler shift would be $P_o v/c\Delta P_I = vT/cP_o \approx 40x7.2x60^2/3x10^5x112 \approx 3$ % for an orbit inclined at an angle of 90°. Therefore if the values of the orbital elements suggested by Cutler, Dennis and Dolan (1986) are close to the truth, then an inability to transform Cerenkov arrival times to the binary rest frame is not of any consequence to a search for pulse periodicity.

The pulsar spin-down rate of $\approx 4 \times 10^{-8}$ s s^{-1} implied by the contemporary X-ray measurements would change the X-ray pulse period by approximately 0.03 s over the course of the 9-day observing sequence at Narrabri. This is approximately 6 % of the spacing between independent candidate periods therefore the value of the contemporary X-ray pulse period has been assumed to be constant when analysing the database.

Each of the 5 time series have been tested for periodicity using the Rayleigh test. As for the analysis of the 47 Tucanae database described earlier, the chance probabilities observed at each candidate value of period were combined (equation 1): the results are shown in Figure 10.3. No evidence is found for pulse periodicity. Separate analyses of the individual time series also yielded null results.

Figure 10.3

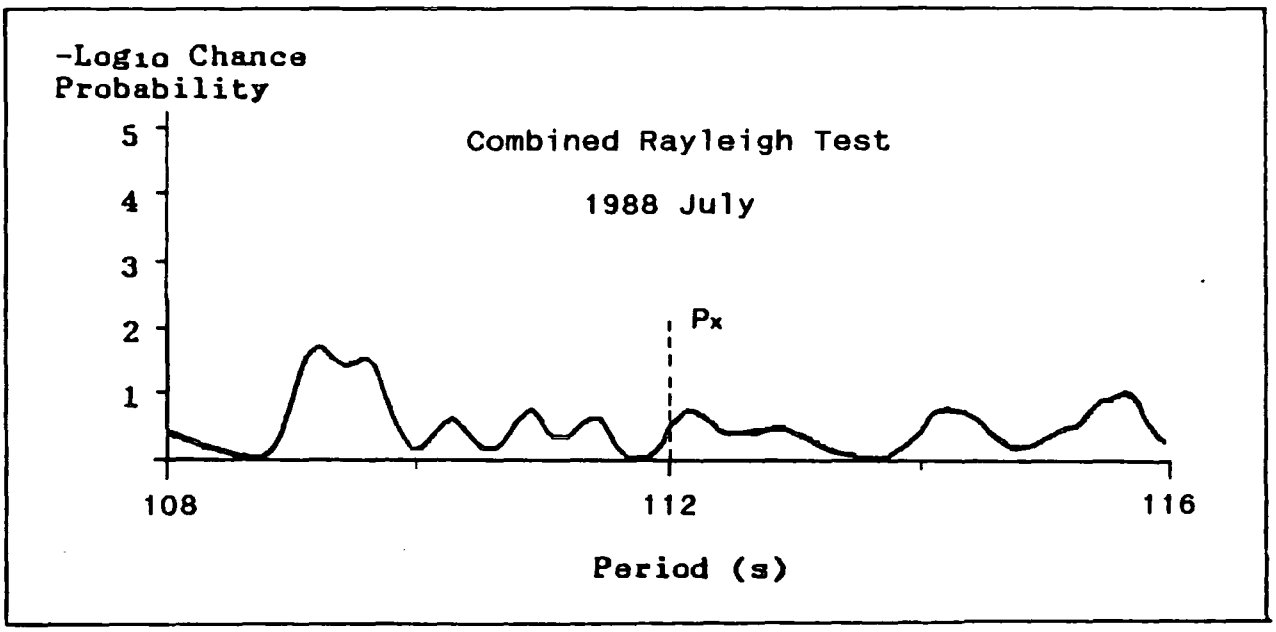

GX 1+4: Period Analysis of Narrabri Data

10.3.6 Discussion

A 3σ upper limit on the luminosity of γ-ray emission from GX 1+4 pulsed at the X-ray pulse period is computed using the method described in section 10.2.5 and is defined as that which would have led to a combined chance probability $Pr(\chi^2 \geq {}_{10}\chi^2) \approx 5 \times 10^{-4}$. The total number of Cerenkov arrival times is 56,564, for which the required pulsed signal strength (equation 3) would be R = 1.67 % of the cosmic ray background. The cosmic ray flux detected by the Mark III telescope at the zenith is $\approx 6 \times 10^{-9}$ cm^{-2} s^{-1}, at which the threshold γ-ray energy is estimated to be 0.25 TeV. The upper limit on the flux of pulsed γ-rays is therefore 1.0×10^{-10} cm^{-2} s^{-1}. This is converted to an upper limit to the time-averaged pulsed γ-ray luminosity of approximately 4×10^{35} ergs s^{-1} ($E > 0.25$ TeV) assuming a differential spectral index of -2.6 and a distance of 10 kpc to GX 1+4. This is estimated to be correct to within a factor of 10. (The Potchefstroom Group (Raubenheimer *et al.* 1988) have published a 3σ upper limit of 7.7×10^{-11} cm^{-2} s^{-1} ($E > 1$ TeV) to the pulsed γ-ray flux from GX 1+4. Using the same values of spectral index and distance to the binary, this implies an upper limit to the luminosity of $\sim 1 \times 10^{36}$ ergs s^{-1} ($E > 1$ TeV). Extrapolation of this limit to the zenithal threshold energy of the Mark III telescope predicts a value $\sim 10^{36} \times (1/0.25)^{0.6} \approx 2 \times 10^{36}$ ergs s^{-1}, which is within the bounds of the uncertainty on the upper limit derived using the Narrabri GX 1+4 data)

It is interesting to compute the phase of the Narrabri observations according to the ephemeris of enhanced rate of spin-up presented by Cutler, Dennis and Dolan (1986). The central date of the Narrabri observations was at JD 2,447,356.5, or 19.02 cycles relative to the ephemeris. A phase of 0.02 corresponds to just 6 days of the 304-day period, or approximately 10 % of the width of the episodes of increased spin-up. Although large rates of spin-down have been observed at X-ray energies since Cutler, Dennis and Dolan proposed this ephemeris, it might still be expected that the epochs of periastron passage (which were taken to correspond to the earlier episodes of increased spin-up) would remain as occasions when the accretion rate at the neutron star will be relatively high and, perhaps, when the rate of TeV γ-ray emission might be greatest. The fact that no evidence has been found for emission under such potentially favourable circumstances indicates that GX 1+4 may be only a very weak TeV γ-ray source for much of the time, if it emits γ-rays at all.

The positive detections of binary systems at TeV energies indicate that they may typically be transient sources of observable γ-ray emission. See also Chapter 11. Confirmed transient γ-ray binary sources identified to date are Centaurus X-3 (Carraminana *et al.* 1989b, North *et al.* 1989, Brazier *et al.* 1989b, 1990a), 4U0115+63 (Brazier *et al.* 1989c, 1990d), Hercules X-1 (Brazier *et al.* 1989c, 1990d), and Cygnus X-3 (Brazier *et al.* 1990c). It would therefore be premature to discourage further observations of GX 1+4 with the Mark III telescope when it is remembered that they currently number only 5 with a total of 31

hours. Further measurements are also encouraged by the unusual nature of the GX 1+4 binary and the unique period history of the pulsar, if only to reduce the upper limit on the source luminosity at TeV energies. However, they should probably be postponed so long as new or more hopeful source candidates compete for observing time during the Southern Hemisphere winter.

Chapter 11

TeV γ-Ray Emission Sites in X-Ray Binary Systems

11.1 Introduction

In Chapter 1 it was noted that all contemporary models of high energy γ-ray production in X-ray binary systems invoke the acceleration of charged particles (nuclei, e^-, and e^+) to ultrahigh energies, followed by the emission of photons via one or more of five processes. These are the electromagnetic decay of neutral pions produced by collisions of ultrarelativistic nucleons (the most commonly suggested mechanism), bremsstrahlung radiation, inverse Compton scattering, synchrotron radiation, and curvature radiation. Four particle acceleration mechanisms have been studied to date: (1) the dynamo mechanism, which utilises large-scale electric fields generated by the rotation of a neutron star magnetosphere; (2) shock acceleration, in which particles are scattered by magnetic irregularities back and forth across shock fronts and gain some energy during each traversal; (3) magnetic reconnection, where acceleration is provided by electric potential drops induced by the transient reconnection of magnetic field lines brought together by a plasma flow; (4) plasma turbulence: if a magnetic field is present in a turbulent plasma, then the turbulent motion can lead to randomly oriented

induced electric fields. Particles may then be accelerated across the potential drops.

Whatever is the nature of the particle acceleration it must, in order to explain the high-energy γ-ray detections described earlier in Chapter 6, be capable of depositing ultrahigh energy particles into environments where the local magnetic field strength is low enough so that substantial losses of γ-rays to electron-positron pair production can be avoided. Neutron star surface field strengths up to values $\sim 10^{12}$ G have been measured for X-ray sources in binary systems (Nagase 1989 and references therein): a photon energy threshold of 1 TeV for pair production in such a field occurs at distances as great as $\sim$ 100 neutron star radii (Chapter 1), which is comparable with the Alfven radius for an X-ray source radiating close to the Eddington limit (Chapter 5). In order that the γ-rays will be observable, it is also required that the column densities within the ambient plasma should be no greater than a few pair production radiation lengths ($\approx$ 40 g cm^{-2} at TeV γ-ray energies). The most popular high-energy γ-ray production mechanism is via the interaction of particle beams with material in the environment of the neutron star or at the limb of the companion, and the subsequent decay of neutral pions. This mechanism can therefore automatically avoid the problem of pair production in the intense fields close to the X-ray pulsar. (In the case of the isolated pulsar sources, high-energy photons are thought to be emitted either by inverse Compton scattering or curvature radiation. See for example Usov (1983), Cheng, Ho and Ruderman (1986a,b) and Cohen and Mustafa

(1987)). Keeping the foregoing upper bound on column density in mind, a lower bound is set by the requirement that a significant fraction of incident particles are involved in collisions; e.g. the TeV proton radiation length is ~ 80 g cm^{-2}. High-energy particle collision models have been considered for the γ-rays from Cygnus X-3 by Vestrand and Eichler (1982), Protheroe (1984), Hillas (1984), Eichler and Vestrand (1984), Chanmugam and Brecher (1985), Kazanas and Ellison (1986), Protheroe and Stanev (1987), Stanev (1987), Katz and Smith (1988), Hillas and Johnson (1990), and Mitra (1990). For explanations of the claims for high-energy γ-ray emission from other binaries such as Hercules X-1 and Vela X-1, see Eichler and Vestrand (1985), Gorham and Learned (1986), Kiraly and Meszaros (1988), Cheng and Ruderman (1989, 1990a,b), and Cheng *et al.* (1990).

The present chapter is concerned with the sites of the high-energy γ-ray emission in the X-ray binaries. Constraints on models which are imposed by the results of the observations are examined. Section 11.2 provides a summary of the observed characteristics of the high energy γ-ray emission, which include luminosity, sensitivity to orbital phase, and long-term behaviour. Indirect evidence for the interaction of ultrahigh energy particles with material that is far removed from the neutron star (so-called "beam-dumping") is found from observations of approximately one half of the binary systems detected to date. Section 11.3 considers beam-dumping in various target media: accretion disks, accretion disk bulges,

accretion wakes, and the limbs of the companion stars. Gorham and Learned (1986) considered the latter target medium in relation to a detection of TeV γ-rays from Hercules X-1 during X-ray eclipse and suggested the possibility of the steering of charged particle beams in the magnetosphere of the companion. This model is adapted in the present work in order to investigate the narrow Centaurus X-3 TeV γ-ray orbital light curve in terms of high-energy particle collisions in an accretion wake. The model is also applied to Vela X-1 to explore claims by North *et al.* (1987) and Raubenheimer *et al.* (1989) that bursts of γ-ray emission have been observed which arise from beam-dumping onto the limb of the supergiant companion star. Section 11.4 briefly considers the possible demands on particle energy and source geometry for γ-ray emission at the limbs of the primary stars in SMC X-1, Cen X-3 and LMC X-4.

11.2 Observed Characteristics of TeV γ-Ray Emission from X-ray Binaries

Table 11.1 lists the results of the observations of the nine X-ray binary systems which have led to claims for the positive detection of TeV γ-rays. The table is divided according to the three main classes of X-ray binary. Quantities tabulated are the reported peak and time-averaged TeV γ-ray luminosity, the ratio of the average γ-ray luminosity to the average X-ray luminosity, the γ-ray pulse period (where observed), the sensitivity to orbital phase (if any) and, where appropriate, the long-term

NAME	BINARY CLASS	PEAK L_γ ergs s^{-1}	$\langle L_\gamma \rangle$ ergs s^{-1}	$\langle L_\gamma \rangle / \langle L_x \rangle$	P sec	ORBITAL PHASE SENSITIVITY	TEMPORAL BEHAVIOUR	REMARKS
Cen X-3	SXRB	$\sim 6\times10^{36}$ (D)	$\sim 4\times10^{36}$ (P)	$\sim$ 5 %	4.82	0.77 to 0.82 (D) 0.70 to 0.81 (P)		Time-variable X-ray absorption dips known at phase 0.5 to 0.75. Confirmed source.
LMC X-4	" "	-	$\sim 2\times10^{37}$	$\sim$ 3 %	13.49	0.5 to 0.7	Modulated by 30.4d X-ray cycle ?	Unconfirmed source.
Vela X-1	" "	$\sim 2\times10^{35}$ (P)	$\sim 2\times10^{34}$ (P) $\sim 4\times10^{34}$ (D)	$\sim$ 1 %	283	Emission over broad range. Enhancements in & near X-ray eclipse (P).	Persistent TeV source.	Gamma-ray eclipse may be at most 0.96 - 0.06, or half duration of X-ray eclipse. Confirmed source.
4U0115+63	Be	-	$\sim 2\times10^{36}$	$\sim$ 10 %	3.61	No sensitivity to phase (D).		Confirmed source
1E2259+586	"	-	$\sim 5\times10^{35}$	$\sim$ 250 %	3.49 ($=P_x/2$)	-	Detected once during two sequences of observations one year apart.	Unconfirmed source.
Her X-1	LMXRB	$\sim 2\times10^{37}$ in outburst			1.24	Predominantly 0.6 to post entry into X-ray eclipse.	Often detected in bursts - 10^2-10^3 seconds.	All detections confined to the 2 high-states of 35d X-ray cycle. Evidence for blue-shifted pulse periods. Confirmed source.
Cyg X-3	" "	$\sim 10^{37}$ in outburst			0.0126	$\approx$10 min after X-ray maximum, or phase 0.625.	Witnessed in bursts $\approx$ 10 min.	Intensity can vary by factor of $\sim$ 10. Confirmed source.
Sco X-1	" "	-	$\sim 2\times10^{34}$ (D) $\sim 6\times10^{33}$ (P)	$\sim$ 0.01 %	-	Possible enhancement at 0.4 (D).	Persistent.	Confirmed source.
X0021.8-7221 (in 47 Tuc)	" "	$\sim 10^{36}$ (P)	$\sim 2\times10^{35}$ (P)	$\sim$ 1000 %	120.2	-	Two intervals of activity seen, each $\approx$ 5 days (P).	Source classification uncertain. Unconfirmed source.

(D) Durham (P) Potchefstroom

Table 11.1

Characteristics of TeV γ-Ray Emission from X-Ray Binaries

variation of γ-ray intensity.

Any attempt to identify a trend (e.g. correlations between luminosity, production geometry, temporal behaviour) is hampered by the small number of entries in Table 11.1. This is especially so when it is remembered that only six of the nine binaries (Cen X-3, Vela X-1, 4U0115+63, Her X-1, Cyg X-3, and Sco X-1) have been detected by more than one independent research group. However, some comments can be made. The possible relative importance of non-thermal emission processes to the overall energetics of the accretion flow can be gauged by comparing the γ-ray and X-ray luminosities for each binary. The ratio of $\langle L_{gamma} \rangle$ to $\langle L_X \rangle$ tends to be lower ($\sim$ 1 %) for the supergiant X-ray binaries. The low-mass binaries Her X-1 and Cygnus X-3 can exhibit luminosities from $\sim 10^{35}$ to $\sim 10^{37}$ ergs s^{-1} in outburst, the upper limits being comparable with their average X-ray luminosities. The Be binaries also show relatively high ratios of average γ-ray to X-ray luminosity: 1E2259+586 may even be brighter at γ-ray energies than it is in X-rays. Two of the low-mass binaries are particularly noteworthy: though both X0021.8-7221 and Sco X-1 have low average γ-ray powers and radiate at the 10^{34} to 10^{35} ergs s^{-1} level, their measured X-ray luminosities are very different. X0021.8-7221 is a weak X-ray source and is brighter at γ-ray energies by a factor $\sim$ 10. This may be due to obscuration of the pulsar by material which acts both as an efficient absorber of X-rays and a favourable target medium for high-energy particles. Sco X-1, in contrast, radiates

X-rays typically at the Eddington limit, whilst the observed γ-ray power is the lowest of all the binaries studied so far. Seven of the binaries listed in Table 11.1 show variation in high-energy γ-ray intensity due to orbital or X-ray cycle phase modulation (Cen X-3, Her X-1, Cyg X-3) and/or to possible intrinsic variability (4U0115+63, 1E2259+586, X0021.8-7221, Cen X-3, LMC X-4). Two of the three binary classes has an example of a γ-ray source which appears to be persistent: Vela X-1 (SXRB) and Sco X-1 (LMXRB).

11.3 Particle Beam-Dumping in X-Ray Binary Systems

11.3.1 Introduction

Evidence for orbital phase modulation of the intensity of the observable TeV γ-ray flux has been found for the high-mass binary Cen X-3 and, at a lower level of statistical significance, for LMC X-4. The γ-ray observations of the low-mass binaries Her X-1 and Cyg X-3 also display a dependence on orbital phase. Observations of TeV γ-rays during X-ray eclipse have been reported for Her X-1 and Vela X-1.

These results are examined in the context of the interaction of charged particle beams with the neutron star and companion star magnetospheres. The target material considered for the particle beams are, in turn, accretion disks, accretion disk bulges, accretion wakes, and the limbs of the companion stars.

11.3.2 Neutron Star Magnetic Steering Onto Accretion Disk

The acceleration of protons in the magnetosphere of an X-ray pulsar in a binary, followed by collisions and π^0-production in the accretion disk, has been suggested by Cheng and Ruderman (1989) to explain the ~ 10^2-10^3 s bursts of TeV γ-rays observed from Her X-1 and Vela X-1 (Dowthwaite *et al.* 1984c; Gorham *et al.* 1986; North *et al.* 1987; Lamb *et al.* 1988; Resvanis *et al.* 1988; Raubenheimer *et al.* 1989). (Without invoking magnetic steering, Eichler and Vestrand (1985) have considered the interaction of particles with the Her X-1 accretion disk following shock acceleration in the accretion flow near to the neutron star. Also, Slane and Fry (1989) have proposed the interaction of broad particle beams with target material removed from the disk by instabilities at the interface of the disk and the Her X-1 pulsar magnetosphere, which could also account for the anomalous γ-ray periodicities reported for this binary: e.g. Resvanis *et al.* 1988 and Lamb *et al.* 1988).

Proton/ion trajectories in the disk target model of Cheng and Ruderman are sketched in Figure 11.1. The particle accelerator model, which has been discussed in detail recently by Cheng and Ruderman (1990a,b), proposes that, when the accreting neutron star rotates more slowly than the inner edge of the accretion disk, a plasma void, or "gap", develops between those parts of the magnetosphere which co-rotate with the star and those which co-rotate with the disk. Charged particles are accelerated down a high electric potential drop across the gap and travel along

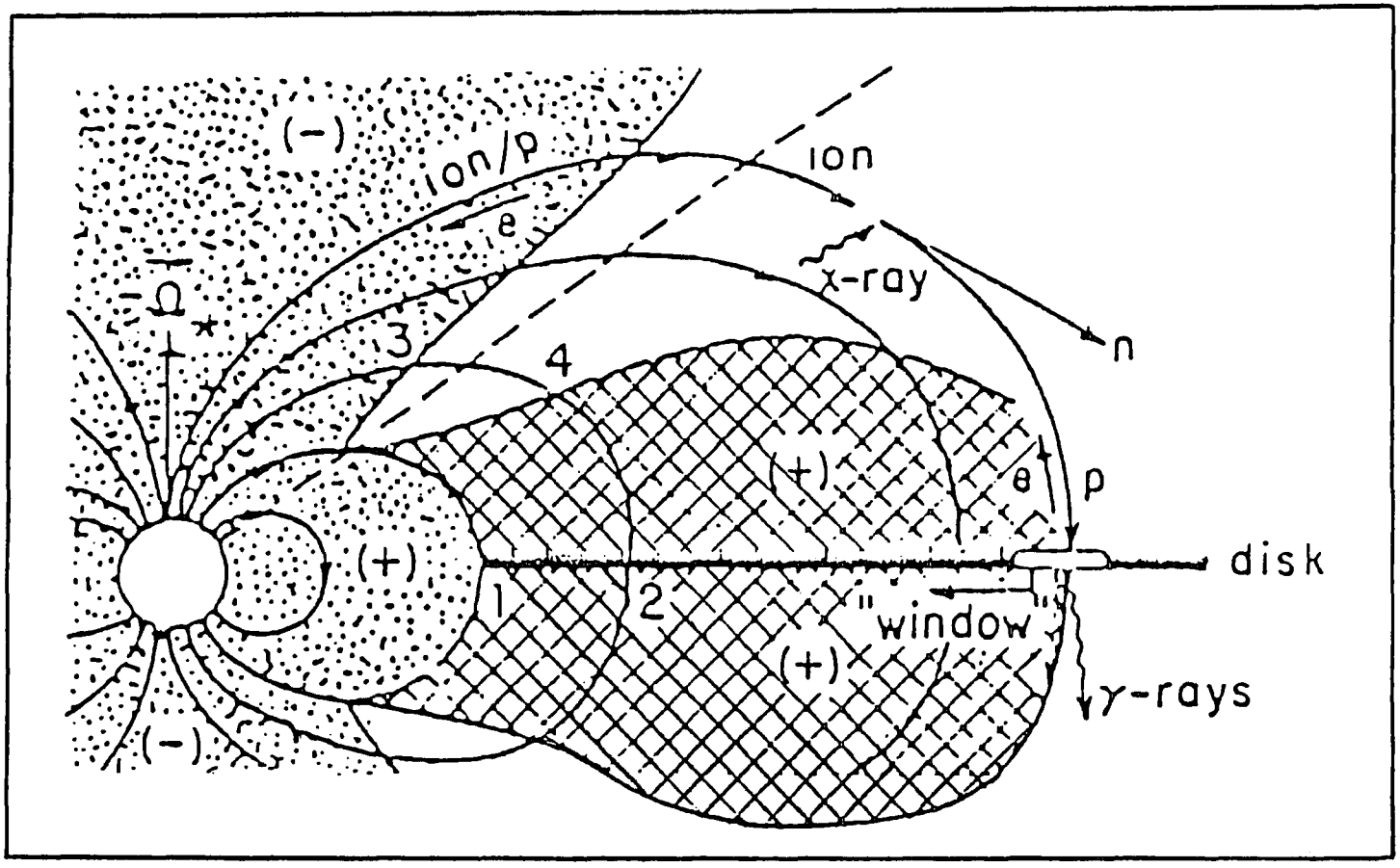

Figure 11.1

Proton/ion trajectories in pulsar magnetosphere according to gap accelerator/disk target model of TeV γ-ray emission at Her X-1 and Vela X-1. From Cheng and Ruderman (1989).

the field lines toward the disk. The trajectories of the particles upon exit from the accelerator site are considered briefly here.

Consider the neutron star magnetosphere and the accretion disk as shown in Figure 11.1. When a proton enters the charge-free gap at point 3, for example, it is accelerated along a $\underline{B}$-field line to point 4 and passes into the disk at 2. If the disk is "thin" (column density $\sigma < 80$ g cm^{-2}) then the proton will emerge and will be reflected back along the same field line after encountering a second gap below the disk. The proton eventually loses all its energy to collisions during multiple disk traversals, after which it is conducted in towards the neutron star from 2 to 1 and along a field line to one of the magnetic poles. Using the observed Her X-1 X-ray luminosity, Cheng and Ruderman (1989) compute a time-averaged vertical disk column density $\sim 10^3$ g cm^{-2}, which is a factor of ~ 25 too high for the escape of π^o-decay γ-rays. The $\sim 10^2$-10^3-second bursts of TeV γ-ray emission from Her X-1 referred to above are accounted for in this model by the radial drift of lower density ($\sigma \sim 10^2$ g cm^{-2}) annular "windows" which, given the mass, radius and magnetic field strength of the neutron star, together with the observed X-ray power, would traverse the disk in a time which is comparable with the burst duration.

The model of Cheng and Ruderman (1989) for Her X-1 is strict because it predicts a narrow beam of high-energy γ-rays and demands that the line of sight should be approximately parallel

to the neutron star dipole axis during at least a fraction of the pulsar rotation period, if the beam is to be observed.

In the case of the wind-driven supergiant X-ray binary Vela X-1, the accretion disk density is computed by Cheng and Ruderman (1989) to be $< 10^2$ g cm^{-2}. Gamma-ray windows should therefore be common and may be multiple or perhaps even tend to permeate the entire disk. This could explain the observed persistence of TeV γ-ray emission from Vela X-1 (North *et al.* 1987; Carraminana *et al.* 1989a; Brazier *et al.* 1989b; Raubenheimer *et al.* 1989; Brazier *et al.* 1990i). In an interesting reversal of the conditions postulated for Her X-1, higher intensity bursts may occur when a region of enhanced density (but with σ still $< \sim 100$ g cm^{-2}) crosses the disk, thereby increasing the probability of π^o production. Such enhancements could be responsible for some of the relatively intense γ-ray bursts ($L/\langle L\rangle \approx 3$) lasting for two to four pulsar rotations (P_x = 283 s) reported by the Potchefstroom group (North *et al.* 1987 and Raubenheimer *et al.* 1989).

11.3.3 Particle Beam Trajectories in the Magnetic Fields of Companion Stars

a) Target Material: Accretion Flow Bulge

Protheroe and Stanev (1987) have modelled the observed Cygnus X-3 high-energy γ-ray orbital light curve. In contrast to the nearly sinusoidal flux modulation seen at X-ray energies (e.g.

Bonnet-Bidaud and van der Klis 1981) the TeV γ-ray light curve observed during the 1970s was composed of two extremely narrow peaks ($\Delta\varphi \approx 0.05$) near X-ray phases $\varphi \approx 0.2$ and 0.8 (e.g. Neshpor *et al.* 1979); during the 1980s, a single narrow peak was observed from $\varphi = 0.625$ to 0.655 (Dowthwaite *et al.* 1983, Brazier *et al.* 1990c). Cygnus X-3 is assumed by Protheroe and Stanev (1987) to be a close binary system of 4.8 hr orbital period consisting of a neutron star and either a main sequence dwarf (radius $R \approx 1.25$ ls; binary separation $a_x \approx 4.2$ ls) or a helium star ($R \approx 2.75$ ls; $a_x \approx 5.8$ ls). Following on from an explanation of the X-ray orbital light curve of X1822-377 by White and Holt (1982), Protheroe and Stanev postulate for Cygnus X-3 the existence of two bulges: a main bulge at the confluence of the accretion stream with the accretion disk about the neutron star, and a pre-bulge located upstream from the main bulge. It is postulated that protons accelerated near the neutron star are steered onto both bulges by a companion star dipole magnetic field with a surface strength $\sim 10^3$ G. High-energy γ-rays are then emitted by π^o decay. This model could account not only for the observed orbital phase modulation of the γ-ray flux, but also for the time-variability of the phase at which peak emission occurs: changes in the orientation of dipole fields in main sequence dwarfs have been observed on timescales $\sim$ 5-20 yr, similar to that observed for the Sun

b) Target Material: Accretion Wake

The supergiant eclipsing X-ray binary Centaurus X-3 comprises a 4.8-second X-ray pulsar in a 2.1-day circular orbit of radius ≈ 40 ls. Cen X-3 was discovered to be a source of pulsed TeV γ-rays by the Durham Group during observations made from Narrabri on 58 nights in the interval 1987 January to 1989 June (Carraminana *et al.* 1989b; Brazier *et al.* 1989b, 1990a). Though the observations were made over a broad sample of orbital phases, evidence for pulsed γ-ray emission is confined to the data recorded on eight nights (spread throughout the two-year observing interval) when the neutron star was near to the ascending node of the orbit (φ = 0.75). The Potchefstroom Group (North *et al.* 1989) have reported confirmation that Cen X-3 is a source of pulsed TeV γ-rays and find that observable emission is similarly restricted to the vicinity of the ascending node.

The plane of the binary is highly inclined to the plane of the sky ($i \approx 80^\circ$ to 85°), so that a regular modulation of the flux with the binary period at this orbital phase indicates strongly that the observed γ-rays originate in material which is trailing behind the neutron star as it revolves about its high-mass companion. The present author has investigated the possible implications of the orbital phase modulation of the Cen X-3 γ-ray flux. The simple model described below has also been summarised in a recent review by Turver (1990b).

Direct evidence for the presence of material trailing the neutron star was first discovered by Tuohy and Cruise (1975)

using X-ray measurements obtained with the *Copernicus* satellite. Absorption dips which were attributed to an accretion 'wake' were found in the X-ray orbital light curve after inferior conjunction of the neutron star (X-ray phase 0.5). Additional observations of absorption dips between phase 0.5 to 0.75 were reported by Pounds *et al.* (1975) shortly afterwards using X-ray observations by the *Ariel V* satellite. Pronounced variations in the peak X-ray intensity and the depth of the pre-eclipse dips were found from one binary cycle to the next. North *et al.* (1989) have calculated column densities within the wake using the measurements of Pounds *et al.* (1975) and find values ranging from ~ 5 g cm^{-2} up to a maximum ~ 100 g cm^{-2}, which is favourable for collisions of high-energy nucleons and the escape of π^{o}-decay γ-rays.

The Cen X-3 binary and the accretion disk are drawn to scale in the upper panel of Figure 11.2, where the parameters determined by Khruzina and Cherepashchuk (1986) have been used. The Durham Group (Carraminana *et al.* 1989b; Brazier *et al.* 1989b, 1990a) have found that γ-rays from Cen X-3 are observable from orbital phase φ = 0.77 to 0.82, during which time the neutron star travels approximately 3 ls in the plane of the field of view. This distance will be assumed to be the approximate scale-width of a portion of the accretion wake with column densities ~ 10^{2} g cm^{-2}, which sweeps across the line-of-sight as the neutron star moves through the phase band 0.77 to 0.82. It is postulated here that particles are accelerated to ultrahigh energies within

Figure 11.2

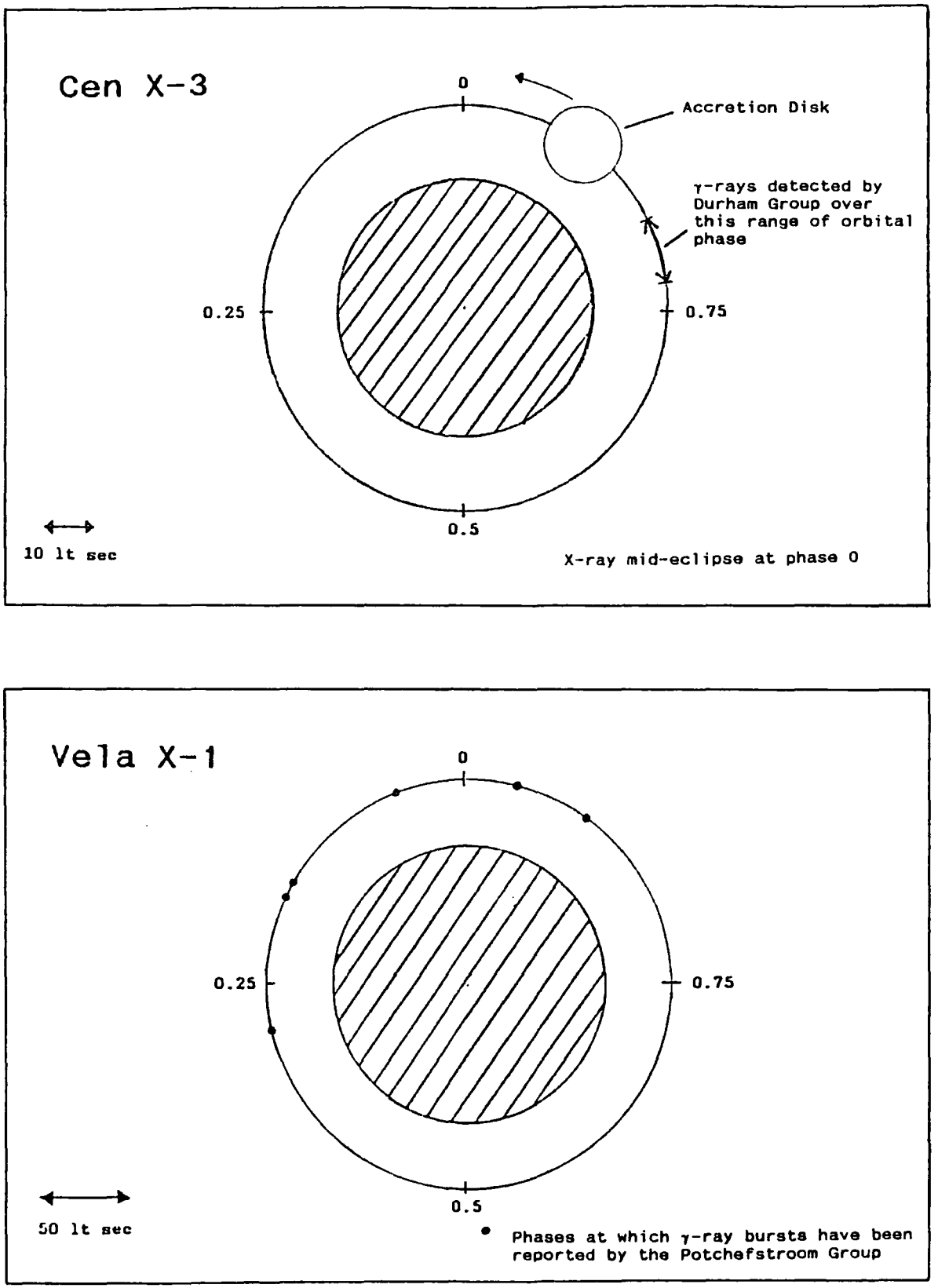

Cen X-3 & Vela X-1 Binary Systems

(Drawn to Scale)

the immediate vicinity of the neutron star and that a fraction of these are injected into the environment of the accretion disk and beyond. They would be required to travel a distance of at least ~ 10 ls (= accretion disk radius) from the neutron star before they could meet the wake material. If these particles are charged then their trajectories will be curved by the resultant magnetic field at this location. This is likely to be dominated by the field of the companion star, for the radius of the pulsar light cylinder is just $r = cP_x/2\pi \approx 0.8$ ls, beyond which any charged particles would be shielded from the magnetic field of the neutron star. Even if such shielding did not operate, the contribution of the pulsar field would probably be negligible at the outer edge of the accretion disk. Although the strength of the companion star magnetic field has not been measured, a rough estimate can be made: by conservation of magnetic flux, the field strength (B_*) at the surface of the supergiant progenitor (radius r_*) of a neutron star must be in the region of

$$B_* \approx B_N (r_N/r_*)^2 \sim 1 \text{ G} \qquad (1)$$

where the neutron star surface field strength has been taken as $B_N \sim 10^{12}$ G, and the neutron star and supergiant radii are assumed to be $r_N \approx 10^4$ m and $r_* \sim 40$ ls, respectively. This value of B_* is assumed to be appropriate for the magnetic field strength at the surface of the Cen X-3 primary star. Let P be the point where the accretion disc meets the accretion wake and

let this occur at distance r_{NP} ($\approx$ 10 ls) from the surface of the neutron star and distance r_{*P} from the companion's surface ($\approx a_x \sin i - r_*$; $r_* \approx$ 25 ls for the Cen X-3 primary). Then, if B_{*P} and B_{NP} are the field strengths at P due to the primary and neutron stars respectively, the constancy of the magnetic dipole moments gives

$$\frac{B_{*P}}{B_{NP}} \approx \frac{B_*}{B_N} \left[\frac{r_* . r_{NP}}{r_N . r_{*P}} \right]^3 \qquad (2)$$

so that

$$\frac{B_{*P}}{B_{NP}} \sim 10^5$$

The companion's magnetosphere therefore dominates the resultant field at the location of the accretion wake and will exert the prime influence on the motion of charged particles arriving there following acceleration near to the neutron star. The fact that the observed TeV γ-rays are modulated with the 4.8-second rotation period of the Cen X-3 pulsar may impose a constraint on this simple picture: the curving of particle trajectories would mean that the magnetic field is acting as a time-of-flight mass (energy) spectrometer. Pulse phase coherence of the γ-ray emission might therefore require a steep energy spectrum for particles arriving at the target medium. Shallower particle

spectra might lead to a correspondingly greater unpulsed component in the high-energy γ-ray flux.*

In order to test the feasibility of this scheme, charged particle trajectories near the Cen X-3 accretion wake have been computed. (The details of such computations will be provided later when the possibility of particle steering onto the limbs of companion stars is explored). Following the work of Protheroe and Stanev (1987), who considered proton beams at Cygnus X-3, the beam particles in the Centaurus X-3 system are also taken here to be protons. The magnetic field is assumed to be a single dipole through the centre of the companion star which is directed normally to the plane of the eclipsing binary. The target medium is represented in Figure 11.3 by a rectangular block of material (radial width $\approx$ 3 ls, as implied by the observations, and arbitrary length) which begins at a distance $\approx$ 10 ls from the neutron star (using the accretion disk radius given by Khruzina and Cherepashchuk, 1986) and which is directed almost tangentially to the orbit. The requirement is that protons have sufficient energies to traverse this distance with little deviation from a straight-line trajectory, in order that a) pulse phase coherence will be preserved b) collision-produced high-energy γ-rays may be observed in a direction which is

*Unfortunately the γ-ray fluxes from Cen X-3 observed by the Durham and Potchefstroom Groups at threshold energies of 0.25 and 1.9 TeV, respectively, cannot be compared easily since, as noted in Chapter 10, the two Groups differ in their methods of estimating effective collecting areas.

Figure 11.3

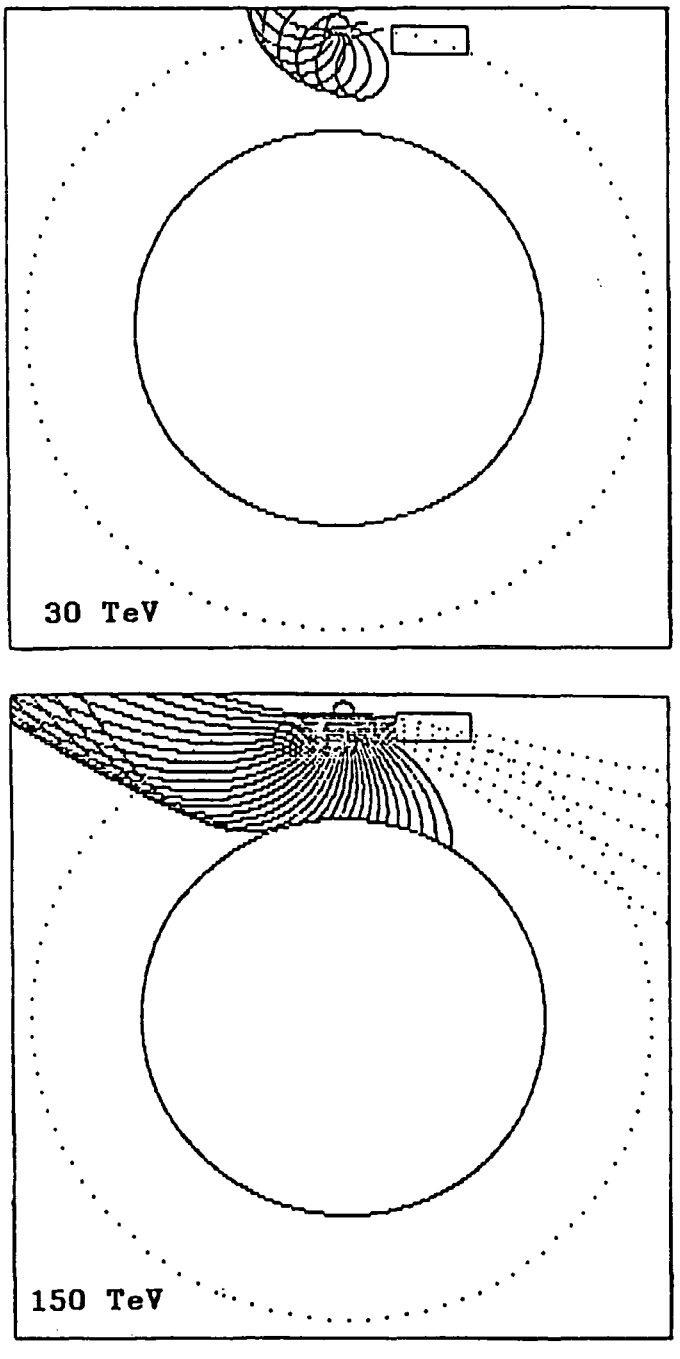

Proton Trajectories in the Cen X-3 Binary System

Solid circle: companion star
Dotted circle: pulsar orbit

Solid curves: proton trajectories
Dotted lines: γ-ray paths following proton collisions at accretion wake

Proton energies are indicated

$B_* = 1$ G
Dipole directed into page through centre of companion star

approximately along the axis of the sampled portion of the accretion wake. Examples of trajectories are shown in Figure 11.3 for proton energies of 30 and 150 TeV. The neutron star is represented near the top of each of the two panels and proton beams are shown emerging with successive 10° steps in the pulsar rotation. Given the simple assumptions on field strengths and source geometry made here, near straight-line trajectories would appear to be possible at proton energies $> \sim$ 150 TeV. This is encouraging for, with a proton-proton $\longrightarrow$ γ-ray conversion efficiency $\sim$ 10 % at TeV energies (e.g. Lang 1986), it implies that the threshold proton energy would be sufficiently low to permit the emission of γ-rays at energies within a factor $\sim$ 10 of those detected by the Durham and Potchefstroom Groups.

A lower limit on the lifetime of the beam target can be estimated using both the observed phase modulation of the TeV γ-ray flux and the typical Cen X-3 X-ray power. If the accretion wake is assumed to be approximately tubular, then the source geometry described above suggests that the cross-sectional area presented by the beam target is $A \sim \pi r_t^2$, where r_t ($\approx$ 3 ls) is the target scale-width. The mass of the target sampled is then $m_t \sim \sigma \pi r_t^2$. Cen X-3 radiates X-rays typically at the Eddington limit $L_x \sim 10^{38}$ ergs s^{-1} (e.g. White 1989). For an average mass neutron star ($M_N \approx 1.4\ M_\odot$) the corresponding Eddington upper limit on the mass accretion rate at the neutron star surface was shown in Chapter 5 (equation 6) to be $\dot{m} \sim 10^{-8}\ M_\odot\ yr^{-1}$. If *all* the beam target were to feed the X-ray pulsar at this rate then the lifetime would be $t \sim m_t/\dot{m} \sim$ 2 months. Since the target

probably represents just a small fraction of the mass transferred from the companion star, it is likely to be stable for times considerably longer than this. Though these calculations are clearly only very approximate, they are at least consistent with the fact that TeV γ-rays were detected from Cen X-3 during the majority of observations in the phase band 0.77 - 0.82 (8 nights in 12) over the two years in which the binary was monitored from Narrabri.

North *et al.* (1989) have suggested an alternative to proton bombardment of the Cen X-3 accretion wake and propose that high-energy neutrons might be the incident particles. (A similar scheme was suggested by Kazanas and Ellison (1986) for neutron bombardment of the companion star in Cygnus X-3). One advantage of this idea is that it makes no demands on the steepness of the particle energy spectrum in order to maintain phase coherence in the high-energy γ-ray emission. The gap accelerator/disk target model of Cheng and Ruderman (1989) was described earlier in relation to the production of π^0-decay γ-rays at the Her X-1 and Vela X-1 binaries. In addition to protons, nuclei accelerated to ultrahigh energies may also follow the field lines until they are photodisintegrated by the copious soft X-rays originating at the base of the accretion flow. (Such photons would have an energy $\sim$ 10 MeV in the nucleus rest frame). Using this model therefore, North *et al.* (1989) suggest that most or all of the protons would strike the Cen X-3 accretion disk, as proposed by Cheng and Ruderman (1989) for the accretion disk in Her X-1. Since, for

the case of Cen X-3, the vertical accretion disk column density is estimated by North *et al.* (1989) at $\sigma \sim 5 \times 10^3$ g cm^{-2}, high-energy γ-rays would be almost entirely absorbed. The neutron products of the photodisintegration, however, are no longer constrained to move along the pulsar field lines and are free to travel much further away from the neutron star and on into the accretion wake.

Consider now the giant X-ray binary LMC X-4. TeV γ-ray emission from this system was detected by the Durham Group during one of four observing sequences made over a large sample of orbital phases during the interval 1987 January to 1989 November (Brazier *et al.* 1990e). Although this detection remains to be confirmed, it is interesting that it was made when the neutron star was in the orbital phase range φ = 0.5 to 0.7. If this is again indicative of the presence of an accretion wake then it would imply that column densities which are suitable for the production of observable high-energy γ-rays might occupy a much broader angle in the wake than is proposed here for the case of Cen X-3.

c) <u>Target Material: Limb of the Companion Star</u>

Gorham *et al.* (1986) made a remarkable observation of Hercules X-1 on 1985 June 16 which provided a strong indication that ultrarelativistic charged particles emanating from an X-ray pulsar can be steered by the magnetosphere of a companion star.

Pulsed TeV γ-rays from Her X-1 were detected only after the time of the expected onset of X-ray eclipse (corresponding to orbital phase 0.93) and continued to be detected for approximately 70 minutes until the end of the 2-hr observation. During this time, the neutron star had passed through $\approx$ 20 % of the eclipse by the companion, HZ Her. Assuming solar corona column densities at the limb of HZ Her, Gorham *et al.* (1986) estimated that line-of-sight column densities would exceed ~ one hundred 1 TeV γ-ray pair production radiation lengths or ~ ten 10 TeV proton radiation lengths after just ~ 2 % of the eclipse time and therefore concluded that the X-ray and γ-ray emission sites were not co-located during most or all of the time of the observation.

This detection provides a rare opportunity to identify the site of high-energy γ-ray emission. A test of the sensitivity of period analysis of Cerenkov arrival time series to the transformation of times to the Her X-1 binary rest frame would offer, for a typical observation length $\approx$ 3 to 4 hr, a resolution in the value of the projected semi-major axis which at best is $\Delta a \approx 4$ ls ($\Delta a / a_x \sin i \approx 0.3$). Similarly, the value of the epoch of mid-eclipse can be determined only to within approximately 2 hr of the true value, which corresponds to some 20° in orbital phase.

Gorham and Learned (1986) have explored the geometry, magnetic field strengths and particle energies at the Her X-1 binary which might explain the emission of high-energy γ-rays during eclipse. (For interpretations of other TeV γ-ray

observations of Her X-1, see (i) Eichler and Vestrand (1985), who consider the interaction of shock-accelerated particle beams with the accretion disk; (ii) Kiraly and Meszaros (1988): ejection of jets of protons by radiation pressure along the pulsar magnetic axis, followed by shock acceleration in the accretion flow and γ-ray production from collisions in the shock itself and the accretion disk (iii) Slane and Fry (1989), who postulate collisions of proton beams with matter removed from the inner edge of the accretion disk by instabilities in the disk/magnetosphere interface; (iv) Cheng and Ruderman (1989), described earlier in Section 11.3.2).

The radius of the Her X-1 pulsar light cylinder is $r_c = cP_x/2\pi \approx 0.2$ ls. So, as for the simple model of Cen X-3 presented earlier, the resultant magnetic field over much of the region separating the pulsar and the companion star is dominated by the latter's magnetosphere. Gorham and Learned (1986) model the companion star field as a simple dipole through the centre of the star directed normally to the plane of the orbit. The present author has used the same technique to compute the trajectories of ultrahigh energy protons at Vela X-1, SMC X-1, Cen X-3 and LMC X-4 in order to quantify (to order of magnitude) the conditions that might be required for the observation of post-eclipse γ-ray emission at the limb of the companion.

The trajectory of a charged particle in such a field is easily computed. The Lorentz force ($\underline{F}$) on a particle of charge Ze travelling in a pure magnetic field $\underline{B}$ with velocity $\underline{v}$ in the

observer's rest frame is

$$\underline{F} = \frac{Ze}{c} \underline{v} \times \underline{B} \qquad (3)$$

where $|\underline{B}|$ is measured in units of Gauss. Since $|\underline{v}| \approx c$ here and since the velocity and magnetic field vectors are here orthogonal for particles travelling in the plane of the orbit,

$$F = \frac{mv^2}{r_L} \approx \frac{\gamma m_o c^2}{r_L} = ZeB(r) \qquad (4)$$

where r_L is the Larmor radius, m and m_o are the relativistic and rest masses of the particle, respectively, and B(r) is the field strength at distance r from the centre of the companion star. Thus if E is the total energy of the particle, the Larmor radius at r is just

$$r_L = E\,[ZeB(r)]^{-1} \qquad (5)$$

The dipole moment at r is $B(r)r^3 \approx B_* r_*^3$, where B_* is the field strength at the surface of the companion star and r_* is the stellar radius. So,

$$r_L = E\,[ZeB_*(r_*/r)^3]^{-1} \qquad (6)$$

which is just the instantaneous radius of curvature of the path of the particle. At the same time, the direction of travel is given simply by the Larmor radius unit vector:

$$\frac{\hat{r}_L}{} = \frac{\underline{v}(r) \times \underline{B}(r)}{|\underline{v}(r) \times \underline{B}(r)|} \qquad (7)$$

So, for a given particle energy and injection velocity vector at the vicinity of the neutron star, the subsequent trajectory in the companion star magnetosphere can be directly computed using equations 6 and 7.

1) Hercules X-1

The companion star (HZ Her) has a spectral type of A9 and a mass $M_* \approx 2.2\ M_o$. The magnetic field strength (B_*) is not known and is arbitrarily taken by Gorham and Learned (1986) to be a simple extrapolation from the solar field. (The trajectories computed for the charged particles can be applied to different field strengths by just keeping the value of E/B_* in equation 6 constant). If φ_x is the phase of X-ray eclipse egress (φ_x = 0.068), then the radius of the companion star is $r_* = (M_*/M_N)a_x \sin i . \sin\varphi_x \approx 9$ ls, where the average neutron star mass $M_N \approx 1.4\ M_o$ is assumed. Using the solar surface field (~ 1 G), the HZ Her surface field strength is therefore taken to be $B_* \approx B_o(r_o/r_*)^2 \sim 0.1$ G.

The trajectories of protons injected into the system by the Her X-1 pulsar are illustrated in Figure 11.4. Proton energies of 1, 5, 10, 15, 20 and 50 TeV have been used and, for clarity, particle beams are shown only after the neutron star has rotated through successive steps of 10°. The orbital plane of the Her X-1 binary is inclined at an angle ≈ 80° to the sky so that, for an orthogonal dipole field, the observer and the particle beams are here assumed to be in the same plane. The neutron star is shown at orbital phase 0 (mid-eclipse) in each of the panels of Figure 11.4. Below energies ~ 5 TeV, the protons execute multiple loops, whilst the trajectories approach straight lines for E > ~ 50 TeV. The suggestion that TeV γ-rays can arise as a result of magnetic steering onto the limb of HZ Her appears to provide a plausible model of the origin of the high energy γ-ray emission observed after X-ray eclipse ingress since, subject to the validity of the simplifying assumptions made, gently curved trajectories leading to the limb of the star can be achieved for protons which have sufficient energies (~ 10 TeV) to generate ~ 1 TeV π^0-decay γ-rays.

2) <u>Vela X-1</u>

The supergiant X-ray binary Vela X-1 ($P_x \approx 283$ s, $P_{orb} \approx 9$ d, $a_x \sin i \approx 113$ ls, $i \approx 80°$, $e \approx 0.09$) appears to be a persistent source of pulsed TeV γ-ray emission beyond episodes of X-ray eclipse (Brazier *et al.* 1989b, Carraminana *et al.* 1989a, Raubenheimer *et al.* 1989, Brazier *et al.* 1990i). In addition it

Figure 11.4

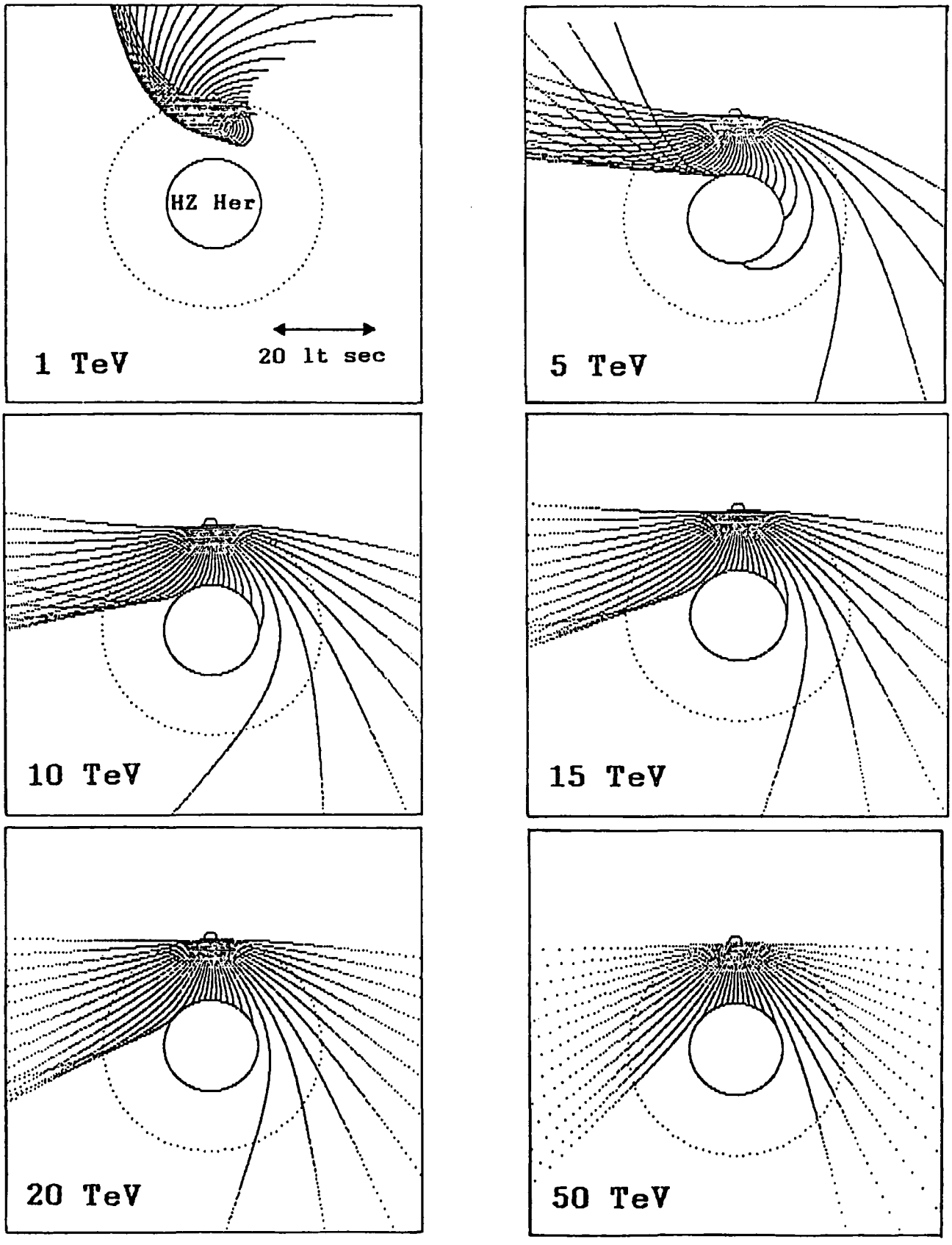

Proton Trajectories in the Her X-1 Binary System

Solid circle: companion star
Dotted circle: pulsar orbit
Pulsar at mid-eclipse

Curves: proton trajectories
Proton energies are indicated

$B_* = 0.1$ G
Dipole directed into page through
centre of companion star

has been claimed to be an occasional source of brief bursts (< ~ 20 minutes) of pulsed TeV γ-rays, some of which have occurred when the neutron star is eclipsed by the companion star. A total of six short-term enhancements in the pulsed high-energy γ-ray flux from Vela X-1 have been reported by the Potchefstroom Group. See North *et al.* (1987) and Raubenheimer *et al.* (1989). Vela X-1 was observed by the Durham Group during 34 nights between 1986 October and 1988 May (Carraminana *et al.* 1989a). No transitory enhancements in the γ-ray signal strength have been identified in the data obtained on any of these nights (P.J. Edwards, private communication). Periodic modulation of the flux during the bursts observed by the Potchefstroom Group is claimed to be in phase with the persistent pulsed γ-ray emission. Each of the enhancements lasted for between two and four pulsar rotations. See the lower panel of Figure 11.2, where the Vela X-1 binary is drawn to scale and the orbital phases of the γ-ray bursts are indicated. The first of these events was witnessed in 1986 and occurred at orbital phase 0.899, or four hours after the predicted time of X-ray eclipse ingress. The strength of this outburst was approximately eight times that of the persistent emission. The remaining five bursts were observed in 1987 and occurred at phases 0.96, 0.06, 0.17, 0.18 and 0.29, each at a level of $\approx$ 2 to 3 times the steady pulsed γ-ray emission. X-ray eclipse persists from orbital phase $\approx$ 0.88 to 0.12: the first two phases of the 1987 enhancements are therefore particularly interesting for they imply that the duration of γ-ray eclipse might sometimes be, at most, approximately half that of X-ray

eclipse. Following the conclusion drawn by Gorham *et al.* (1986) and Gorham and Learned (1986) from the observation of high-energy γ-rays from Her X-1 in eclipse, the narrow Vela X-1 TeV γ-ray eclipse is cited by Raubenheimer *et al.* (1989) as an indication that ultra-relativistic charged particle beams emitted at the Vela X-1 neutron star may be steered in the magnetic field of the supergiant companion.

The present author has examined this suggestion by computing the trajectories of protons in the Vela X-1 binary using the known geometry of the system (Boynton *et al.* 1986) and a reasonable value for the magnetic field strength at the surface of the companion star. Let the field strengths due to both stars balance at a distance r_{NP} from the neutron star surface and a distance r_{*P} from the surface of the companion. Using simple arguments, the companion star in the Cen X-3 high-mass binary was calculated earlier to have a surface magnetic field strength $B_* \sim 1$ G. This value will be adopted for the Vela X-1 companion star. From the X-ray eclipse geometry (orbital phase $\varphi = 0.12$ at egress), the radius of the supergiant must be $r_* \approx 75$ ls. Equation 2 then gives $r_{*P}/r_{NP} = (r_*/r_N)(B_*/B_N)^{1/3} \sim 230$ (with B_N, the neutron star surface field, assumed to be $\sim 10^{12}$ G, and the neutron star radius $r_N \sim 10^4$ m). If the barycentre of the binary is taken to be coincident with the centre of the supergiant, then $r_{NP} \approx (a_x \sin i - r_* - r_N)/230 \approx 0.2$ ls. So, from beyond less than one light-second from the neutron star, the path taken by a high-energy charged particle ejected from the neighbourhood of the pulsar will, according to the simple approximations made here, be

deviated principally by the companion star magnetosphere. The latter is again assumed to be a single dipole through the centre of the primary and directed normally to the highly inclined plane ($i \approx 80^{\circ}$) of the neutron star orbit.

Trajectories of protons computed for the Vela X-1 system are shown in Figure 11.5, where energies of 0.1, 0.3, 1 and 5 PeV have been used. Protons are found to perform multiple loops at energies $E_P < \sim 0.1$ PeV. The trajectories are almost linear at energies above ~ 5 PeV. Post-ingress emission of observable high-energy γ-rays following the mild curving of proton trajectories onto the limb of the primary star appears to be plausible only when $E_P \sim 1$ PeV. Assuming once again a proton-proton $\longrightarrow$ γ-ray conversion efficiency ~ 10 %, the π^{o}-decay γ-ray emission would therefore occur beyond a cut-off energy which is a factor ~ 10^2 higher than the threshold γ-ray energy (~ 1 TeV) of the air Cerenkov telescopes operated by the Potchefstroom Group. Is it feasible that some or all of the outburst γ-ray signal claimed by the Potchefstroom Group could be at such high energies ? Independent evidence indicating that particles may in fact be accelerated by the Vela X-1 pulsar up to energies of at least E ~ 30 PeV was reported by Protheroe, Clay and Gerhardy (1984). Measurements at a threshold γ-ray energy ~ 3 PeV were made with the Buckland Park (South Australia) air shower array during 1979-1981. Evidence at the ~ 10^{-4} chance probability level was found for an excess of showers in the direction of Vela X-1 which were modulated with the $\approx$ 9-day orbital period. All

Figure 11.5

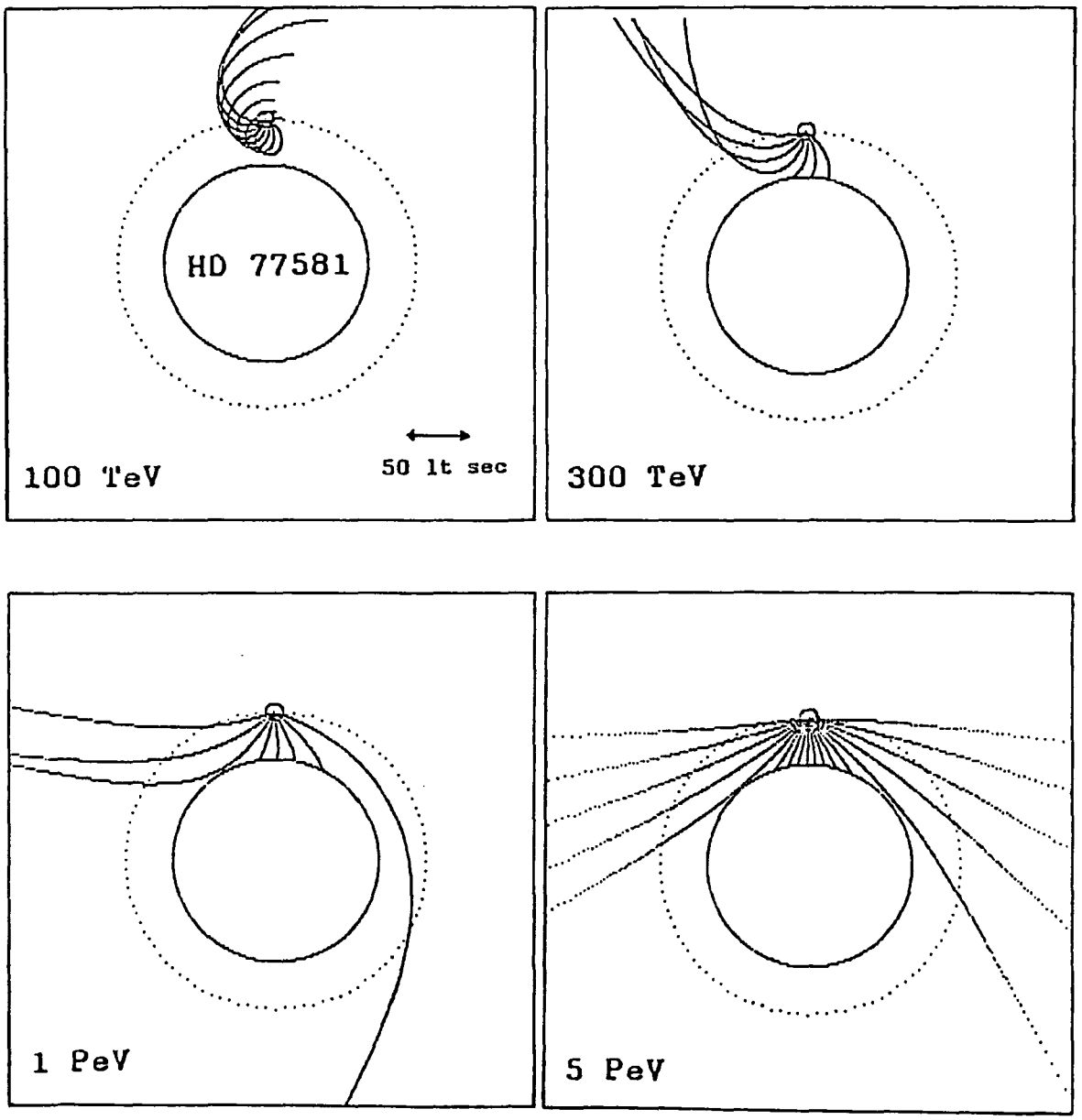

Proton Trajectories in Vela X-1 Binary System

Solid circle: companion star
Dotted circle: pulsar orbit
Pulsar at mid-eclipse

Curves: proton trajectories
Proton energies are indicated

$B_* = 1$ G
Dipole directed into page through
centre of companion star

the excess showers were observed when the neutron star was within a narrow orbital phase band ($\Delta\varphi \approx 2$ %) centred on phase 0.63, shortly after inferior conjunction. The estimated time-averaged luminosity was ~ 2.2×10^{34} ergs s^{-1} per decade of energy at 3 PeV. (The errors on this value were not given). Assuming an integral spectral index of -1.6, i.e. that of the cosmic ray spectrum, this converts to a luminosity of ~ 2.9×10^{34} ergs s^{-1} for $E > 3$ PeV. The value of the distance to Vela X-1 used by Protheroe, Clay and Gerhardy (1984) was 1.4 kpc whilst that used by the Potchefstroom Group (North *et al.* 1987) was 1.9 kpc: scaling up the luminosity accordingly suggests a value of ~ 5.3×10^{34} ergs s^{-1} ($E > 3$ PeV). The outbursts reported by the Potchefstroom Group at $E > 1.5$ TeV are claimed to be approximately 8 times stronger than the persistent Vela X-1 emission which, using their value of time-averaged luminosity ($(2.4 \pm 1.1) \times 10^{34}$ ergs s^{-1}), would imply an outburst luminosity at a level ~ 2×10^{35} ergs s^{-1}, or within a factor of 4 of the luminosity observed above 3 PeV. The PeV γ-ray measurements therefore suggest that the Vela X-1 binary may be capable of producing a) particles with energies at the level required by the present model to account for the Potchefstroom detections during eclipse b) fluxes of such particles which are roughly in agreement with the luminosities claimed by North *et al.* (1987). A direct prediction using the present model is that PeV γ-ray emission might also be observed by an air shower array during times when Vela X-1 is in X-ray eclipse.

It is therefore feasible that the Vela X-1 γ-ray eclipse could, as is claimed by Raubenheimer *et al.* (1989), be narrower than the X-ray eclipse. There could, in principle, be no high-energy γ-ray eclipse at all. Depending upon the energy spectrum of particles emanating from the pulsar there may be, at all phases near and during X-ray eclipse, a fraction of particles deposited at the limb of the companion which send a beam of γ-rays into the line-of-sight to the binary. The sign of the Lorentz force exerted by the magnetic field on the charged particles does not change as the neutron star moves through mid-eclipse so that there could be an asymmetry about $\varphi = 0$ in the emission detected at any given γ-ray threshold. This could provide information on the orientation of the companion star magnetosphere.

3) Other X-Ray Binaries

Figure 11.6 shows the typical proton energies that might be required in order to observe high-energy γ-rays from the limbs of the companion stars in the SMC X-1, Cen X-3 and LMC X-4 X-ray binaries during eclipse of the neutron star. Typical values of E_P lie in the range ~ 0.1 to 1 PeV.

Period analysis of the data from the SMC X-1 observations made at Narrabri reveal no evidence for pulsed high-energy γ-ray emission from this binary during X-ray eclipse, nor is there any indication of short-term bursts of pulsed or unpulsed emission.

Figure 11.6

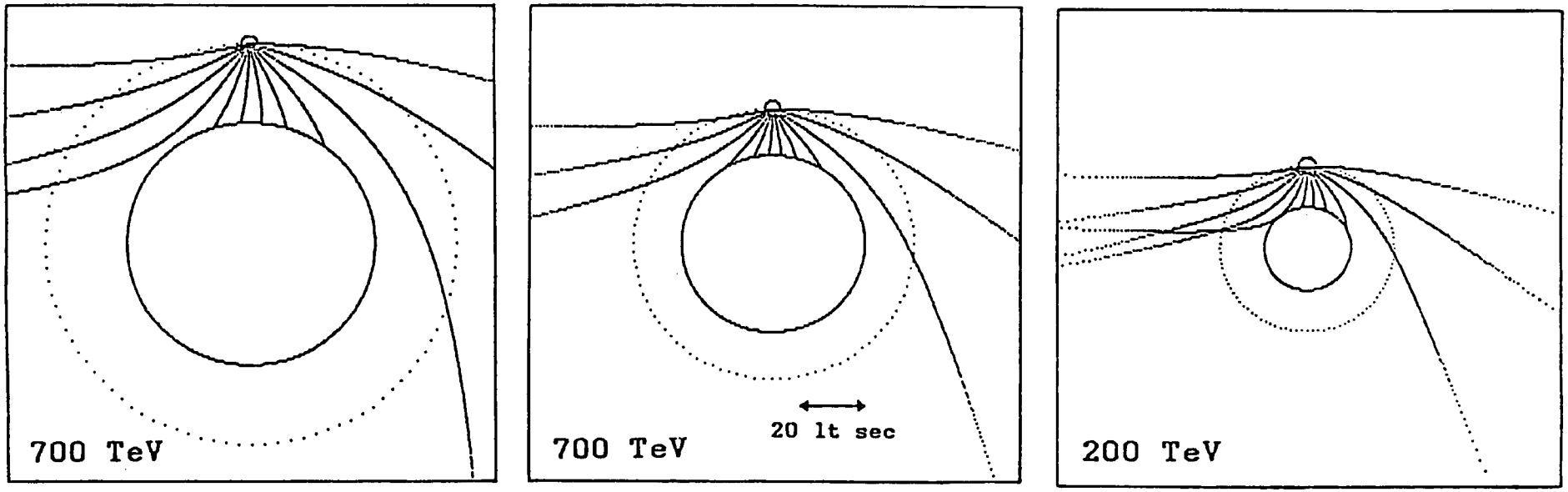

Proton Trajectories at SMC X-1, Cen X-3 & LMC X-4

Solid circle: companion star
Dotted circle: pulsar orbit
Pulsar at mid-eclipse

Curves: proton trajectories
Proton energies are indicated

$B_* = 1$ G
Dipole directed into page through centre of companion star

Each binary is drawn to same scale

Similarly, no reports have been made of the detection of TeV γ-rays from Cen X-3 and LMC X-4 during X-ray eclipse. PeV γ-rays were observed from LMC X-4 by Protheroe and Clay (1985). LMC X-4 is a high-mass binary which contains a 13.5-second X-ray pulsar in a circular orbit of period 1.41 d and $a_x \sin i$ 26 ls, inclined at $i \approx 70^\circ$. X-ray eclipse lasts from orbital phase $\varphi = 0.92$ to 0.08. Protheroe and Clay (1985) examined the orbital phase distribution of air showers observed in the direction of the binary using phase bins of width $\Delta\varphi = 0.05$. Evidence for an excess of events was confined to the 0.90-0.95 phase bin, which is consistent with the emission of γ-rays at the limb of the companion star as the X-ray source enters eclipse. LMC X-4 must therefore be a strong candidate for TeV γ-ray emission at similar orbital phases. The claims for the detection of TeV γ-rays from Hercules X-1 and Vela X-1 at eclipse ingress are encouraging: future observations of LMC X-4 from Narrabri at times of ingress and egress would be of great interest.

Chapter 12

Conclusion and Future Work

A new approach has been introduced for the period analysis of Cerenkov arrival time series obtained during observations of TeV γ-ray pulsar source candidates in binary systems. The aim of this new method goes beyond the testing of time series for modulation at the expected value of the pulsar period: a search is also made for information on the location of the putative site of pulsed γ-ray emission in the binary system.

For many of the source candidates in X-ray binaries, it is important that period analysis of the data is preceded by a transformation of the arrival times to the binary rest frame. Such transformations are made in order to eliminate the effect of Doppler shifting of the observed pulse period and it is this process which can provide the positional information. The Doppler corrections require a knowledge of the location of the emission site with respect to the centre-of-mass of the binary system at the time of the observation. For circular orbits, this position can be expressed simply in terms of the radius (= projected semi-major axis, or $a_x \sin i$) and orbital phase angle (≡ epoch of mid-eclipse). Both these quantities have finite ranges over which Doppler corrections are indistinguishable and a coherent periodic signal can be recovered. These ranges vary,

depending upon the parameters of the binary in question and the orbital phase at which it is observed. Beyond these limits, the signal will be smeared by Doppler shifting. Information on the location of a γ-ray source can therefore be obtained by:

1) specifying bounds on the range of possible γ-ray site locations, e.g. the full extent of an accretion disk in an X-ray binary system;

2) systematically exploring the sensitivity of the results of the period analysis to values of $a_x \sin i$ and epoch of mid-eclipse within the pre-specified limits.

The spatial resolution provided by this test is greatest for X-ray binaries with short pulsar periods, where the retention of γ-ray pulse phase coherence is more demanding of the Doppler corrections. SMC X-1 has one of the smallest known X-ray pulse periods and an orbital ephemeris which is very well measured at X-ray energies. Here the potential spatial resolution ($\Delta d < \sim 5$ lt-sec) is, in principle, sufficient to distinguish between a γ-ray source which is positioned near to the edge of the accretion disk surrounding the neutron star, and one that is co-located with the powerful X-ray pulsar. The analysis of a large database obtained during observations of SMC X-1 over an interval of three years at Narrabri has been described in the present work. This analysis has highlighted a problem which can occur when applying the new technique to data with low signal-to-noise, namely that the potential gain of valuable information on the γ-ray pulse

period and the location of the γ-ray source must be weighed against the number of independent trials which have to be made in order to obtain that information. When the γ-ray signal is weak, it is not possible to recover the periodicity without automatically lowering the statistical significance of the effect. A periodic component can certainly be recognised (and a possible location identified), but it may not be presented as conclusive evidence for pulsed γ-ray emission. This has proved to be the case for SMC X-1. Although this system is a very interesting γ-ray source candidate on the grounds of the super-Eddington luminosity at X-ray energies and the promising spatial resolution, it is unfortunately a very distant X-ray binary.

It is hoped that in the future this new analysis technique will be applied with success to some of the closer binary sources. The average distance to the Galactic binary TeV γ-ray sources discussed in Chapters 6 and 11 is $\approx$ 5 kpc, which is less than 10 % of the distance to SMC X-1. Hence the threshold intrinsic γ-ray luminosity required for a statistically significant detection is reduced by a factor in excess of $\sim 10^2$ for source candidates within the Galaxy. On-going analyses by the Durham Group are using this new method to examine data collected for the Be X-ray binary 4U0115+63 ($d \approx 3.5$ kpc) and for the millisecond binary radio pulsars PSR 1855+09 ($d \approx 0.35$ kpc), PSR 1957+20 ($d \approx 0.9$ kpc), and PSR 1953+29 ($d \approx 3.5$ kpc).

The benefits of directly obtaining information on the location of a γ-ray source within a binary system would be tremendous. Previously, the possible emission sites have been suggested only on the basis of indirect evidence. These have been discussed in Chapter 11. Both the accretion disk and the limb of the companion star in the Hercules X-1 binary have been proposed as emission sites using knowledge of the phase of the 35-day X-ray cycle (e.g. Eichler and Vestrand 1985) and the orbital phase of the X-ray pulsar (Gorham *et al.* 1986) at the times of the γ-ray observations. The detection of TeV γ-rays from Her X-1 after the neutron star had entered eclipse was explained by Gorham and Learned (1986) using the steering of charged particles in the magnetosphere of the companion star. Like Her X-1, the high-mass X-ray binary Vela X-1 has been reported to be a transient source of TeV γ-rays during X-ray eclipse (North *et al.* 1987), in addition to being a persistent source at other orbital phases (Carraminana *et al.* 1989a). Again, the magnetic steering of charged particles onto the limb of the companion star has been suggested (Raubenheimer *et al.* 1989) in order to account for the observations of γ-rays deep into X-ray eclipse; calculations presented in this thesis indicate that particle energies of $\sim$ 1 PeV might be required in order for such a process to operate in the Vela X-1 binary. The observed orbital phase modulation of the pulsed TeV γ-ray flux from the high-mass binary Centaurus X-3 (Carraminana *et al.* 1989b, North *et al.* 1989, and Brazier *et al.* 1989b, 1990a) has also been studied in the present work. Such orbital phase dependence is concluded to be indirect evidence

for a γ-ray emission site which is located within an accretion wake trailing behind the X-ray pulsar as it revolves about its companion star. The new analysis technique described in the present work may therefore be capable of providing a more sensitive probe of the nature of the high-energy γ-ray emission in binary systems. The presence of an emission site directly identified with this technique towards the outer edge of an accretion disk, for example, or at the limb of a companion star, would be important and would provide unambiguous evidence for the escape of ultrahigh-energy particles from the neighbourhood of the neutron star to locations well beyond the X-ray pulsar magnetosphere. Future observations of TeV γ-rays therefore might not only provide information on particle energies, energy spectra and the geometries and intensities of the magnetic fields prevailing in X-ray binaries, they could also conclusively demonstrate that at least some of the X-ray binary systems must be contributing to the Galactic cosmic ray population.

Future observations of the X-ray binaries at TeV γ-ray energies therefore hold the promise of revealing much information. Observations at all orbital phases are of interest, particularly at X-ray eclipse ingress and egress. The X-ray observations can point to those potential γ-ray sources which might show flux enhancements following inferior conjunction of the neutron star. In addition to Cen X-3, absorption dips have also been observed in the X-ray orbital light curves of SMC X-1 (Gruber and Rothschild 1984) and Vela X-1 (Haberl and White 1990) which might indicate the existence of an accretion wake.

For Vela X-1, Haberl and White (1990) also report erratic increases by a factor of ten in X-ray absorption across a wide range of orbital phases lasting for times of between minutes and hours. These increases imply an enhancement in the column density of intervening material and, therefore, a possible transient increase in the density of a target for high energy particle beams.

Simultaneous or at least near-contemporary measurements of orbital light curves at both X-ray and TeV γ-ray energies would be very desirable. It would also be fascinating to compare long-term variations of the intensity of binary sources in both energy bands. For example, White (1989) has noted that low and high state X-ray transitions in Cen X-3, together with variability in X-ray absorption, may be caused by variations in the thickness of the accretion disk. This, in turn, could be indicative of changes in the flow of material from the supergiant. A simultaneous observing campaign at TeV energies could be made to search for corresponding long-term fluctuations in the γ-ray luminosity.

The period analysis of data obtained on the globular cluster 47 Tucanae has also been described in this work. Globular clusters have several points of interest here. The number densities of stars in the cluster cores are so great that low-mass X-ray binaries are thought to be formed relatively frequently as a consequence of the near encounters of neutron stars and main sequence stars. X-ray sources occur ~ 100 times

more frequently per unit stellar mass in the clusters than in the Galactic bulge. The globular clusters must surely therefore be prime source candidates for TeV γ-ray emission, especially when it is remembered that they appear compact and can easily be accommodated within the ~ 1°-wide field of view of an air Cerenkov telescope.

It would be fair to say that the prospects for TeV γ-ray astronomy in the 1990s are better than at any time before. There are now a total of thirteen air Cerenkov experiments operating worldwide, five of which are located in the Southern Hemisphere. The Whipple Collaboration at Mount Hopkins (Arizona) have pioneered and developed the Cerenkov imaging technique and their work has produced evidence for unpulsed γ-ray emission from the Crab Nebula (Weekes *et al.* 1989) with unprecedented statistical significance. The University of Durham Cerenkov Observatory at Narrabri is well placed for observations of the Galactic centre, the Galactic bulge X-ray binary systems, and the Large and Small Magellanic Clouds. The Mark III and Mark IV γ-ray telescopes are now the most sensitive instruments monitoring the Southern Hemisphere skies.

It may be reasonable to predict that, by the turn of the century, the current debate on the reality of many of the γ-ray sources claimed by the various research groups in the field will have been largely supplanted by disagreements on the interpretation of a rich body of information provided by TeV γ-ray observations of great sensitivity.

APPENDIX

Further Notes on the Transformation of Time Series

Introduction

This appendix is concerned with the transformation of Cerenkov arrival time series to the rest frame of a binary system. Such a procedure is often a necessary stage of the pre-processing of data recorded during observations of γ-ray pulsar source candidates in binaries and is performed in order to compensate for the Doppler shift in the observed value of the pulse period due to the orbital motion of the pulsar. Further details have been given in Chapters 8 and 9. For circular orbits, the input data required to make the transformations are the projected semi-major axis ($a_x \sin i$) and the orbital phase of the pulsar. The latter is computed relative to a known epoch of mid-eclipse ($\equiv$ orbital phase zero) which is provided by radio or X-ray measurements. These two quantities ($a_x \sin i$ and epoch) have, for a time series of given duration, finite ranges over which the Doppler corrections are indistinguishable. These ranges depend upon the neutron star rotation and orbital periods, the orbital phase of the pulsar, and the value of $a_x \sin i$ itself. Simple expressions are derived here which enable computation of the separation between independent values of both $a_x \sin i$ and the epoch of mid-eclipse. Examples of their values are determined

for several X-ray binaries for time series of fixed duration recorded when the neutron star passes through the descending and ascending nodes, and through inferior and superior conjunction.

A.1 $a_x \sin i$

Let t be the time of emission of a γ-ray as measured in the rest frame of a binary system. The durations (T_s) of Cerenkov arrival time series recorded at Narrabri are usually between 3 and 6 hours. Under these circumstances the pulsar phase equation needs to be taken only up to the term in $^1/_P$ (where P is the pulsar period) since the term in $\dot{P}$ and the higher order terms are invariably small and can be neglected:

$$\varphi(t) = \varphi_o + \frac{t}{P} - \frac{\dot{P}t^2}{2P^2} + \frac{t^3}{3!}\left[\frac{2(\dot{P})^2}{P^3} - \frac{\ddot{P}}{P^2}\right] + \ldots\ldots \qquad (1)$$

For example, SMC X-1 exhibits a secular pulse period derivative $\dot{P} \approx -1.2 \times 10^{-11}$ s s^{-1}. The phase error introduced during time T_s = 6 hours is therefore $\Delta\varphi = \dot{P}T_s^2/2P_x^2 \approx 0.5$ %. Or, consider Centaurus X-3, which has $\dot{P} \sim 10^{-10}$ s s^{-1} and $P_x \approx 5$ s, so that $\Delta\varphi \approx 0.1$ %. LMC X-4: $\dot{P} \sim 10^{-10}$ s s^{-1} and $P_x \approx 13.5$ s; $\Delta\varphi \approx 0.01$ %. Equation 1 can therefore be safely approximated by

$$\varphi = \varphi_o + \frac{t}{P}$$

or $$\varphi = \varphi_o + ft \qquad (2)$$

where f is the rest frame pulse frequency.

If t' is the time of emission of the same γ-ray as recorded in the rest frame of the observer (in which the binary rotates) then the transformation to the binary frame is simply

$$t = t' - a_x \sin i \sin\theta \qquad (3)$$

with $a_x \sin i$ in units of light-travel time. (See Figure A.1 and see also Chapter 8). The angle θ is the orbital phase of the site of emission, as defined by the observer. Orbital phase is here measured anticlockwise from the ascending node.

The pulse phase number may then be written

$$\varphi = \varphi_o + ft' - f\, a_x \sin i \sin\theta \qquad (4)$$

The pulse phase numbers corresponding to Cerenkov times (t') registered at the beginning and end of an observation are

Figure A.1

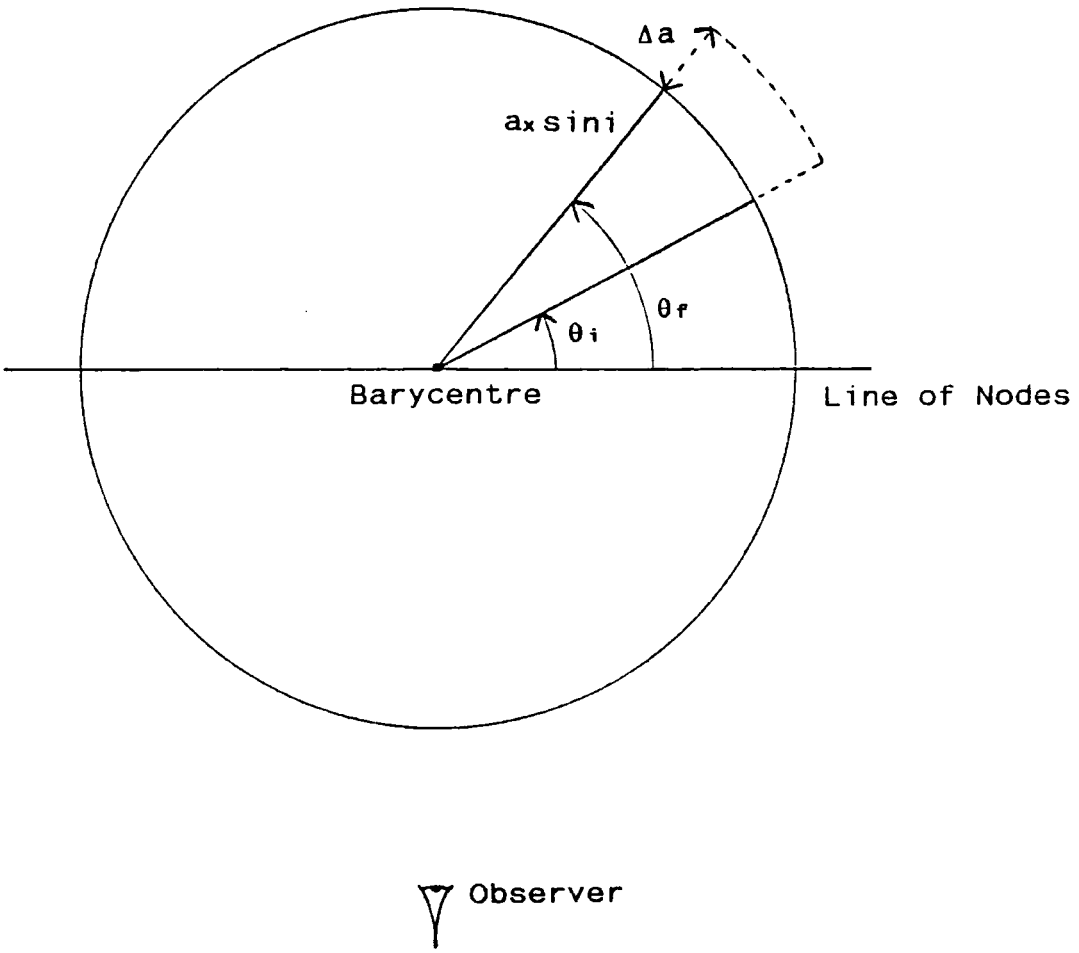

Geometry for the computation of sampling intervals for $a_x \sin i$

$$\varphi_i = \varphi_o + f P_{orb} \frac{\theta_i}{2\pi} - f a_x \sin i \sin\theta_i \qquad (5a)$$

$$\varphi_f = \varphi_o + f P_{orb} \frac{\theta_f}{2\pi} - f a_x \sin i \sin\theta_f \qquad (5b)$$

where P_{orb} is the binary orbital period.

Let $\varphi_f - \varphi_i = k$. The independent sampling interval in $a_x \sin i$ is defined as the increment required in order to alter the value of k by unity. In other words, $a_x \sin i$ is adjusted to some new value so that the computed values of the initial and final pulse phases become φ_{i1} and φ_{f1}, with

$$(\varphi_{f1} - \varphi_{i1}) - (\varphi_f - \varphi_i) = 1 \qquad (6)$$

Let the change in $a_x \sin i$ be Δa. Then,

$$\varphi_{i1} = \varphi_o + f P_{orb} \frac{\theta_i}{2\pi} - f (a_x \sin i + \Delta a) \sin\theta_i \qquad (7a)$$

$$\varphi_{f1} = \varphi_o + f P_{orb} \frac{\theta_f}{2\pi} - f (a_x \sin i + \Delta a) \sin\theta_f \qquad (7b)$$

Equations 5, 6, and 7 yield

$$\Delta a = \frac{1}{f\,(\sin\theta_i - \sin\theta_f)} \qquad (8)$$

For a given pulsar frequency and binary orbital period, the sampling interval in $a_x \sin i$ is therefore dependent upon the orbital phase of the emission site and the duration of the observation.

The sensitivity of the period analysis to the value adopted for $a_x \sin i$ may be gauged by fixing the interval $\theta_f - \theta_i$ ($\equiv$ observation length) and sliding it along a sine curve. For small values of $\theta_f - \theta_i$, the gradient of this curve is approximatley proportional to the difference between the sines of these angles, which is included in the denominator in equation 8. The gradient decreases to zero when the neutron star is at inferior or superior conjunction ($\theta = n\pi/2$, where n is odd). The value taken for $a_x \sin i$ is then unimportant. However, the sampling interval decreases to a non-zero minimum when the neutron star is at the ascending or descending node ($\theta = n\pi$, n = any integer). It is at these orbital phases that accurate knowledge of the value of $a_x \sin i$ can become important. Take the example of a five-hour observation centred at either node: the independent sampling interval in $a_x \sin i$ is computed for several X-ray binaries -

Binary	P_x (s)	P_{orb} (d)	$\Delta a/a_x \sin i$
Vela X-1	283	8.97	$\approx$ 1200 %
LMC X-4	13.5	1.41	60 %
Cen X-3	4.82	2.09	20 %
SMC X-1	0.71	3.89	5 %

A.2 Epoch of Mid-Eclipse

The value of $a_x \sin i$ is now held constant while the epoch is changed by a small amount $\Delta\tau$; with the corresponding shift in orbital phase just $\Delta\theta = 2\pi\Delta\tau/P_{orb}$, the new equations for the pulse phase numbers are

$$\varphi_{i1} = \varphi_o + f P_{orb} \frac{(\theta_i+\Delta\theta)}{2\pi} - f a_x \sin i \sin(\theta_i+\Delta\theta) \quad (9a)$$

$$\varphi_{f1} = \varphi_o + f P_{orb} \frac{(\theta_f+\Delta\theta)}{2\pi} - f a_x \sin i \sin(\theta_f+\Delta\theta) \quad (9b)$$

See Figure A.2. Combining equations 5, 6, and 9,

$$q_1 \sin^2(\Delta\theta) + q_2 \sin(\Delta\theta) + q_3 = 0 \qquad (10)$$

where

$$q_1 = B^2 + C^2$$

$$q_2 = -2AB$$

$$q_3 = A^2 - C^2$$

and

$$A = \frac{1}{f a_x \sin i} - \sin\theta_f + \sin\theta_i$$

$$B = \cos\theta_i - \cos\theta_f$$

$$C = \sin\theta_i - \sin\theta_f$$

Equation 10 is solved for $\Delta\theta$, which is sketched in Figure A.3 as a function of orbital phase for a fixed interval $\theta_f - \theta_i$. Note how the sampling interval in epoch minimises at inferior and superior conjunction, in contrast to the behaviour observed for $a_x \sin i$. It is at these phases that the period analysis will be most sensitive to the value selected for the epoch of mid-eclipse. For a five-hour observation performed near either conjunction:

Binary	P_x (s)	P_{orb} (d)	$a_x \sin i$ (ls)	$\Delta\theta/2\pi$
Vela X-1	283	8.97	113	>100 %
LMC X-4	13.5	1.41	26	10 %
Cen X-3	4.82	2.09	39.8	3 %
SMC X-1	0.71	3.89	53.5	0.6 %

Figure A.2

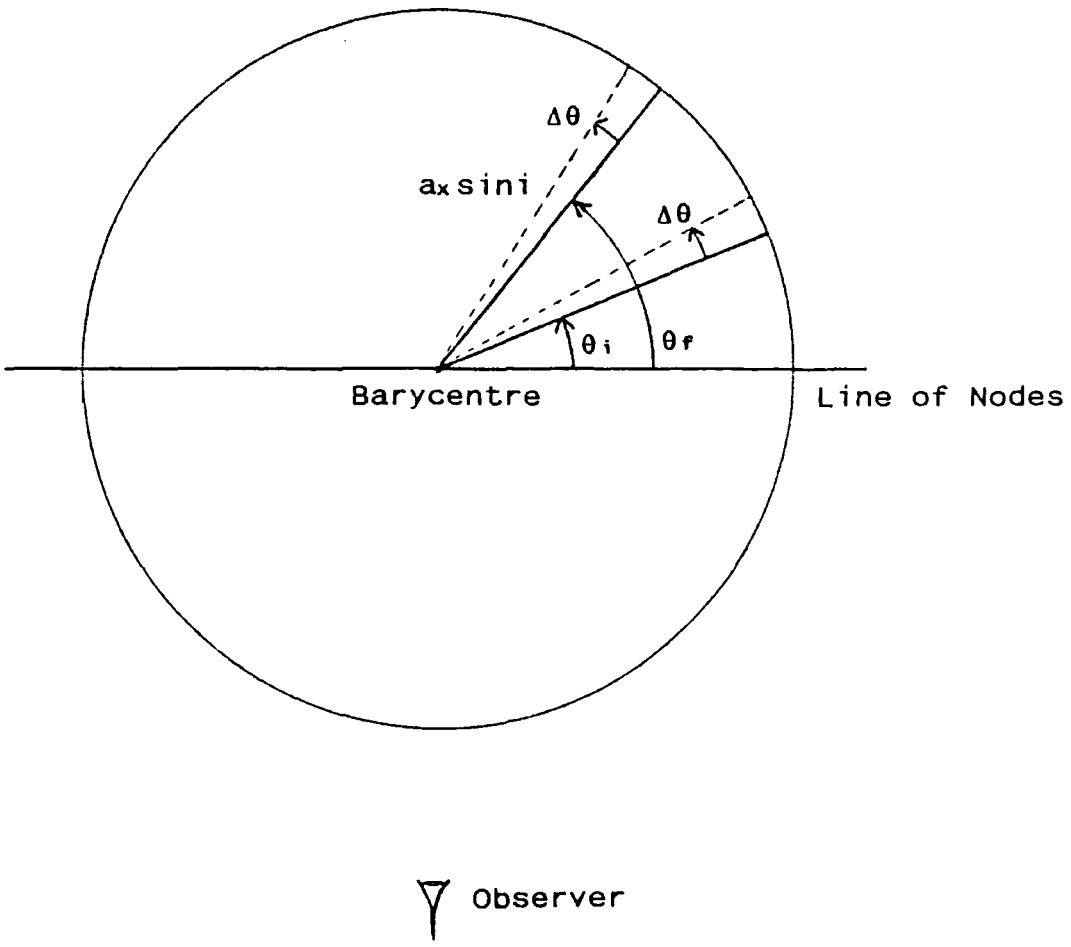

Geometry for the computation of sampling intervals for mid-eclipse epoch

Figure A.3

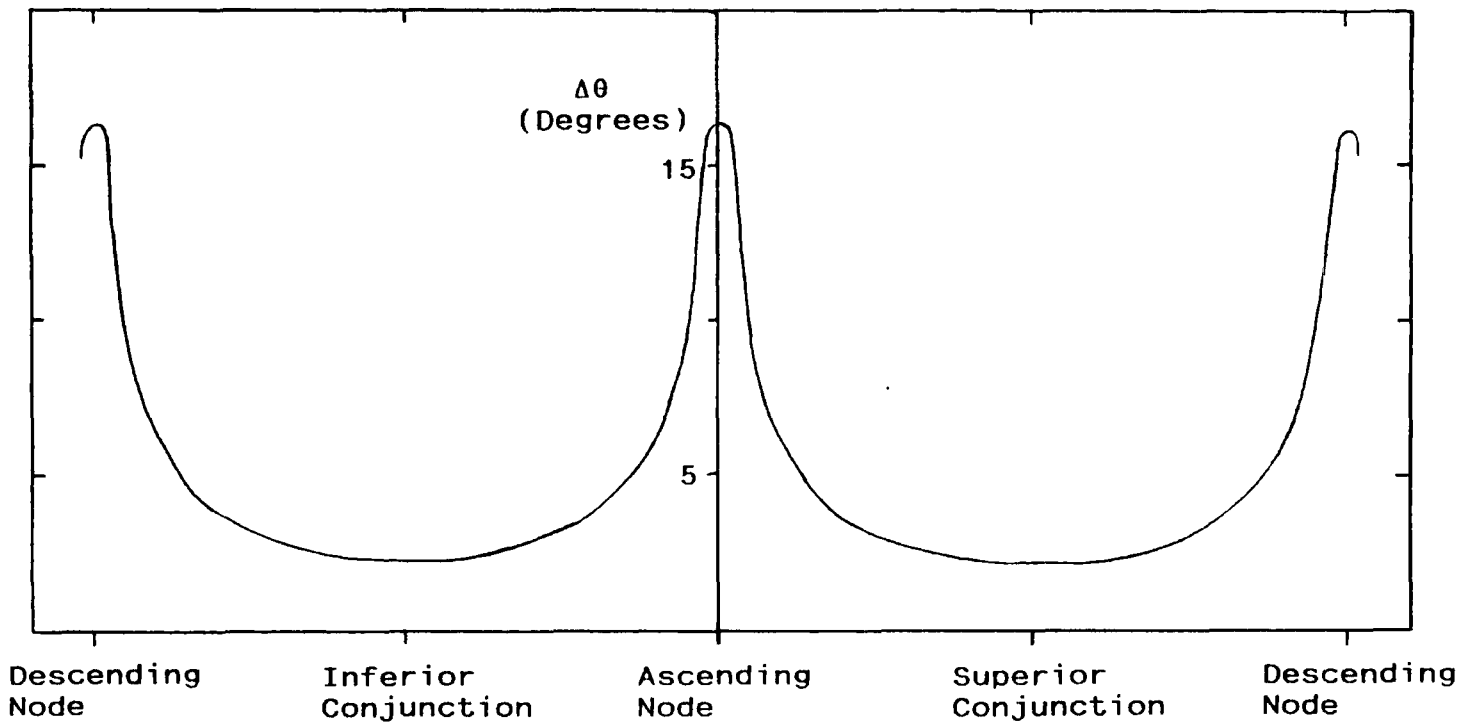

Independent sampling interval for epoch of mid-eclipse (represented by a change in orbital phase). The example shown here is for an observation of SMC X-1 lasting 5 hours.

A.3 Summary

Expressions have been provided for the magnitude of the sampling intervals between independent values of the projected semi-major axis ($a_x \sin i$) and between independent values of the epoch of mid-eclipse. These quantities are found to be functions of pulsar period, orbital period, the magnitude of $a_x \sin i$ itself, the duration of the observation, and the orbital phase at which the pulsar is observed.

The properties of the transformation of arrival time series to the rest frame of a binary system can be summarised by considering the extremes of behaviour observed at the orbital nodes and conjunctions. Such transformations are insensitive to the value of $a_x \sin i$ when the neutron star is located at inferior or superior conjunction, where the sampling interval between independent values of $a_x \sin i$ is infinite. This is because at these orbital phases the pulsar is travelling at right angles to the line-of-sight and the observed magnitude of the Doppler shift in the value of the pulsar period is instantaneously zero. At the orbital nodes, however, the radial velocity of the neutron star reaches a maximum with respect to the observer, hence the Doppler shift is greatest and the sampling interval in $a_x \sin i$ is at a minimum. The sensitivity of the arrival time transformations to the value of epoch of mid-eclipse is greatest at conjunction because the rate of change of the Doppler shift with orbital phase is then at a maximum. It is at these phases that the sampling interval in epoch is smallest. Conversely,

this interval reaches its greatest value at the nodes, where the rate of change of Doppler shift with orbital phase falls to zero.

References

Acharya, B.S., Bhat, P.N., Gandhi, V.N., Ramana-Murthy, P.V., Sathyanarayana, and Vishwanath, P.R., *Proceedings of the 21st International Cosmic Ray Conference,* ed. Protheroe, R.J., **2**, 319-321 (Adelaide, 1990).

Achterberg, A., *Nature*, **342**, 51-52 (1989).

Ajne, B., *Biometrika*, **55**, 343-354 (1968).

Arnett, W.D., and Clayton D.D., *Nature*, **227**, 780 (1970).

Auriere, M., Koch-Miramond, L., and Ortolani, S., *Astron. & Ap.*, **214**, 113-122 (1989).

Azzopardi, M., and Vigneau, J., *Astr. & Ap.*, **56**, 151, (1977).

Bagge, E.R., Samorski, M., and Stamm, W., *Proceedings of the 16th International Cosmic Ray Conference* (Kyoto), **13**, 260 (1979).

Basiuk, V., Bazer-Bachi, A.R., Bonduelle, B., Ducros, R., Goret, P., Hote, C., Mougin, B., Petrou, N., Raviart, A., Rivoire, B., Tabary, A., Treguer, L., *Proceedings of the 21st International Cosmic Ray Conference,* ed. Protheroe, R.J., **4**, 231-233 (Adelaide, 1990).

Batschelet, E., *Circular Statistics in Biology*, Academic Press, London (1981)

Battistoni, G., Bellotti, E., Bloise, C., Bologna, G., Campana, P., Castagnoli, C., Castellina, A., Chiarella, V., Ciocio, A., Cundy, D., D'Ettorre-Piazzoli, B., Fiorini, E., Galeotti, P., Iarocci, E., Liguori, C., Mannocchi, G., Murtas, G., Negri, P., Nicoletti, G., Picchi, P., Price, M., Pullia, A., Ragazzi, S., Rollier, M., Saavedra, O., Satta, L., Serri, P., Vernetto, S., and Zanotti, L., *Phys. Lett.*, **155B**, 465-467 (1985).

Bennett, K., Burger, J.J., Gorisse, M., Mayer-Hasselwander, H.A., Pfeffermann, E., Shukla, P.G., Stiglitz, R., Swanenburg, B.N., Taylor, B.G., and Wills, R.D., *Proceedings of the 9th ESLAB Symposium*, ESRO SP-106, 323 (1974).

Bhat, P.N., Gupta, S.K., Ramana Murthy, P.V., Sreekantan, B.V., Tonwar, S.C., and Vishwanath, P.R., *Proceedings of the NATO Advanced Research Workshop on Very High-Energy γ-Ray Astronomy*, ed. Turver, K.E., Reidel, p. 143 (1987).

Blackett, P.M.S., *Physical Society of London Gassiot Committee Report on Emission Spectra of the Night Sky and Aurorae*, p. 34-35 (1948).

Boldt, E.A., Holt, S.S., Rothschild, R.E., and Serlemitsos, P.J., *Astron. Ap.*, **50**, 161 (1976).

Boley, F., *Rev. Mod. Phys.*, **36**, 792-808 (1964).

Bond, I.A., Budding, E., Conway, M.J., Fenton, K.B., Fujii, H., Fujii, Z., Fujimoto, M., Hasegawa, H., Hayashida, N., Honda, M., Hotta, N., Humble, J.E., Kabe, S., Kashara, K., Kifune, T., Lythe, G.D., Masaike, A., Matsubara, Y., Mitsui, K., Miura, Y., Mori, M., Murakami, K., Muraki, Y., Nagano, M., Makamura, K., Nakamura, T., Norris, P.M., Ogio, S., Ohashi, Y., Okada, A., Saito, T., Sakata, M., Sato, H., Shibata, S., Shima, M., Shimizu, H.M., Spencer, M., Storey, J.R., Tanimori, T., Teshima, M., Torii, S., Uchino, K., Watase, Y., Woodhams, M.D., Yamamoto, Y., Yock, P.C.M., and Yuda, T., *Proceedings of the 21st International Cosmic Ray Conference,* ed. Protheroe, R.J., **2**, 198-201 (Adelaide, 1990).

Bonnet-Bidaud, J.M., and van der Klis, M., *Astron. Ap.*, **97**, 134-138 (1981).

Boynton, P.E., Crosa, L.M., and Deeter, J.E., *Ap. J.*, **237**, 169 (1980).

Boynton, P.E., Deeter, J.E., Lamb, F.K., and Zylstra, G., *Ap. J.*, **307**, 545-563 (1986).

Brazier, K.T.S., Carraminana, A., Chadwick, P.M., Currell, T.R., Dipper, N.A., Lincoln, E.W., Mannings, V.G., McComb, T.J.L., Orford, K.J., Rayner, S.M., and Turver, K.E., *Experimental*

Astronomy, 1, 77-99 (1989a).

Brazier, K.T.S., Carraminana, A., Chadwick, P.M., Dipper, N.A., Lincoln, E.W., Mannings, V.G., McComb, T.J.L., Orford, K.J., Rayner, S.M., and Turver, K.E., *Proc. 23rd ESLAB Symp. on Two Topics in X-Ray Astronomy*, Bologna, Italy; ed. Hunt, J. and Battrick, B., ESA SP-296; 1, 311-314 (1989b).

Brazier, K.T.S., Carraminana, A., Chadwick, P.M., Dipper, N.A., Lincoln, E.W., Mannings, V.G., McComb, T.J.L., Orford, K.J., Rayner, S.M., and Turver, K.E., *Proc. 23rd ESLAB Symp. on Two Topics in X-Ray Astronomy*, Bologna, Italy; ed. Hunt, J. and Battrick, B., ESA SP-296; 1, 321-324 (1989c).

Brazier, K.T.S., Carraminana, A., Chadwick, P.M., Dipper, N.A., Lincoln, E.W., Mannings, V.G., McComb, T.J.L., Orford, K.J., Rayner, S.M., and Turver, K.E., *Proceedings 21st International Cosmic Ray Conference*, ed. Protheroe, R.J., 2, 296-299 (1990a).

Brazier, K.T.S., Carraminana, A., Chadwick, P.M., Dipper, N.A., Lincoln, E.W., Mannings, V.G., McComb, T.J.L., Orford, K.J., Rayner, S.M., and Turver, K.E., *Astron. and Ap.*, **232**, 383-386 (1990b).

Brazier, K.T.S., Carraminana, A., Chadwick, P.M., Dipper, N.A., Lincoln, E.W., Mannings, V.G., McComb, T.J.L., Orford, K.J., Rayner, S.M., and Turver, K.E., *Ap. J.*, **350**, 745 (1990c).

Brazier, K.T.S., Carraminana, A., Chadwick, P.M., Dipper, N.A., Lincoln, E.W., Mannings, V.G., McComb, T.J.L., Orford, K.J., Rayner, S.M., and Turver, K.E., *Proceedings 21st International Cosmic Ray Conference*, ed. Protheroe, R.J., 2, 379-382 (1990d).

Brazier, K.T.S., Carraminana, A., Chadwick, P.M., Dipper, N.A., Lincoln, E.W., Mannings, V.G., McComb, T.J.L., Orford, K.J., Rayner, S.M., and Turver, K.E., *Proceedings 21st International Cosmic Ray Conference*, ed. Protheroe, R.J., 2, 300-303 (1990e).

Brazier, K.T.S., Carraminana, A., Chadwick, P.M., Dipper, N.A., Lincoln, E.W., Mannings, V.G., McComb, T.J.L., Orford, K.J., Rayner, S.M., and Turver, K.E., in preparation (1990f).

Brazier, K.T.S., Carraminana, A., Chadwick, P.M., Dipper, N.A., Lincoln, E.W., Mannings, V.G., McComb, T.J.L., Orford, K.J., Rayner, S.M., Turver, K.E., and Williams, D.G., *Proceedings 21st International Cosmic Ray Conference*, ed. Protheroe, R.J., 4, 274-277 (1990g).

Brazier, K.T.S., Carraminana, A., Chadwick, P.M., Dipper, N.A., Lincoln, E.W., Mannings, V.G., McComb, T.J.L., Orford, K.J., Rayner, S.M., Turver, K.E., and Williams, D.G., *Proceedings to International Conference on High-Energy Gamma-Ray Astronomy*, Ann Arbor,(1990h in preparation).

Brazier, K.T.S., Carraminana, A., Chadwick, P.M., Dipper, N.A.,

Lincoln, E.W., Mannings, V.G., McComb, T.J.L., Orford, K.J., Rayner, S.M., Turver, K.E., and Williams, D.G., *Proceedings 21st International Cosmic Ray Conference*, ed. Protheroe, R.J., 2, 292-295 (1990i)

Browning, R., and Turver, K.E., *Nuovo Cimento*, **38A**, 223 (1977).

Buccheri, R., and de Jager, O.C., in *Timing Neutron Stars*, pp. 95-111; ed. Ogelman, H., and van den Heuvel, E.P.J.; Kluwer Academic Publishers, The Netherlands (1989).

Buccheri, R., Bennett, K., Bignami, G.F., Bloemen, J.B.G.M., Boriakoff, V., Caraveo, P.A., Hermsen, W., Kanbach, G., Manchester, R.N., Masnou, J.L., Mayer-Hasselwander, H.A., Ozel, M.E., Paul, J.A., Sacco, B., Scarsi, L., and Strong, A.W., *Astronomy and Astrophysics*, **128**, 245-251 (1983).

Carraminana, A., Chadwick, P.M., Dipper, N.A., Lincoln, E.W., Mannings, V.G., McComb, T.J.L., Orford, K.J., Rayner, S.M., and Turver, K.E., *Ap. J.*, **346**, 967-970 (1989a).

Carraminana, A., Chadwick, P.M., Dipper, N.A., Lincoln, E.W., Mannings, V.G., McComb, T.J.L., Orford, K.J., Rayner, S.M., Turver, K.E., and Williams, D.G., in *Timing Neutron Stars*, ed. Ogelman, H., and van den Heuvel, E.P.J., Kluwer Academic Publishers, The Netherlands (1989b).

Cassiday, G.L., Cooper, R., Dawson, B.R., Elbert, J.W., Fick, B.E., Green, K.D., Ko, S., Liebing, D.F., Loh, E.C., Salamon, M.H., Smith, J.D., Sokolsky, P., Sommers, P., and Thomas, S.B., *Phys. Rev. Lett.*, **62**, 383-386 (1989).

Cawley, M.F., Murphy, D.W., Murphy, N.M., Lanigan, W.P., Fegan, D.J., and Nolan, K., *Proceedings 21st International Cosmic Ray Conference,* ed. Protheroe, R.J., **4**, 258-261 (Adelaide, 1990).

Cerenkov, P.A., *C.R. Acad. Sci, U.S.S.R.*, 2, 457 (1934).

Cerenkov, P.A., *Ibid.*, 3, 414 (1936).

Cerenkov, P.A., *Ibid.*, **14**, 105 (1937).

Cerenkov, P.A., *Phys. Rev.*, **52**, 378 (1937).

Cerenkov, P.A., *C.R. Acad. Sci., U.S.S.R.*, **21**, 116, 319 (1938).

Chadwick, P.M.C., Dowthwaite, J.C., Harrison, A.B., Kirkman, McComb, T.J.L., Orford, K.J., Turver, K.E., *Nature*, **317**, 236-238 (1985a).

Chadwick, P.M.C., Dowthwaite, J.C., Harrison, A.B., Kirkman, I.W., McComb, T.J.L., Orford, K.J., and Turver, K.E., *Astron. & Ap.*, **151**, L1-L3 (1985b).

Chadwick, P.M.C., Dipper, N.A., Dowthwaite, J.C., Gibson, A.I., Harrison, A.B., Kirkman, I.W., MacRae, J.H., McComb, T.J.L., Orford, K.J., Turver, K.E., and Walmsley, M., *Nature*, **318**, 642-644 (1985c).

Chadwick, P.M., Dipper, N.A., Lincoln, E.W., Mannings, V.G., McComb. T.J.L., Rayner. S.M., Orford, K.J., Turver, K.E., and Williams, D.G., *Ap. J.*, **333**, L19-L21 (1988).

Chanmugam, G., and Brecher, K., *Nature*, **313**, 767-768 (1985).

Charman, W.N., Jelley, J.W., Orman, P.R., Drever, R.W.P., and McBreen, B., *Nature*, **220**, 565 (1968).

Cheng, K.S., Cheung, T., de Jager, O.C., Lau, M.M., and Yu, K.N., *Proceedings 21st International Cosmic Ray Conference,* ed. Protheroe, R.J., 2, 374-377 (1990).

Cheng, K.S., Ho, C., and Ruderman, M., *Ap. J.*, **300**, 500-521 (1986a).

Cheng, K.S., Ho, C., and Ruderman, M., *Ap. J.*, **300**, 522-539 (1986b).

Cheng, K.S., and Ruderman, M., *Ap. J.*, **337**, L77-L79 (1989).

Cheng, K.S., and Ruderman, M., *Ap. J.* (1990a: in press).

Cheng, K.S., and Ruderman, M., *Ap. J.* (1990b: in press).

Chudakov, A.E., Zatsepin, V.I., Nesterova, N.M., and Dadykin, V.L., *J. Phys., Soc. Jpn.*, **17** (A-III), 106 (1962).

Clark, G, Doxsey, R., Li, F., Jernigan, J. G., and van Paradijs, J., *Ap. J. Letters*, **221**, L37-L41 (1978).

Coe, M.J., Engel, A.R., Quenby, J.J., and Dyer, C.S., *Nature*, **268**, 508 (1977).

Coe, M.J., Bell-Burnell, S.J., Engel, A.R., Evans, A.J., and Quenby, J.J., *Mon. Not. R. ast. Soc.*, **197**, 247-251 (1981).

Cohen, J.M., and Mustafa, E., *Astrophysics and Space Science*, **128**, 355-361 (1986).

Cohen, J.M., and Mustafa, E., *Ap. J.*, **319**, 930-938 (1987).

Conti, P.S., *Astron. Ap.*, **63**, 225-235 (1978).

Cressie, N., *J. Appl. Prob.*, **14**, 272-283 (1977).

Critchfield, C.L., Ney, E.P., and Oleksa, S., *Phys. Rev.*, **85**, 461 (1952).

Cutler, E.P., Dennis, B.R., and Dolan, J.F., *Ap. J.*, **300**, 551-556

(1986).

Danaher, S., Fegan, D.J., Porter, N.A., and Weekes, T.C., *Nature*, **289**, 568 (1981).

Darbro, W., Ghosh, P., Elsner, R.F., Weisskopf, M.C., Sutherland, P.G., and Grindlay, J.E., *Ap. J.*, **246**, 231-237 (1981).

Davidsen, A., Malina, R., and Bowyer, S., *Ap. J.*, **211**, 866-871 (1977).

Davies, S.R., Coe, M.J., Payne, B.J., and Hanson, C.G., *Mon. Not. R. Astron. Soc.*, **237**, 973 (1989).

Davison, P.J.N., *Mon. Not., R. astr. Soc.*, **179**, *Short Communication*, 15P-20P (1977).

de Jager, O.C., *The Analysis and Intrepretation of VHE Gamma-Ray Measurements*, Ph.D. Thesis, Potchefstroom University, South Africa (1987).

de Jager, H.I., de Jager, O.C., North, A.R., van der Walt, D.J., and van Urk, G., *South African J. Phys*, **9**, 107-118 (1986).

de Jager, O.C., Raubenheimer, B.C., North, A.R., Nel, H.I., and van Urk, G., *Ap. J.*, **329**, 831-837 (1988).

de Jager, O.C., Meintjes, P.J., Brink, C., Nel, H.I., North, A.R., Raubenheimer, B.C., van der Walt, D.J., and Waanders, F.B., IAU Circular # 4858 (1989).

de Jager, O.C., Swanepoel, J.W.H., and Raubenheimer, B.C., *Astron. and Ap.*, **221**, 180-190 (1989).

de Jager, O.C., Raubenheimer, B.C., Brink, C., Meintjes, P.J., Nel, H.I., North, A.R., van Urk, G., and Visser, B., *Astron. & Ap.* (1990; in press).

Dingus, B.L., Chang, C.Y., Goodman, J.A., Gupta, S.K., Haines, T.J., Krakauer, D.A., and Talaga, R.L. , Phys. Rev. Lett., **60**, 1785-1788 (1988).

Dingus, B.L., Chang, C.Y., Goodman, J.A., Gupta, S.K., Haines, T.J., Krakauer, D.A., and Talaga, R.L. , Phys. Rev. Lett., **61**, 1906-1909 (1989).

Dowthwaite, J.C., Gibson, A.I., Harrison, A.B., Kirkman, I.W., Lotts, A.P., MacRea, J.H.K., Orford, K.J., Turver, K.E., and Walmsley, M., *Astron. and Ap.*, **126**, 1 (1983).

Dowthwaite, J.C., Harrison, A.B., Kirkman, I.W., MacRea, J.H.K., McComb, T.J.L., Orford, K.J., Turver, K.E., and Walmsley, M., *Ap. J.*, **286**, L35-L38 (1984a).

Dowthwaite, J.C., Harrison, A.B., Kirkman, I.W., MacRea, J.H.K., Orford, K.J., Turver, K.E., and Walmsley, M., *Astron. & Ap.*, **136**, L14-L15 (1984b).

Dowthwaite, J.C., Harrison, A.B., Kirkman, I.W., MacRea, J.H.K., Orford, K.J., Turver, K.E., and Walmsley, M., *Nature*, **309**, 691-693 (1984c).

Dowthwaite, J.C, Harrison, A.B., Kirkman, I.W., MacRea, J.H.K., Orford, K.J., Turver, K.E., and Walmsley, M., *Astron. and Ap.*, **142**, 55-58 (1985).

Eadie, W.T., Drijard, D., James, F.E., Roos, M., and Sadoulet, B., *Statistical Methods in Experimental Physics*, North-Holland, Amsterdam (1971).

Eichler, D., and Vestrand, W.T., *Nature*, **307**, 613-614 (1984).

Eichler, D., and Vestrand, W.T., *Nature*, **318**, 345-347 (1985).

Elbert, J.W., in *New Particles Conference*, Madison, WI (1985).

Erber, T., *Rev. Mod. Physics*, **38**, 626 (1966).

Fazio, G.G., *Ann. Rev. Astron. and Ap.*, **5**, 481 (1967).

Fazio, G.G., Helmken, H.F., Rieke, G.H., and Weekes, T.C.,

Nature, 220, 892 (1968).

Fichtel, C.E., *Phil. Trans. Roy. Soc. Lond.*, **277**, 367 (1974).

Firkowski, R., Gawin, J., Hioner, J., Wdowczyk, J., Zawadski, A., and Maze, R., *Proceedings of the 9th International Cosmic Ray Conference* (London), 2, 696 (1965).

Frank, J., King, A.R., and Raine, D.J., *Accretion Power in Astrophysics*, Cambridge University Press (1985).

Gaisser, T.K., in *Workshop on Very High Energy Cosmic Ray Interactions* (pp. 492-514), University of Pennsylvania; ed. Cherry, M.L., Lande, K., and Steinberg, R.I. (1982).

Galbraith, W., and Jelley, J.V., *Nature*, **171**, 349 (1953).

Galbraith, W., and Jelley, J.V., *J. Atmos. Terr. Phys.*, **6**, 250 (1955).

Ghosh, P., Elsner, R.F., Sutherland, P.G.., and Weisskopf, M.C., *Ap. J.*, **251**, 230-245 (1981).

Giacconi, R., Murray, S., Gursky, H., Kellogg, E., Schreier, E., and Tananbaum, H., *Ap. J.*, **178**, 281 (1972).

Giacconi, R., and Gursky, H., *X-Ray Astronomy*, Dordrecht: Reidel

(1974).

Gibson, A.I., Harrison, A.B., Kirkman, I.W., Lotts, A.P., MacRae, J.H.K., Orford, K.J., Turver, K.E., and Walmsley, M., *Nature*, **296**, pp. 833-835 (1982).

Gibson, A.I., Harrison, A.B., Kirkman, I.W., Lotts, A.P., MacRae, J.H., Orford, K.J., Turver, K.E., and Walmsley, M., in *International Workshop on Very High Energy Gamma-Ray Astronomy* (pp. 97-115), Ootacamund, India; ed. Ramana Murthy, P.V., and Weekes, T.C. (1982).

Gilfanov, M., Sunyaev, R., Churazov, E., Loznikov, V., Efremov, V., Kaniovskiy, A., Kuznetsov, A., Yamburenko, N., Melioranskiy, A., Skinner, G.K., Al-Emam, O., Patterson, T.G., Willmore, A.P., Brinkman, A.C., Heise, J., Int, J.J., Jager, R., Pietsch, W., Doebereiner, S., Englhauser, J., Reppin, C., Truemper, J., Voges, W., Kendziorra, E., Maisack, M., Mony, B., Staubert, R., Parmar, A.N., Smith, A., *Proc. 23rd ESLAB Symp. on Two Topics in X-Ray Astronomy*, Bologna, Italy; ed. Hunt, J. and Battrick, B., ESA SP-296; 1, 71-79 (1989).

Glass, I.S., and Feast, M.W., *Nature Phys. Sci.*, **245**, 39 (1973).

Goodman, J.A., Freudenreich, H., Mincer, A., Tonwar, S.C., Yodh, G.B., Ellsworth, R.W., in *Workshop on Very High Energy Cosmic Ray Interactions* (pp. 174-199), University of Pennsylvania; ed.

Cherry, M.L., Lande, K., and Steinberg, R.I. (1982).

Gorham, P.W., Cawley, M.F., Fegan, D.J., Gibbs., K.G., Lamb, R.C., Liebing, D.F., Porter, N.A., Stenger, V.J., and Weekes, T.C., *Ap. J.*, **308**, L11-L15 (1986).

Gorham, P.W., and Learned, J.G., *Nature*, **323**, 422-424 (1986).

Gould, R.J., and Schreder, G.P., *Phys. Rev. Lett.*, **16**, 252 (1966).

Greenhill, J.G., Giles, A.B., Sharma, D.P., Dieters, S., Sood, R.K., Thomas, J.A., Waldron, L., Manchanda, R.K., Carli, R., Hammer, P., Kendziorra, E., Staubert, R., Bazzano, A., Ubertini, P., and La Padula, G.,

Greenwood, J.A., and Durand, D., *Annals of Mathematical Statistics*, **26**, 233-246 (1955).

Gregory, A.G., Patterson, J.R., Roberts, M.D., Smith, N.I., and Thornton, G.J., submitted to *Astron. and Ap.* (1990).

Greisen, K. *The Physics of Cosmic X-ray, γ-Ray and Particle Sources*, Gorden and Breach (1971).

Grindlay, J.E., Helmken, H.F., Hanbury-Brown, R., Davis, J., and Allen, L.R., *Ap. J.*, **197**, L9 (1975).

Grindlay, J.E., Hertz, P., Steiner, J.E., Murray, S.S., and Lightman, A.P., *Ap. J.*, **282**, L13-L16 (1984).

Gruber, D.E., and Rothschild, R.E., *Ap. J.*, **283**, 546-551 (1984).

Haberl, F., and White, N.E., accepted *Ap.J.* (1990).

Halzen, F., Hikasa, K., and Stanev, T., *Phys. Rev.*, **D 34**, 2061 (1986).

Harding, A.K., *Proceedings of Workshop on Physics and Experimental Techniques of High-Energy Neutrinos and VHE and UHE Gamma-Ray Astrophysics*, ed. Yodh, G.B., and Wold, D.C., NASA Goddard Space Flight Center, Maryland (1989).

Harding, A.K., *Proceedings to Energetic Gamma-Ray Experiment Telescope (EGRET) Science Symposium*, ed. Fichtel, C., Hunter, S., Sreekumar, P., and Stecker, F., NASA Goddard Space Flight Center, Maryland (1990).

Harding, A.K., and Gaisser, T.K., *Ap. J.*, **358**, 561-574 (1990).

Hartman, R.C., in *Proceedings of the Workshop on High-Resolution Gamma-Ray Cosmology* (1988: UCLA).

Harwit, M. *Astrophysical Concepts*, Wiley, New York (1973).

Hayakawa, S., *Cosmic Ray Physics: Nuclear and Astrophysical Aspects*, John Wiley & Sons (1969).

Henry, P., and Schreier, E., *Ap. J. (Letters)*, **212**, L13-L16 (1977).

Hertz, P., and Grindlay, J.E., *Ap. J.*, **267**, L83-L87 (1983a).

Hertz, P., and Grindlay, J.E., *Ap. J.*, **275**, 105-119 (1983b).

Hillas, A.M., *Nature*, **312**, 50-51 (1984).

Hillas, A.M., *Proceedings of the NATO Advanced Research Workshop on Very High Energy Gamma-Ray Astronomy*, Turver, K.E., (Ed.), Reidel, p. 71 (1987).

Hillas, A.M., *Proc. 12th European Cosmic Ray Symposium*, Nottingham (1990: in preparation).

Hillas, A.M., and Johnson, P.A., *Proceedings 21st International Cosmic Ray Conference*, ed. Protheroe, R.J., **4**, 19-22 (1990)

Hillier, R., *Gamma-Ray Astronomy*, Clarendon Press, Oxford (1984).

Hirata, K., Kajita, T., Koshiba, M., Nakahata, M., Oyama, Y., Sato, N., Suzuki, A., Takita, M., and Totsuka, Y., *Phys. Rev. Lett.*, **58**, 1494 (1987).

Hjellming, R.M., *Science*, **182**, 1089 (1973).

Hodges, J.L., *Annals of Mathematical Statistics*, **26**, 523-527 (1955).

Hoeffding, W., *Annals of Mathematical Statistics*, **19**, 293-325 (1948).

Howarth, I.D., *Mon. Not. R. Astr. Soc.*, **198**, 289-296 (1982).

Hutchings, J.B., in *Galactic X-Ray Sources*, pp. 3-26; ed. Sanford, P.W., Laskarides, P., and Salton, J.; Wiley (1982).

Jauch, J.M., and Rohrlich, F., *Theory of Photons and Electrons*, Addison-Wesley (1955).

Jayanthi, U.B., Jablonski, F., and Braga, J., *Astrophys. & Space Sci.*, **137**, 233-238 (1987).

Jelley, J.V., in *Progress in Elementary Particle and Cosmic Ray Physics* (pp. 40-159), ed. Wilson, J.G., and Wouthuyen, S.A., North Holland Publishing Co. (1967).

Jiang, Y., Xu, C., Chen, D., He, H., Wang, J., He, E., and Huo, A., *Proceedings of the 21st International Cosmic Ray Conference*, ed. Protheroe, R.J., **4**, 220-223 (Adelaide, 1990).

Jones, W.V., in *High Energy Astrophysics* (pp. 59-76): *Proceedings of the Nineteenth Rencontre de Moriond Meeting*, Savoie, France; ed. Van, J.T.T (1984).

Katz, J.I., *High Energy Astrophysics*, Addison-Wesley, California (1987).

Katz, J.I., and Smith, I.A., *Ap. J.*, **326**, 733-737 (1988).

Kazanas, D., *Adv. Space Res.*, **8**, 2559-2561 (1988).

Kazanas, D., *Nature*, **338**, 300 (1989).

Kazanas, D., and Ellison, D.C., *Nature*, **319**, 380-382 (1986).

Kenter, A.T., *A Search for Very High Energy Gamma-Rays from the Crab Pulsar-Nebula*, Ph.D. Thesis, University of Wisconsin-Madison (1989).

Khruzina, T.S., and Cherepashchuk, A.M., *Sov. Astron.*, **30**, 295 (1986).

Khruzina, T.S., and Cherepashchuk, A.M., Sov. Astron., **31**(2), 180-187 (1987).

Kiraly, P., and Meszaros, P., *Ap. J.*, **333**, 719-728 (1988).

Kirov, I.N., Stamenov, J.N., Ushev, S.Z., Janminchev, V.D., Aseikin, V.S., Nikolsky, S.I., Nikolskaya, N.M., Yakovlev, V.I., and Morozov, A.E., *Proceedings of the 19th International Cosmic Ray Conference* (La Jolla), **1**, 135 (1985).

Koul, R., Bhat, C.L., Tickoo, A.K., Kaul, S.K., Qazi, R.A., Kaul, R.K., Rawat, H.S., Sanecha, V.K., Rannot, R.C., Sapru, M.L., and Razdan, H., *J. Phys. E: Sci Instrum.*, **22**, 47-52 (1989).

Kraushaar, W.L., Clark, G.W., Garmire, G.P., Borken, R., Higbie, P., Leong, C., and Thorsos, T., *Ap. J.*, **177**, 341 (1972).

Kuiper, N.H., *Konikl. Nederl. Akad. Wet. Proc.*, Ser. A, **63**, 38-47 (1960).

Kwok, P.W., *Very High Energy Gamma-Rays from the Crab Nebula and Pulsar*, Ph.D Thesis, University of Arizona (1989).

Lamb, R.C., Fichtel, C.E., Hartman, R.C., Kniffen, D.A., and Thompson, D.J., *Ap. J.*, **212**, L63 (1977).

Lamb, R.C., Godfrey, C.P., Wheaton, W.A., and Tumer, T., *Nature*, **296**, 543 (1982).

Lamb, R.C., Cawley, M.F., Fegan, D.J., Gibbs, K.G., Gregory, A.G., Gorham, P.W., Lewis, D.A., Porter, N.A., Stenger, V.J., and Weekes, T.C., in *Very High Energy γ-Ray Astronomy*; ed. Turver.

K.E., Reidel (Dordrecht); pp. 139-142 (1987).

Lamb, R.C., Cawley, M.F., Fegan, D.J., Gibbs, K.G., Gorham, P.W., Hillas, A.M., Lewis, D.A., Porter, N.A., Reynolds, P.T., and Weekes, T.C., *Ap. J.*, **328**, L13-L16 (1988).

Lang, F.L., Levine, A.M., Bautz, M., Hauskins, S., Howe, S., Primini, F.A., Lewin, W.H.G., Baity, W.A., Knight, F.K., Rothschild, R.E., and Petterson, J.A., *Ap. J.*, **246**, L21 (1981).

Lang, K.R., *Atrophysical Formulae*, Springer-Verlag (1986).

Lang, M.J., Cawley, M.F., Fegan, D.J., Hillas, A.M., Kwok, P.W., Lamb, R.C., Lewis, D.A., Macomb, D., Reynolds, P.T., Vanti, G., and Weekes, T.C., *Proceedings 21st International Cosmic Ray Conference,* ed. Protheroe, R.J., 2, 139-142 (1990).

Leahy, D.A., Darbro, W., Elsner, R.F., Weisskopf, M.C., Sutherland, P.G., Kahn, S., and Grindlay, J.E., *Ap. J.*, **266**, 160-170 (1983).

Leahy, D.A., Elsner, R.F., and Weisskopf, M.C., *Ap. J.*, **272**, 256-258 (1983).

Lecar, M., Wheeler, J.C., and McKee, C.F., *Ap. J.*, **205**, 556 (1976).

Leong, C., Kellogg, E., Gursky, H., Tananbaum, H., and Giacconi, R., *Ap. J. Letters*, **170**, L67-L71 (1971).

Leventhal, M., MacCallum, C.J., Barthelmy, S.D., Gehrels, N., Teegarden, B.J., and Tueller, J., *Nature*, **339**, 36-38 (1989).

Lewin, W.H.G., and van den Heuvel, E.P.J., *Accretion-Driven Stellar X-Ray Sources*; (ed.) Cambridge University Press (1983).

Lewin, W.H.G., Ricker, G.R., and McClintock, J.E., *Ap. J. Letters*, **169**, L17-L21 (1971)

Liller, W., *Ap. J. (Letters)*, **184**, L37-L39 (1973).

LLoyd-Evans, J., Coy, R.N., Lambert, A., Lapikens, J., Patel, M., Reid, R.J.D., and Watson, A.A., *Nature*, **305**, 784 (1983a).

LLoyd-Evans, J., Coy, R.N., Lambert, A., Lapikens, J., Patel, M., Reid, R.J.D., and Watson, A.A., *Proc. 18th Int. Cosmic Ray Conf.*, Bangalore, **9**, 65 (1983b).

Longair, M.S., *High Energy Astrophysics*, Cambridge University Press (1981).

Lucke, R., Yentis, D., Friedman, H., Fritz, G., and Shulman, S., *Ap. J. (Letters)*, **206**, L25-L28 (1976).

MacRae, J.H.K., *The Detection of Very High Energy Cosmic Gamma-Rays Using the Atmospheric Cerenkov Technique*, Ph.D. Thesis, University of Durham (1985).

Makino, F., IAU Cirular # 4855 (1989)

Makishima, K., Ohashi, T., Sakao, T., Dotani, T., Inoue, H., Koyama, K., Makino, F., Mitsuda, K., Nagase, F., Thomas, H.D., Turner, M.J.L., Kii, T., and Tawara, Y., *Nature*, **333**, 746-748 (1988).

Manchester, R.N, and Taylor, J.H., *Pulsars*, Freeman, San Francisco (1977).

Manchester, R.N., Lyne, A.G., D'Amico, N., Johnston, S., Lim, J., and Kniffen, D.A., *Nature*, **345**, 598-600 (1990).

Mardia, K.V., *Statistics of Directional Data*, Acadmeic Press, New York (1972).

Marshak, M.L., Bartelt, J., Courant, H., Heller, K., Joyce, T., Peterson, E.A., Ruddick, K., and Shupe, M., *Phys. Rev. Lett.*, **54**, 2079-2082 (1985).

Martin, N., Prevot, L., Rebeirot, E., and Rousseau, J., *Astron. Ap.*, **51**, 31 (1976).

McClintock, J., Rappaport, S., Joss, P.C., Bradt, H., Buff, J., Clark, G.W., Hearn, D., Lewin, W.H.G., Matilsky, T., Mayer, W., and Primini, F., *Ap. J. (Letters)*, **206**, L99 (1976).

McClintock, J.E., and Leventhal. M., *Ap. J.*, **346**, 143-150 (1989).

McGee, R.X., and Hindman, J.V., quoted by F. J. Kerr in *The Magellanic Clouds*, ed. A. B. Muller (Dordrecht: Reidel 1971).

Meyer, P., in *Origin of Cosmic Rays* (pp.233-266), ed. Osborne, J.L., and Wolfendale, A.W.; Reidel Publishing Co., Dordrecht-Holland (1975).

Mitra, A.K., *Proceedings 21st International Cosmic Ray Conference,* ed. Protheroe, R.J., **4**, 15-18 (1990).

Morrison, P., *Nuovo Cimento*, **7**, No. 6, p. 858 (1958).

Morse, R., *Proceedings of the 21st International Cosmic Ray Conference,* ed. Protheroe, R.J., **4**, 262-265 (Adelaide, 1990).

Nagase, F., *Publ. Astron. Soc. Japan*, **41**, 1-79 (1989).

Nagle, D.E., Gaisser, T.K., and Protheroe, R.J., *Ann. Rev. Nucl. Part. Sci.*, **38**, 609-657 (1988).

Naranan, S., Elsner, R.F., Darbro, W., Hardee, P.E., Ramsey,

B.D., Leahy, D.A., Weisskopf, M.C., and Williams, A.C, *Ap. J.*, **290**, 487-495 (1985).

Neshpor, Y.I., Stepanian, A.A., Fomin, V.P., Gerasimov, S.A., Vladimirsky, B.M., and Ziskin, Y.L., *Astrophys. & Space Sci.*, **61**, 349 (1979).

Nikishov, A.I., *Zh. Eksp. Teor. Fiz.*, **41**, 549; *Soviet Physics* - JETP, **14**, 393 (1961).

North, A.R., Raubenheimer, B.C., de Jager, O.C., van Tonder, A.J., and van Urk, G., *Nature*, **326**, 567-569 (1987).

North, A.R., Brink, C., Cheng, K.S., de Jager, O.C., Nel, H.I., and Raubenheimer, B.C.,*Proc. 23rd ESLAB Symp. on Two Topics in X-Ray Astronomy*, Bologna, Italy; ed. Hunt, J. and Battrick, B., ESA SP-296; 1, 563-566 (1989).

Ogelman, H., Ayasli, S., and Haciliyar, A., *Proceedings of Gamma-Ray Symposium*, Goddard Space Flight Center (1976).

Ogelman, H., in *Timing Neutron Stars*, pp. 169-189; ed. Ogelman, H., and van den Heuvel, E.P.J., Kluwer Academic Publishers, The Netherlands (1989b).

Orford, K.J., submitted to *Experimental Astronomy* (1990).

Parsignault, D.R., Schreier, E., Grindlay, J., and Gursky, H., *Ap. J. (Letters)*, **209**, L73 (1976).

Perlow, G.J., and Kissinger, C.W., *Phys. Rev.*, **81**, 552 (1951).

Petterson,J.A., in *Accretion-Driven Stellar X-Ray Sources*; ed. Lewin, W.H.G., and van den Heuvel, E.P.J., Cambridge University Press; pp.367-391 (1983).

Porter, N.A., and Weekes, T.C., *Smithsonian Astrophysical Report* No. 381 (1978).

Pounds, K.A., Cooke, B.A., Ricketts, M.J., Turner, M.J., and Elvis, M., *M.N.R.A.S.*, **172**, 473-481 (1975).

Price, R.E., Groves, D.J., Rodrigues, R.M., Seward, F.D., Swift, C.D., and Toor, A., *Ap. J. Letters*, **168**, L7-L9 (1971).

Primini, F., Rappaport, S., Joss, P.C., Clark, G.W., Lewin, W., Li, F., Mayer, W., and McClintock, J., *Ap. J. (Letters)*, **210**, L71-L74 (1976).

Primini, F., Rappaport, S., and Joss, P.C., *Ap. J.*, **217**, 543-548 (1977).

Protheroe, R.J., *Nature*, **310**, 296-298 (1984).

Protheroe, R.J., *Astron. Express*, **1**, 137 (1985).

Protheroe, R.J., *Proc. Astron. Soc. Australia*, **7**, 167 (1988).

Protheroe, R.J., and Clay, R.W., and Gerhardy, P.R., *Ap. J.*, **280**, L47-L50 (1984).

Protheroe, R.J., and Clay, R.W., *Nature*, **315**, 205-207 (1985).

Protheroe, R.J., and Stanev, T., *Nature*, **328**, 136-139 (1987).

Protheroe, R.J., and Turver, K.E., *J. Phys.*, G 5, p. 1613 (1979)

Quenby, J.J., *Acceleration of Cosmic Rays*, *Mitt. Astron. Ges.*, **65** (1986).

Ramana-Murthy, P.V., and Wolfendale, A.W., *Gamma-Ray Astronomy*, Cambridge University Press (1986).

Rappaport, S., and Joss, P.C., *Nature*, **266**, 683 (1977).

Raubenheimer, B.C., North, A.R., de Jager, O.C. and Nel, H.I., *S. Afr. J. Sci.*, **84**, 461 (1988).

Raubenheimer, B.C., North, A.R., de Jager, O.C. and Nel, H.I., *Ap. J.*, **336**, 394-402 (1989).

Rayner, S.M., Ph.D. thesis, Department of Physics, University of Durham (1989).

Resvanis, L., Learned, J., Stenger, V., Weeks, D., Gaidos, J., Loeffler, J., Olson, T., Palfrey, T., Sembroski, G., Wilson C., Camerini, U., Finley, J., Fry, W., Jaworski, M., Jennings, J., Kenter, A., Lomperski, M., Loveless, R., March, R., Matthews, J., Morse, R., Reeder, D., Slane, P., and Szentgyorgyi, A., in *Very High Energy γ-Ray Astronomy*; ed. Turver. K.E., Reidel (Dordrecht); pp. 131-134 (1987).

Resvanis, L.K., Szentgyorgyi, A., Hudson, J., Kelley, L., Learned, J.G., Sinnis, C., Stenger, V., Weeks, D.D., Gaidos, J., Kertzman, M., Loeffler, F., Palfrey, T., Sembroski, G., Wilson C., Camerini, U., Finley, J.P., Jennings, J., Kenter, A., Lomperski, M., Loveless, R., March, R., Matthews, J., Morse, R., Reeder, D., and Slane, P., *Ap. J.*, **328**, L9-L12 (1988).

Reynolds, P.T., Cawley, M.F., Fegan, D.J., Hillas, A.M., Kwok, P.W., Lamb, R.C., Lang, M.J., Lewis, D.A., Macomb, D., Vacanti, G., and Weekes, T.C., *Nuclear Physics B* (Proc. Suppl.), North-Holland, **14A**, 200-204 (1990).

Ricketts, M.J., Hall, R., Page, C.G., Whitford, C.H., and Pounds, K.A., *Mon. Not. R. astr. Soc.*, **201**, 759-768 (1982).

Rossi, B., and Greisen, K., *Rev. Mod. Phys.*, **13**, 240 (1941).

Rybicki, G.B., and Lightman, A.P., *Radiative Processes in Astrophysics*, Wiley, New York (1979).

Salvati, M., and Massaro, E., *Astron. and Astrophys.*, **67**, 55 (1978)

Samorski, M. and Stamm, W., *Ap. J.*, **268**, L17 (1983a).

Samorski, M. and Stamm, W., *Proc. 18th Int. Cosmic Ray Conf.*, Bangalore, 1, 135 (1983b).

Samorski, M. and Stamm, W., *Proc. 18th Int. Cosmic Ray Conf.*, Bangalore, 11, 244 (1983c).

Sanduleak, N., *Astron. J.*, **73**, 246 (1968).

Schreier, E., Gursky, H., Kellogg, E., Tananbaum, H., and Giacconi, R., *Ap. J. (Letters)*, **170**, L21 (1971).

Schreier, E., Levinson, R., Gursky, H., Kellogg, E., Tananbaum, H., and Giacconi, R., *Ap. J. Letters*, **172**, L79-L89 (1972a).

Schreier, E., Giacconi, R., Gursky, H., Kellogg, E., and Tananbaum, H., *Ap. J. Letters*, **178**, L71-L75 (1972b).

Slane, P., and Fry, W.F., *Ap. J.*, **342**, 1129-1133 (1989).

Smith, F.G., *Proceedings of the NATO Advanced Research Workshop on Very High Energy Gamma-Ray Astronomy*, Turver, K.E. (Ed.), Reidel, p. 1 (1987).

Standish, E.M., *Astron. and Ap.*, 114, 297 (1982).

Stanev, T., *Fourth Moriond Workshop: Searches for New and Exotic Phenomena*, Les Arcs (1987).

Stanev, T., Vankov, Ch. P., and Halzen, F., *Proceedings of the 19th International Cosmic Ray Conference* (La Jolla), 7, 219 (1985).

Strickman, M.S., Johnson, W.N., and Kurfess, J.D., *Ap. J. Letters*, L21-L25 (1980).

Strom, R.G., van Paradijs, J., and van der Klis, M., *Nature*, 337, 234-236 (1989)

Sturrock, P.A., *Ap. J.*, **164**, 529 (1971).

Swanepoel, J.W.H. and de Beer, C.F., *Ap. J.*, **350**, 754-757 (1990).

Takeshima, *Private Communication* (1987).

Tamm, I., and Frank, I., *C.R. Acad. Sci., U.S.S.R.*, **14**, 109 (1937).

Tananbaum, H., Gursky, H., Kellogg, E., Levinson, R., Schreier, E., and Giacconi, R., *Ap. J. (Letters)*, **174**, L143 (1972).

Taylor, J.R., *An Introduction to Error Analysis*, University Science Books (1982).

Teshima, M., Nagano, M., Hara, T., Hayashida, N., Honda, M., Kamata, K., Kifune, T., Ohoka, H., and Matsubara, Y., *Phys. Rev. Lett.*, **64**, 1628-1631 (1990).

Tjemkes, S.A., Zuiderwijk, E.J., and van Paradijs, J., *Astron. & Ap.*, **154**, 77-91 (1986).

Tonwar, S.C., in *Workshop on Very High Energy Cosmic Ray Interactions* (p. 160-172), University of Pennsylvania; ed. Cherry, M.L., Lande, K., and Steinberg, R.I. (1982).

Toyoda, Y., Suga, K., Murakami, K., Hasegawa, H., Shibata, S., Domingo, V., Escobar, I., Kamata, S., Bradt, H., Clark, G., LaPointe, M., *Proceedings of the 9th International Cosmic Ray Conference* (London), **2**, 708 (1965).

Trumper, J., Pietsch, W., Reppin, C., Voges, W., Staubert, R., and Kendziorra, E. *Ap. J. (Letters)*, **219**, L105 (1978).

Tucker, W.H., *Radiation Processes In Astrophysics*, MIT Press (1975).

Tumer, O.T., Hammond, J.S., White, R.S., and Zych, A.D., *Proceedings 21st International Cosmic Ray Conference*, ed. Protheroe, R.J., 2, 155-158 (1990).

Touhy, I.R., and Cruise, A.M., *M.N.R.A.S.*, **171**, 33p-39p (1975).

Tuohy, I.R., and Rapley, C.G., *Ap. J. (Letters)*, **198**, L69-L72 (1975).

Turver, K.E., in *Proc. Workshop on Particle Acceleration in Accreting Compact Objects*, Amsterdam (1990a: in preparation).

Turver, K.E., in *Proc. 12th European Cosmic Ray Symposium*, Nottingham (1990b: in preparation).

Ulmer, M.P., Baity, W.A., Wheaton, W.A., and Peterson, L.E., *Nature Phys. Sci.*, **242**, 121 (1973).

Usov, V.V., *Nature*, **305**, 409-410 (1983).

van Paradijs, J., in *Timing Neutron Stars*, pp. 191-207; ed. Ogelman, H., and van den Heuvel, E.P.J., Kluwer Academic Publishers, The Netherlands (1989).

van Paradijs, J., Lub, J., Pel, J.W., Pakull, M., and van Amerongen, S., *Astron. & Ap.*, **124**, 294 (1983).

van Paradijs, J. and Kuiper, L., *Astron. & Ap.*, **138**, 71-76 (1984).

Vavilov, S.I., *C.R. Acad. Sci., U.S.S.R.*, 2, 457 (1934).

Verbunt, F., van Paradijs, J., and Elson, R., *Mon. Not. Roy. Ast. Soc.*, **210**, 899-914 (1984).

Vestrand, W.T., and Eichler, D., *Ap. J.*, **261**, 251-258 (1982).

Vladimirsky, B.M., Stepanian, A.A., and Fomin, V.P., *Proceedings of the 13th International Cosmic Ray Conference* (Denver), **1**, 456 (1973).

Waltman, F.B., Fiedlar, R.L., and Johnston, K.J., IAU Circular # 5075 (1990).

Wang, Y.M., *Astron. Space Sci.*, **121**, 193-200 (1986).

Watson, G.S., *Biometrika*, **49**, 57-63 (1962).

Webster, B.L., Martin, W.L., Feast, M.W., and Andrews, P.J., *Nature Phys. Sci.*, **240**, 183 (1972).

Weekes, T.C., *Physics Reports*, **160**, 1-121 (1988).

Weekes, T.C., Cawley, M.F., Fegan, D.J., Gibbs, K.G., Hillas,

A.M., Kwok, P.W., Lamb, R.C., Lewis, D.A., Macomb, D., Porter, N.A., Reynolds, P.T., and Vacanti, G, *Ap. J.*, **342**, 379-395 (1989).

Wheaton, W.A., Doty, J.P., Primini, F.A., Cooke, B.A., Dobson, C.A., Goldman, A., Hecht, M., Hoffman, J.A., Howe, S.K., Scheepmaker, A., Tsiang, E.Y., Lewin, W.H.G., Matteson, J.L., Gruber, D.E., Baity, W.A., Rothschild, R., Knight, F.K., Nolan, P., and Peterson, L.E., *Nature*, **282**, 240 (1979).

Wheeler, J.C., Lecar, M., and McKee, C.F., *Ap. J.*, **200**, 145 (1975).

White, N.E., *X-Ray Binaries*, in *The Astronomy and Astrophysics Review*, **1** (1989).

White , N.E., and Holt, S.S., *Ap. J.*, **257**, 318-337 (1982).

Yentis, D., Shulman, S., McKee, J.D., and Rose, W.K., *Astrophysical Letters*, **19**, 53 (1977).

Figure 1.2

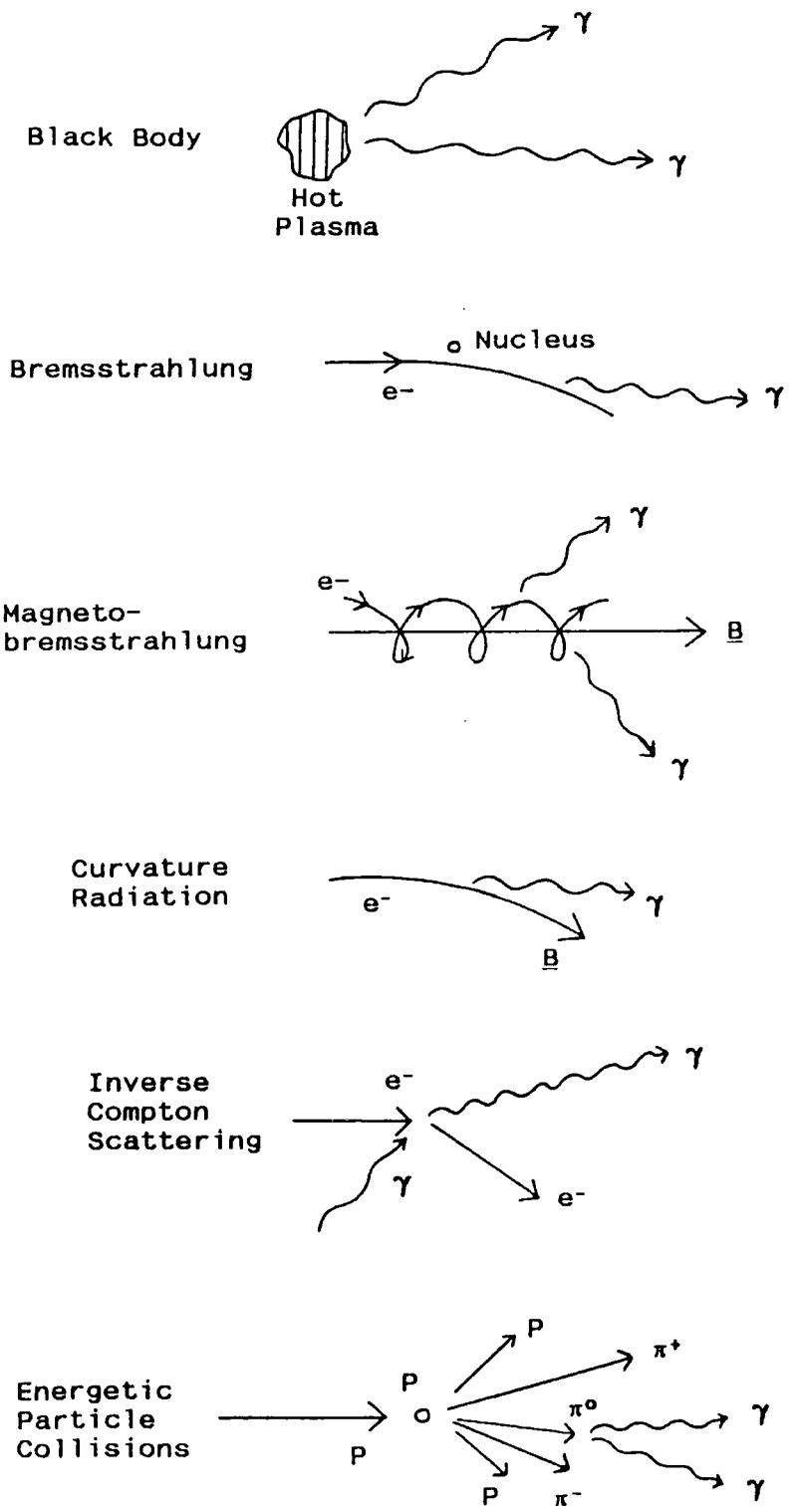

Continuum Radiation Processes

Figure 2.5a

Durham University Mark III Telescope:

Geometrical Shower Discrimination

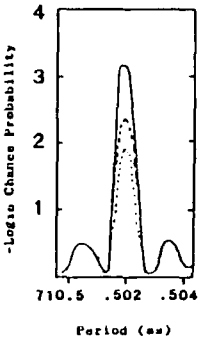

—— Hardware & Software Selection

---- Hardware Selection

····· No Selection

Results of test for uniformity in phase of SMC X-1 time series recorded on 1987 July 23

SMC X-1 23/07/87	Total Events	% Rejected	% Signal Strength	Gamma-Ray Candidates	Chance Prob.
No Selection	9517	-	2.14	204	1.3×10^{-2}
Hardware Selection	8235	34	2.69	180	5.5×10^{-4}
Software Selection	5557	11	3.54	197	8.5×10^{-6}

Figure 2.5b

Whipple Collaboration: Air Shower Discrimination By Cerenkov Imaging

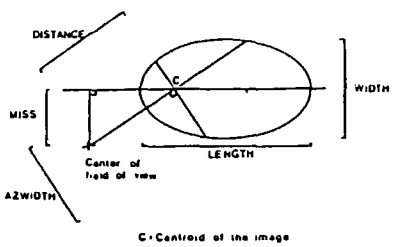

Definition of image parameters

(Adapted from Weekes *et al.* 1989)

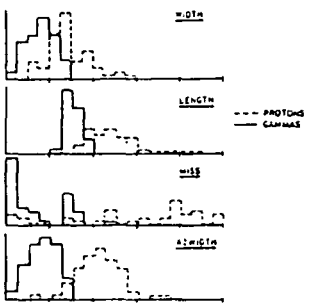

Image parameter distribution predicted by simulations for γ-ray source at zenith and an isotropic cosmic ray background

Horizontal scale: degrees
Vertical: arbitrary linear scale

Figure 2.5c

Riverside & Caltech: Shower Discrimination by Inspection of Temporal Distribution of Pulse

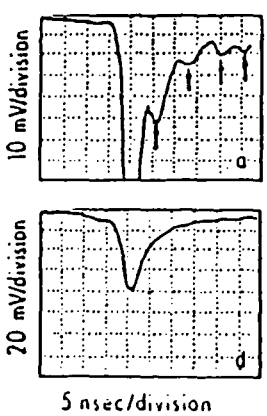

OSCILLOSCOPE TRACES OF CERENKOV PULSES

Hadron Candidate.

Multiple kinks, large tail offset, pulse height > 100 mV

Gamma-Ray Candidate.

No kinks, no tail offset, pulse height = 80 mV.

(Adapted from Tumer *et al.* 1990)

Figure 8.5

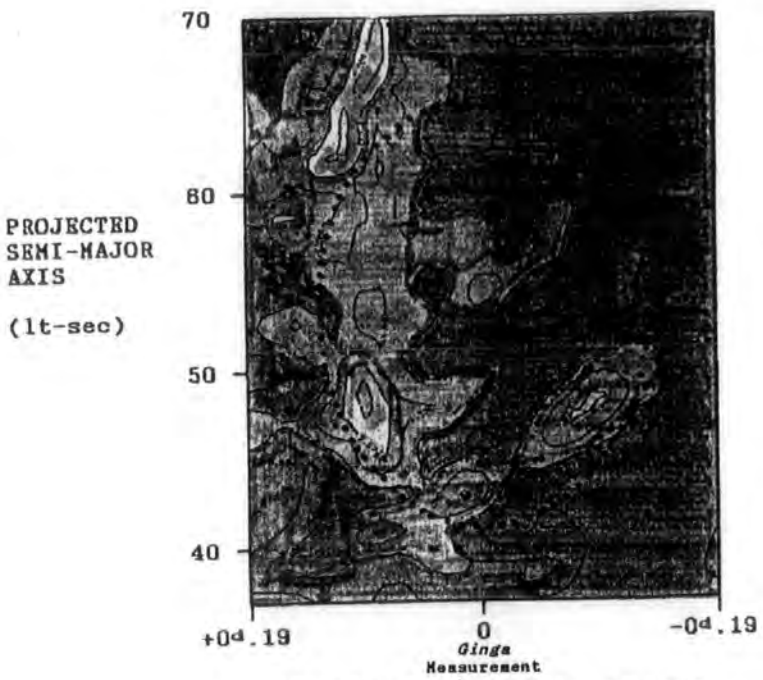

1986 Oct 24 - Nov 04

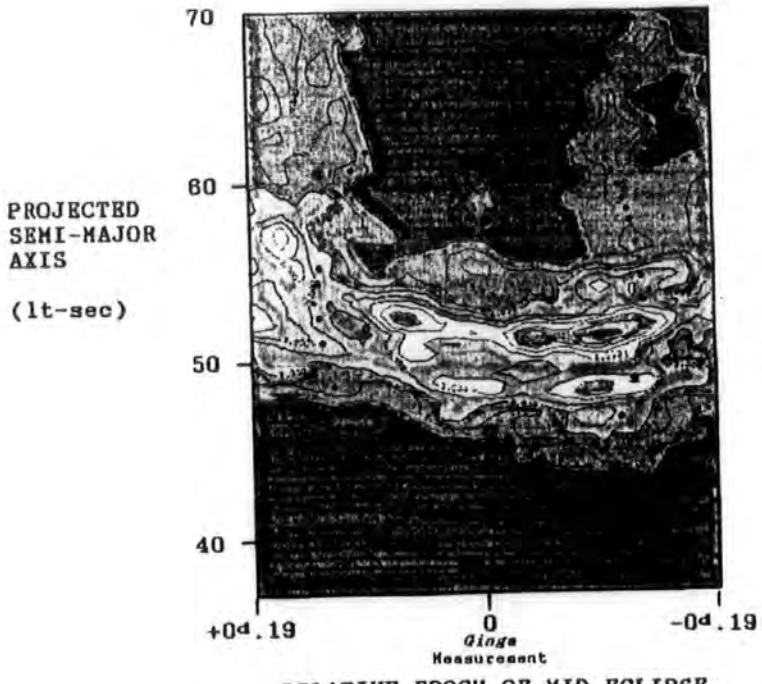

1987 Jul 21-31

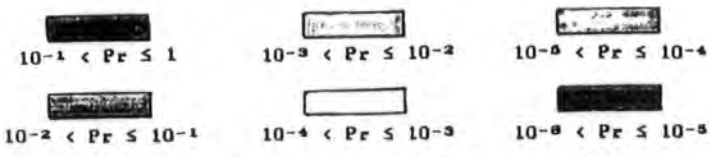

Figure 8.5 (cont.)

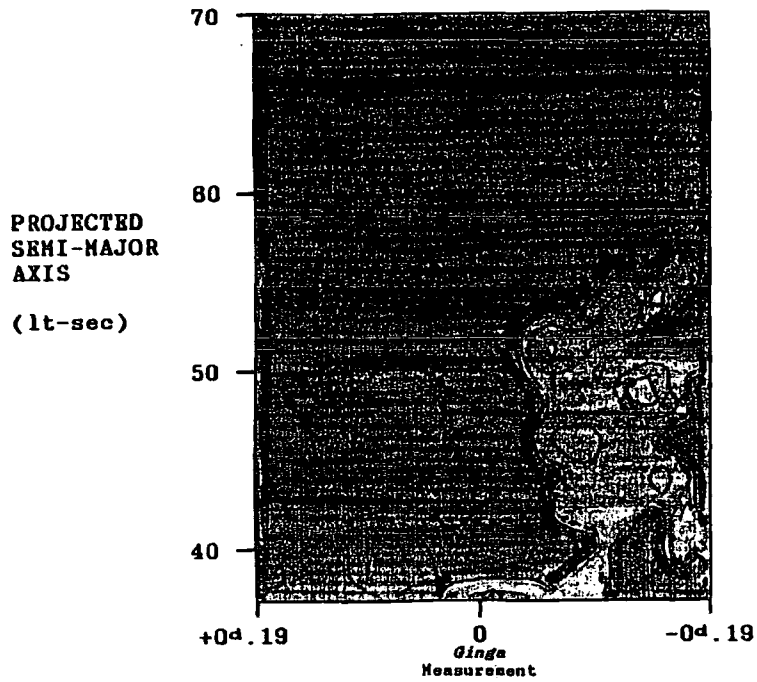

1987 Aug 20-28

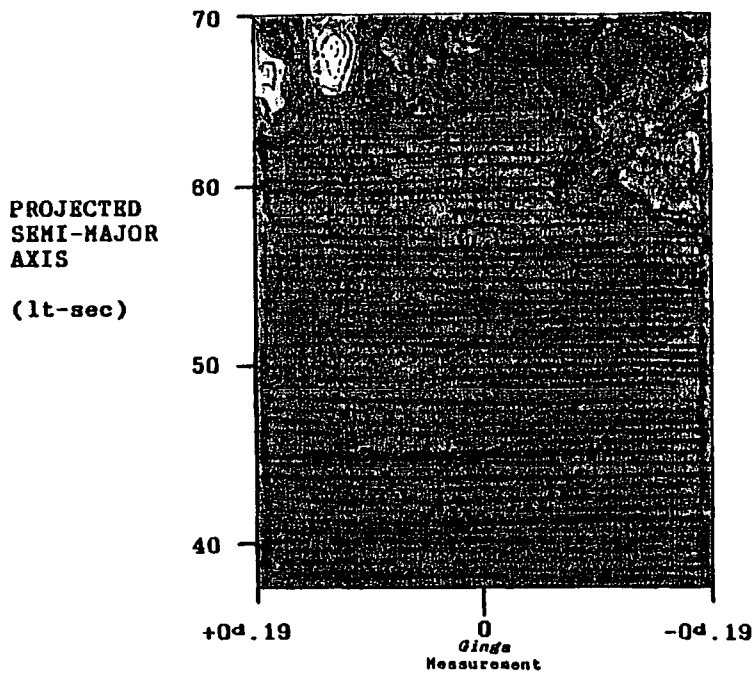

1987 Sep 14-27

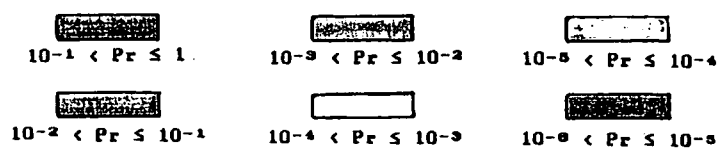

Figure 8.5 (cont.)

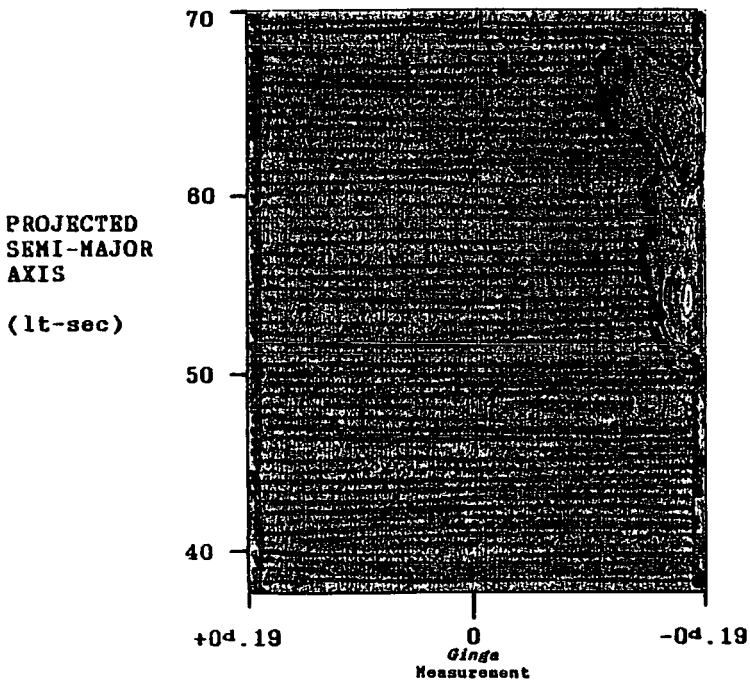

1987 Oct 10-25

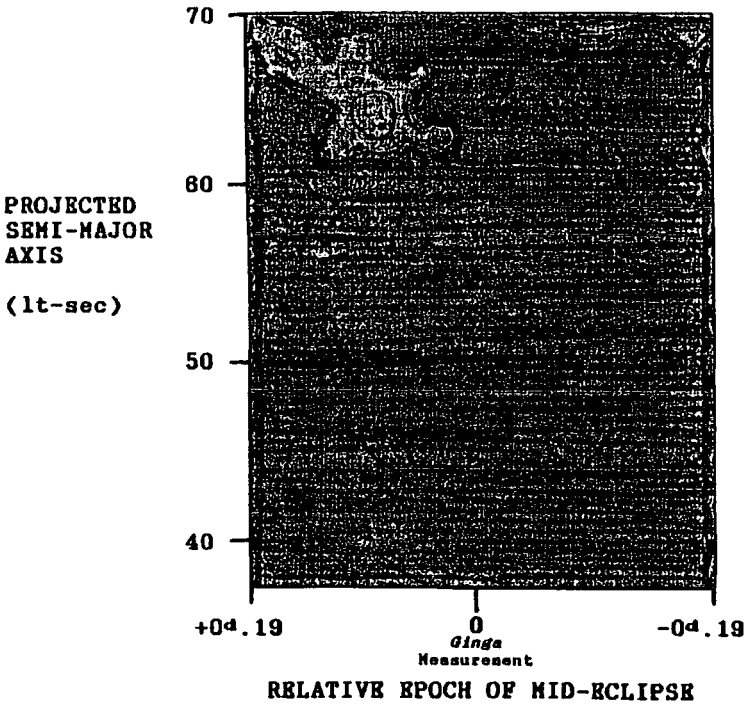

1987 Nov 13-19

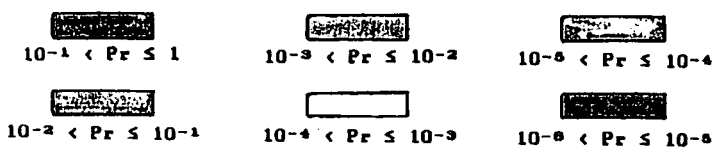

Figure 8.5 (cont.)

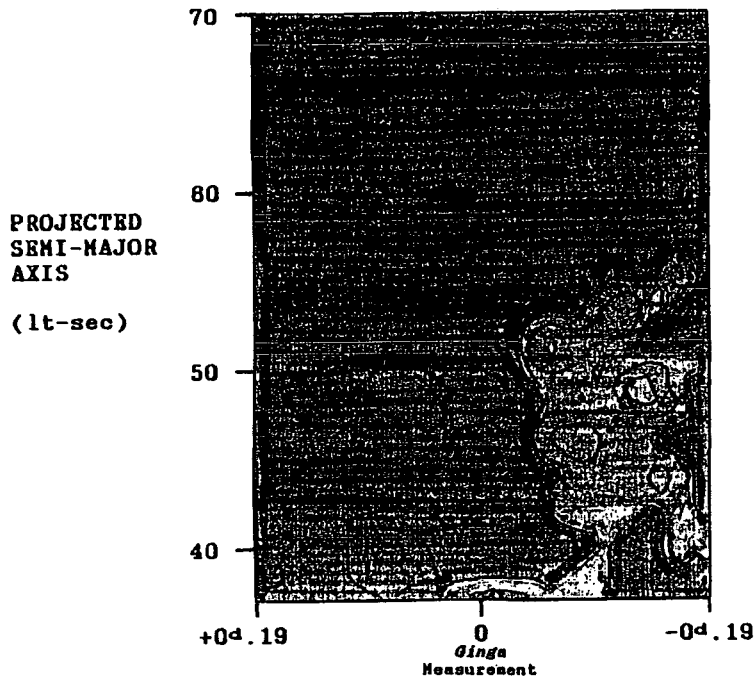

1987 Aug 20-28

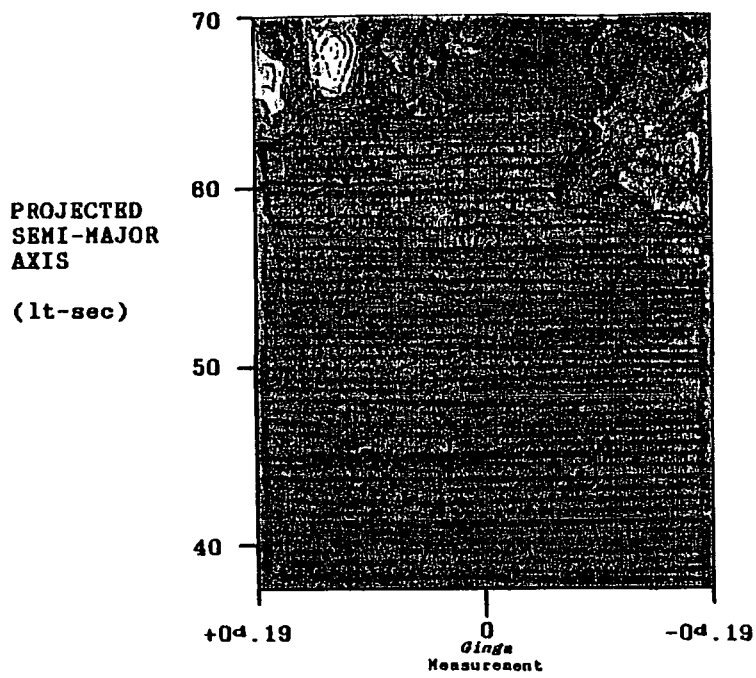

1987 Sep 14-27

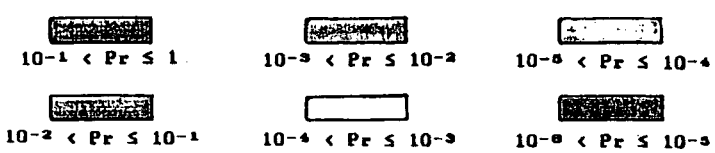

Figure 8.5 (cont.)

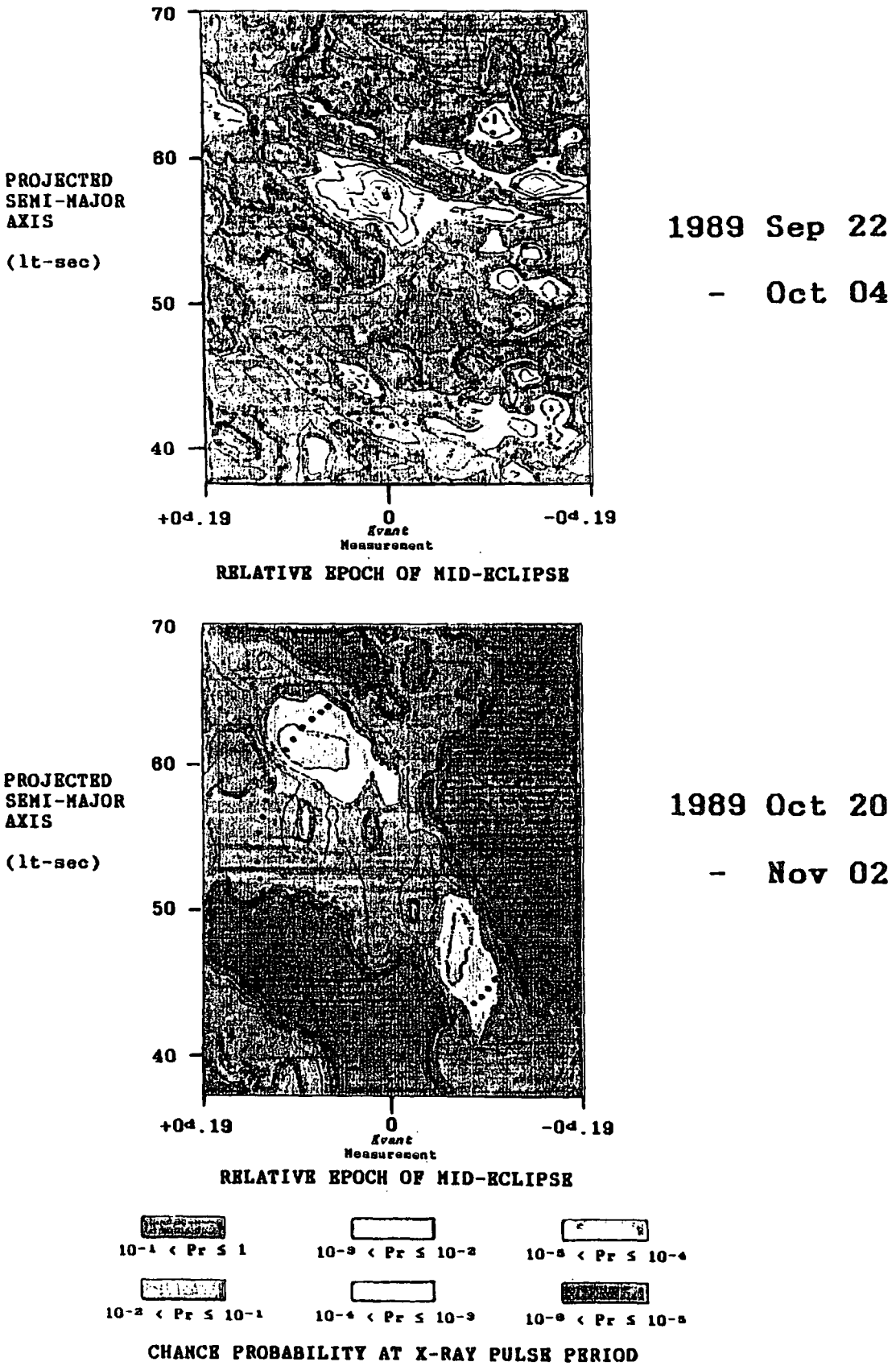

Figure 8.6a

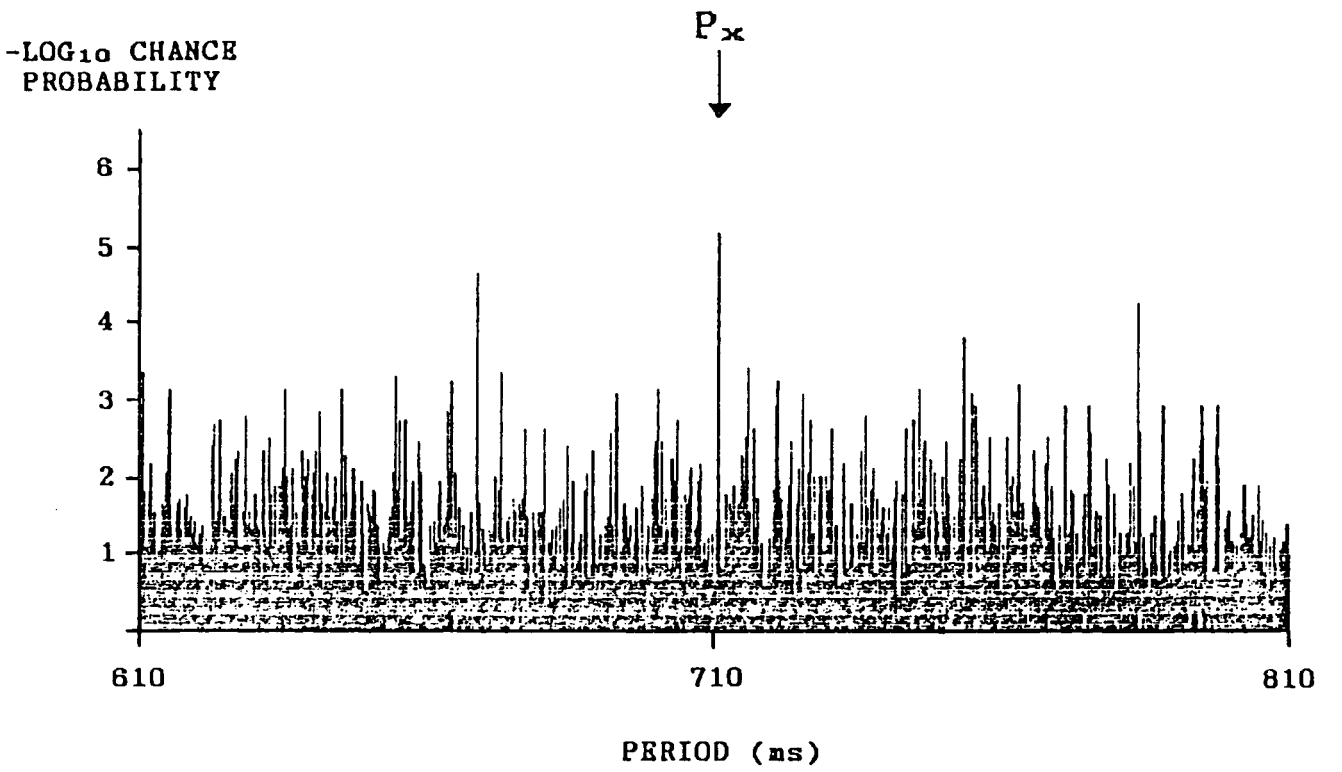

SMC X-1: Period Analysis of the

1987 July 21-31 Data

Figure 8.6b

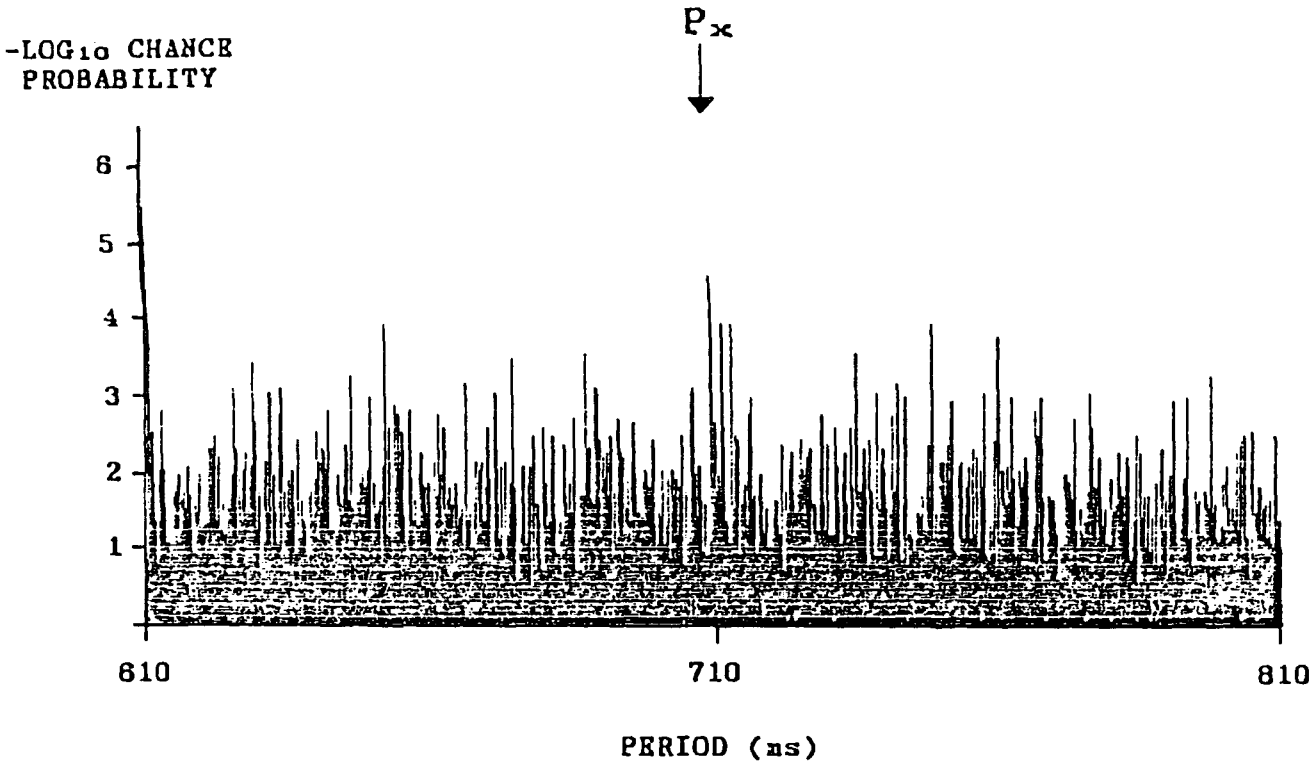

SMC X-1: Period Analysis of the

1989 September 22 -

October 04 Data

Figure 8.8a

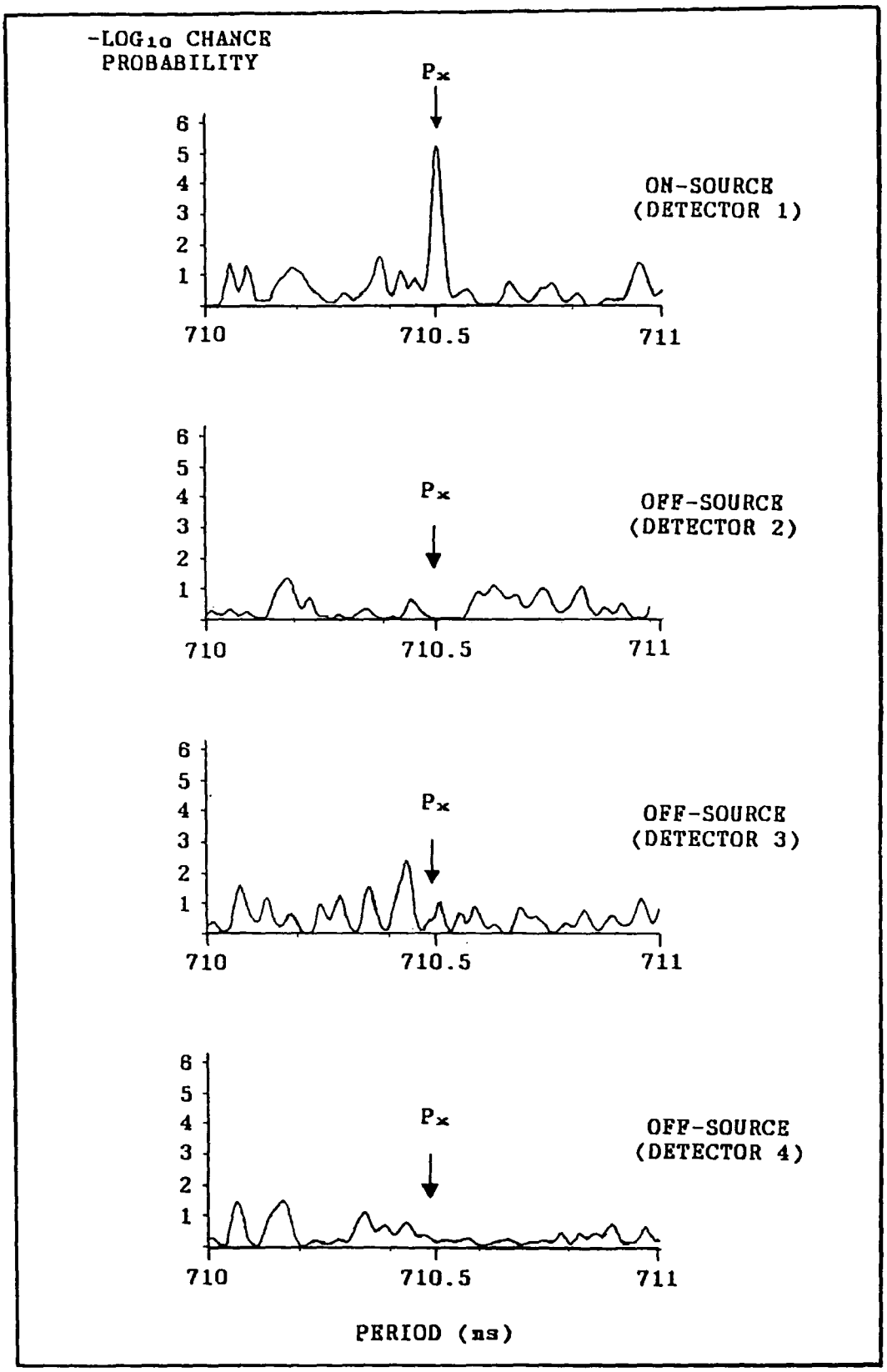

SMC X-1: Control Tests on the 1987 July 21-31 Data

Figure 8.8b

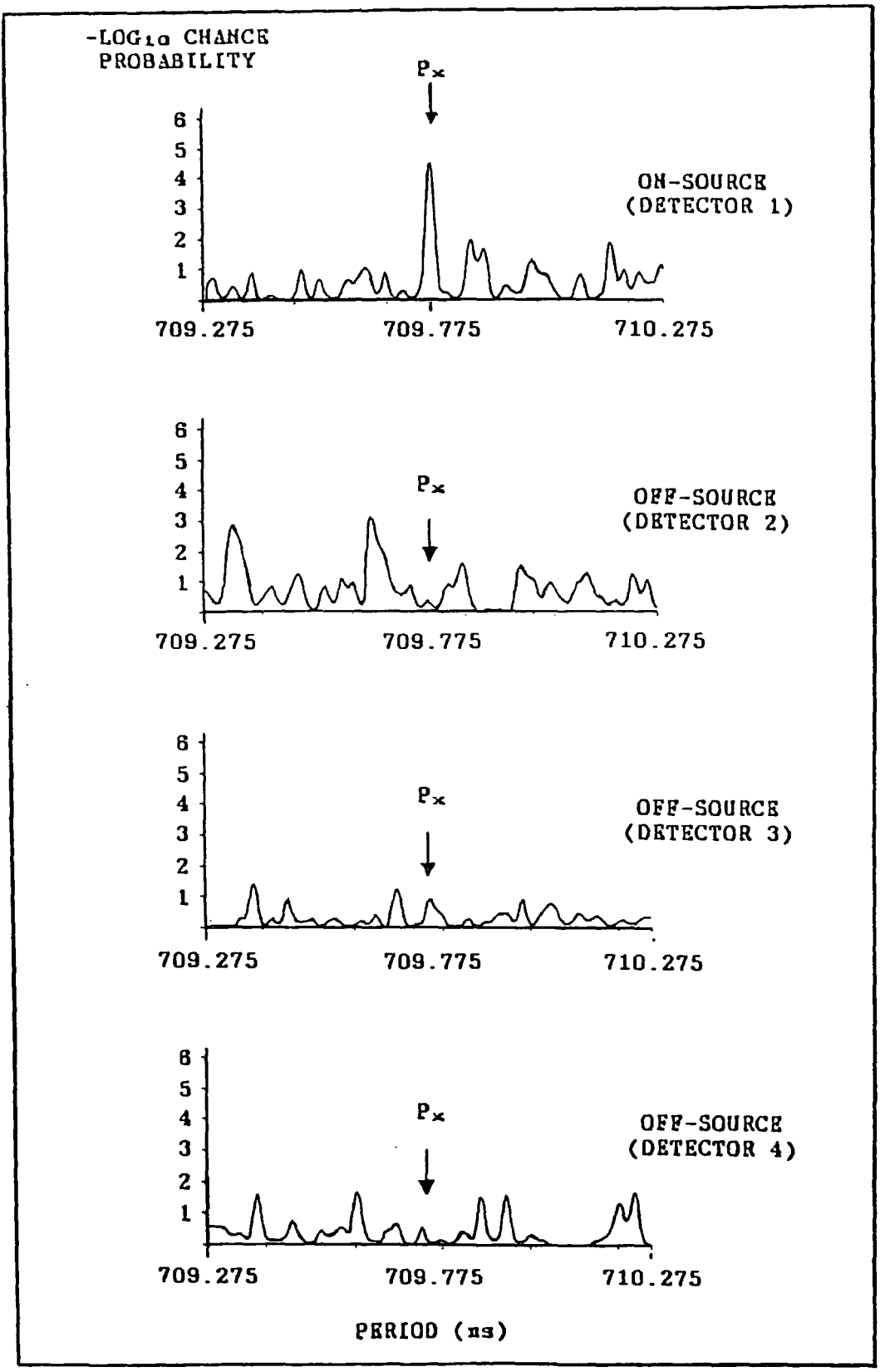

SMC X-1: Control Tests on the 1989

Sep 22 - Oct 04 Data

Figure 9.2a

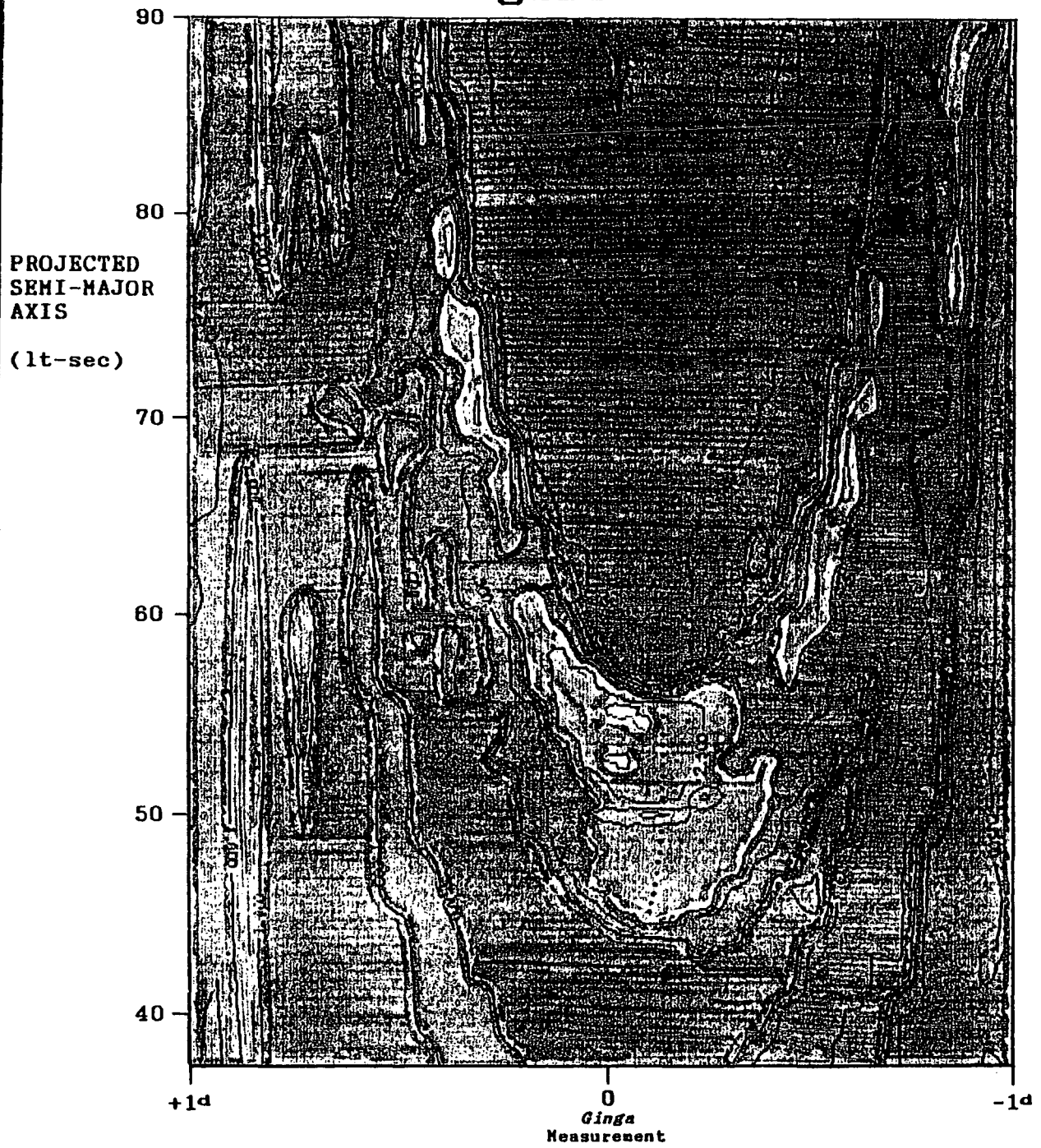

SMC X-1: Analysis of 1987 July 23 Data

Figure 9.2b

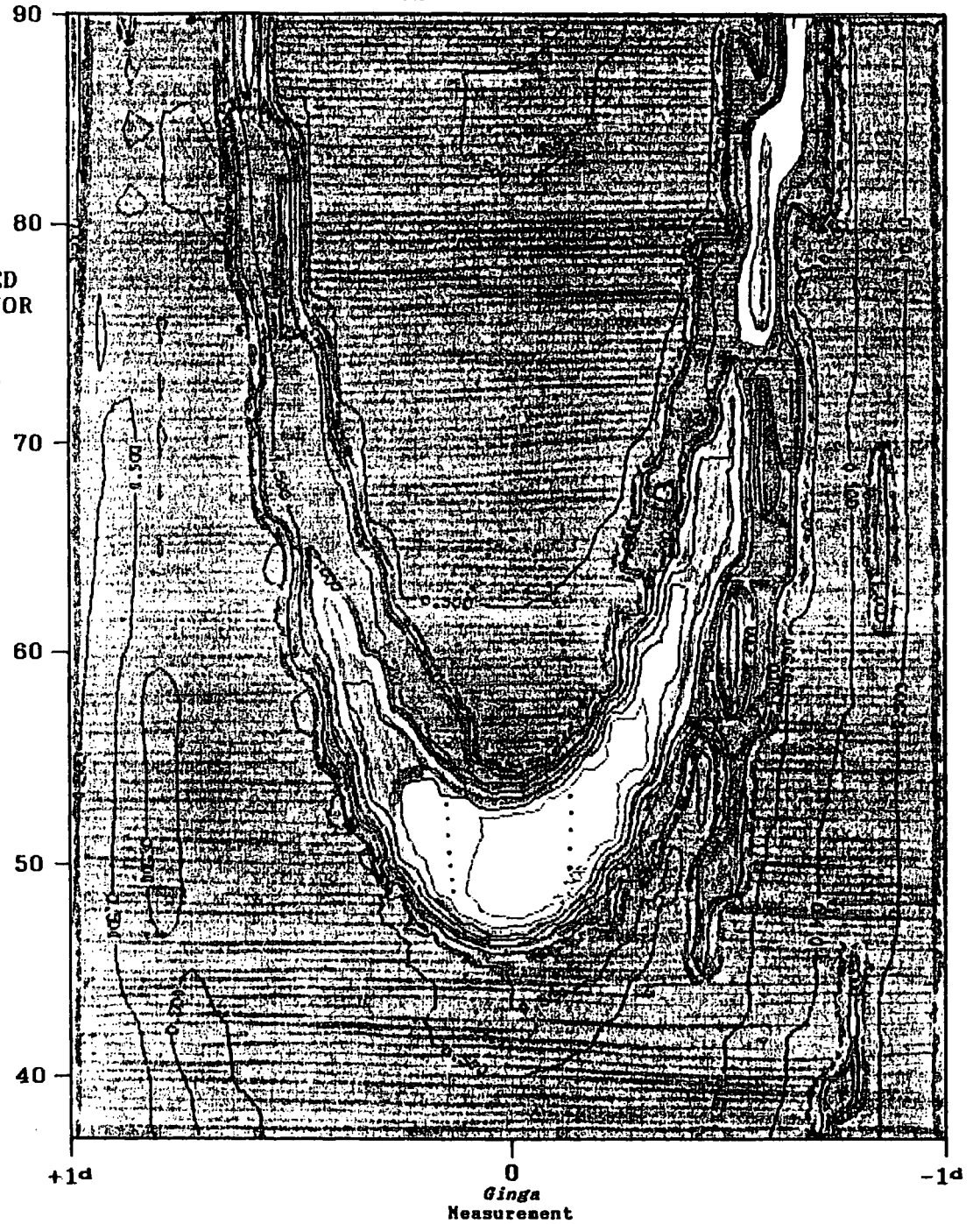

SMC X-1: Analysis of 1987 July 29 Data

Figure 9.3a

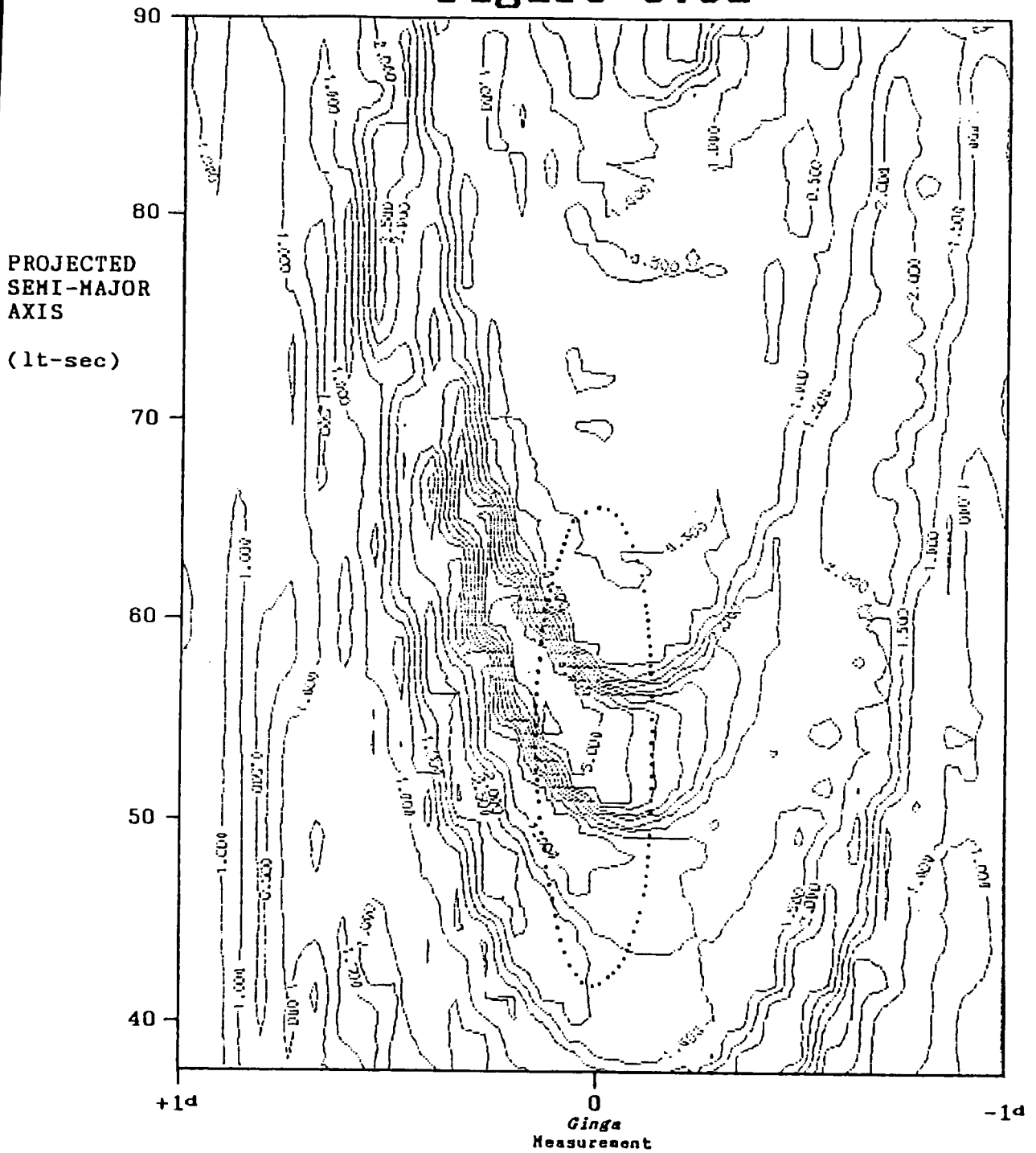

SMC X-1: SIMULATION of 1987 July 23 Data

with uniform pulsed signal

Figure 7.5

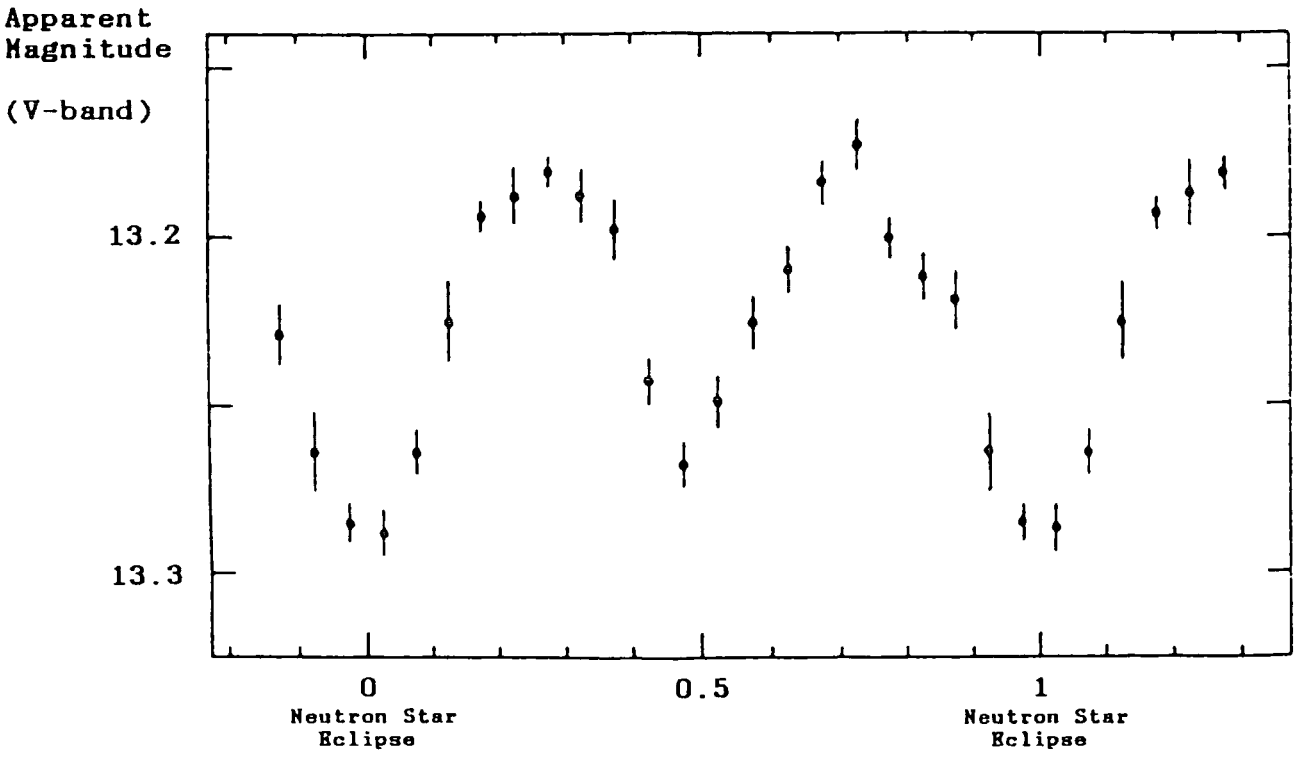

SMC X-1: Average Optical Light Curve

(From van Paradijs and Kuiper 1984)

Figure 8.3

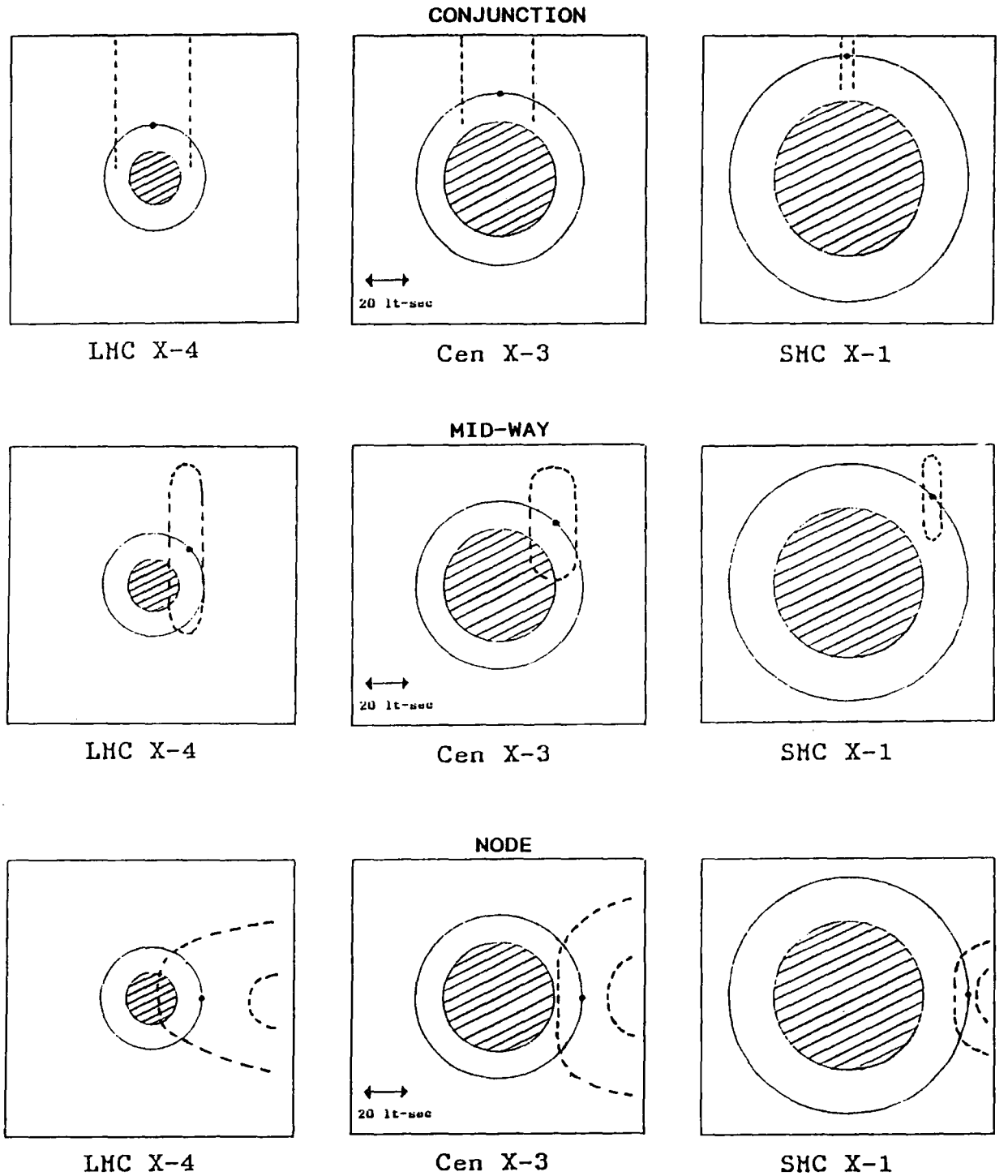

Sampling intervals for $a_x \sin i$ and epoch of mid-eclipse

Solid circle: neutron star orbit

Disk: companion star

Dashed line: Sampling interval 'error box' about position of neutron star

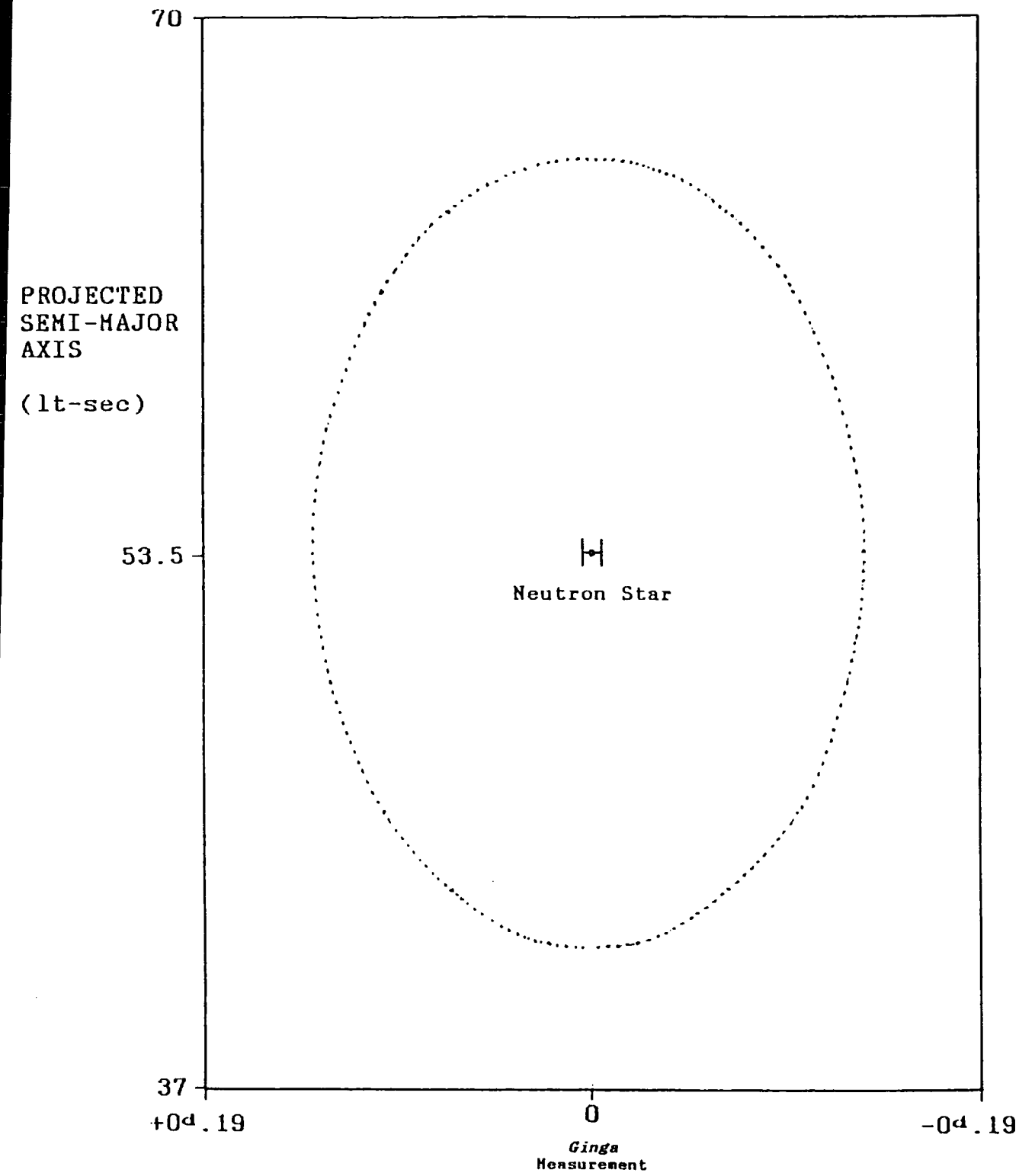

Figure 8.4

[Epoch, $a_x \sin i$] plane in which contours of chance probability will be drawn

..... Boundary of accretion disk

Figure 9.3b

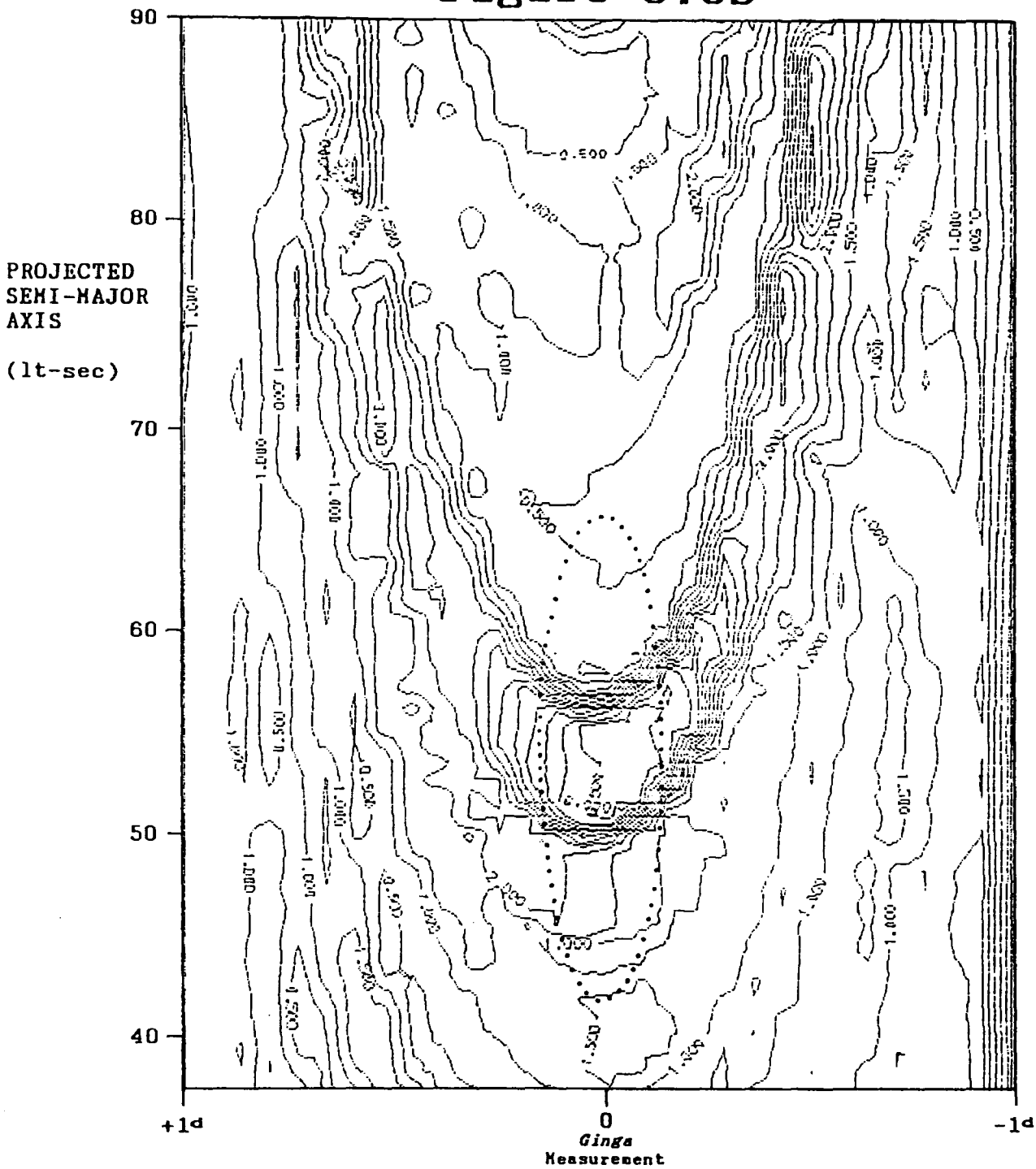

SMC X-1: SIMULATION of 1987 July 29 Data

with uniform pulsed signal

Figure 9.5a

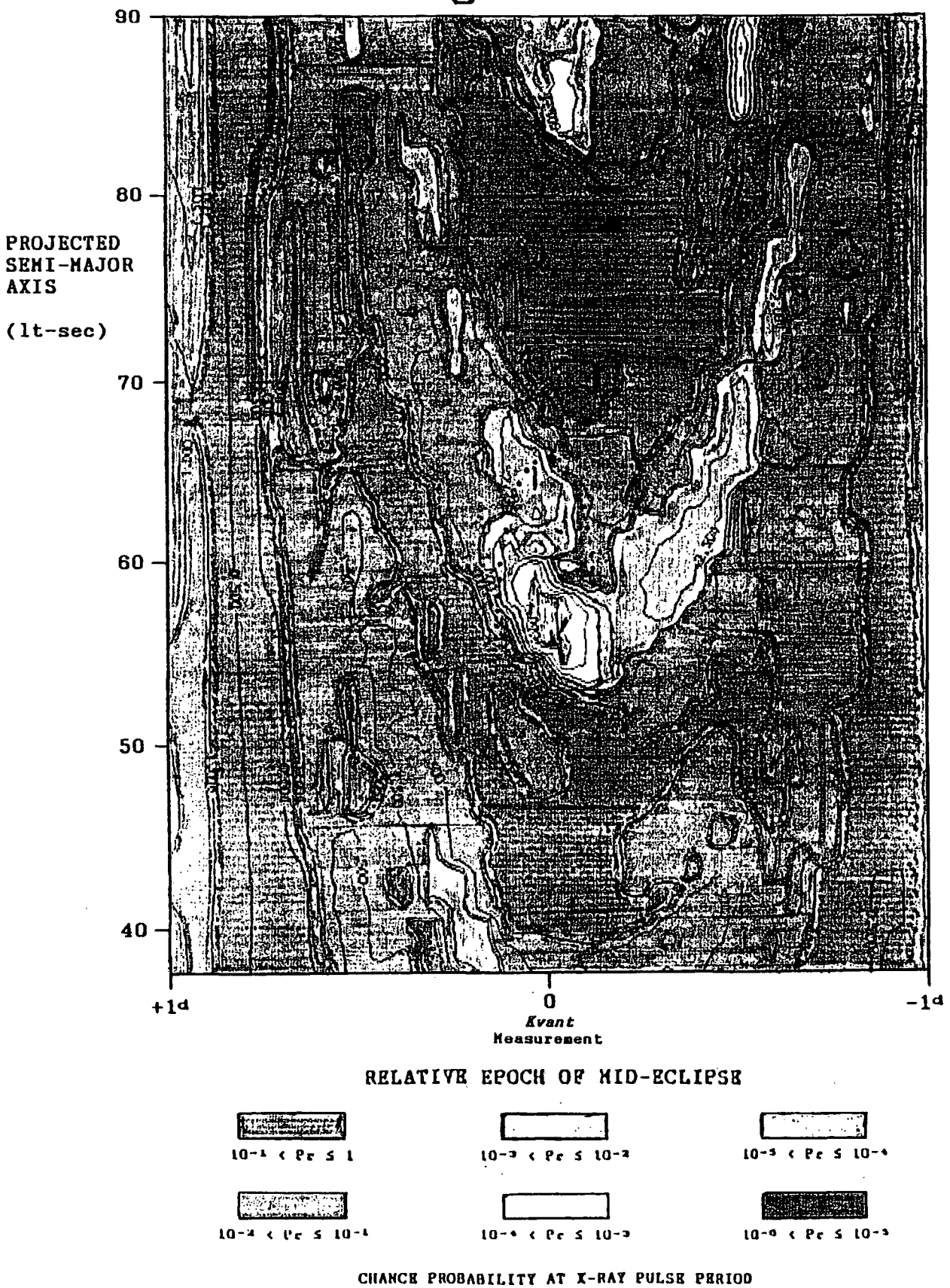

SMC X-1: Analysis of 1989 October 02 Data

Figure 9.5b

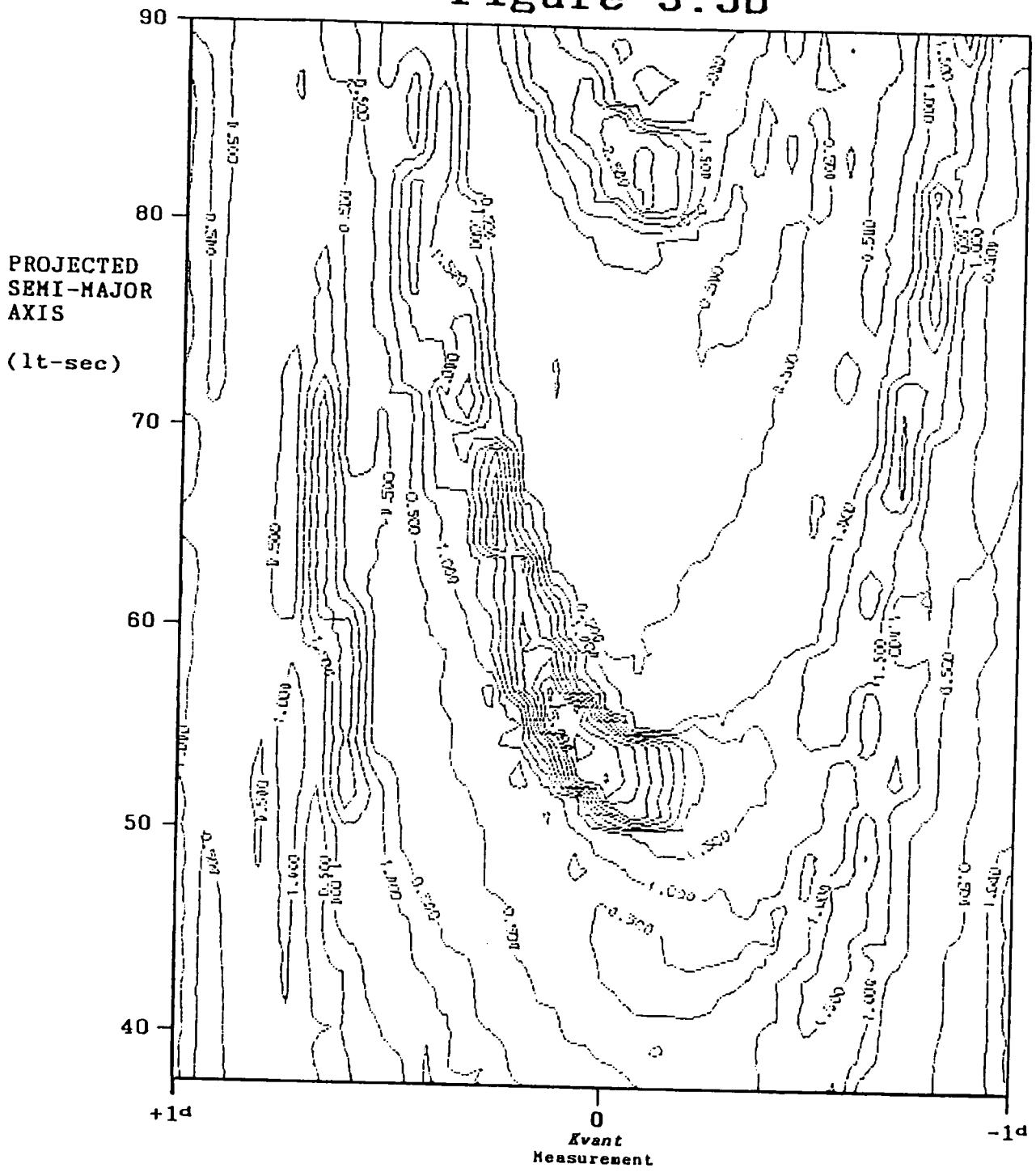

SMC X-1: SIMULATION of 1989 October 02 Data

with uniform pulsed signal

Figure 9.6

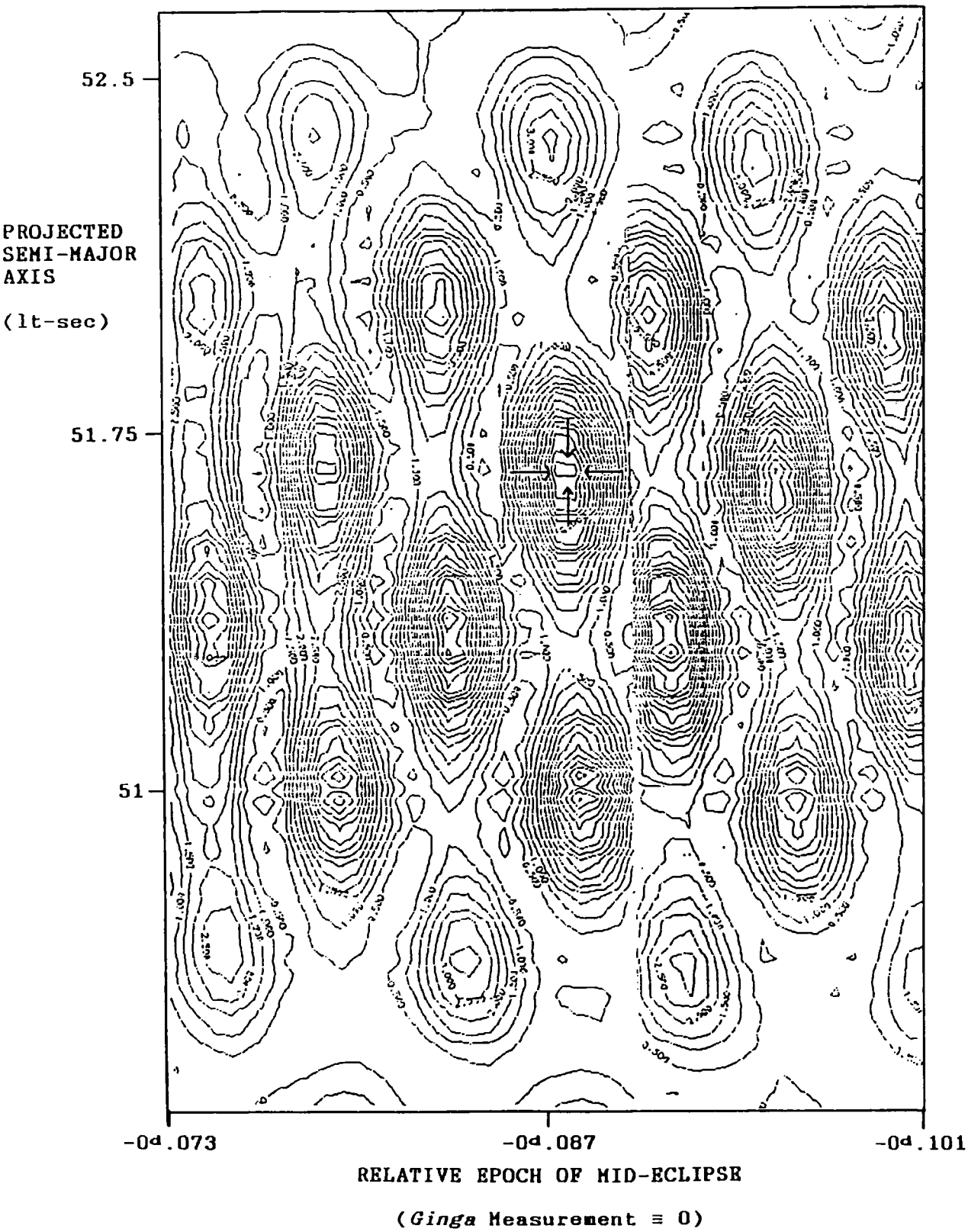

SMC X-1: Test for phase coherence in 1987 July data. Chance probability contours are drawn at X-ray period

Figure 9.8

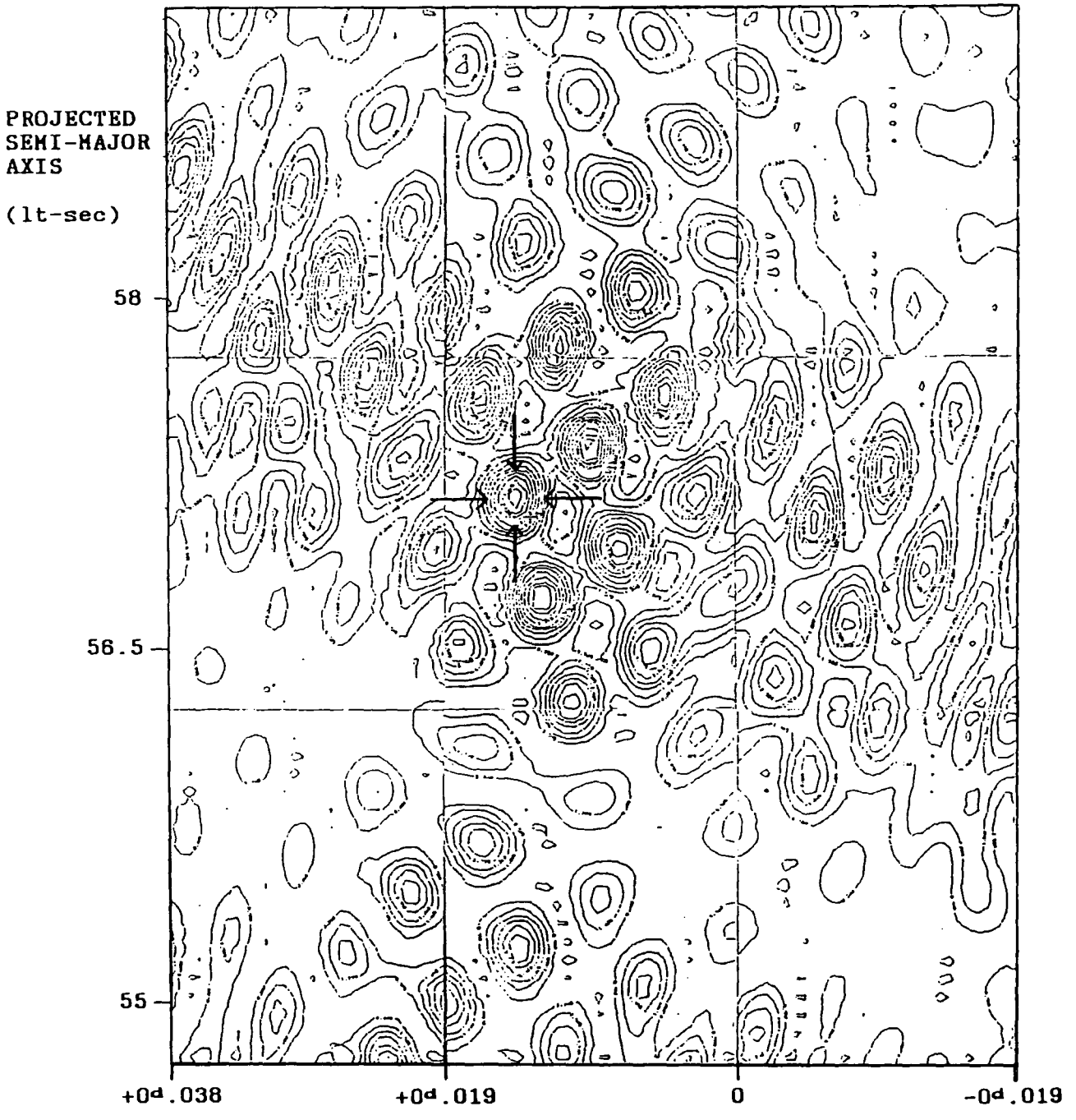

SMC X-1: Test for phase coherence in data of 1989 September 22 - October 04. Chance probability contours are drawn at X-ray period.

Figure 10.1

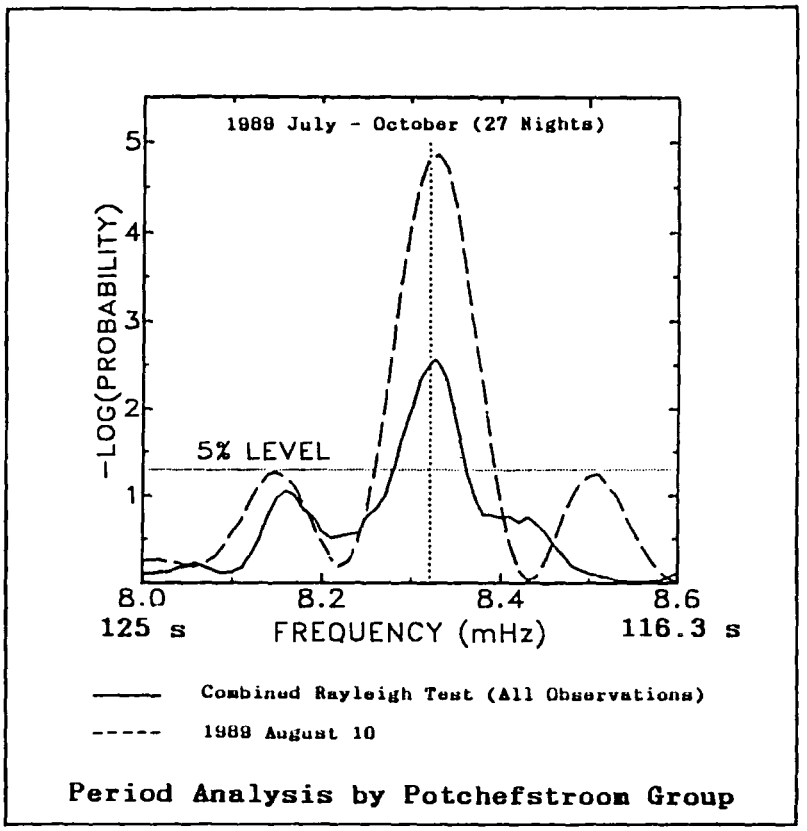

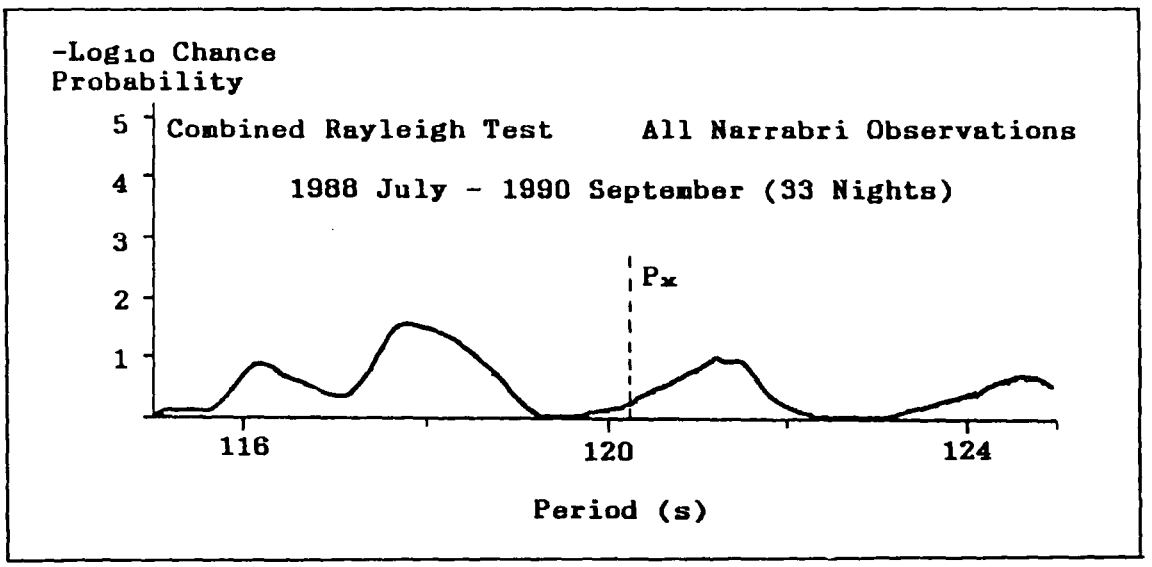

47 Tucanae: Period Analyses by Potchefstroom and Durham Groups

Figure 11.4

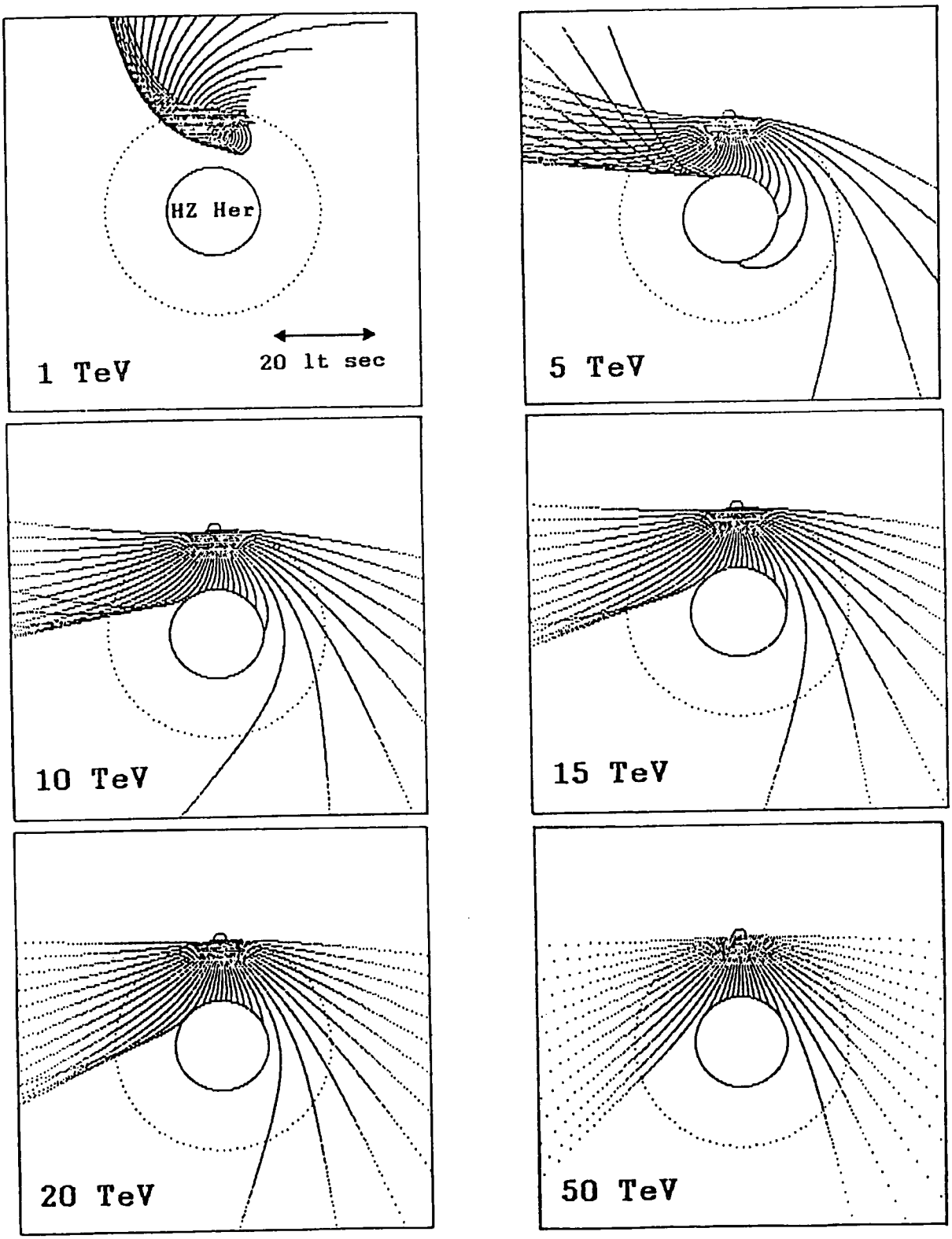

Proton Trajectories in the Her X-1 Binary System

Solid circle: companion star
Dotted circle: pulsar orbit
Pulsar at mid-eclipse

Curves: proton trajectories
Proton energies are indicated

$B_\bullet$ = 0.1 G
Dipole directed into page through
centre of companion star